Design, Synthesis and Evaluation of Amino- and Guanidino-Substituted Oligomers and Oligonucleotides for Better Cellular Uptake

Thesis Submitted to
The University of Pune for the degree of

Doctor of Philosophy
in
Chemistry

BY

Kiran M. Patil

Research Supervisor

Dr. Vaijayanti A. Kumar

Division of Organic Chemistry
National Chemical Laboratory
Pune-411008

November 2013

CERTIFICATE

This is to certify that the work presented in the thesis entitled "**Design, Synthesis and Evaluation of Amino- and Guanidino-Substituted Oligomers and Oligonucleotides for Better Cellular Uptake**" submitted by Mr. Kiran M. Patil, was carried out by the candidate at the CSIR-National Chemical Laboratory Pune, under my supervision. Such materials as obtained from other sources have been duly acknowledged in the thesis.

Dr. Vaijayanti A. Kumar   **November 2013**

(Research Supervisor)

Division of Organic Chemistry

CSIR-National Chemical Laboratory

Pune 411008

CANDIDATE'S DECLARATION

I hereby declare that the thesis entitled "**Design, Synthesis and Evaluation of Amino- and Guanidino-Substituted Oligomers and Oligonucleotides for Better Cellular Uptake**" submitted for the award of degree of *Doctor of Philosophy* in Chemistry to the University of Pune has not been submitted by me to any other university or institution. This work was carried out by me at the National Chemical Laboratory, Pune, India. Such materials as obtained from other sources have been duly acknowledged in the thesis.

Kiran M. Patil   **November 2013**

CSIR-National Chemical Laboratory

Pune- 411 008

Dedicated to

Family and Friends

Acknowledgement

Contents

	Chapter 2	
2	**Design and synthesis of proline/hydroxy-proline-derived monomers, peptide and their biological evaluation**	
	SECTION A	
A	**Synthesis of *trans*-4-hydroxy-L-proline-derived orthogonally protected monomer, peptides and their cell uptake studies**	
2A.1	Introduction	46
2A.2	Rationale, design and objectives of the present work	48
2A.3	Synthesis, results and discussion	50
2A.3.1	Synthesis of monomer	50
2A.3.2	Solid phase peptide synthesis	52
2A.3.2a	General principles of solid phase peptide synthesis	52
2A.3.2b	Solid phase peptide synthesis of novel CPPs	53
2A.3.2c	Cleavage and purification of resin bound peptide	54
2A.3.3	Guanidinylation of pendant amines on solid and in solution phase	55
2A.3.4	Fluorescence-Activated Cell Sorting (FACS) analysis	57
2A.3.4a	General principle of FACS analysis	57
2A.3.4b	FACS analysis of *cf*-labeled peptides (P1-P10)	59
2A.4	Summary and Conclusion	60
	SECTION B	
B	**Synthesis of L/D-Proline-derived monomers, peptides and their cell uptake studies**	
2B.1	Introduction	62
2B.2	Rationale, design and objectives of the present work	62
2B.3	Synthesis, results and discussion	63
2B.3.1	Synthesis of proline-derived conformationally restricted spacer units	63
2B.3.2	Solid phase peptide synthesis	64
2B.3.3	Circular Dichroism analysis of synthesized oligomers	66
2B.3.4	Fluorescence-activated cell sorting (FACS) Analysis	67
2B.3.5	Confocal microscopy analysis	69
2B.3.5a	Principle of confocal microscopy	69
2B.3.5b	Confocal microscopic analysis of synthesized oligomers	70
2B.3.6	pDNA delivery to cells by unlabeled oligomers	71
2B.3.7	Cytotoxicity analysis of synthesized oligomers	72
2B.4	Summary and conclusion	74
2.1	Experimental	75
2.1.1	Synthesis of compounds/monomers	75
2.1.1a	Experimental procedure and spectral data	76

Chapter 4

Design and synthesis of novel oligocarbamates and monomer synthesis for dendron and dendrimers

List of research publications:

1. "Highly Efficient (R-X-R)-Type Carbamates as Molecular Transporters for Cellular Delivery"
   Kiran M. Patil, Rangeetha J. Naik, Rajpal, Moneesha Fernandes, Munia Ganguli,* and Vaijayanti A. Kumar* *J. Am. Chem. Soc.* **2012**, *134*, 7196-1799.

2. "Second generation arginine-rich (R-X'-R)$_4$-type cell-penetrating α-ω-α-peptides with constrained, chiral ω-aminoacids (X') for enhanced cargo delivery inside cells"
   Kiran M. Patil, Rangeetha J. Naik, Manika Vij, Vaijayanti A. Kumar, Munia Ganguli*, and Moneesha Fernandes* Submitted manuscript.

Symposia Attended/ Poster Presentations:

1. Participation in Indian Peptide Society, Second "Indian Peptide Symposium" held at National Institute of Immunology, New Delhi, INDIA on February 26-27th, 2009.

2. Participation in "1st CRSI zonal meeting" held at CSIR-NCL, Pune, INDIA in May 2011.

3. Presented Poster in "6th Cambridge Symposium on Nucleic Acid and Biology" held at Queens' college, University of Cambridge, Cambridge, UK on September 04 -07th, 2011.

4. Attended "ACS on campus" meeting held at CSIR-NCL, Pune, INDIA 4th on October 10th, 2012.

5. Presented Poster in International Conference of ISCB on "Recent advances in Chemistry and Biology" held at Udaipur, Rajasthan, INDIA on March 02-05th, 2013

6. Presented Poster in "International Meeting on Chemical Biology" (IMCB-2013) at Indian Institute of Science Education and Research, Pune held on May 26-28th, 2013

Abbreviations

μL	Microlitre
μM	Micromolar
A	Absorbance
Å	Angstrom
Ac	Acetate
Ac_2O	Acetic anhydride
ACN	Acetonitrile
Ahx	6-Amino hexanoic acid
asONs	Antisense oligonucleotides
Boc	Di-tert butyl carbonate
BOP	Benzotriazol-1-yloxy)tris(dimethylamino)phosphonium hexafluorophosphate
Calc.	calculated
Cat.	Catalytic/catalyst
Cbz	Benzyloxycarbonyl
CD	Circular Dichroism
cf	5,(6)-carboxyfluorescein
CH_2Cl_2	Dichloromethane
CHO cell	Chinese Hamster Ovary cell
Conc.	Concentrated
CPOs	Cell-penetrating oligomers
CPPs	Cell-penetrating peptides
Dau	Daunomycin
DCC	N'N'- Diclyclohexylcarbodiimide
DCM	Dichloromethane
DEPT	Distortionless Enhancement by Polarization Transfer
DI	Deionized
DIC	Differential Interface Contrast Image
DIPCDI	N,N'Diisopropylcarbodiimide
DIPEA/DIEA	Diisopropylethylamine
DMAP	4',4'-Dimethylaminopyridine
DMD	Duchenne Muscular Dystrophy
DMF	*N*,*N*-dimethylformamide

DMSO	*N*,*N*-Dimethyl sulfoxide
DNA	2'-deoxyribonucleic acid
ds	Double stranded
EDTA	Ethylenediaminetetraacetic acid
Et$_3$N	Triethylamine
EtOAc	Ethyl acetate
EtOH	Ethanol
FACS	Fluorescence-activated Cell Sorting
Fmoc	Fluorenylmethyloxycarbonyl
g	Gram
h	Hours
HDMS	High Defination Mass Spectroscopy
HOBt	Hydroxy benztriazole
HPLC	High Performance Liquid Chromatography
HRMS	High Resolution Mass Spectrometry
Hz	Hertz
IR	Infra red
L	litre
LCMS	Liquid Chromatography-Mass Spectrometry
M	Molar
MALDI-TOF	Matrix Assisted Laser Desorption Ionisation-Time of Flight
MBHA	4-(methyl)benzhydrylamine-resin
MeOH	Methanol
MF	Molecular formula
mg	milligram
MHz	Megahertz
min	Minutes
mL	Millilitre
mM	millimolar
mmol	millimoles
MS	Mass spectrometry
mts	mesitylene-2-sulfonyl
MW	Molecular weight
N	Normal
nm	Nanometer

NMR	Nuclear Magnetic Resonance
Obsd.	Observed
ONs	Oligonucleotides
pDNA	Plasmid deoxyribonucleic acid
pDNA	Plasmid DNA
Pet-ether	Petroleum ether
PNA	Peptide Nucleic Acid
ppm	Parts per million
Py	Pyridine
R	Arginine
R_f	Retention factor
RNA	Ribose Nucleic Acid
RP	Reversed Phase
RP-HPLC	Reversed Phase-HPLC
sec	Second
siRNA	Small interfering RNA
Ss	Single stranded
SSOs	splice switching oligonucleotides
tat	trans-activating transcriptional activator
TBTU	O-(Benzotriazol-1-yl)-N,N,N',N'-tetramethyluronium
TFA	Trifluoroacetic acid
TFMSA	Trifluoromethanesulfonic acid
THF	Tetrahydrofuran
TLC	Thin layer chromatography
T_m	Melting temperature
t_R	Retention time
UV-Vis	Ultraviolet-Visible
w/w	Weight by weight

<u>Abstract</u>

The thesis entitled **"Design, Synthesis and Evaluation of Amino- and Guanidino-Substituted Oligomers and Oligonucleoties for Better Cellular Uptake"** has been divided into four chapters.

Chapter 1:	Introduction: Cell-penetrating oligomers for drug delivery
Chapter 2:	Design and synthesis of proline/hydroxy proline-derived monomers, peptide and their biological evaluation
Section 2A:	Synthesis of *trans*-4-hydroxy-L-proline-derived orthogonally protected monomer, peptides and their cell uptake studies
Section 2B:	Synthesis of L/D-Proline-derived monomers, peptides and their cell uptake studies
Chapter 3:	Design and synthesis of (R-X-R)-type oligocarbamate transporters for cellular delivery *via*: Non-covalent complexation and covalent conjugation strategies
Chapter 4:	Design and synthesis of novel oligocarbamates and monomer synthesis for dendron and dendrimers
Section 4A:	Synthesis of tartaric acid-derived novel di-guanidine carbonate monomer and its incorporation in oligocarbamate
Section 4B:	Synthesis of *trans*-4-L-hydroxy-L-proline-derived carbonate monomer for incorporation in carbamate linked dendron and dendrimer

Chapter 1: Introduction: Cell-penetrating oligomers for drug delivery

Cell-penetrating Oligomers (CPOs) have proved very useful as carriers for the intracellular delivery of several types of small molecular drugs as well as peptide/oligonucleotides cargoes for therapeutic applications. A significant number of CPOs are cationic in nature and contain at least six amino acids such as lysine or arginine which are positively charged at physiological pH. The repertoire of naturally derived Cell-penetrating peptides (CPPs) such as Tat-peptide, penetratin, and pAntp was later augmented by synthetic homopolymers of cationic α-amino acids.

It was demonstrated that the guanidine headgroup of arginine (R) in polyarginine peptides was the critical component for their efficiency. The arginines separated by ω-amino acids (-X-) with variable chain lengths as in the (R-X-R) peptide motif were shown to be far better than the only natural α-amino acid-containing peptides, probably due to their amphipathic nature. The arginine peptides interspersed with ε-aminohexanoic acid (Ahx) and γ-aminopropionic acid (Apr) were found to be among the most effective synthetic CPPs for highly efficient cargo transportation. The mechanism of uptake of CPPs is still under debate, and it is postulated that it could be operating in multiple modes. The (R-X-R)-type of peptides were found to be comparatively more stable to peptidase than the natural α- amino acid-containing peptides. The peptide linkages at arginine sites were still amenable to cleavage for the (R-X-R)$_4$ peptides and caused toxicity. Peptidomimetics such as oligocarbonates, oligocarbamates, peptoids, oligoureas, α-aminoxy based amino acid containing peptides, etc. transporters have been explored with an aim to increase the stability of the oligomers *in vivo*. In addition to CPOs; dendrimers, liposomes, etc. are also been reported to deliver variety of cargo molecules across the cell membrane. Different strategies such as covalent conjugation or charge complexation to attach cargo molecules to carriers are studied. Many of these analogues were found to have enhanced uptake properties with good biocompatibility and these cargo carriers are currently been evaluating in various clinical trials. A concise review of the literature is given in chapter 1.

Chapter 2: Design and synthesis of proline/hydroxy proline-derived monomers, oligomers and their biological evaluation

It has we describe the proline hinge was responsible for the cell-penetrating ability of buforin II, a 21-amino acid-containing potent antimicrobial peptide. Later, it was showed that a 10-residue proline-rich peptide with two arginine residues was capable of delivering a non-covalently complexed protein into cells. Thus, the proline-rich peptides were found to be a potentially new class of cell-penetrating peptides for intracellular delivery of cargo.

<u>Section 2A:</u> Synthesis of *trans*-4-hydroxy-L-proline-derived orthogonally protected monomer, peptides and their cell uptake studies

In this section, our aim was to design and synthesize a *trans*-4-hydroxy-L-proline-derived-monomer, as a conformationally restricted analogue of lysine or arginine. Due to the presence of the pyrrolidinyl ring and attached flexible side-chain at the ring nitrogen atom in the designed monomer, there is scope to optimize the flexibility and conformational restriction in resulting peptides. We envisioned the synergistic contributing properties of lysine/proline and arginine/proline units in our designed monomer (Figure 1).
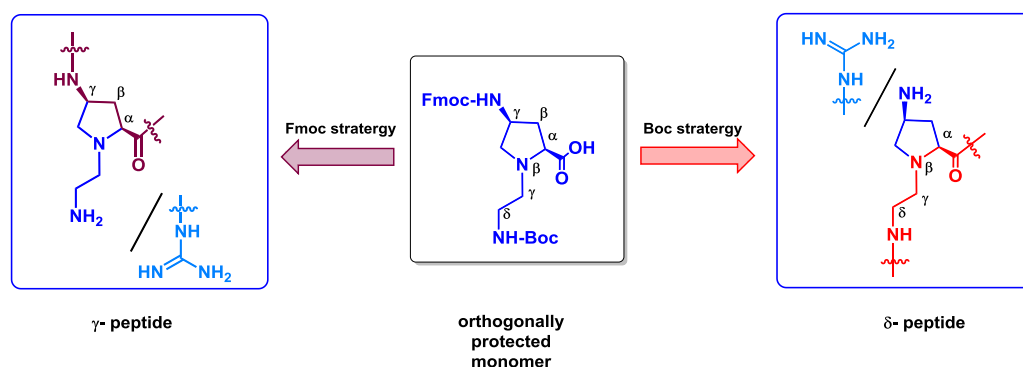
Figure 1. Schematic presentation of γ- and δ-peptides derived from single orthogonally protected monomer unit.

The strategy for synthesis of orthogonally protected monomer from *trans*-4-hydroxy-L-proline is depicted in Scheme 1.
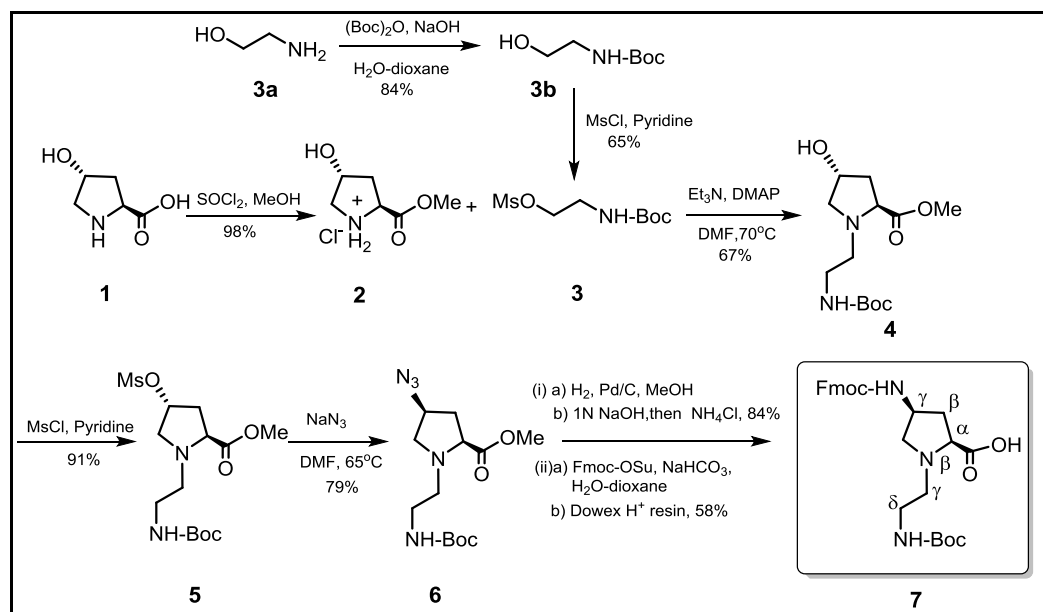
Scheme 1. Synthesis of orthogonally protected monomer.

The synthesized peptides were designed to compare the impact of amino or guanidino functionality on the cell uptake efficiency. At the same time, the effect of the position where these functionalities are attached to the pyrrolidinyl ring (on flexible side chain or directly to pyrrolidinyl ring) would also be examined. Incorporation of 6-aminohexanoic acid as a spacer moiety was planned to modulate the optimal space between adjacent amino or guanidino functionalities and to amend the amphipaticity in designed peptides.

The control heptapeptide made up of α-L-arginine was also synthesized to compare with the newly synthesized γ-peptide (by Fmoc strategy synthesis without spacer moiety), δ-peptide (by Boc strategy synthesis without spacer moiety), γ, ω-peptide (by Fmoc strategy synthesis with spacer moiety), and δ, ω-peptide (by Boc strategy synthesis with spacer moiety).

Table 1 Synthesized peptides of study and their MALDI-TOF analysis.

Code	Sequence	Mass (MALDI-TOF)	
		Calcd	Obsd
P1	cf-(aeP^{NH2})$_7$-NH$_2$	1461.7	1461.7
P2	cf-(aeP^{NH2}-Ahx)$_6$-Aaep-NH$_2$	2139.3	2140.0, 2161.8
P3	cf-(AEP^{NH2})$_7$-NH$_2$	1461.7	1481.2
P4	cf-(AEP^{NH2}-Ahx)$_6$- AEP^{NH2}-NH$_2$	2139.3	2141.5
P5	cf-(aeP^g)$_7$-NH$_2$	1755.9	1767.9, 1710.02
P6	cf-(aeP^g-Ahx)$_6$-aeP^g-NH$_2$	2433.4	2370.1, 2354.7
P7	cf-(AEP^g)$_7$-NH$_2$	1755.9	1716.4, 1561.8
P8	cf-(AEP^g-Ahx)$_6$-AEP^g-NH$_2$	2433.4	2238.7
P9	cf-(R)$_7$_control	1468.6	1468.8
P10	cf-(Arg-Ahx)$_6$-Arg-NH$_2$_Control	2147.6	2145.2

[a]cf = 5(6)-carboxyfluorescein; Ahx = 6-aminohexanoic acid; Arg = L-Arginine; aeP^{NH2} = (4-amino-(*N*-2-aminoethyl)prolyl); aeP^g = (4-guanidino-(*N*-2-aminoethyl)prolyl); AEP^{NH2} = (*N*-2-aminoethyl)-4-aminoprolyl; AEP^g = (*N*-2-guanidinoethyl)-4-aminoprolyl).

Synthesized monomer was further utilized in solid phase peptide synthesis (SPPS) by either Boc- or Fmoc- chemistry protocols to synthesize small set of peptides. The conversion of free amino groups in the synthesized peptides into guanidine groups was further attempted on solid support as well as in solution phase by using 1*H*-

Pyrazole-1-carboxamidine hydrochloride reagent, this strategy lead only in partial guanidinylated peptides.

The synthesized carboxyfluoresce (*cf*)-labeled peptides **P1-P10** were cleaved from resin, purified by HPLC, characterized by MALDI-TOF mass analysis and further evaluated for cell uptake studies by Fluorescence-activated cell sorting (FACS) analysis.
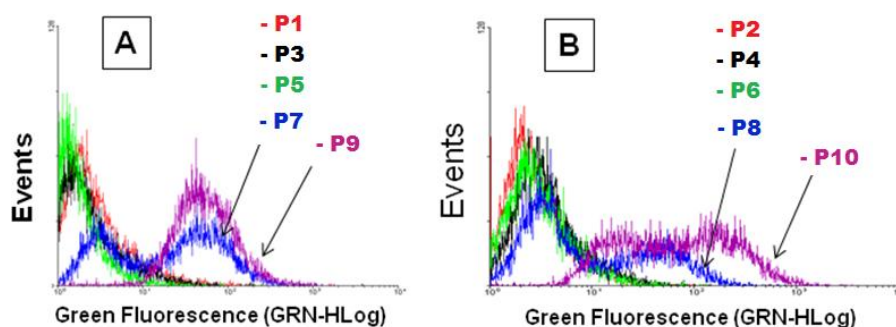
Figure 2. FACS analysis of peptides **P1-P10** in CHO cells at 37°C.

The flow cytometry analysis results are shown in Figure 2. As seen in the Figure 2; panel A, peptide **P7** (blue colour) showed comparable cellular uptake to the control peptide **P9** (purple colour) of poly-lysine/arginine-type peptides. As seen in the Figure 2; panel B, in the case of RX-type peptides peptide **P8** (blue colour) showed comparable cellular uptake to the control RX-peptide **P10** (purple colour).

Conclusion:

▪ We designed and synthesized conformationally restricted analogue of lysine/argnine amino acid from *trans*-4-hydroxy-L-proline and incorporated in (RX)-type of peptides.

▪ FACS results (Figure 2; Panel A; peptides without spacer) suggested guanidinylated peptide were superior over free amine-containing peptides. The peptides in which guanidines are attached through flexible hydrocarbon chain were found to be more active in cell uptake than when the guanidines are attached directly to the constrained pyrrolidinyl ring. Similar results (Figure 2; Panel B; peptides with spacer) were observed in case of 6-aminohexanoic acid-spaced containing peptides,

but overall addition of spacer moieties to peptides showed little improvement in the cell uptake properties.

▪ To improve cell uptake efficiency of CPPs, guanidine groups are thus, superior than amines and significant when attached through flexible linker. Spacing between adjacent amines or guanidines also has a role in cell uptake efficiency.

Section 2B: Synthesis of L/D-Proline-derived monomers, peptides and their cell uptake studies

The (R-X-R)$_4$-motif peptides, where 'R' is arginine and '-X-' is the unnatural 6-aminohexanoic acid (Ahx) or 4-aminobutanoic acid spacer moiety, are the leading cell-penetrating peptides used in many studies and these type of peptides have been evaluated in various clinical trials. However, there is still a need to increase the efficacy of these peptides. Chemical modifications could be used to achieve high therapeutic effect of attached drug molecules.

In this section, we evaluate the effects of conformational rigidity and configurational identity in designed (R-X-R)$_4$-motif peptides, where 'R' is L-arginine and '-X-' is the designed spacer amino acid. Instead of conformational restriction on arginine/lysine monomer (Section 2A) unit, the spacer chain amino acid (-X-) is now altered. The designed spacer aminoacid (-X-) bears a positively charged tertiary *N*-atom, which can counterbalance the hydrophobicity in the alkyl chain. These proline-derived spacer amino acids also exert conformational constraint in their structure. The designed spacer (-X-) units are shown in Figure 3.

aeLP   aeDP   apLP   apDP

Aminoethylprolyl   **Aminopropylprolyl**
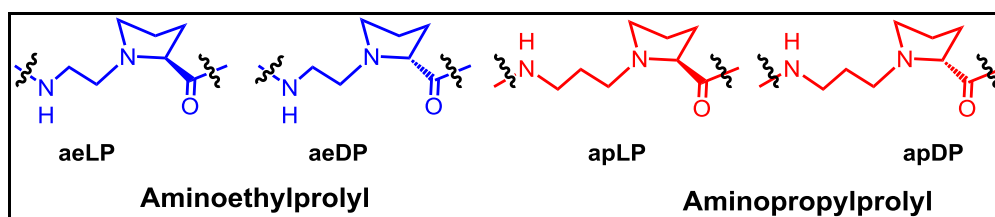
Figure 3. The designed spacer (-X-) amino acid units in (R-X-R)$_4$ peptides.

The four *N*-alkyl-prolinyl spacers (-X-) differ in the stereochemistry at C-2 position, being derived from either L-proline (LP) or D-proline (DP) and in the length of the spacer using aminoethyl (ae) or aminopropyl (ap) alkyl groups and their synthesis shown in Scheme 2.
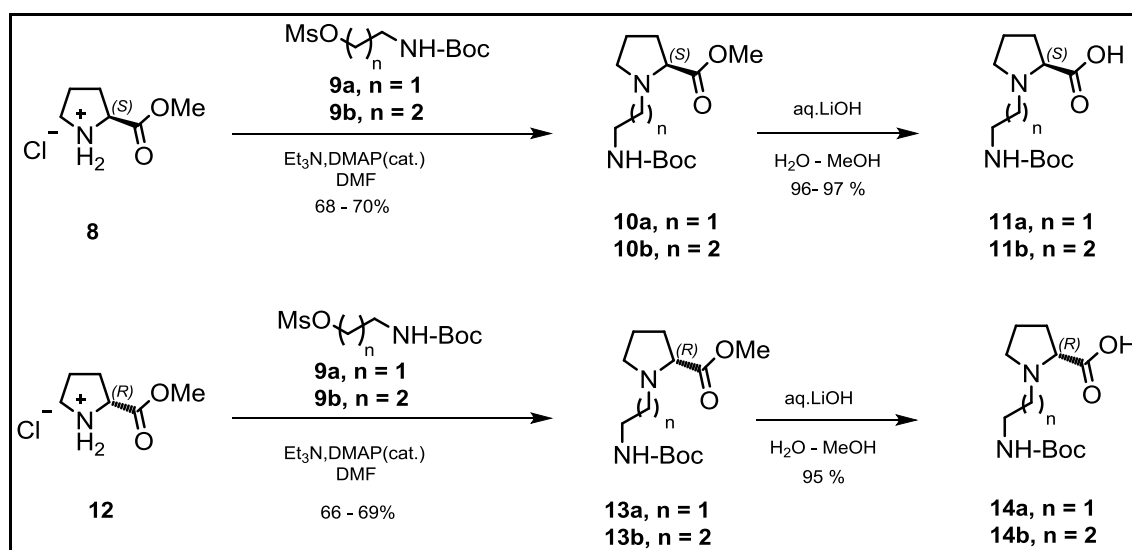
Scheme 2. Synthesis of aeLP, aeDP, apLP and apDP spacer monomers.

The synthesized spacer moieties were incorporated at appropriate positions in the desired *cf*-labeled and non-fluorescence *N*-terminal acetate, $(R-X-R)_4$-type peptide sequences on solid support (MBHA resin). After cleavage from resin these peptides were purified by HPLC and characterized them by MALDI-TOF analysis (Table 2).

Table 1. Synthesized peptides of the study.[a]

Code	Sequences	Mass (MALDI-TOF)	
		Calcd	Obsd
[cf]**P11**	*cf*-(R-aeLP-R)$_4$-NH$_2$	2184.26	2185.02
[cf]**P12**	*cf*-(R-aeDP-R)$_4$-NH$_2$	2184.26	2184.79
[cf]**P13**	*cf*-(R-apLP-R)$_4$ -NH$_2$	2240.32	2241.69
[cf]**P14**	*cf*-(R-apDP-R)$_4$ -NH$_2$	2240.32	2241.60
[cf]**P15**	*cf*-(R-Ahx-R)$_4$ -NH$_2$ control	2077.48	2078.07
[Ac]**P12**	Ac-Phe-(R-aeDP-R)$_4$ -NH$_2$	2016.50	2020.86
[Ac]**P14**	Ac-Phe-(R-apDP-R)$_4$ -NH$_2$	2072.61	2076.71
[Ac]**P15**	Ac-Phe-(R-Ahx-R)$_4$ -NH$_2$ control	1907.25	1907.33

[a] *cf* denotes carboxyfluorescein and *Ac* denotes *N*-terminal acetate.

The *cf*-labeled peptides initially studied by Circular Dichroism (CD) analysis in water as well as in TFE (trifluoroethanol) solvents. In water, all four CPPs showed approximately similar CD spectra (Figure 4; panel A). In TFE, also only slight changes were observed in CD signature of all peptide studied. Thus, the differing chirality of the

spacer and conformational restrictions due to ring structures seem to have a very less effect on the CPP secondary structure at concentration studied in both the solvents.
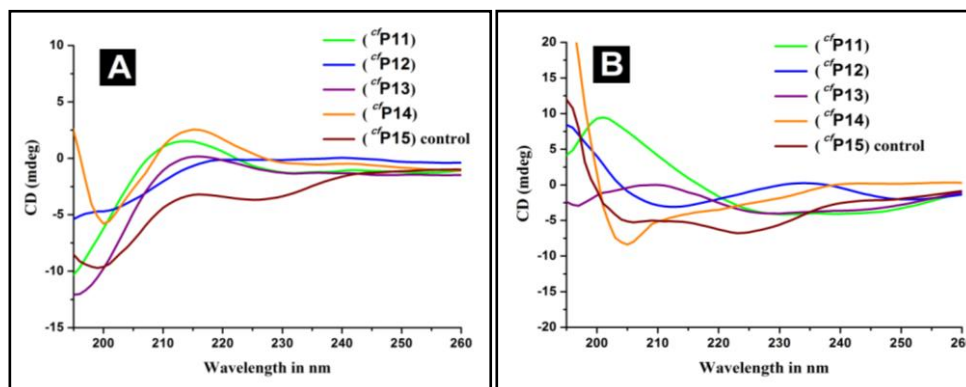
Figure 4. CD spectras of peptides ^{cf}**P11-**^{cf}**15** in water (Panel A) and TFE (Panel B) at 10 μM peptide concentration.

Quantitative cell uptake studies of CPPs ^{cf}**P11-**^{cf}**P15** were carried out by FACS analysis in CHO-K1 cells at 37°C as well as 4°C.
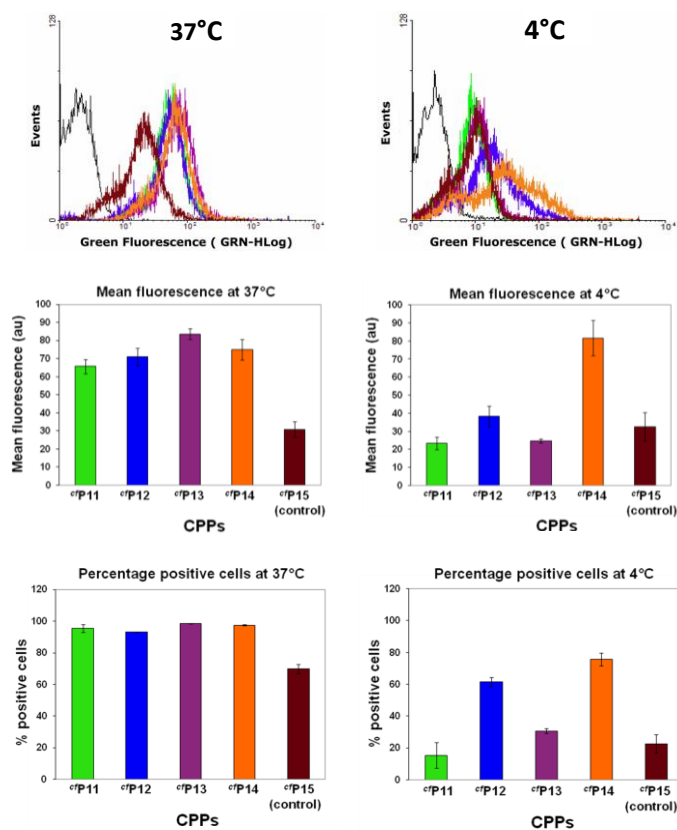
Figure 5. FACS analysis of peptides ^{cf}**P11-**^{cf}**15** in CHO-K1 cells at 37°C and 4°C, at 10 μM concentration and after 4h incubation time.

Studies carried at 37°C, the peptides ^{cf}**P11**-^{cf}**P14** showed enhanced uptake with high mean fluorescence in almost all cells compared to control peptide ^{cf}**P15.** FACS analysis at 4°C, resultant in hampering cellular uptake for all the synthesized peptides including the control (R-Ahx-R)$_4$. However, the peptides with D-stereochemistry of the proline (^{cf}**P12** and ^{cf}**P14**) retained their ability to enter cells at least in part, even at lower temperature. These results thus draw attention to the importance of different parameters that optimize the CPPs for better Cell-Penetrating properties (Figure 5).

Further, in order to determine the intracellular localization of the CPPs, confocal microscopic analysis was carried out at 37°C by incubating labeled CPPs (^{cf}**P11**-^{cf}**P15**) for 4h with CHO-K1 cells. All the newly synthesized CPPs showed cytoplasmic entry and preferentially accumulated near the nuclear membrane.

The efficiency of selected CPPs at cargo delivery in CHO-K1, HaCaT and WM melanoma cells was tested using pMIR-Report Luciferase plasmid DNA (pDNA) as the cargo. For this study the two unlabeled CPPs containing *N*-alkyl-D-proline spacers (peptide ^{Ac}**P12** and ^{Ac}**P14**) were chosen, since these were shown to have superior cell-penetration properties by the FACS analysis. As seen in Figure 6, both these CPPs were able to transport the plasmid into CHO-K1 and WM melanoma cells better than the control peptide (^{Ac}**P15**). However, this increase in transfection efficiency was not observed in HaCaT cells.
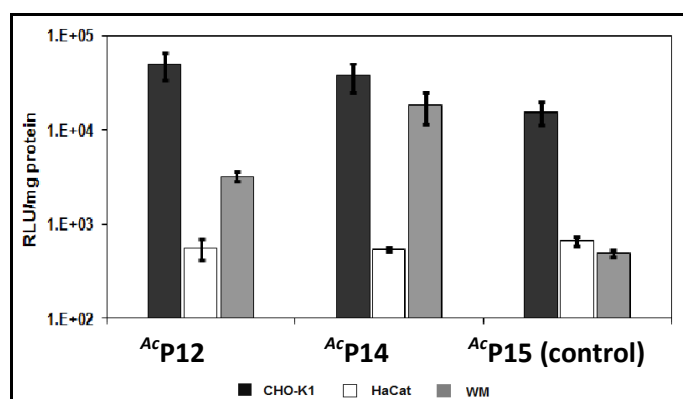
Figure 6. Transfection of pMIR-Report luciferase in CHO-K1 cells with peptides ^{Ac}**P12**, ^{Ac}**P14** and ^{Ac}**P15**.

The cytotoxicity of the synthesized CPPs was estimated in CHO-K1 and HeLa cells. All the synthesized CPPs ^{cf}**P12**-^{cf}**14** except *cf*-(R-aeLP-R)$_4$-NH$_2$ (^{cf}**P11**) were found to be almost non-toxic to both cell types studied. The polyplexes of peptides

^{Ac}**P12,** ^{Ac}**P14** and ^{Ac}**P15** were found to be relatively non-toxic in comparison to lipofectamine, which displayed a marked decrease in cell viability after 24h.

Conclusion:

▪ We designed and synthesized novel conformationally restricted spacer amino acids from L- and D-proline and incorporated them in polyarginine peptides.

▪ Structure of these peptides were studied by CD analysis and found constrained spacer moiety in (R-X-R)$_4$-type of peptides did not revealed significant change in peptide structure at concentration and in solvent studied.

▪ FACS studied in CHO-K1 cell for *cf*-labeled peptides showed enhance cell uptake efficiency over control peptide and confocal studied revealed, accumulation in cytosol.

▪ Efficient pDNA transfection was observed when pDNA was complexed with synthesized ^{Ac}**P12,** ^{Ac}**P14** peptides, also these complexes were found to be relatively non-toxic to cells.

Chapter 3: Design and synthesis of (R-X-R)-type oligocarbamate transporters for cellular delivery *via*: Non-covalent complexation and covalent conjugation strategies

(R-X-R)-types of peptides are shown to be the leading CPPs for cargo delivery. We designed and synthesized the oligocarbamate analogues (r-x-r)$_4$ of these CPPs. We envisioned the carbamate linkages would make the oligomers more flexible and the increased spacing between two guanidine units would lead oligomers with overall optimum amphipaticity to advance them in cell uptake and cargo delivery property.
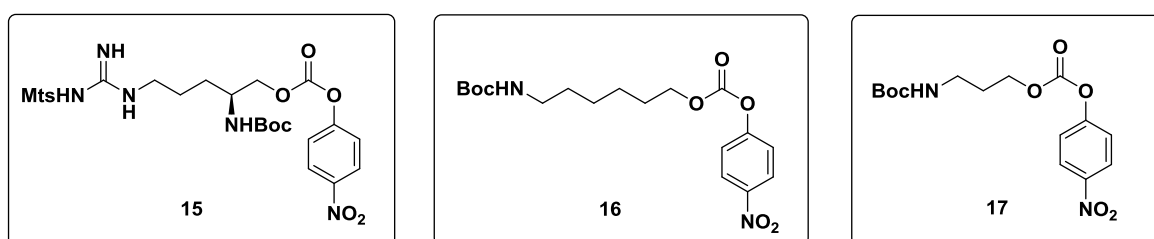
Figure 7. Synthesized monomer units for solid phase oligocarbamate synthesis.

For synthesis of (r-x-r)$_4$-type oligocarbamates initially, we synthesized *para*-nitrophenyl activated carbonate monomers (Figure 7) and used them in solid phase oligocarbamate synthesis (Table 2). The representative structure of synthesized oligocarbamate in comparison with synthesized control peptide is shown in Figure 8.

Newly synthesized (r-x-r)-type oligocarbamate

Literature reported (R-X-R)-type peptide
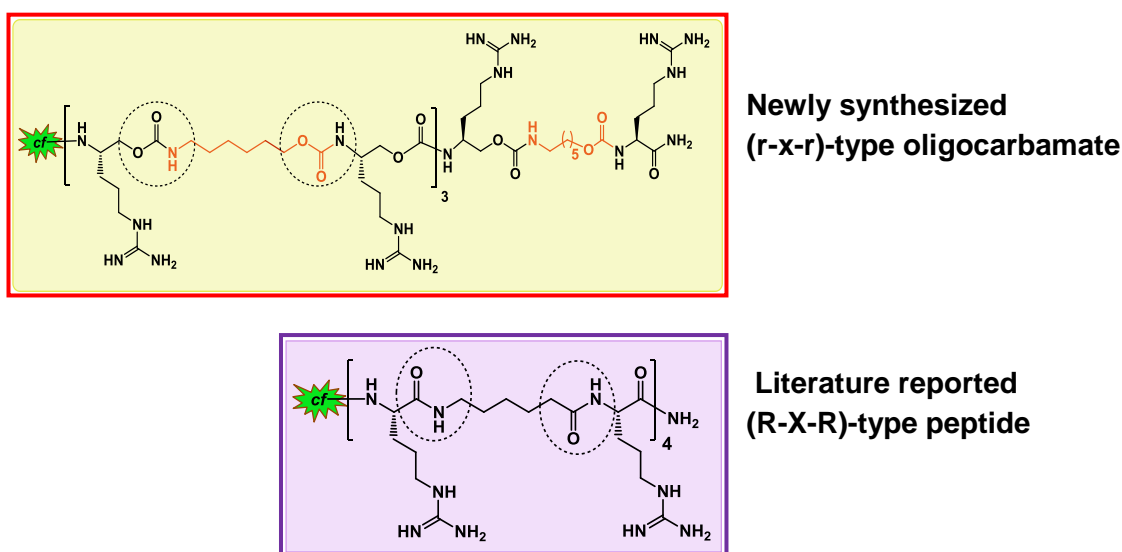
Figure 8. Structural comparison of $(R-X-R)_4$ peptide and synthesized $(r-x-r)_4$ oligocarbamate

According to design expectations, the synthesized oligocarbamtes were found to be more flexible than the corresponding peptide counterpart, revealed by Circular Dichroism studies. We tested synthesized oligomers in octanol-water partioning experiments and these oligomers were found amphiphatic in nature.

Table 2. Synthesized peptides of the study[a]

Code	Sequence	Mass (MALDI-TOF)	
		Calcd.	**Obsd.**
^{cf}**P15**	cf-(R-Ahx-R)$_4$ -NH$_2$ control	2077.48	2078.07
^{cf}**C1**	cf-(r-ahx-r)$_4$-NH$_2$	2406.33	2408.40
^{cf}**C2**	cf-(r-ahx-r-r-apr-r)$_2$ -NH$_2$	2322.24	2324.81
^{cf}**C3**	cf-(r)$_8$ –NH$_2$ control	1833.95	1834.49
^{Ac}**P15**	Ac-Phe-(R-Ahx-R)$_4$ -NH$_2$ control	1907.25	1907.33
^{Ac}**C1**	Ac-Phe-(r-ahx-r)$_4$ -NH$_2$	2237.36	2238.33
^{Ac}**C3**	Ac-Phe-(r)$_8$ -NH$_2$ control	1664.98	1666.71

[a] *cf* denotes carboxyfluorescein and *Ac* denotes *N*-terminal acetate

FACS analysis in CHO-K1 (Figure 9) and HeLa cells at 37°C and 4°C revealed that newly synthesized oligocarbamate showed temperature-independent and increased cellular uptake over control peptide. Confocal microscopic analysis in CHO-K1 (Figure 8), HeLa cells revealed that high cytosolic and fare nuclear distribution for oligocarbamate in comparison to peptide or oligoamide counterpart (Figure 8).
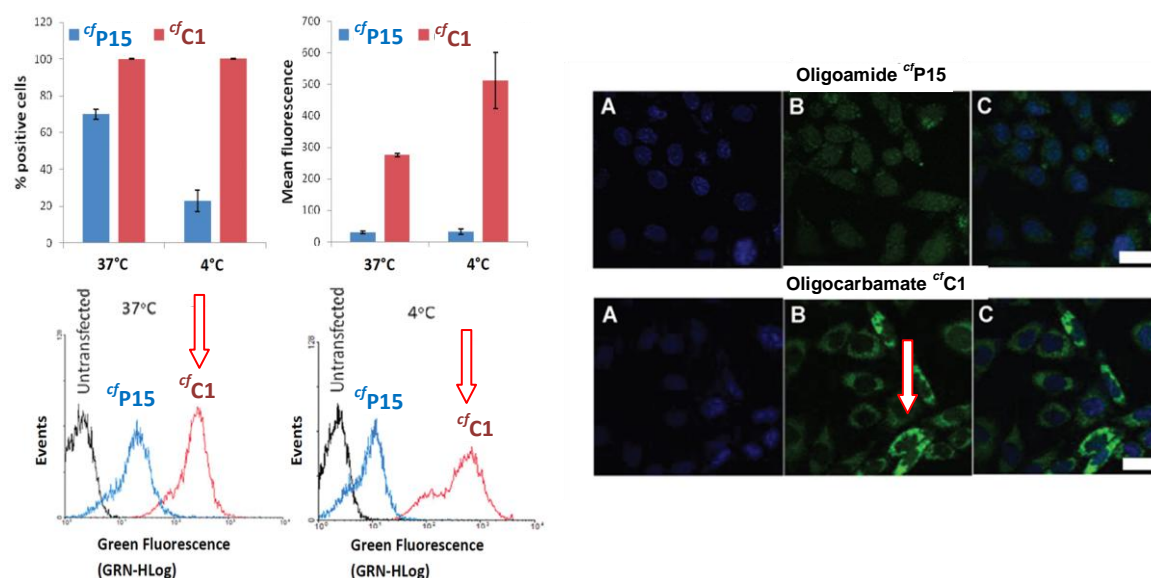
Figure 9. FACS (at 37 and 4°C) and confocal analysis in CHO-K1 cells (at 37°C) of oligomer ^{cf}**P15** and ^{cf}**C1**.

Further, to get inside in cell uptake mechanism for these newly synthesized oligocarbamates, confocal microscopic analysis of the oligocarbamate ^{cf}**C1** was carried after incubation of CHO-K1 cells in the presence of ^{cf}**C1** at lower temperature (4°C) as well as the cell uptake experiment in the presence of sodium azide (inhibitor for energy-dependent cell entry). The microscopic images revealed no remarkable difference observed in cellular uptake efficiency for this oligocarbamate even after incubation at low temperature or presence of sodium azide. These results suggested energy-independent or non-endocytosis cell uptake mechanism could work for this oligocarbamate, which is advantageous in drug delivery applications.

To verify the applicability of synthesized oligocarbamates, we tested transportation various cargoes such as labeled, siRNA, and pDNA (Figure 10A) *via* noncovalent complexation strategy with oligocarbamates and also the synthesized *cf*-labeled anti-tumor tripeptide (Figure 10B) *via* covalent conjugation *in vitro*.

The FACS analysis shown in Figure 10 clearly indicates the high efficiency of synthesized oligocarbamate over control oligoamide in transportation of cargo molecules *via* complexation strategy (pDNA transfection; Figure 10A) as well as covalent conjugation (*cf*-Tyroserleutide; Figure 10B). The cytotoxicity experiment revealed that the synthesized oligomers were relatively non-toxic to cells.
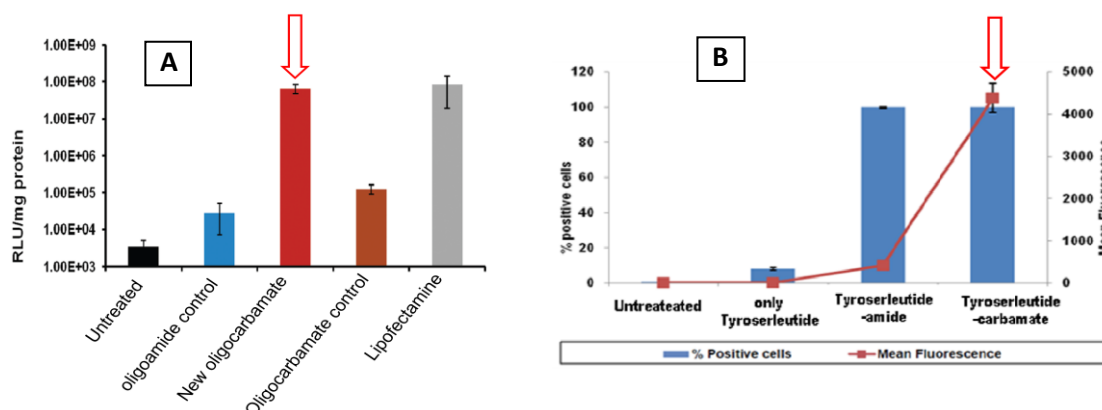
Figure 10. Transfection of pMIR-Report luciferase **[A]** and Tyroserleutide delivery studies **[B]** to CHO-K1 cells.

Antisense phosphorodiamidate morpholino oligonucleotides (PMO) was also conjugate covalently to synthesized oligocarbamate and studied their efficiency *in vito* as well as *in vivo*.

Daunomycin a potent anticancer drug also been attached covalently to synthesized oligocarbamate and their further evaluation is in progress.

Conclusion:

- CD analysis and octanol-water partitionic experiments revealed that synthesized oligocarbamates are less structured and amphiphathic in nature respectively than oligoamide or peptide control.

- FACS and confocal analysis suggested their high efficiency over control oligoamide in cell uptake studied at different incubation conditions.

- Newly synthesized oligocarbamates showed high efficiency than oligoamide counterpart in transportation of cargoes such as labelled, siRNA, and pDNA *via* noncovalent complexation strategy and synthesized anti-tumor tripeptide *via* covalent conjugation *in vitro*, with low cytotoxicity.

- Delivery and application of covalently attached antisense PMO to oligocarbamate was also studied *in vitro* and *in vivo*. Also the covalent attachment of anticancer drug daunomycin to synthesized oligocarbamate was shown.

Chapter 4: Design and synthesis of novel oligocarbamates and monomer synthesis for dendron and dendrimers

Section 4A: Synthesis of tartaric acid-derived novel di-guanidine carbonate monomer and its incorporation in oligocarbamate

In this section we describe the synthesis of a novel carbonate monomer containing two amino groups which can further be converted to guanidine functionality and substituted in consecutive 'r-r' groups in (r-x-r)$_n$-type oligocarbamates such as 'x-r-r-x-r-r-x-r-r-x-r-r-x' (Scheme 4). The synthesis of monomer unit was accomplished from L-(+)-tartaric acid and synthetic strategy was shown in Scheme 3.
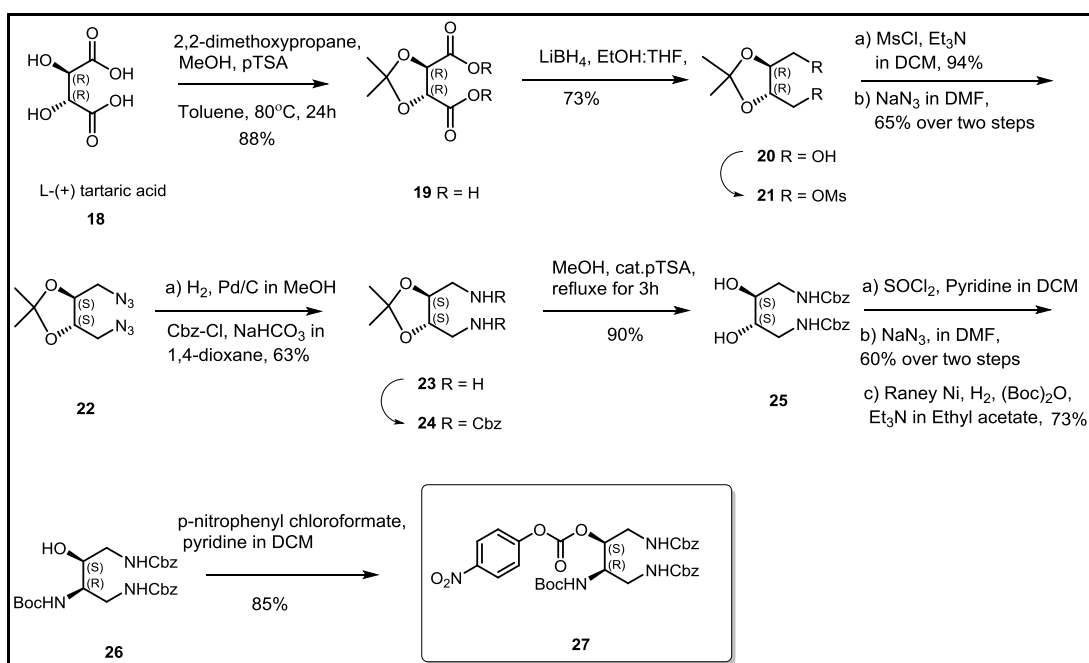
Scheme 3. Synthesis of *p*-nitrophenyl activated carbonate monomer from tartaric acid.

Synthesized oligomer was further incorporated in solid phase oligocarbamate synthesis and synthesized (r-x-r)$_4$-type oligomers where '-x-' is aminopropanol unit. Free amines in synthesized oligocarbamate ^{Ac}C4$_{NH2}$ was further converted to guanidines by solution phase guanidinylation method (Scheme 4) and synthesized guanidinylated oligocarbamate ^{Ac}C4$_{gua}$.
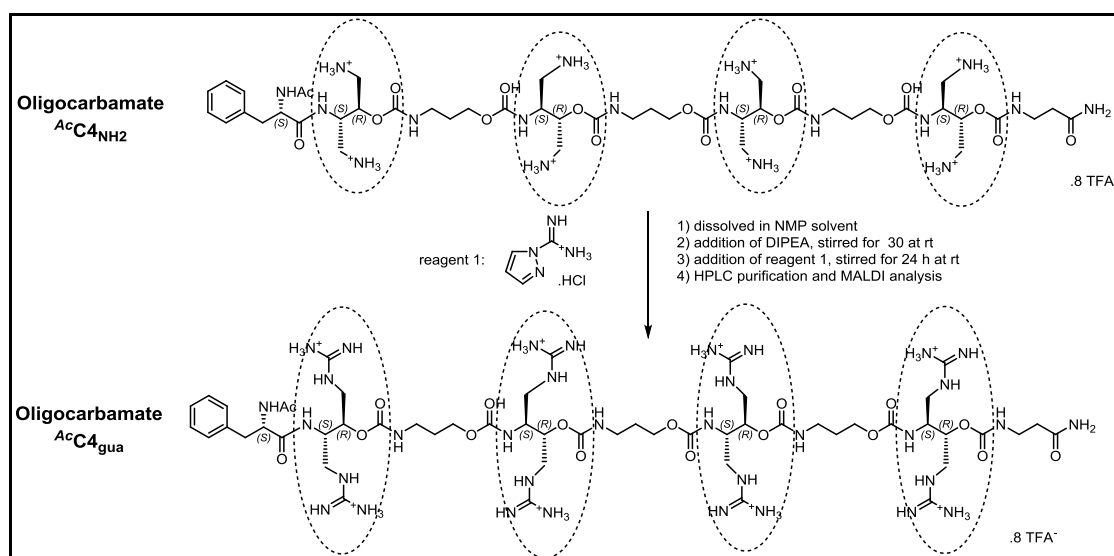
Scheme 4. Schematic presentation of free amines in oligomer into guanidines.

Further biological applications to deliver negatively charged cargoes such as siRNA, pDNA to cells *via* non-covalent conjugation strategy using synthesized oligocarbamates are underway.

Conclusion:

- Design and synthesis of novel *p*-nitrophenyl activated carbonate monomer was accomplished by appropriate functional group transformation, starting from inexpensively available L (+) tartaric acid.

- Synthesized monomeric unit was incorporated on solid support and desired oligocarbamate was synthesized using Boc-chemistry protocol.

- Eight free amines in synthesized oligocarbamate were successfully guanidinylated in solution phase.

- Synthesized oligocarbamates were purified by HPLC and characterized by MALDI-TOF mass analysis and their biological evaluation for cargo delivery applications are in progress.

Section 4B: Synthesis of *trans*-4-hydroxy-L-proline-derived monomer for incorporation in carbamate linked dendron and dendrimer

In addition to structural diversity of cell-penetrating peptides, cell-penetrating dendrimers are one of the important cell delivery vectors that have been studied in the literature. Here, we have designed and synthesized *p*-nitrophenyl activated monomer which will be suitable for synthesis of variety of dendrons, dendrimers, (r-x-r)-type dendrimers, etc. which will contain polycarbamate linkages by solid phase or solution phase synthesis method. Our strategy for synthesis of *p*-nitrophenyl activated carbonate monomer is depicted in Scheme 5.
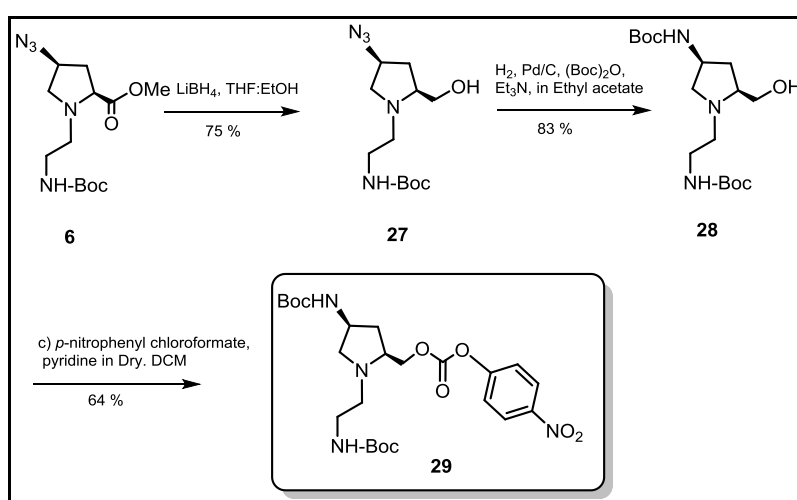
Scheme 5. Synthesis of *p*-Nitrophenyl activated carbonate monomer.

Conclusion:

- We designed and synthesized a novel monomeric unit from easily accessible *trans*-4-hydroxy-L-proline as a starting material.

- Synthesized *para*-nitrophenyl activated monomer a building block can further use to build various dendrons and dendrimers.

- Hydrophobic interior and surface pendant group anchoring is envisioned in planned dendrons and dendrimers, and those can further explored in drug delivery applications.

- --------------------

CHAPTER 1

Introduction: Cell-penetrating Oligomers for Drug Delivery
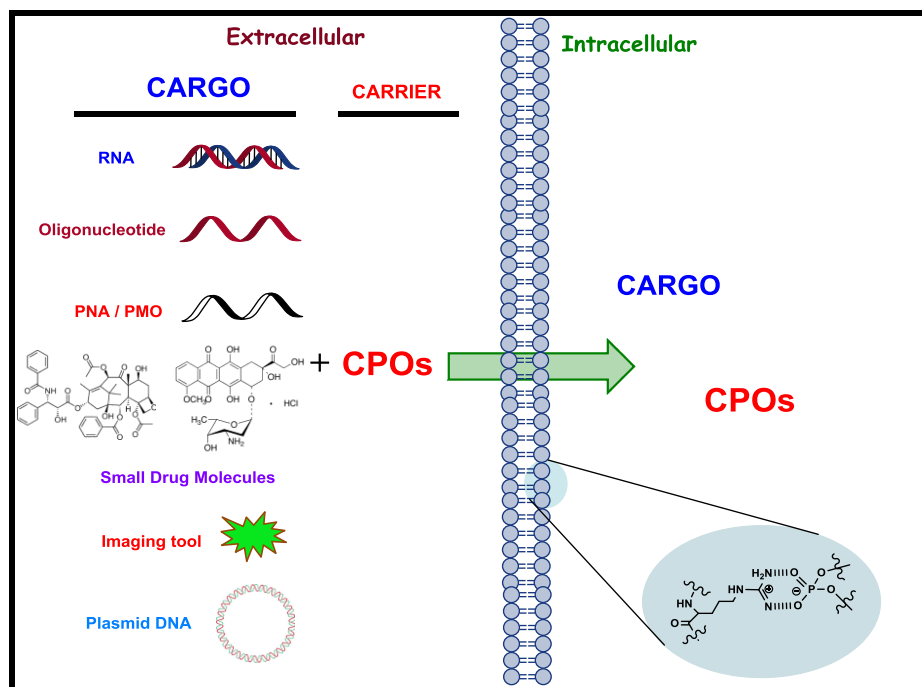
Cell-Penetrating Oligomers (CPOs) are useful tools to deliver variety of cell impermeable bioactive cargoes across the cell membrane. Structural study and chemical modifications in naturally occurring CPOs could enhance the efficacy of these oligomers. Numerous type of CPOs have been reported such as Cell-Penetrating Peptides (CPPs), oligocarbamates, oligocarbonates, etc. Cell uptake mechanism of these oligomers is not understood completely, but it is known that it may vary and depend on their structural backbone, amphipathicity, associated cargo, etc. Various strategies have been demonstrated in literature to attach cargo molecules to CPOs and their release inside the cell from the associated CPO. Along with CPOs, liposomes and dendrimers have also been studied for drug delivery applications. Many of these CPOs were found to have enhanced uptake properties with good biocompatibility. These cargo carriers are currently being evaluated in various clinical trials. A concise review of the literature is discussed in this chapter.

1.1 Introduction

Despite numerous successes in identification and capacity to tackle therapeutic targets inside cells, therapeutic drug molecules fail to be effective because of their insufficient and/or non-specific cellular uptake. The hydrophobic plasma membrane of the cells is an indispensable barrier which allows trafficking of essential molecules while preventing access to extracellular unnatural drugs or macromolecules. This highly selective barrier of the cell membranes does not easily allow the entry of essential therapeutic drug molecules inside cells. Thus in the treatment of diseases, breaching the membrane barrier is sometimes necessary but a difficult task, particularly in the absence of active transport.[1]

Many promising drug candidates do not advance clinically because they are unable to confirm the necessary physical properties such as water solubility, lipophilicity and amphipathicity, which allow them to cross the cell membrane. They are either too non-polar (water insoluble) for administration and distribution or too polar for passive cellular entry. These drug molecules can be natural or synthetic, such as peptides, oligonucleotides, small molecules, nanoparticles, etc. To overcome this bottleneck, a smart drug delivery agent[2] is required, which will have good pharmacokinetic properties and effectiveness to transport associate cargoes to intracellular targeted sites.[3] Currently, drug delivery is not only important in the treatment of diseases but also becoming important in prevention and diagnosis of diseases. In recent years, efficient drug delivery to the specific sites are preferred because it influences the vital sites and hence are useful to avoid any undesirable side effects or repetitive high doses of the drug. Nanocarriers with optimized physicochemical (such as size and amphipathicity with surface functional groups) and biological (such as enzymatic stability) properties are taken up by cells more easily and can be used as successful drug delivery agents. Surface PEGylation to decorate some of these nano-drug carriers has also been studied widely to improve the blood circulation time,[4] which could also enhance accumulation of drug near to targeted tumor site and hence passively transport drug to the targeted tumor cells.[5,6]

In this chapter we would briefly discuss different strategies to develop agents, with particular emphasis on cell-penetrating oligomers, capable of acting as vehicles for

intracellular delivery of pharmacologically important small/large molecules.

1.2 Cell-Penetrating Oligomers (CPOs)

Numerous literature reports show application of different Cell-Penetrating Oligomers (CPOs) for drug/oligonucleotide delivery. To improve therapeutic efficiency of a variety of drug molecules particularly oligonucleotide (ON) based drugs, CPOs have been studied and are proved to be useful for cellular tissues or organelle delivery. Most importantly, in majority of the cases, they were found to be with no or negligible toxicity. Various types of CPOs such as natural and synthetic peptides, oligocarbamates, oligocarbonates, oligoureas, collagen-like peptides, etc. are reported in the literature (Figure 1.1) for ONs and other drug delivery applications, some of which are discussed herein.
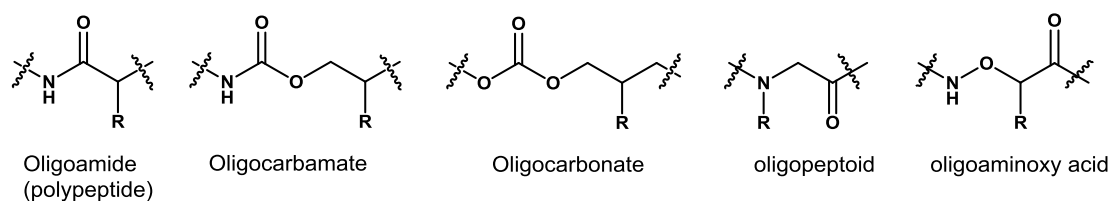
Figure 1.1 Structures of backbones used to synthesize a variety of CPOs.

1.2.1 Cell-Penetrating Peptides (CPPs)

Delivery of cell impermeable drugs across the cell membrane using Cell-Penetrating Peptides (CPPs) is one of most promising strategies of drug delivery; and so far, it has been proved very successful in diverse drug delivery applications. CPPs are capable of translocation into the cell by themselves or together with associated cell impermeable cargo. CPPs have been evaluated for the ability to transport cargoes into cells, tissues, and organs[7]. CPPs are the special class of short peptides usually 5-30 residues long. CPPs typically have a composition that either contains a relatively high abundance of positively charged (at physiological pH) amino acids such as lysine and/or arginine or they have sequences that contain an alternating pattern of polar/charged amino acids and non-polar, hydrophobic amino acids. These two types of CPPs are referred as polycationic or amphipathic peptides respectively. Initially naturally occurring 'tat' peptide was modified to polyarginines and further several different scaffolds were

synthesized and tested them for cell penetration and drug delivery applications (Figure 1.2). In contrast with other classes of peptides (such as fusogenic peptides of viral origin and antimicrobial peptides which are also capable of crossing cellular membranes), the CPP internalization is highly efficient and harmless to the cells, avoiding membrane destabilization and loss of cellular integrity.
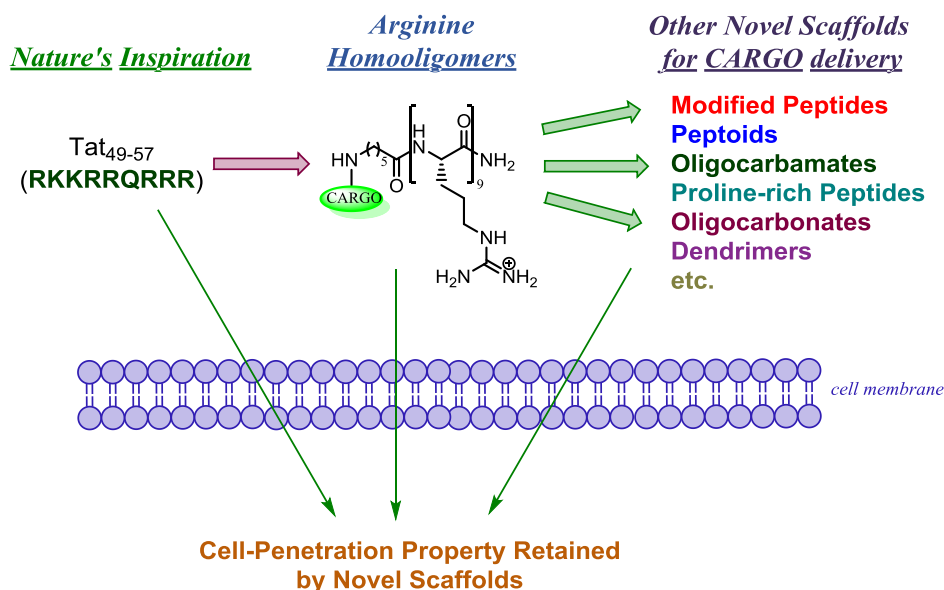
Figure 1.2 Discovery and progress of arginine rich CPPs and other scaffolds.

CPPs are also applied in delivery of therapeutic Oligonucleotides (ONs) and are currently being evaluated in human clinical trials. ONs display great therapeutic potential due to their ability to interfere with gene expression. Several classes of ONs have emerged either based on double stranded RNAs, such as short interfering RNAs that confer gene silencing activity or single stranded ONs of various chemistries for antisense targeting of small regulatory micro RNAs or mRNAs. In particular, the use of splice switching oligonucleotides (SSOs) to manipulate alternative splicing, by targeting pre-mRNA, has proven to be a highly promising therapeutic strategy to treat various genetic disorders, including Duchenne Muscular Dystrophy (DMD) and Spinal Muscular Atrophy (SMA).[8] Although efficient to alter splicing patterns, the hydrophilic macromolecular nature of ONs prohibits efficient cellular internalization. Various chemical oligonucleotides (ON) delivery vehicles have been developed aiming at improving the bioavailability of nucleic acid-based drugs. In the context of SSOs, CPPs

display extremely high potency to transport these drugs across the cell and nuclear membrane in a relatively non-toxic fashion.[9] Several guanidine rich analogues[10] for drug delivery application have been synthesized, studied and the promising results obtained in a number of studies indicate that CPPs/CPOs have an important role in the development of novel therapeutics.

1.2.1.1 Classification of CPPs

1.2.1.1a Classification of CPPs based on their source of derived

CPPs can be classified into following three categories based on their source form which they derived.[11] Some of them are listed in Table 1.1.

I) <u>Protein-derived peptides or protein transduction domain:</u>
Many of the viral as well as non-viral naturally occurring proteins have been identified to penetrate biological cell membrane. After systematic dissection of these naturally derived long proteins, their functional domains have been identified, which are comparatively short in length. Further these peptide sequences were used as a drug delivery tool. e.g. tat, penetratin, chimeric peptides.[12,13] The first CPP was derived in 1988 from naturally occurring viral protein named 'tat', produced by HIV-1 type of virus.[14,15] Further the 86 amino acid long peptide revealed that the amino acid region between 48-60 (rich in basic amino acids) was responsible to cross the cell membrane. The term 'tat' has been used for the entire 86 amino acid sequence as well as for different regions of this peptide, and also with different ways of representation, e.g. tat (49-57) RKKRRQRRR,[16] or tat (48-61),[17] or 'Tat', etc.

In 1994, Derossi *et al.*[18] showed that the third helix of the Antennapedia homeodomain (pAntp) could translocate through biological membranes. Later, several natural or synthetically modified proteins and peptides have shown the capability of internalization into mammalian, plant and bacterial cells to mediate the transport of a variety of biologically active molecules and cargoes.[11a,19] Several preclinical and clinical evaluations have been conducted and are currently in progress. Despite many successes, none of the CPP or CPP-conjugates have obtained the FDA approval or reached the clinic.[11a]

Table 1.1 Representative CPPs listed according to their source of which derived[a].

CPP Name or code	Sequence	Source
tat (48-60)	GRKKRRQRRRQC	Protein-derived
Penetratin	RQIKIWFQNRRMKWKK-NH$_2$	Protein-derived
pVEC	LLIILRRRIRKQAHAHSK-NH$_2$	Protein-derived
SynB1	RGGRLSYSRRRFSTSTGR	Protein-derived
SynB3	RRLSYSRRRF	Protein-derived
Maurocalcine	GDCLPHLKLCKENKDCCSKKCKRRGTNIEKR CR	Protein-derived
PTD4	YARAAARQARA	Protein-derived
MPG8	AFLGWLGAWGTMGWSPKKKRK-cya	Chimeric
Transportan	GWTLNSAGYLLGKINLKALAALAKKIL-NH$_2$	Chimeric
Transportan10	AGYLLGKINLKALAALAKKIL-NH$_2$	Chimeric, modified
PepFect3	Stearyl-AGYLLGKINLKALAALAKKIL-NH$_2$	Chimeric, modified
PepFect 6	Stearyl-AGYLLGK(ε-NH$_2$)INLKALAALAKKIL-NH$_2$	Chimeric, modified
PepFect 14	Stearyl-AGYLLGKLLOOLAAAALOOLL-NH$_2$	Chimeric, modified
Polyarginine/ Sterylarginine	R$_n$ where n = 6–12	Designed
RXR-type/ Stearyl RXR-type	(RXR)$_n$ where n= 2-4, X = Aminocaproic acid, β-alanine, etc.	Designed
Pep-1	Ac-KETWWETWWTEWSQPKKKRKV-cya	Designed
Pep-3	KWFETWFTEWPKKRK-cya	Designed
CADY	Ac-GLWRALWRLLRSLWRLLWRA-cya	Designed
YTA2	YTAIAWVKAFIRKLRK-NH$_2$	Designed
YTA4	IAWVKAFIRKLRKGPLG-NH$_2$	Designed

[a] cys is cysteamide

II) <u>Chimeric peptides:</u>

Several CPPs are chimeric peptides, which are obtained by covalent attachment of hydrophobic peptide domain to the Nuclear Localization Sequences (NLS) for targeted cellular delivery of cargo molecules. These peptides which may contain two or more motifs from the other peptides like transportan which is derived from mastoparan and galanin and its short analogue TP10. For example, MPG (GLAFLGFLGAAGSTMGAWSQPKKKRKV) and Pep-1 (KETWWETWWTEWSQPKKKRKV) both peptides are based on the SV40 Nuclear Localization Sequence peptide PKKRKV. The hydrophobic domain of MPG was derived from the fusion sequence of the HIV glycoprotein 41 (GALFLGFLGAAGSTMGA), while that of Pep-1 corresponds to a tryptophan-rich cluster (KETWWETWWTEW), which has high affinity for membranes. Both in MPG and Pep-1, the hydrophobic domain is separated from the NLS through a linker (WSQP).[20]

IIIa) <u>Designed or Synthetic peptides:</u>

Synthetic peptides such as polyarginines, polylysines and amphipathic peptides e.g. RXR-type peptides, where R is arginine and X is a hydrophobic spacer, which are enriched in cationic amino acids have been demonstrated to be good at cell penetration. The peptides can also be designed with the help of computer simulations and theoretical calculations[21] e.g. Steered molecular dynamics simulations on the wild-type pVEC and retro-pVEC, which has the pVEC sequence in reverse order, and scramble-pVEC, which has the same amino acid composition but a scrambled sequence, were performed. This analysis gave information at an atomic level on the translocation mechanism of pVEC.[22]

IIIb) <u>Mix (α-β, α-γ, etc.) type of peptides:</u>

In the year 2000, Wender and co-workers[23] showed the cell uptake efficiency of synthesized family of arginine peptoids could be improved by increasing the length and flexibility in the side chain with increase conformational freedom.[24] Later in 2002, molecular modelling studies were carried out on one of the preferred family of arginine

peptides. Only seven out of the 10 guanidinium groups displayed directionality towards cell membrane which was opposite to the other three side chain guanidines (at the 2nd, 5th, and 8th residues). Only these seven residues from deca-arginine were interacting with cell surface and hence the other three arginine residues were replaced by other natural α-amino acids. All the synthesized peptides were internalized into cells. Two of the mixed decamers containing seven arginine residues having spacer moieties in it, entered cells more effectively than the corresponding heptaarginine control, suggesting that the spacing between the arginine residues effectively influence transport. After the synthesis of the library of heptarginine peptides containing one or more non-consecutive non-α-amino acid subunits, it was found that cellular uptake increased as more aminocaproic acid or 6-amino hexanoic acid (Ahx) residues were added, until reaching the fully substituted analogue containing six spacer amino acids, one between each of the seven arginines.

Later, many studies showed that the (R-Ahx-R)$_4$ pattern with four units (12mer peptide) showed better cellular uptake. This peptide was explored further for transportation of various cargo molecules such as steric-block ON,[25] etc. and currently analogues of this peptide are in various stages of clinical trials.[11a, 26]

1.2.1.1b Classification of CPPs based on their binding properties to the lipids

Another way of classifying CPPs is based upon different peptide sequences and their binding properties to the lipids.

I) <u>Primary amphipathic CPPs (paCPPs):</u>

This class of CPPs are typically more than 20 amino acids e.g. transportan or TP10. They have sequentially hydrophilic and hydrophobic residues along their primary sequence.[27] In addition to endocytosis, the proposed mechanism for this group of CPPs is direct membrane transduction. Model studies[28] have suggested that the direct transduction occurs *via* pore formation, carpet-like perturbations, or inverted micelles formed in the bilayer membrane.

II) <u>Secondary amphipathic CPPs (saCPPs):</u>

saCPPs such as penetratin, pVEC,[29] and M918[30] frequently contain less number of

amino acids in comparison to primary amphipathic CPPs. Their amphipathic property is revealed when they form α-helix or a beta sheet structure upon interaction with a phospholipid membrane. They typically bind to model membranes with a certain fraction of anionic lipids.[27]

III) <u>Nonamphipathic CPPs (naCPPs):</u>

This class of CPPs are moderately short with a high content of cationic amino acids (e.g. arginine) such as nona-arginine and tat (48–60). They bind to the lipid membrane with a high amount of anionic lipids. Membrane leakage was not observed at low micromolar concentrations for these class of CPPs.[27]

1.2.1.2 Proposed mechanisms for cellular uptake of CPPs

The mechanism of how CPPs enter into cells is not yet fully understood and seems ambiguous from different literature reports. It is now considered that each CPP and CPP-cargo can enter cells *via* one or simultaneously more than one mechanisms. The mechanism of cellular uptake of CPPs may vary with the attached cargo and the method of cargo attachment (either covalent or non-covalent), its amino acid residues, cells or biological model of the study and other experimental conditions. Few suggested mechanisms that implies by CPOs in delivering associated cargo to cells are shown in Figure 1.3.

Several studies suggested that the mechanisms of cell entry for majority of the CPPs could be:

       a) Energy-dependent or endocytotic penetration

       b) Energy-independent or non-endocytotic or direct penetration

       c) Receptor-mediated cell penetration

1.2.1.2a Energy-dependent or endocytotic penetration

Endocytosis is one of the major mechanisms that have been reported for CPPs. Despite several reports suggesting endocytosis as the major route of CPPs entry to various cells, there is still some ambiguity between explanations and facts.

Endocytosis can be divided into two main categories:

I) Phagocytosis: a process which occurs in specialized cells e.g. macrophages

II) Pinocytosis: a process which is active in most of the cells. Pinocytosis is the set of pathways that include macropinocytosis, clathrin-mediated endocytosis, caveolae-mediated endocytosis and other less well-characterized pathways.[31]
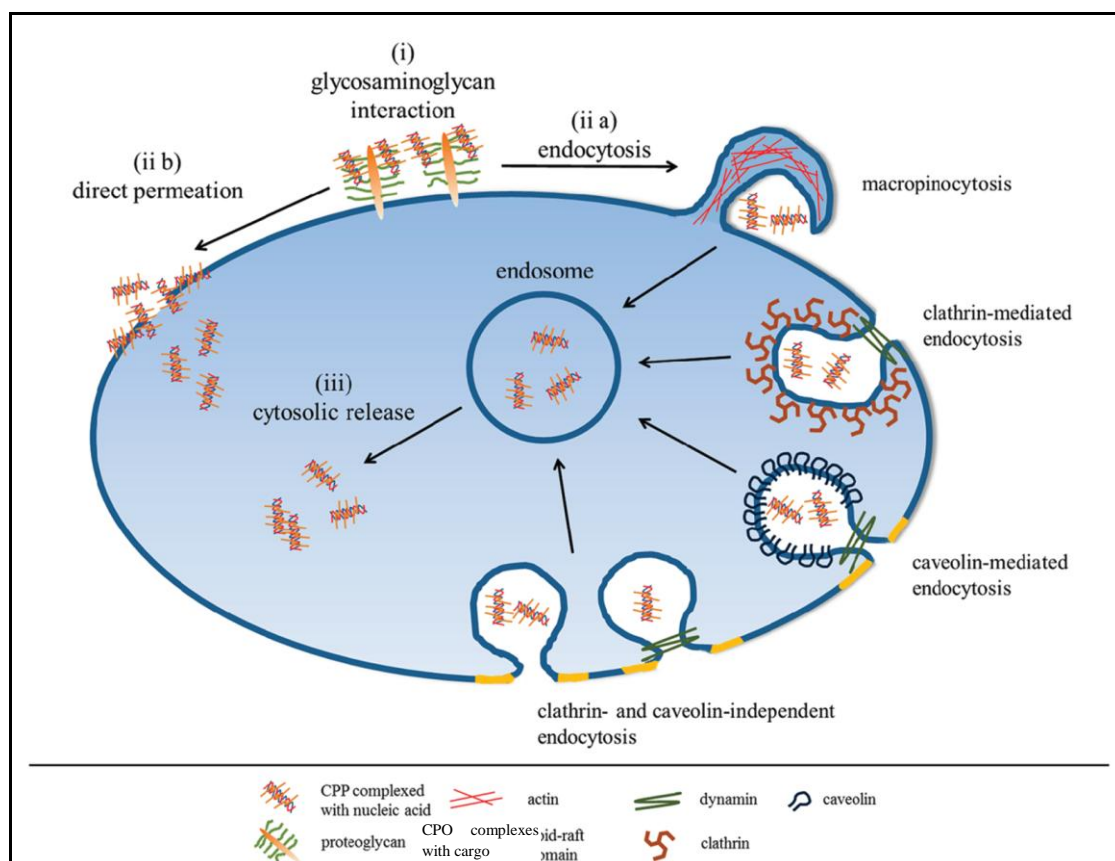
Figure 1.3 Various mechanisms of cellular uptake of CPOs complexed with cargo.[32]

There are several experimental evidences to support the above energy dependent mechanisms of CPPs translocation to biological membrane. These experiments include: (i) Cellular uptake studies carried out at low temperature (usually at 4°C) or in energy/ATP depleted condition; (ii) cell uptake studies in the presence of drug which will specifically arrest a known internalization pathway; (iii) incubation with molecular markers of known internalisation pathways (e.g., Caveolin-1, early endosome antigen-1 - EEA1) or evaluation of peptide or peptide conjugate co-localization with their specific endocytosis internalization pathways ; (iv) over expression of dominant negative mutants of proteins involved in the internalization process (e.g., Dynamin). (v) use of

endosomal release agent. By using these approaches, cell uptake mechanisms of many CPPs have been demonstrated and for 'tat' peptide, pinocytosis pathways have been suggested. However, in parallel experiments, the authors took advantage of physical methods, such as temperature decrease, to inhibit all endocytotic pathways simultaneously. In this study 'tat' was not excluded from the cells in any of the tested conditions, suggesting that tat cell uptake can also be endocytosis-independent.[33]

After revised experimental procedure which included new protocols from different literature reports, several endocytotic pathways such as caveolae mediated endocytosis,[34] macropinocytosis[35] and clathrin-mediated endocytosis,[36] found to be involved in CPPs internalization. Further, differences in cellular uptake for the same CPP in the presence and in the absence of attached cargo, suggested different mechanisms of internalization.

1.2.1.2b Energy-independent or non-endocytotic or direct penetration

Initial experimental results showed cellular uptake which was carried out at low temperature (usually at 4°C) did not significantly affect the entry of some CPPs. These results suggested the presence of energy-independent (non-endocytosis or direct penetration) mechanism in addition to the known energy dependent endocytosis as a mechanism involved in cell entry of CPPs.[18] Many physical models have been therefore proposed to show the direct penetration of CPPs. The work of Lundberg *et al.* for viral derived protein VP22 and of Richard *et al.* for tat (48-60) and nonarginine CPPs was published in year 2000. These reports suggested that flow cytometry analysis could not be used validly to evaluate cellular uptake unless a step of trypsin digestion of the cell membrane-adsorbed peptide is included in the protocol. Similarly the use of methanol or formaldehyde in cell fixation, even in mild conditions, leads to the artifactual uptake of some CPPs.[37]

Direct penetration of cell membrane by CPPs has been suggested by different models such as inverted micelle formation,[38] pore formation,[39] the carpet-like model[40] and the membrane thinning model.[41] Sara *et al.*[33] reviewed and compared most of these models and stated that even though these models have some common features, there are some significant differences which are explained herein

(i) According to the "inverted micelle model", the peptides remain associated to the membrane surface during translocation and never experience direct contact with the hydrophobic interior of the lipid bilayer, in contrast to what is described in the models that assume pore formation, where the insertion of the peptides in the membrane and the resulting transmembrane conformation are important steps of the translocation process.

(ii) Both the "toroidal pore" and the "carpet model" describe an extensive reorganization of membrane phospholipids, in contrast to the "barrel stave" model, in which the structure of the lipid bilayer would not be significantly disturbed.

(iii) The interaction of cell-penetrating peptides with cellular membranes would result in the formation of concave membrane surfaces according to the "inverted micelle" model, whereas convex membrane surfaces would be formed according to the "toroidal pore" model.

(iv) The models involving the formation of "barrel-stave" or "toroidal" pores, in which homo-oligomerization of the membrane-inserted peptides occurs, predicts the existence of a well-defined structure, in contrast with the highly disorganized structure responsible for the destabilization of the cellular membrane described in the "carpet model".

Later they concluded that all reported models show direct entry of CPPs and CPP-large molecular cargo conjugates across the cell membrane suited except in the case of "inverted micelles model". These models require the presence of amphipathic alpha-helix secondary structures, a feature shared by many CPPs. However, the translocation of large molecules by any of these mechanisms would imply an extensive destabilization of the cellular membrane. This feature is not compatible with the low cytotoxicity usually associated with the membrane translocation of CPPs and their conjugates. Accordingly, it can be concluded that none of the above described models completely explain all the experimental data obtained with different CPPs, indicating that alternative mechanisms should play a role in peptide translocation, especially when conjugated with high molecular weight cargoes.

1.2.1.2c Receptor-mediated cell penetration

Binding of CPPs to cell surface proteoglycans prior to internalization of cells is still the

subject of debate. Recently, Jacob *et al.* stated that, "based primarily on microscopic visualization, previous studies concluded that cells lacking proteoglycans are refractory to cellular transduction by several PTDs, including tat PTD,[42] whereas the other researchers obtained conflicting results".[43] Their experiments using a cellular phenotypic assay, not merely visualization, demonstrated that cells lacking Heparan sulfate or sialic acid are fully competent to efficiently transduce TAT PTD-Cre into CHO cells.[44] Ziegler *et al.* recently showed glycosamino glycan (GAG) binding without and with GAG clustering induced two different pathways of CPP uptake.[45]

Synthesis of retro-isomers (reversed sequences of amino acid) and D-isomer (changed from natural L- to un-natural D-stereochemisty) of amino acids contained in CPPs does not hamper the cellular uptake of CPPs, excluding receptor mediated cell entry;[24, 46] it suggested that receptor mediated cellular uptake mechanism is also involved.

An interesting result published by Boisguerin and co-workers[47] compared 22 different but known CPPs, and presented the first analytical screening in 4 selected cell lines (MDCK, HEK293, HeLa, and Cos-7). They used different experimental conditions, such as effect of protease inhibitors, incubation conditions, different endocytosis inhibitors, temperature as well as monitored cytotoxicity. They clearly demonstrated that the 22 CPPs of the study can be classified by their behaviour into three main groups showing high, medium and low cellular uptake, even after trypsinization. Moreover, they showed additional agents (e.g. chloroquine as endosome rupture reagent), which should increase cellular uptake or spread out endosomal/entrapped CPPs in cytoplasm, only have low effects.

Cell uptake of cargoes such as negatively charged oligonucleotides (ONs) with CPPs:

The group of Divita and Heitz[48] introduced the idea of noncovalent association of nucleic acids with a carrier CPP for cellular delivery and their first report about efficient cellular uptake of CPP-oligonucleotide complexes was published in 1997. Now, it has been well documented that when negatively charged oligonucleotides are mixed with positively charged CPPs they form nanoparticles *via* electrostatic and/or hydrophobic interactions. Both endocytotic and non-endocytotic pathways are proposed for cellular uptake of non-covalent CPP-ON complexes. siRNA and antisense oligonucleotides

(asONs) need to reach the cytoplasm for exerting activity, and the splice switching ONs function in the nucleus of the cell. Therefore, the endocytic mechanism may not seem effective at the first glance because the internalized material remains entrapped in the endosomes. In living cells, however, the non-endocytic uptake is not the prevailing mechanism for majority of CPPs, especially if coupled to cargo molecules[49] and currently, most of the published data points to endocytic internalization of noncovalent ON-CPP complexes. Similar to the cellular uptake of CPPs themselves,[50] ON-CPP complexes initially interact with the negatively charged glycosaminoglycans of the extracellular matrix. This interaction triggers the activation of Rho GTPase Rac1 and actin network remodelling, which favours macropinocytosis and increases membrane fluidity.[50a, 51] Thus, the endocytic uptake of positively charged CPP–ON complexes is typically of oligoarginine-based delivery.[52]

1.2.1.3 Structure-activity studies of CPPs

The systematic structure activity study done for tat (49-57) by Wender and co-authors[53,54] showed that the guanidine groups are most essential in cellular uptake of CPPs. They evaluated a series of guanidine-rich molecular transporters; including polyarginine modified oligocarbamates, oligocarbonates, and branched guanidine rich sequences. Initially a series of systematic *N-* and *C*-termini truncations of tat (49-57) was carried out and was found that the full-length nonamer provided optimal cell uptake. An alanine scan, in which each residue of tat (49-57) was individually replaced by an alanine, showed that all substitutions reduced uptake, except substitution of the only non-charged residue, glutamine, which produced a 9-mer peptide with cell uptake similar to the native peptide.[54] To address the then unknown relative contributions of lysines and arginines to the cell-penetrating function, homooligomers of L-and D-arginine were synthesized and compared with homooligomers of lysine, ornithine and histidines for cell uptake. This study showed that homooligomers of lysine were less effective than tat (49-57) in cell-penetrating function, but homooligomers of arginine were dramatically better than tat (49-57). Thus, it was concluded that the cationic charge of lysines alone was not sufficient for cell uptake while cationic guanidinium groups of arginines and their number were critical (5-20 arginines, with 7-9 being the best compromise of cost and performance).

The reason for the difference between the efficiency of cellular uptake found in oligo-arginine and oligo-lysine peptides was experimentally proved by replacement of hydrogen atoms on guanidine by methyl group and it was found that this replacement reduced the cellular uptake
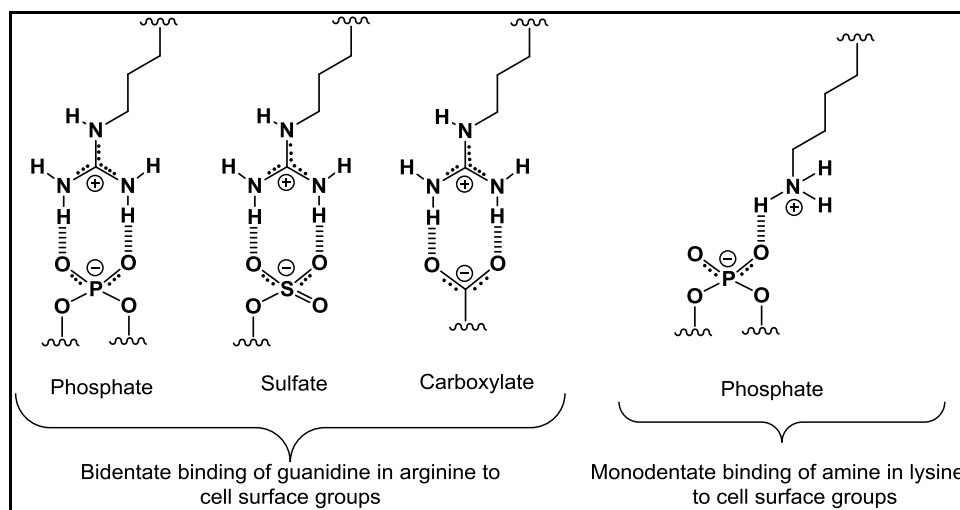
Figure 1.4 Representative interactions between guanidine and amine present in arginine and lysine respectively with cell surface functional groups.

Further, it was hypothesized that guanidine in arginine has the capability to form a bidentate hydrogen bond with anionic cell surface phosphates, carboxylates and/or sulphates, whereas the interaction of lysine residues is through monodentate binding of ammonium groups. This hydrogen bonding is crucial in initial binding of guanidine-rich CPPs to the cell surface prior to internalisation (Figure 1.4).[55]

1.3 Cell-Penetrating Oligomers other than peptides

Subsequent studies from several groups showed that a variety of other scaffolds, including beta-peptides, carbohydrates, heterocycles, and peptide nucleic acids, upon perguanidinylation, exhibit cell-penetrating activity. Similarly, the peptide backbone of CPPs has been replaced by carbamates, carbonates, peptoids, etc. and these changes showed variations in cell uptake property for these CPOs. Some of these CPOs are discussed herein and shown in Figure 1.5.
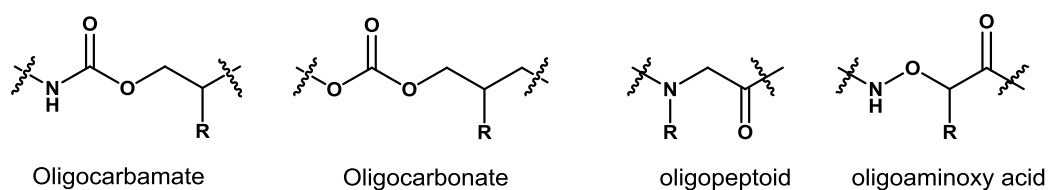
Figure 1.5 Representative backbone structures of various CPOs other than polyamides.

1.3.1 Oligocarbamates

In 1993, Schultz and co-workers[56] demonstrated the solid phase methodology to synthesize unnatural biopolymers such as oligocarbamates (Figure 1.6), composed of building blocks other than amino acids. Their aim was to design chiral aminocarbonate monomer units and to link them on solid support *via* carbamate linkages. They also showed these new type of biopolymers to be stable to proteolytic degradation.[57]
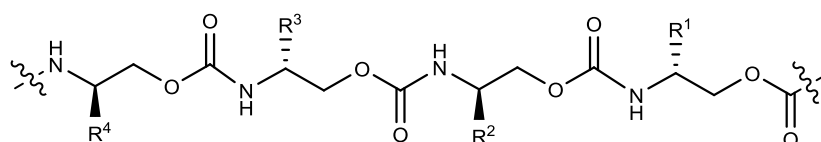
Figure 1.6 Representative structure of oligocarbamate; where R^{1-4} are side chain functional groups.

In 1997, Rana and co-workers[58] synthesized oligocarbamate mimic of tat (47-57) peptide and showed that this tat-derived unnatural biopolymer could specifically bind TAR RNA with high affinity. After site-specific photo-cross-linking experiments using a photoactive analogue (4-thiouracil) containing TAR RNA, it was revealed that this unnatural biopolymer interacts with RNA in the major groove. The oligocarbamate-RNA complexes were stable to proteolytic digestion. These results identify a new class of unnatural polymers for structure-specific recognition of RNA. Further extension of these unnatural polymers synthesis and applications showed that the oligocarbamate and oligourea could also be used to inhibit transcriptional activity of tat protein in human cells.[59] In the year 2004, they covalently conjugated siRNA to tat (47-57) derived oligocarbamate and tat (47-57) peptide to effectively induce RNAi activity.[60] This report compared siRNA cellular uptake, localization and function using tat peptide and tat derived oligocarbamate as delivery vectors.

Wender and co-workers reported in the year 2002, a new class of molecular

transporters, so called, guanidinylated oligocarbamates. They reported stepwise solid phase oligomerization to obtain oligocarbamates with free amine groups and in a single step perguanidinylation of free amines introduced guanidine groups in oligocarbamates. The 9-mer oligocarbamate was found to be the most efficient transporters, entering cells faster than even nonamer of D-Arg and HIV-1 tat (49-57) peptide. Significantly, this new family of transporters also enable uptake into the formidable skin barrier of a probe molecule which by itself does not penetrate skin.[61]

1.3.2 Oligocarbonates

Wender and co-workers[62] recently reported a new class of molecular transporters having polyguanidines attached by carbonate linkage (Figure 1.7). After synthesizing numerous guanidine-rich oligomers for drug delivery application, they explored the new type of polyguanidines assembled in one-step organocatalytic ring-opening oligomerization process that also allowed concomitant probe (or drug) attachment and control over transporter length.
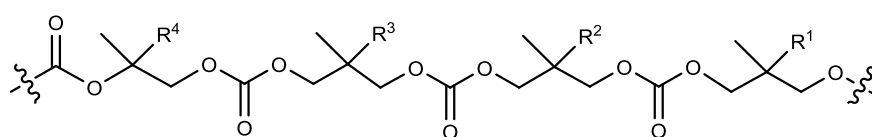
Figure 1.7 Representative structure of oligocarbonate; where R[1-4] are side chain functional groups.

To show the applicability of these synthesized guanidine rich oligocarbonates, covalent conjugation of luciferin cargo with intracellular cleavable disulfide linkage was done. The activity was measured by the light emitted when luciferin is converted by luciferase to oxyluciferin and as a photon of detectable light in HepG2 cells.

1.3.3 α-aminoxy acid based peptides

Zhang *et al.*[63] synthesized novel CPPs which were constructed by D- and L-α-aminoxy acids (Figure 1.8) to study their cellular uptake property and stability towards proteolytic degradation.
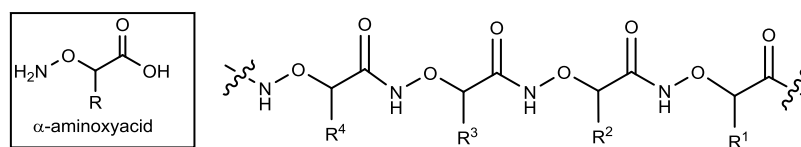
Figure 1.8 Structure of α-aminoxy acid and its derived peptides.[63] where R[1-6] are side chain functional groups.

These synthesized CPPs containing α-aminoxy acids were tested for cellular uptake by FACS and confocal analysis, which showed that these peptides were internalized and showed diffuse cytosolic distribution. These peptides also showed serum stability and low cytotoxicity.

1.3.4 Peptoids, peptoid-peptide hybrids and oligoureas

Peptoids, or poly-*N*-substituted glycines, are a class of peptidomimetics in which the side chains are appended to the nitrogen atom of the peptide backbone, rather than to the α-carbons (as in amino acids). Peptoids (Figure 1.9; A) are more flexible than peptides because intramolecular CO---HN hydrogen bonds are removed and the steric interactions that induce secondary structure are different. For pharmacological applications, peptoids have the advantage of being stabilized against enzymatic degradation and many hybrid peptoids were used in drug delivery applications.[64]
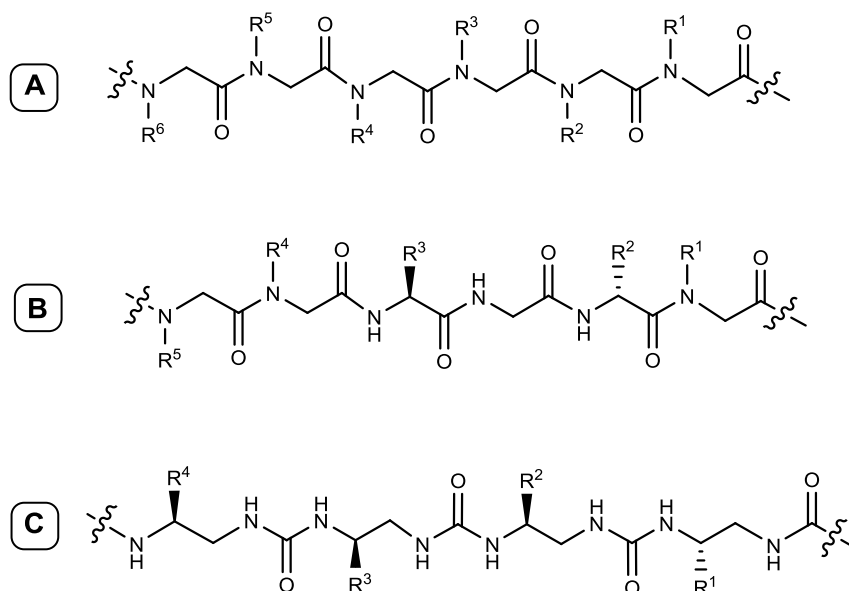
Figure 1.9 Representative structures of [A] Peptoid, [B] Peptoid-peptide hybrid, [C] Oligourea; where R[1-6] are side chain functional groups.

Zuckermann and co-workers demonstrated peptoid can be used as drug delivery agent. They synthesized *N*-substituted glysine oligomers (peptoids) and showed its application to condense plasmid DNA efficiently with enzymatic stability and studied their cell delivery property in variety of cell lines.[65] In the year 2000, Wender and co-authors[24] designed and synthesized a series of polyguanidine peptoid derivatives that preserve the 1, 4-backbone spacing of side chains of arginine oligomers but have an oligoglycine backbone devoid of stereogenic centres.

Brase and co-workers[66] reported targeted delivery to cell cytosol or to nucleus using peptoid-carriers containing either amino or guanidino functional group in the side chains and further investigated their cellular uptake and toxicity. There has been also a report to show the use of α-peptide/β-peptoid chimeras (Figure 1.9;B) in cellular delivery.[67] Recently Barron and co-workers[68] reported design and synthesis of a library of cationic, amphipathic peptoids as molecular transporters and investigated how peptoid structures influenced their cellular uptake and cytotoxicity. Birgit and co-authors work studied the photophysical properties of fluorescently-labeled peptoids.[69]

Synthesis of oligourea[70] (Figure 1.9; C) and peptoid-peptide hydride,[64, 71] of tat (47-59) was also reported earlier by other groups, but their cellular uptake was not explicitly studied. These selected peptoids incorporated arginine-like side chains on the amide nitrogen, because of their expected resistance to proteolysis, ease and cost effective synthesis.

1.4 Strategies to transport drug molecules across the cell membrane by CPOs

The CPOs have remarkably contributing in the delivery applications of rapidly progressing oligonucleotides drugs *in vitro* as well as *in vivo*. Numerous CPOs, majorly CPPs, have been extensively studied to transport variety of biomolecular cargoes of pharmacological interest to various cells and tissues. More importantly, they could deliver these cargoes to various compartments of cells such as mitochondria, lysosome, nucleus, and cytoplasm as well as across the blood brain barrier (BBB).[72] Sometimes endosomal escape might be needed for efficiency of CPP attached cargoes to their target sites, which has been accomplished by the use of fusogenic lipids, membrane-disruptive peptides, membrane-disruptive polymers and lysosomotropic agents.[73]

CPPs successfully transported a large number of different sizes of cargoes efficiently both *in vitro* and *in vivo.* These cargoes include therapeutic peptides, proteins, antibodies, nucleic acids (oligonucleotides, cDNA, RNA, siRNA), fluorochromes, nanoparticles, lipid-based formulations, viruses, quantum dots, contrast agents for magnetic resonance imaging, and drugs.[11a, 74] Attachment of cargoes to CPOs can be carried out by following two ways:

1.4.1 Covalent attachment of cargo to CPOs

This method involves chemical synthesis of peptides that are modified to enable covalent conjugation to oligonucleotides or other cargo types. Such conjugation reactions may be carried out either on solid support or in solution, and often result in high yields. An advantage of covalent conjugation is that it results in a well-defined single entity that simplifies drug development. Linker types may be chemically stable, which ensure that the peptide-oligonucleotide conjugates remain intact throughout *in vivo* administration and subsequent delivery process and that degradation now reflects only the proteolytic susceptibility of the particular peptide.

Alternatively, a labile linker cleavable within the cell, such as a disulphide linkage (Figure 1.10), has proven to be very successful in studies of peptide-mediated delivery, both in cells and *in vivo*.[41, 42] Such disulphide bridges may remain sufficiently stable, if administration is rapid, but may be cleaved later when the conjugate reaches the reducing environment of the endosome/ cytoplasm. This approach was initially favoured in therapeutic design, because cleavage diminishes the risk of any detrimental effect of the peptide on the interaction of the oligonucleotides with its target. However, recent *in vivo* applications using stable linkages suggested that peptide-cargo cleavage is not essential. Recent studies have also suggested that thiol or disulfide groups might enhance cellular uptake, although the reasons for this are not as yet fully understood.[43,44]
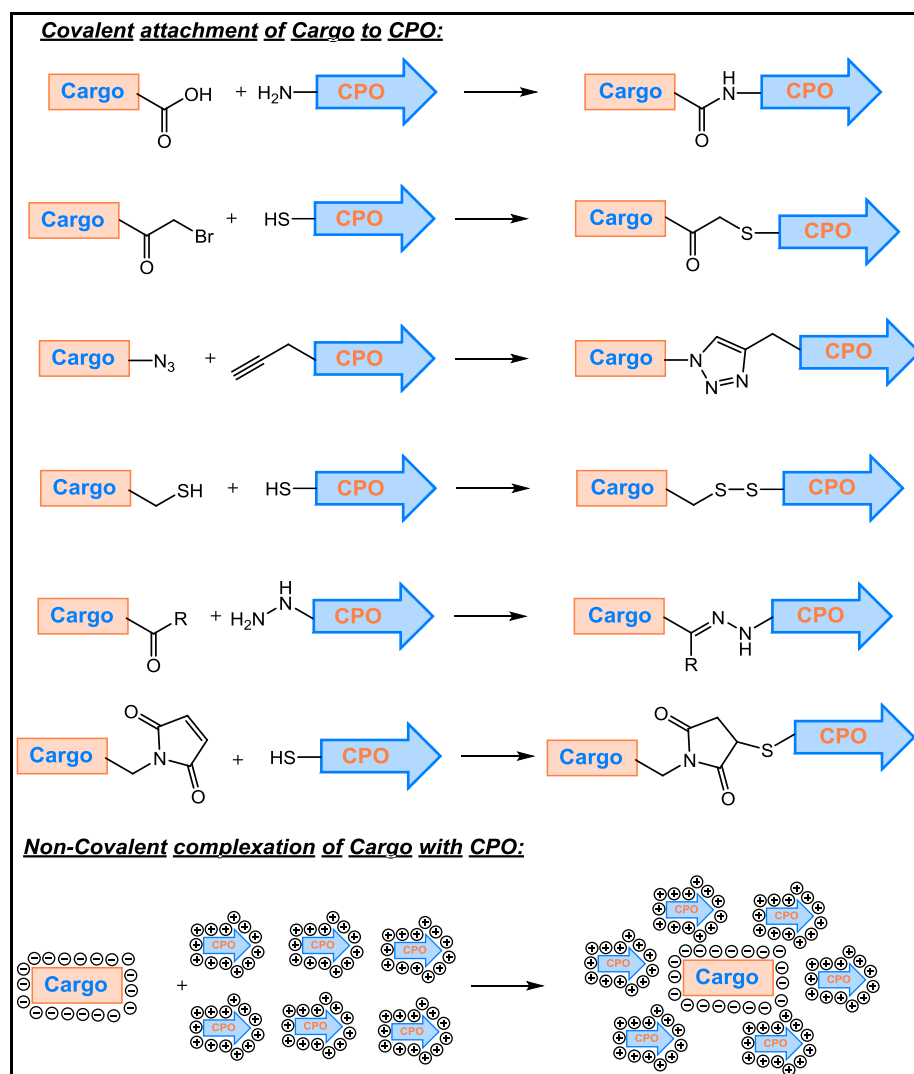
Figure 1.10 Representative strategies to show the attachment of cargo with CPO by covalent conjugation and by non-covalent complexation.

Although covalent conjugation is very suitable for charge neutral oligonucleotide analogues, there are technical difficulties in conjugation and purification of conjugates of highly cationic peptides with negatively charged oligonucleotides that have limited the type of peptide that can be conjugated.[45] However, meaningful comparative data on the effects of different peptide-oligonucleotide linkages in biological antisense assays are mostly lacking.

CPPs have also been used to mediate the delivery of PNAs and PMOs through covalent linkage (Figure 1.10)[75]. Our group reported, the covalent attachment of PNA as

well as DNA oligomer to the (R-Ahx-R)$_4$-peptide using click chemistry protocol.[76a] The formation of efficient non-covalent complexes comprising CPPs and both charged and uncharged steric block oligonucleotides like 2'-O-methyl, LNA, PNA and charged PNA derivatives, have also been described.[76b]

There are various methods and functional groups that have been used to attach the cargo to CPOs. Also various strategies such as pH sensitive release[72a] are used to detach these cargoes from CPOs after delivery to their site of action.

1.4.2 Non-covalent attachment cargo to CPOs

This method of peptide-mediated oligonucleotides delivery exploits the complex forming properties of CPPs and their derivatives. For example, cationic CPPs can form complexes efficiently with negatively charged oligonucleotides[8] or cargo molecules (Figure 1.10). Further, some peptide vectors also contain hydrophobic elements (hydrophobic amino acids or addition of hydrophobic amino acids and/or other moieties such as fatty acids, lipids or cholesterol), which are designed for complex formation with both negatively charged and charge-neutral analogue types. Such complex forming peptides form nano-sized particles together with the oligonucleotides that are better able to translocate across the plasma membrane (in some cases perhaps avoiding the endosomal uptake system altogether)[46] and can deliver the oligonucleotide cargo to the target with greater efficiency.[8]

1.5 Applications of CPOs

Several CPOs have been evaluated for the ability to transport diverse type of imaging agents, carriers and cargoes (Figure 1.11), into cells, tissues, and organs. Certain CPPs have been used for the intracellular delivery of information-rich molecules to modulate protein-protein interactions and thereby inhibit key cellular mechanisms of disease. The ability to introduce drugs into cells allows the conventional bio-distribution of drugs to be altered in order to favorably impact toxicity, patient compliance, and other treatment factors.
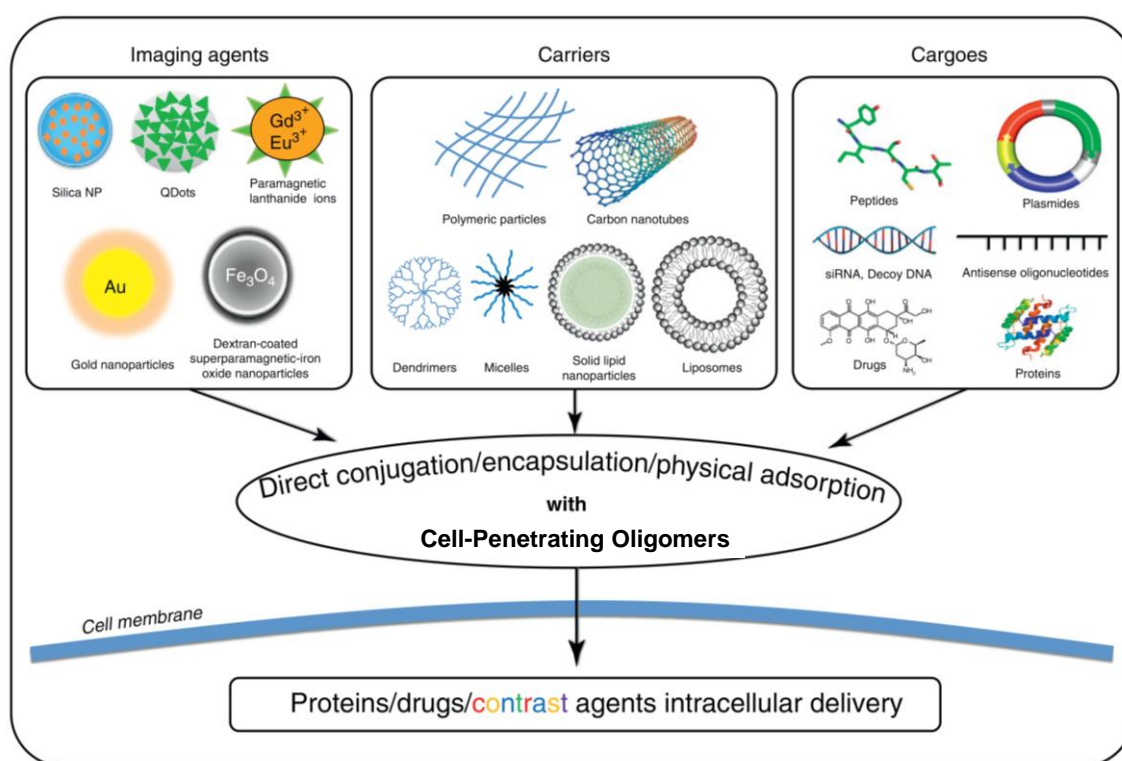

Figure 1.11 Strategies for attachment of cargo to CPPs; adopted image.[11a]

CPP-conjugated moieties are directed against a growing variety of targets and disease areas, including cancer, cardiology, pain and stroke. The promising results obtained in a number of studies indicate that CPOs may have an important role in the development of novel therapeutics (Table 1.2).

Table 1.2 Selective CPOs-drug attachment strategies and their applications.

CPO	Cargo	Application	References
CPO-cargo covalent attachment:			
Low molecular weight protamine (LMWP) VSRRRRRRGGRRRR-albumin	Doxorubicin	Anticancer agent	Gua Q. *et al.*[77]
TH (AGYLLGHINLHHLAHL (Aib)HHIL-NH$_2$	Paclitaxel, coumarin 6, etc loaded liposomes	pH responsive delivery and release to tumor cells	Zhang Q. *et al.*[78]
Xentry (LCLRPVG)	β-galactosidase, Anti-B-raf antibodies and siRNAs	Delivery of β-galactosidase to most of the tissues in mice	Montrose K. *et al.*[79]
tat	Immunoglobulin-like protein superoxide dismutase 1 (SOD1)	Structural and functional analysis carried by in-cell NMR	Danielsson J. *et al.*[80]
Modified tat nanofibers	Paclitaxel	Designed peptide used for anticancer drug delivery agent	Zhang P. *et al.*[81]
tat, (RXR)$_4$, B-pep, Pip2b	BH4-protein domain of the Bcl-xL anti-apoptotic protein	Studies conjugates help to reduced infarct size and to inhibit apoptosis in the left ventricle of treated mice	Boisegurin P. *et al.*[82]
PepFectss, TP10, tat, stearyl-(RxR)$_4$ Peptides	Plasmid pEGFP-C1	Comparison of activity and Cxytotoxicity of different CPPs	Suhorutsenko J. *et al.*[83]
(RXRRBR)$_2$XB where X is 6-aminohexanoic acid, B is β-alanine residues	Antisense morpholino oligonucleotides (AMOs)	Delivery of AMOs in the brain of mice	Du L. *et al.*[84]
Cyclic [W(RW)$_4$]	Doxorubicin	Attachment by hydrolytic linker which release drug inside the cell	Nasrolahi *et al.*[85]
CPO-cargo Non-covalent attachment:			
Arginine clusters	pEGFP-C1 DNA	DNA transfection	Bagnacani *et al.*[86]

Stearyl-[D]-K6L9	Plasmid DNA	Plasmid delivery to Cos-7 cells	Zhang W. *et al.*[87]
PepFect6	Semliki Forest virus (genus alphavirus) based RNA and DNA vectors	Intracellular delivery of DNA without interfering with the viral life cycle	Pärn *et al.*[88]
Cyclic peptides-gold nanoparticles containing tryptophan and lysine residues	Anti-HIV drugs (emtricitabine (FTC) and lamivudine (3TC))	cellular uptake of F′-GpYEEI was enhanced 12.8-fold by c[KW]$_5$-AuNPs	Nasrolahi *et al.*[89]
Stearyl-(RXR)$_4$, stearyl-R$_9$	plasmids and splice-correcting oligonucleotides (SCOs)	Found enhanced spice correction activity after stearylation of peptides	Lehto *et al.*[90]
Series of cyclic peptides containing hydrophobic residues (e.g., W, F, L) and charged residues (e.g., K, R, E)	Lamivudine, doxorubicin	Successful application of drug entrapment in cyclic structure of peptide	Mandal *et al.*[91]
Covalent and Non-covalent strategies:			
GV1001 (EARPALLTSRLRFIPK)	Conjugated and non-conjugated siRNA targeting luciferase, DNA,	Same peptide vector could used for various cargo delivery	Lee *et al.*[92]
(rxr)$_4$ -type oligocarbamates	Covalently conjugated Tyroserleutide, non-covalently conjugated siRNA, pDNA	Enhanced efficacy in cargo delivery by oligocarbamates over its peptide counterpart	Patil *et al.*[93]

1.6 Limitations and drawbacks of CPOs

Many times efficiency of CPOs, is depends on the concentration of the oligomer, the guanidine contents, and also on the length of the oligomer (upto approximately 15 residues). However, longer oligomers enter cells effectively but also precipitate in serum and exhibit cellular cytotoxicity at high micromolar concentrations.[94] CPOs without directing ligands or antibody enters the cells non-specifically and hence their efficacy to required cells decreases and shows the non-specific cytotoxicity. Properties such as amphipathicity and water solubility changes for each different cargo or CPO and results in different cellular uptake efficiency and toxicity of each cargo-CPO conjugates, hence designing of universal CPO to transport variety of cargoes across the cell membrane is not possible.

1.7 Dendrimers as drug delivery tool

Dendrimers are a class of polymers with well-defined nanostructure that possess tree-like architecture distinguished by exponential numbers of discrete dendritic branches connected to a common core. These dendrimers can either be symmetric or asymmetric in structure. These unique structural attributes confer a spherical shape to dendrimers after several layers of branching (i.e. generations).

1.7.1 Design and synthesis of dendrimers

Numerous dendrimer molecules have been designed and synthesized as drug delivery tools. The core (central moiety), dendrons (branch or arms of dendrimer) or surface moieties (outer shell of dendrimer) can be synthesized according to application needs (Figure 1.12). The scope to use different linkages (such as polyethylene gylcol, peptide chains, carbon chains, etc.) to connect dendron arms and variety of surface functional groups make them suitable to use in variety of drug delivering systems and imaging applications.
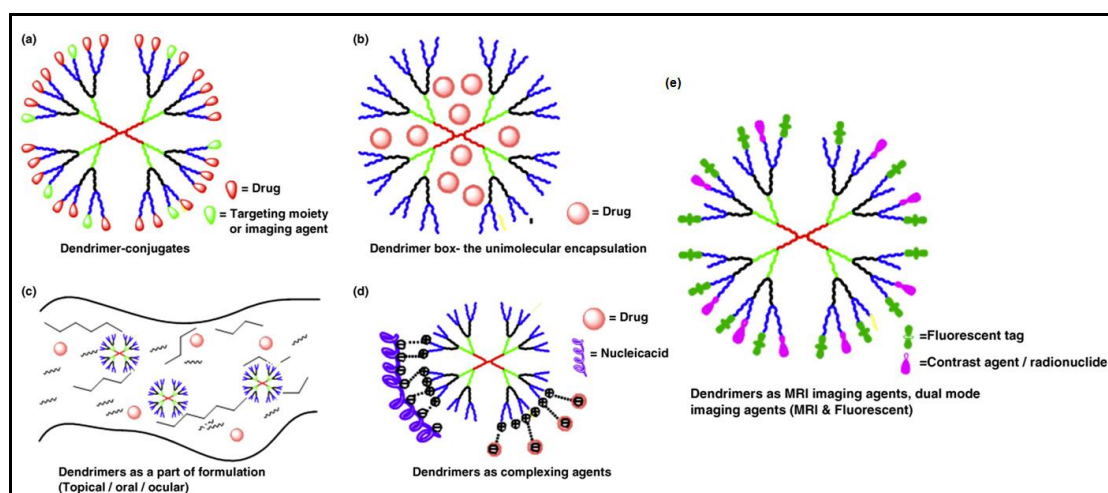
Figure 1.12 Potential applications of dendrimers. (a) Dendrimer drug conjugates, dendrimers linked to targeting moieties and imaging agents. (b) Encapsulation of the drugs in the dendritic interiors. (c) Dendrimers incorporated into various delivery systems for enhancing permeation, solubility and so on. (d) Dendrimers as complexing agents. (e) Dendrimers as carriers for MRI and fluorescent imaging.[95]

Poly(amidoamine) (PAMAM) is a dendrimer which is frequently used in biomedical applications (Figure 1.13). Its structure and the distribution of drugs or genes inside these molecules have been intensively investigated. PAMAM has been used in the targeted drug delivery applications and its surfaces has been functionalized with folic acid,[96] cyclic RGD peptides,[97] antibodies,[98] selective A3 adenosine[99] receptor etc.

1.7.2 Applications of dendrimers in drug delivery

Other than amido amide linked dendrimers, peptide based dendrimers are also reported to enhance the cellular uptake efficiency of attached cargoes. Wender *et al.* synthesized fluorescently labeled, structurally varied polyguanidino dendrimers based on diaminoacid monomeric units and studied their cellular uptake.[100] Fluorescein attached branched arginines were also studied in cells and increased cell uptake of these newly synthesized oligomers was found.[101] A series of polyguanidylated dendritic structures that can be used as molecular transporters have been designed and synthesized based on non-peptide units and has also been reported.[102] Huang *et al*. reported biocompatible macromolecular vectors that not only enable transport of bioactive cargo across the cell membrane but also control the delivery into defined intracellular compartments.[103]
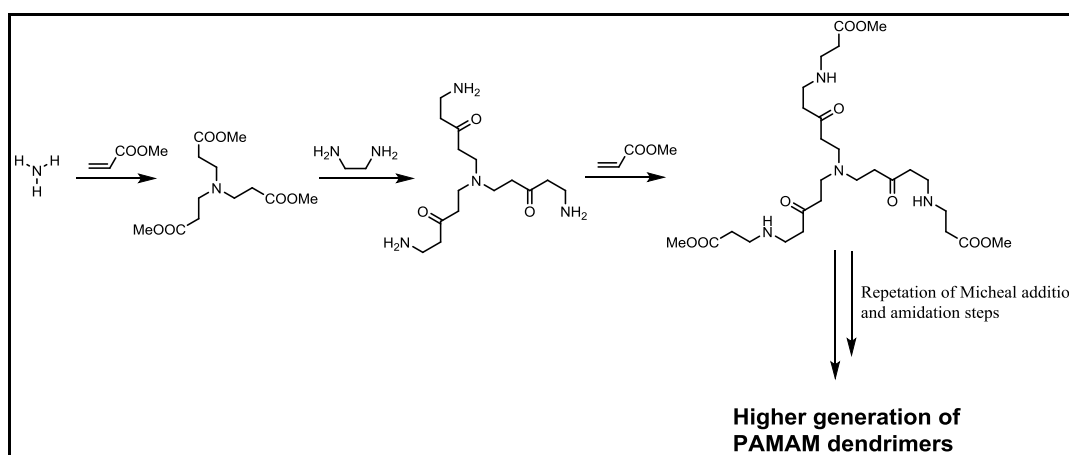
Figure 1.13 Representative example for synthesis of PAMAM dendrimer.

1.7.3 Limitations and drawbacks of dendrimers as drug delivery tool

The size and charge on dendrimers influence their cytoxicity. In case of PAMAM dendrimers, the positively charged surface containing dendrimers are found comparatively more cytotoxic than negative or neutral surface dendrimers. Positively charged dendrimers introduced into the systemic circulation interact with blood components causing destabilization of cell membranes and cell lysis.[104] Dendrimer cytotoxicity depends on the central core moiety and is strongly influenced by the nature of the dendrimers surface. For example, changing the surface amine groups to hydroxyl groups may result in lower levels of cytotoxicity.

1.8 Liposomes as drug delivery tool

In the early stage of development in drug delivery tools, liposomes were realized as one of the promising and non-toxic tools due to their high degree of biocompatibility and the enormous diversity of structure and composition. They are tiny vesicles consisting of an aqueous core entrapped within one or more natural phospholipids forming closed bilayered structures.

1.8.1 Design and synthesis of Liposomes

Liposomes have been extensively designed, functionalized and used as potential drug delivery system for a variety of cell impermeable drugs. Li *et al.* designed and constructed a multifunctional theranostic liposomal drug delivery system, which

incorporated multimodality magnetic resonance (MR), near-infrared (NIR) fluorescent and nuclear imaging for therapy monitoring and prediction.[105]
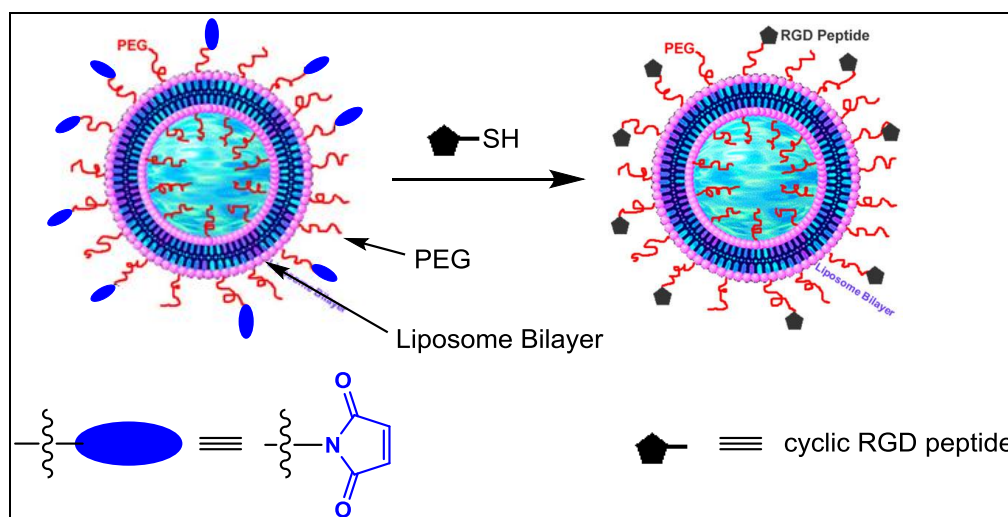

Figure 1.14 A schematic representation of the synthesis of targeted liposome delivery system depicting the cyclic RGD peptides that targets the $\alpha\nu\beta3$ integrin receptors on the vascular tumor cells, Nallamothu *et al.*[106]

Stealth liposome technology has revolutionized the field of liposomal drug delivery.[107] This strategy was developed to overcome most challenging problems encountered by the use of conventional liposome technology such as the inability to evade interception by the immune system, toxicity due to charged liposomes, low blood circulation half-life, and steric stability. Stealth liposome strategy was achieved simply by modifying the surface of the liposome membrane; a process that was achieved by engineering hydrophilic polymer conjugates (e.g. attachment of polyethyleneglycol chains). Nallamothu *et al.* synthesized liposomes composed of hydrogenated soybean phosphatidylcholine (HSPC), cholesterol, distearoyl phosphoethanolamine-polyethylene- glycol-2000 conjugate (DSPE-PEG), and DSPEPEG- maleimide, prepared by the lipid film hydration and extrusion process (schematically presented in Figure 1.14). These liposomes containing 2% of DSPEPEG- maleimide were conjugated by cystein-maleimide linkage via thiol goups of the RGD peptide (cyclo [Arg-Gly-Asp-D-Phe-Cys]). These surface anchored RGD-liposomes was used further in tumor targeted delivery, because cyclic RGD (Arg-Gly-Asp) peptides have high affinity for αvβ3-integrins expressed on tumor vascular endothelial cells.[106]

1.8.2 Applications of liposomes in drug delivery

Liposomal drug delivery has been studied for a variety of applications including polymeric antisense/antigene therapeutics delivery *in vitro* as well as *in vivo* such as phosphorothioate oligonucleotides,[109] DNA, ribosomes, peptide/proteins, small molecular drugs; few of them are listed in Table 1.3.

Table 1.3 Drugs and their applications using liposomal drug delivery tool.[108]

Cargo type	Effect after liposomal formulation
Antibiotics, chelators, plasmids,antigene and antisense therapeutics such as phosphorothioate oligonucleotides	Improved transfer of hydrophilic, charged molecules, efficient delivery using cationic liposomes
Amphotericin B, porphyrins, minoxidil, some peptides, and anthracyclines, respectively; hydrophilic drugs, such as anticancer agent doxorubicin or acyclovir	Improved solubility of lipophilic and amphiphilic drugs
Antimonials, amphotericin B, porphyrins, vaccines, immunomodulators	Passive targeting to the cells of the immune system, especially cells of the mononuclear phagocytic system
Doxorubicin, cytosine arabinoside, cortisones, biological proteins or peptides such as vasopressin	Sustained release system of systemically or locally administered liposomes
Doxorubicin andamphotericin B	Site-avoidance mechanism
Anti-inflammatory drugs, anti-cancer, anti-infection	Site-specific targeting
Corticosteroids, anesthetics, and insulin	Improved penetration into tissues

Since the first liposomal pharmaceutical product, Doxil, received FDA approval in 1995, liposomes have been extensively applied as drug delivery tool in clinic. There are several important types of liposomes, such as PEGylated liposomes (Doxil and

Lipo-dox), temperature sensitive liposomes (ThermoDox), cationic liposomes (EndoTAG1-1), and virosomes (Expal and Inflexal V), that have been investigated for clinic use. In contrast with liposomal-based drugs on the market, liposome-based drugs in clinical trials focused more on the types of delivered drugs (e.g., Cisplatin, BLP25 lipopeptide, Grb2 antisense oligodeoxynucleotide, Bacteriophage T4 endonuclease 5, etc) and therapeutic applications (from topical delivery systems to portable aerosol delivery systems).[110]

1.8.3 Limitations and drawbacks of liposomes as drug delivery vectors

Although liposomal drug delivery systems demonstrated improved success, there are still some major challenges that are need to be addressed. Incorporation of toxic organic solvents or high heat during fabrication process can inhibit the activity of some bioactive molecules such as protein. While *in vivo* application of drug-loaded liposomes, since the drug release profiles seem to depend most on degradation of polymeric materials, majority of drug-loaded liposomes may remain entrapped within the body or insufficient initial release at commencement of treatment may result in toxicity. At the same time, high overdose may occur during high degradation period.[111]

New liposomal formulations, such as PEGylated liposomes, may extend blood circulation time, vary drug distribution in the body, and hence reduce the possible side effects related to the drugs (e.g. cardiotoxicity). However, PEGylated liposomes (Doxil and Lipo-dox) displayed significant incidence of stomatitis in clinical trials, which may be related to PEGylation.

1.9 Present work

The following chapters of this thesis illustrate the design and synthesis of different chemically modified peptides, oligocarbamates and dendrimers for their applications in the delivery of dugs inside cells.

Chapter 2: Design and synthesis of proline/hydroxy proline-derived monomers, oligomers and their biological evaluation

Section A: Synthesis of trans-4-hydroxy-L-proline-derived orthogonally protected monomer, peptides and their cell uptake studies

After systematic structure activity relationship study of various reported CPOs, we have designed and synthesized new molecular scaffold peptides, oligocarbamates, and monomer for dendrimer synthesis. We chose hydroxyproline amino acid and modified it to get synergistic property of the proline ring constraint and guanidines that are normally present in arginine residues.

Section B: Synthesis of L/D-Proline-derived monomers, peptides and their cell uptake studies

We used L- and D-proline amino acids to synthesize spacer moieties to get conformationally restricted spacers, incorporated them in polyarginine peptides and studied their structural features, cellular uptake property and cargo delivery applications.

Chapter 3: Design and synthesis of (R-X-R)-type oligocarbamate transporters for cellular delivery *via*: Non-covalent complexation and covalent conjugation strategies

In another project we designed (r-x-r)$_4$-type oligocarbamates as efficient molecular transporters,[93] where '-r-' is arginine analogue and '-x-' is aminohexanoic acid or aminopropanoic acid analogue for oligocarbamate synthesis. The synthesis was based on the use of *p*-nitrophenyl carbonate activated monomers and oligomerization on solid support. These oligomers served as efficient cellular delivery vectors for various cargoes such as covalently conjugated carboxyfluorescein (*cf*, model cargo), antitumor tripeptide (tyroserleutide), as well as non-covalently attached siRNA and plasmid DNA to the cells in comparison to its peptide counterpart.

Chapter 4: Design and synthesis of novel oligocarbamates and monomer synthesis for dendron and dendrimers

Section A: Synthesis of tartaric acid-derived novel di-guanidine carbonate monomer and its incorporation in oligocarbamate

Synthesis of novel *p*-nitrophenyl carbonate activated monomer which was derived from cheaply available L-(+)-tartaric acid has been showed. Synthesized monomer was further incorporated in (r-x-r)-type of oligocarbamate where consecutive 'r-r' unit was

replaced by synthesized monomer.

Section B: Synthesis of trans-4-hydroxy-L-proline-derived monomer for incorporation in carbamate linked dendron and dendrimer

Based on understanding from literature reports for dendrimers as drug delivery tools, we designed and synthesized a novel *trans*-4-hydroxy-L-proline-derived monomer unit, which was envisioned to be used for synthesis of various dendron and dendrimers which can further be evaluated for drug delivery applications.

1.10 References

1.   Bae, Y.; Park, K. Targeted drug delivery to tumors: myths, reality and possibility. *Journal of Controlled Release* **2011,** *153*, 198-205.

2.   (a) Xia, H.; Gu, G.; Hu, Q.; Liu, Z.; Jiang, M.; Kang, T.; Miao, D.; Song, Q.; Yao, L.; Tu, Y.; Chen, H.; Gao, X.; Chen, J. Activatable Cell Penetrating Peptide-Conjugated Nanoparticles with Enhanced Permeability for Site-Specific Targeting Delivery of Anticancer Drug. *Bioconjugate Chemistry* **2013,** *24*, 419-430. (b) Jin, E.; Zhang, B.; Sun, X.; Zhou, Z.; Ma, X.; Sun, Q.; Tang, J.; Shen, Y.; Van Kirk, E.; Murdoch, W. J.; Radosz, M. Acid-Active Cell-Penetrating Peptides for in Vivo Tumor-Targeted Drug Delivery. *Journal of the American Chemical Society* **2012,** *135*, 933-940.

3.   Kelley, S.; Stewart, K.; Mourtada, R. Development of Novel Peptides for Mitochondrial Drug Delivery: Amino Acids Featuring Delocalized Lipophilic Cations. *Pharmaceutical Research* **2011,** *28*, 2808-2819.

4.   De Jong, W.; Borm, P. Drug delivery and nanoparticles:applications and hazards. *International Journal of Nanomedicine* **2008,** *3*, 133-149.

5.   Wilczewska, A.; Niemirowicz, K.; Markiewicz, K.; Car, H. Nanoparticles as drug delivery systems. *Pharmacological Reports* **2012,** *64*, 1020-1037.

6.   Suri, S.; Fenniri, H.; Singh, B. Nanotechnology-based drug delivery systems. *Journal of Occupational Medicine and Toxicology (London, England)* **2007,** *2*, 16.

7.   Johnson, R.; Harrison, S.; Maclean, D. Therapeutic Applications of Cell-Penetrating Peptides. *Methods in Molecular Biology (Clifton N. J.)* **2011** *683,* 535-551.

8. Järver, P.; Coursindel, T.; Andaloussi, S.; Godfrey, C.; Wood, M.; Gait, M. Peptide-mediated Cell and In Vivo Delivery of Antisense Oligonucleotides and siRNA. *Molecular Therapy- Nucleic Acids* **2012,** *1*.

9. El Andaloussi, S.; Hammond, S.; Mäger, I.; Wood, M. Use of cell-penetrating-peptides in oligonucleotide splice switching therapy. *Current Gene Therapy* **2012,** *12*, 161-178.

10. Stanzl, E. G.; Trantow, B. M.; Vargas, J. R.; Wender, P. A. Fifteen Years of Cell-Penetrating, Guanidinium-Rich Molecular Transporters: Basic Science, Research Tools, and Clinical Applications. *Accounts of Chemical Research* **2013**.

11. (a) Koren, E.; Torchilin, V. Cell-penetrating peptides: breaking through to the other side. *Trends in Molecular Medicine* **2012,** *18*, 385-393. (b) Madani, F.; Lindberg, S.; Langel, U.; Futaki, S.; Gräslund, A. Mechanisms of cellular uptake of cell-penetrating peptides. *Journal of Biophysics (Hindawi Publishing Corporation : Online)* **2011,** *2011*, 414729. (c) Jakob, R.; Artita, S.; Ülo, L. Applications of Cell-Penetrating Peptides for Tumor Targeting and Future Cancer Therapies. *Pharmaceuticals* **2012,** *5*.

12. Pooga, M.; Hällbrink, M.; Zorko, M.; Langel, U.; lo. Cell penetration by transportan. *The FASEB Journal* **1998,** *12*, 67-77.

13. Soomets, U.; Lindgren, M.; Gallet, X.; Hällbrink, M.; Elmquist, A.; Balaspiri, L.; Zorko, M.; Pooga, M.; Brasseur, R.; Langel, Ü. Deletion analogues of transportan. *Biochimica et Biophysica Acta (BBA) - Biomembranes* **2000,** *1467*, 165-176.

14. Green, M.; Loewenstein, P. M. Autonomous functional domains of chemically synthesized human immunodeficiency virus tat trans-activator protein. *Cell* **1988,** *55*, 1179-1188.

15. Frankel, A. D.; Pabo, C. O. Cellular uptake of the tat protein from human immunodeficiency virus. *Cell* **1988,** *55*, 1189-1193.

16. Yamazaki, C. M.; Nakase, I.; Endo, H.; Kishimoto, S.; Mashiyama, Y.; Masuda, R.; Futaki, S.; Koide, T. Collagen-like Cell-Penetrating Peptides. *Angewandte Chemie International Edition* **2013,** *52*, 5497-5500.

17. Ruzza, P.; Calderan, A.; Guiotto, A.; Osler, A.; Borin, G. Tat cell-penetrating peptide has the characteristics of a poly(proline) II helix in aqueous solution and in

SDS micelles. *Journal of Peptide Science* **2004,** *10*, 423-426.

18.   Derossi, D.; Joliot, A.; Chassaing, G.; Prochiantz, A. The third helix of the Antennapedia homeodomain translocates through biological membranes. *The Journal of Biological Chemistry* **1994,** *269*, 10444-10450.

19.   (a) Lindgren, M.; Langel, Ü. Classes and Prediction of Cell-Penetrating Peptides. *Methos in Molecular Biology* **2011** *683*,3-19. (b) Stewart, K. M.; Horton, K. L.; Kelley, S. O. Cell-penetrating peptides as delivery vehicles for biology and medicine. *Organic & Biomolecular Chemistry* **2008,** *6*, 2242-2255.

20.   Milletti, F. Cell-penetrating peptides: classes, origin, and current landscape. *Drug Discovery Today* **2012,** *17*, 850-860.

21.   (a) Sanders, W. S.; Johnston, C. I.; Bridges, S. M.; Burgess, S. C.; Willeford, K. O. Prediction of Cell Penetrating Peptides by Support Vector Machines. *PLoS Comput Biol* **2011,** *7*, e1002101. (b) Gautam, A.; Chaudhary, K.; Kumar, R.; Sharma, A.; Kapoor, P.; Tyagi, A.; Open source drug discovery consortium; Raghava, G. In silico approaches for designing highly effective cell penetrating peptides. *Journal of Translational Medicine* **2013,** *11*, 74.

22.   Akdag, I. O.; Ozkirimli, E. The Uptake Mechanism of the Cell-Penetrating pVEC Peptide. *Journal of Chemistry* **2013,** *2013*, 9.

23.   Rothbard, J.; Kreider, E.; VanDeusen, C.; Wright, L.; Wylie, B.; Wender, P. Arginine-rich molecular transporters for drug delivery: role of backbone spacing in cellular uptake. *Journal of Medicinal Chemistry* **2002,** *45*, 3612-3618.

24.   Wender, P.; Mitchell, D.; Pattabiraman, K.; Pelkey, E.; Steinman, L.; Rothbard, J. The design, synthesis, and evaluation of molecules that enable or enhance cellular uptake: peptoid molecular transporters. *Proceedings of the National Academy of Sciences of the United States of America* **2000,** *97*, 13003-13008.

25.   Abes, S.; Moulton, H. M.; Clair, P.; Prevot, P.; Youngblood, D. S.; Wu, R. P.; Iversen, P. L.; Lebleu, B. Vectorization of morpholino oligomers by the (R-Ahx-R)$_4$ peptide allows efficient splicing correction in the absence of endosomolytic agents. *Journal of Controlled Release* **2006,** *116*, 304-313.

26.   Moulton, H.; Moulton, J. Morpholinos and their peptide conjugates: therapeutic promise and challenge for Duchenne muscular dystrophy. *Biochimica et*

Biophysica acta **2010,** *1798*, 2296-2303.

27. Ziegler, A. Thermodynamic studies and binding mechanisms of cell-penetrating peptides with lipids and glycosaminoglycans. *Advanced Drug Delivery Reviews* **2008,** *60*, 580-597.

28. Magzoub, M.; Gräslund, A. Cell-penetrating peptides: small from inception to application. *Quarterly Reviews of Biophysics* **2004,** *37*, 147-195.

29. Elmquist, A.; Lindgren, M.; Bartfai, T.; Langel, Ü. VE-Cadherin-Derived Cell-Penetrating Peptide, pVEC, with Carrier Functions. *Experimental Cell Research* **2001,** *269*, 237-244.

30. El-Andaloussi, S.; Johansson, H.; Holm, T.; Langel, U. A novel cell-penetrating peptide, M918, for efficient delivery of proteins and peptide nucleic acids. *Molecular Therapy : the Journal of the American Society of Gene Therapy* **2007,** *15*, 1820-1826.

31. (a) Conner, S.; Schmid, S. Regulated portals of entry into the cell. *Nature* **2003,** *422*, 37-44. (b) Mayor, S.; Pagano, R. Pathways of clathrin-independent endocytosis. *Nature reviews. Molecular Cell Biology* **2007,** *8*, 603-612. (c) Duchardt, F.; Fotin-Mleczek, M.; Schwarz, H.; Fischer, R.; Brock, R. A comprehensive model for the cellular uptake of cationic cell-penetrating peptides. *Traffic (Copenhagen, Denmark)* **2007,** *8*, 848-866. (d) Fischer, R.; Fotin-Mleczek, M.; Hufnagel, H.; Brock, R. Break on through to the other side-biophysics and cell biology shed light on cell-penetrating peptides. *ChemBioChem* **2005,** *6*, 2126-2142.

32. Nakase, I.; Akita, H.; Kogure, K.; Gräslund, A.; Langel, Ü.; Harashima, H.; Futaki, S. Efficient Intracellular Delivery of Nucleic Acid Pharmaceuticals Using Cell-Penetrating Peptides. *Accounts of Chemical Research* **2011,** *45*, 1132-1139.

33. Sara, T.; Ana Luísa, C.; Miguel, M.; Maria, C. P. d. L. Cell-Penetrating Peptides—Mechanisms of Cellular Uptake and Generation of Delivery Systems. *Pharmaceuticals* **2010,** *3*.

34. Fittipaldi, A.; Ferrari, A.; Zoppé, M.; Arcangeli, C.; Pellegrini, V.; Beltram, F.; Giacca, M. Cell Membrane Lipid Rafts Mediate Caveolar Endocytosis of HIV-1 Tat Fusion Proteins. *Journal of Biological Chemistry* **2003,** *278*, 34141-34149.

35. (a) Wadia, J.; Stan, R.; Dowdy, S. Transducible TAT-HA fusogenic peptide enhances escape of TAT-fusion proteins after lipid raft macropinocytosis. *Nature Medicine* **2004,** *10*, 310-315. (b) Kaplan, I.; Wadia, J.; Dowdy, S. Cationic TAT peptide transduction domain enters cells by macropinocytosis. *Journal of Controlled Release* **2005,** *102*, 247-253.

36. Richard, J. P.; Melikov, K.; Brooks, H.; Prevot, P.; Lebleu, B.; Chernomordik, L. V. Cellular Uptake of Unconjugated TAT Peptide Involves Clathrin-dependent Endocytosis and Heparan Sulfate Receptors. *Journal of Biological Chemistry* **2005,** *280*, 15300-15306.

37. (a) Lundberg, M.; Johansson, M. Is VP22 nuclear homing an artifact? *Nature Biotechnology* **2001** *19*, 713-4. (b) Richard, J. P.; Melikov, K.; Vives, E.; Ramos, C.; Verbeure, B.; Gait, M. J.; Chernomordik, L. V.; Lebleu, B. Cell-penetrating Peptides: a reevaluation of the mechanism of cellular uptake. *Journal of Biological Chemistry* **2003,** *278*, 585-590.

38. Derossi, D.; Calvet, S.; Trembleau, A.; Brunissen, A.; Chassaing, G.; Prochiantz, A. Cell Internalization of the Third Helix of the Antennapedia Homeodomain Is Receptor-independent. *Journal of Biological Chemistry* **1996,** *271*, 18188-18193.

39. Matsuzaki, K.; Yoneyama, S.; Murase, O.; Miyajima, K. Transbilayer Transport of Ions and Lipids Coupled with Mastoparan X Translocation. *Biochemistry* **1996,** *35*, 8450-8456.

40. Pouny, Y.; Rapaport, D.; Mor, A.; Nicolas, P.; Shai, Y. Interaction of antimicrobial dermaseptin and its fluorescently labeled analogs with phospholipid membranes. *Biochemistry* **1992,** *31*, 12416-12423.

41. Lee, M.-T.; Hung, W.-C.; Chen, F.-Y.; Huang, H. W. Many-Body Effect of Antimicrobial Peptides: On the Correlation Between Lipid's Spontaneous Curvature and Pore Formation. *Biophysical Journal* **2005,** *89*, 4006-4016.

42. (a) Tyagi, M.; Rusnati, M.; Presta, M.; Giacca, M. Internalization of HIV-1 Tat Requires Cell Surface Heparan Sulfate Proteoglycans. *Journal of Biological Chemistry* **2001,** *276*, 3254-3261. (b) Nakase, I.; Tadokoro, A.; Kawabata, N.; Takeuchi, T.; Katoh, H.; Hiramoto, K.; Negishi, M.; Nomizu, M.; Sugiura, Y.; Futaki, S. Interaction of Arginine-Rich Peptides with Membrane-Associated

Proteoglycans Is Crucial for Induction of Actin Organization and Macropinocytosis. *Biochemistry* **2006,** *46*, 492-501.

43.   (a) Silhol, M.; Tyagi, M.; Giacca, M.; Lebleu, B.; Vivès, E. Different mechanisms for cellular internalization of the HIV-1 Tat-derived cell penetrating peptide and recombinant proteins fused to Tat. *European Journal of Biochemistry* **2002,** *269*, 494-501. (b) Violini, S.; Sharma, V.; Prior, J. L.; Dyszlewski, M.; Piwnica-Worms, D. Evidence for a Plasma Membrane-Mediated Permeability Barrier to Tat Basic Domain in Well-Differentiated Epithelial Cells: Lack of Correlation with Heparan Sulfate. *Biochemistry* **2002,** *41*, 12652-12661.

44.   Gump, J. M.; June, R. K.; Dowdy, S. F. Revised Role of Glycosaminoglycans in TAT Protein Transduction Domain-mediated Cellular Transduction. *Journal of Biological Chemistry* **2010,** *285*, 1500-1507.

45.   Ziegler, A.; Seelig, J. Contributions of Glycosaminoglycan Binding and Clustering to the Biological Uptake of the Nonamphipathic Cell-Penetrating Peptide WR9. *Biochemistry* **2011,** *50*, 4650-4664.

46.   Huq, I.; Ping, Y.-H.; Tamilarasu, N.; Rana, T. M. Controlling Human Immunodeficiency Virus Type 1 Gene Expression by Unnatural Peptides. *Biochemistry* **1999,** *38*, 5172-5177.

47.   Mueller, J.; Kretzschmar, I.; Volkmer, R.; Boisguerin, P. Comparison of cellular uptake using 22 CPPs in 4 different cell lines. *Bioconjugate Chemistry* **2008,** *19*, 2363-2374.

48. Morris, M.; Vidal, P.; Chaloin, L.; Heitz, F.; Divita, G. A new peptide vector for efficient delivery of oligonucleotides into mammalian cells. *Nucleic Acids Research* **1997,** *25*, 2730-2736.

49.   (a) Lundin, P.; Johansson, H.; Guterstam, P.; Holm, T.; Hansen, M.; Langel, U.; El Andaloussi, S. Distinct uptake routes of cell-penetrating peptide conjugates. *Bioconjugate Chemistry* **2008,** *19*, 2535-2542. (b) Vives, E. Present and future of cell-penetrating peptide mediated delivery systems: "is the Trojan horse too wild to go only to Troy?". *Journal of Controlled Release* **2005,** *109*, 77-85.

50.   (a) Nakase, I.; Tadokoro, A.; Kawabata, N.; Takeuchi, T.; Katoh, H.; Hiramoto, K.; Negishi, M.; Nomizu, M.; Sugiura, Y.; Futaki, S. Interaction of arginine-rich

peptides with membrane-associated proteoglycans is crucial for induction of actin organization and macropinocytosis. *Biochemistry* **2007,** *46*, 492-501. (b) Ziegler, A.; Seelig, J. Binding and clustering of glycosaminoglycans: a common property of mono- and multivalent cell-penetrating compounds. *Biophysical Journal* **2008,** *94*, 2142-2149.

51. Gerbal-Chaloin, S.; Gondeau, C.; Aldrian-Herrada, G.; Heitz, F.; Gauthier-Rouvière, C.; Divita, G. First step of the cell-penetrating peptide mechanism involves Rac1 GTPase-dependent actin-network remodelling. *Biology of the cell / under the auspices of the European Cell Biology Organization* **2007,** *99*, 223-238.

52. (a) Nakamura, Y.; Kogure, K.; Futaki, S.; Harashima, H. Octaarginine-modified multifunctional envelope-type nano device for siRNA. *Journal of Controlled Release* **2007,** *119*, 360-367. (b)Eguchi, A.; Meade, B.; Chang, Y.-C.; Fredrickson, C.; Willert, K.; Puri, N.; Dowdy, S. Efficient siRNA delivery into primary cells by a peptide transduction domain-dsRNA binding domain fusion protein. *Nature biotechnology* **2009,** *27*, 567-571. (c) Tönges, L.; Lingor, P.; Egle, R.; Dietz, G.; Fahr, A.; Bähr, M. Stearylated octaarginine and artificial virus-like particles for transfection of siRNA into primary rat neurons. *RNA (New York, N.Y.)* **2006,** *12*, 1431-1438.

53. Mitchell, D. J.; Steinman, L.; Kim, D. T.; Fathman, C. G.; Rothbard, J. B. Polyarginine enters cells more efficiently than other polycationic homopolymers. *The Journal of Peptide Research* **2000,** *56*, 318-325.

54. Wender, P. A.; Mitchell, D. J.; Pattabiraman, K.; Pelkey, E. T.; Steinman, L.; Rothbard, J. B. The design, synthesis, and evaluation of molecules that enable or enhance cellular uptake: Peptoid molecular transporters. *Proceedings of the National Academy of Sciences* **2000,** *97*, 13003-13008.

55. Rothbard, J. B.; Jessop, T. C.; Lewis, R. S.; Murray, B. A.; Wender, P. A. Role of Membrane Potential and Hydrogen Bonding in the Mechanism of Translocation of Guanidinium-Rich Peptides into Cells. *Journal of the American Chemical Society* **2004,** *126*, 9506-9507.

56. Cho, C.; Moran, E.; Cherry, S.; Stephans, J.; Fodor, S.; Adams, C.; Sundaram, A.; Jacobs, J.; Schultz, P. An unnatural biopolymer. *Science (New York, N.Y.)* **1993,**

261, 1303-1305.

57. Charles, Y. C.; Youngquist, R. S.; Sari, J. P.; Maureen, H. B.; Andrea, R. H.; Lea, T. B.; Corey, W. L.; David, E. W.; Thomas, K.; Peter, G. S. Synthesis and Screening of Linear and Cyclic Oligocarbamate Libraries. Discovery of High Affinity Ligands for GPIIb/IIIa. *Journal of the American Chemical Society* **1998,** *120*.

58. Xilu, W.; Ikramul, H.; Tariq, M. R. HIV-1 TAR RNA Recognition by an Unnatural Biopolymer. *Journal of the American Chemical Society* **1997,** *119*.

59. Tamilarasu, N.; Huq, I.; Rana, T. Targeting RNA with peptidomimetic oligomers in human cells. *Bioorganic & Medicinal Chemistry Letters* **2001,** *11*, 505-507.

60. Chiu, Y.-L.; Ali, A.; Chu, C.-Y.; Cao, H.; Rana, T. Visualizing a correlation between siRNA localization, cellular uptake, and RNAi in living cells. *Chemistry & Biology* **2004,** *11*, 1165-1175.

61. Wender, P. A.; Rothbard, J. B.; Jessop, T. C.; Kreider, E. L.; Wylie, B. L. Oligocarbamate Molecular Transporters: Design, Synthesis, and Biological Evaluation of a New Class of Transporters for Drug Delivery. *Journal of the American Chemical Society* **2002,** *124*, 13382-13383.

62. Cooley, C.; Trantow, B.; Nederberg, F.; Kiesewetter, M.; Hedrick, J.; Waymouth, R.; Wender, P. Oligocarbonate molecular transporters: oligomerization-based syntheses and cell-penetrating studies. *Journal of the American Chemical Society* **2009,** *131*, 16401-16403.

63. Ma, Y.; Yang, D.; Ma, Y.; Zhang, Y.-H. Novel cell-penetrating peptides based on α-aminoxy acids. *ChemBiochem* **2012,** *13*, 73-79.

64. Unciti-Broceta, A.; Diezmann, F.; Ou-Yang, C. Y.; Fara, M. A.; Bradley, M. Synthesis, penetrability and intracellular targeting of fluorescein-tagged peptoids and peptide–peptoid hybrids. *Bioorganic & Medicinal Chemistry* **2009,** *17*, 959-966.

65. Murphy, J. E.; Uno, T.; Hamer, J. D.; Cohen, F. E.; Dwarki, V.; Zuckermann, R. N. A combinatorial approach to the discovery of efficient cationic peptoid reagents for gene delivery. *Proceedings of the National Academy of Sciences* **1998,** *95*, 1517-1522.

66. Schröder, T.; Niemeier, N.; Afonin, S.; Ulrich, A. S.; Krug, H. F.; Bräse, S. Peptoidic Amino- and Guanidinium-Carrier Systems: Targeted Drug Delivery into the Cell Cytosol or the Nucleus. *Journal of Medicinal Chemistry* **2008,** *51*, 376-379.

67. Foged, C.; Franzyk, H.; Bahrami, S.; Frokjaer, S.; Jaroszewski, J. W.; Nielsen, H. M.; Olsen, C. A. Cellular uptake and membrane-destabilising properties of α-peptide/β-peptoid chimeras: lessons for the design of new cell-penetrating peptides. *Biochimica et Biophysica Acta (BBA) - Biomembranes* **2008,** *1778*, 2487-2495.

68. Huang, W.; Seo, J.; Lin, J.; Barron, A. Peptoid transporters: effects of cationic, amphipathic structure on their cellular uptake. *Molecular BioSystems* **2012,** *8*, 2626-2628.

69. Rudat, B.; Birtalan, E.; Vollrath, S. B. L.; Fritz, D.; Kölmel, D. K.; Nieger, M.; Schepers, U.; Müllen, K.; Eisler, H.-J.; Lemmer, U.; Bräse, S. Photophysical properties of fluorescently-labeled peptoids. *European Journal of Medicinal Chemistry* **2011,** *46*, 4457-4465.

70. Tamilarasu, N.; Ikramul, H.; Tariq, M. R. High Affinity and Specific Binding of HIV-1 TAR RNA by a Tat-Derived Oligourea. *Journal of the American Chemical Society* **1999,** *121*.

71. Hamy, F.; Felder, E.; Heizmann, G.; Lazdins, J.; Aboul-ela, F.; Varani, G.; Karn, J.; Klimkait, T. An inhibitor of the Tat/TAR RNA interaction that effectively suppresses HIV-1 replication. *Proceedings of the National Academy of Sciences of the United States of America* **1997,** *94*, 3548-3553.

72. (a) Torchilin, V. P. Cell penetrating peptide-modified pharmaceutical nanocarriers for intracellular drug and gene delivery. *Peptide Science* **2008,** *90*, 604-610. (b) Gupta, B.; Levchenko, T. S.; Torchilin, V. P. Intracellular delivery of large molecules and small particles by cell-penetrating proteins and peptides. *Advanced Drug Delivery Reviews* **2005,** *57*, 637-651. (c) Hoyer, J.; Neundorf, I. Peptide Vectors for the Nonviral Delivery of Nucleic Acids. *Accounts of Chemical Research* **2012,** *45*, 1048-1056. (d) Tian, X.-h.; Wei, F.; Wang, T.-x.; Wang, D.; Wang, J.; Lin, X.-n.; Wang, P.; Ren, L. Blood–brain barrier transport of Tat

peptide and polyethylene glycol decorated gelatin–siloxane nanoparticle. *Materials Letters* **2012,** *68*, 94-96. (e)Giulio, S. Functionalization with TAT-Peptide Enhances Blood-Brain Barrier Crossing In vitro of Nanoliposomes Carrying a Curcumin-Derivative to Bind Amyloid-B Peptide. *Journal of Nanomedicine & Nanotechnology* **2013,** *04*.

73.   El-Sayed, A.; Futaki, S.; Harashima, H. Delivery of Macromolecules Using Arginine-Rich Cell-Penetrating Peptides: Ways to Overcome Endosomal Entrapment. *The AAPS Journal* **2009,** *11*, 13-22.

74.   Trabulo, S.; Cardoso, A. L.; Mano, M.; De Lima, M. C. P. Cell-Penetrating Peptides—Mechanisms of Cellular Uptake and Generation of Delivery Systems. *Pharmaceuticals* **2010,** *3*, 961-993.

75.   Laufer, S.; Recke, A.; Veldhoen, S.; Trampe, A.; Restle, T. Noncovalent peptide-mediated delivery of chemically modified steric block oligonucleotides promotes splice correction: quantitative analysis of uptake and biological effect. *Oligonucleotides* **2009,** *19*, 63-80.

76. (a) Gogoi, K.; Mane, M. V.; Kunte, S. S.; Kumar, V. A. A versatile method for the preparation of conjugates of peptides with DNA/PNA/analog by employing chemo-selective click reaction in water. *Nucleic Acids Research* **2007**, *35* (b) Oehlke, J.; Wallukat, G.; Wolf, Y.; Ehrlich, A.; Wiesner, B.; Berger, H.; Bienert, M. Enhancement of intracellular concentration and biological activity of PNA after conjugation with a cell-penetrating synthetic model peptide. *European Journal of Biochemistry / FEBS* **2004,** *271*, 3043-3049.

77.   Guo, Q.; Wang, H.; Zhao, Y.; Wang, H.; Zeng, F.; Hua, H.; Xu, Q.; Huang, Y. Cell-penetrating albumin conjugates for enhanced doxorubicin delivery. *Polymer Chemistry* **2013,** *4*, 4584-4587.

78.   Zhang, Q.; Tang, J.; Fu, L.; Ran, R.; Liu, Y.; Yuan, M.; He, Q. A pH-responsive α-helical cell penetrating peptide-mediated liposomal delivery system. *Biomaterials* **2013,** *34*, 7980-7993.

79.   Montrose, K.; Yang, Y.; Sun, X.; Wiles, S.; Krissansen, G. Xentry, a new class of cell-penetrating peptide uniquely equipped for delivery of drugs. *Scientific Reports* **2013,** *3*, 1661.

80. Danielsson, J.; Inomata, K.; Murayama, S.; Tochio, H.; Lang, L.; Shirakawa, M.; Oliveberg, M. Pruning the ALS-Associated Protein SOD1 for in-Cell NMR. *Journal of the American Chemical Society* **2013,** *135*, 10266-10269.

81. Zhang, P.; Cheetham, A. G.; Lin, Y.-a.; Cui, H. Self-Assembled Tat Nanofibers as Effective Drug Carrier and Transporter. *ACS Nano* **2013,** *7*, 5965-5977.

82. Boisguerin, P.; Redt-Clouet, C.; Franck-Miclo, A.; Licheheb, S.; Nargeot, J.; Barrère-Lemaire, S.; Lebleu, B. Systemic delivery of BH4 anti-apoptotic peptide using CPPs prevents cardiac ischemia–reperfusion injuries in vivo. *Journal of Controlled Release* **2011,** *156*, 146-153.

83. Suhorutsenko, J.; Oskolkov, N.; Arukuusk, P.; Kurrikoff, K.; Eriste, E.; Copolovici, D.-M.; Langel, Ü. Cell-Penetrating Peptides, PepFects, Show No Evidence of Toxicity and Immunogenicity In Vitro and In Vivo. *Bioconjugate Chemistry* **2011,** *22*, 2255-2262.

84. Du, L.; Kayali, R.; Bertoni, C.; Fike, F.; Hu, H.; Iversen, P.; Gatti, R. Arginine-rich cell-penetrating peptide dramatically enhances AMO-mediated ATM aberrant splicing correction and enables delivery to brain and cerebellum. *Human Molecular Genetics* **2011,** *20*, 3151-3160.

85. Nasrolahi Shirazi, A.; Tiwari, R.; Chhikara, B. S.; Mandal, D.; Parang, K. Design and Biological Evaluation of Cell-Penetrating Peptide–Doxorubicin Conjugates as Prodrugs. *Molecular Pharmaceutics* **2013,** *10*, 488-499.

86. Bagnacani, V.; Franceschi, V.; Bassi, M.; Lomazzi, M.; Donofrio, G.; Sansone, F.; Casnati, A.; Ungaro, R. Arginine clustering on calix[4]arene macrocycles for improved cell penetration and DNA delivery. *Nature Communications* **2013,** *4*, 1721.

87. Zhang, W.; Song, J.; Liang, R.; Zheng, X.; Chen, J.; Li, G.; Zhang, B.; Wang, K.; Yan, X.; Wang, R. Stearylated antimicrobial peptide [D]-K6L9 with cell penetrating property for efficient gene transfer. *Peptides* **2013,** *46*, 33-39.

88. Pärn, K.; Viru, L.; Lehto, T.; Oskolkov, N.; Langel, Ü.; Merits, A. Transfection of Infectious RNA and DNA/RNA Layered Vectors of Semliki Forest Virus by the Cell-Penetrating Peptide Based Reagent PepFect6. *PLoS ONE* **2013,** *8*, e69659.

89. Nasrolahi Shirazi, A.; Tiwari, R. K.; Oh, D.; Sullivan, B.; McCaffrey, K.; Mandal,

D.; Parang, K. Surface Decorated Gold Nanoparticles by Linear and Cyclic Peptides as Molecular Transporters. *Molecular Pharmaceutics* **2013,** *10*, 3137-3151.

90. Lehto, T.; Abes, R.; Oskolkov, N.; Suhorutšenko, J.; Copolovici, D.-M.; Mäger, I.; Viola, J. R.; Simonson, O. E.; Ezzat, K.; Guterstam, P.; Eriste, E.; Smith, C. I. E.; Lebleu, B.; Samir, E. L. A.; Langel, Ü. Delivery of nucleic acids with a stearylated (RxR)4 peptide using a non-covalent co-incubation strategy. *Journal of Controlled Release* **2010,** *141*, 42-51.

91. Mandal, D.; Nasrolahi Shirazi, A.; Parang, K. Cell-Penetrating Homochiral Cyclic Peptides as Nuclear-Targeting Molecular Transporters. *Angewandte Chemie International Edition* **2011,** *50*, 9633-9637.

92. Lee, S.-A.; Kim, B.-R.; Kim, B.-K.; Kim, D.-W.; Shon, W.-J.; Lee, N.-R.; Inn, K.-S.; Kim, B.-J. Heat shock protein-mediated cell penetration and cytosolic delivery of macromolecules by a telomerase-derived peptide vaccine. *Biomaterials* **2013,** *34*, 7495-7505.

93. Patil, K. M.; Naik, R. J.; Rajpal; Fernandes, M.; Ganguli, M.; Kumar, V. A. Highly Efficient (R-X-R)-Type Carbamates as Molecular Transporters for Cellular Delivery. *Journal of the American Chemical Society* **2012,** *134*, 7196-7199.

94. Rothbard, J. B.; Kreider, E.; VanDeusen, C. L.; Wright, L.; Wylie, B. L.; Wender, P. A. Arginine-Rich Molecular Transporters for Drug Delivery: Role of Backbone Spacing in Cellular Uptake. *Journal of Medicinal Chemistry* **2002,** *45*, 3612-3618.

95. Menjoge, A.; Kannan, R.; Tomalia, D. Dendrimer-based drug and imaging conjugates: design considerations for nanomedical applications. *Drug Discovery Today* **2010,** *15*, 171-185.

96. Singh, P.; Gupta, U.; Asthana, A.; Jain, N. K. Folate and Folate−PEG−PAMAM Dendrimers: Synthesis, Characterization, and Targeted Anticancer Drug Delivery Potential in Tumor Bearing Mice. *Bioconjugate Chemistry* **2008,** *19*, 2239-2252.

97. Waite, C. L.; Roth, C. M. PAMAM-RGD Conjugates Enhance siRNA Delivery Through a Multicellular Spheroid Model of Malignant Glioma. *Bioconjugate Chemistry* **2009,** *20*, 1908-1916.

98. Wängler, C.; Moldenhauer, G.; Eisenhut, M.; Haberkorn, U.; Mier, W.

Antibody−Dendrimer Conjugates: The Number, Not the Size of the Dendrimers, Determines the Immunoreactivity. *Bioconjugate Chemistry* **2008,** *19*, 813-820.

99. Wan, T.; Tosh, D.; Du, L.; Gizewski, E.; Jacobson, K.; Auchampach, J. Polyamidoamine (PAMAM) dendrimer conjugate specifically activates the A3 adenosine receptor to improve post-ischemic/reperfusion function in isolated mouse hearts. *BMC Pharmacology* **2011,** *11*, 11.

100. Wender, P. A.; Kreider, E.; Pelkey, E. T.; Rothbard, J.; VanDeusen, C. L. Dendrimeric Molecular Transporters: Synthesis and Evaluation of Tunable Polyguanidino Dendrimers That Facilitate Cellular Uptake. *Organic Letters* **2005,** *7*, 4815-4818.

101. Futaki, S.; Nakase, I.; Suzuki, T.; Youjun, Z.; Sugiura, Y. Translocation of branched-chain arginine peptides through cell membranes: flexibility in the spatial disposition of positive charges in membrane-permeable peptides. *Biochemistry* **2002,** *41*, 7925-7930.

102. Chung, H.-H.; Harms, G.; Seong, C.; Choi, B.; Min, C.; Taulane, J.; Goodman, M. Dendritic oligoguanidines as intracellular translocators. *Biopolymers* **2004,** *76*, 83-96.

103. Huang, K.; Voss, B.; Kumar, D.; Hamm, H.; Harth, E. Dendritic molecular transporters provide control of delivery to intracellular compartments. *Bioconjugate Chemistry* **2007,** *18*, 403-409.

104. Hong, S.; Bielinska, A. U.; Mecke, A.; Keszler, B.; Beals, J. L.; Shi, X.; Balogh, L.; Orr, B. G.; Baker, J. R.; Banaszak Holl, M. M. Interaction of Poly(amidoamine) Dendrimers with Supported Lipid Bilayers and Cells: Hole Formation and the Relation to Transport. *Bioconjugate Chemistry* **2004,** *15*, 774-782.

105. Li, S.; Goins, B.; Zhang, L.; Bao, A. Novel Multifunctional Theranostic Liposome Drug Delivery System: Construction, Characterization, and Multimodality MR, Near-Infrared Fluorescent, and Nuclear Imaging. *Bioconjugate Chemistry* **2012,** *23*, 1322-1332.

106. Nallamothu, R.; Wood, G.; Pattillo, C.; Scott, R.; Kiani, M.; Moore, B.; Thoma, L. A tumor vasculature targeted liposome delivery system for combretastatin A4:

design, characterization, and in vitro evaluation. *AAPS PharmSciTech* **2006,** *7*.

107. Immordino, M.; Dosio, F.; Cattel, L. Stealth liposomes: review of the basic science, rationale, and clinical applications, existing and potential. *International Journal of Nanomedicine* **2006,** *1*, 297-315.

108. Akbarzadeh, A.; Rezaei-Sadabady, R.; Davaran, S.; Joo, S.; Zarghami, N.; Hanifehpour, Y.; Samiei, M.; Kouhi, M.; Nejati-Koshki, K. Liposome: classification, preparation, and applications. *Nanoscale Research Letters* **2013,** *8*, 102.

109. Miyano-Kurosaki, N.; Barnor, J.; Takeuchi, H.; Owada, T.; Nakashima, H.; Yamamoto, N.; Matsuzaki, T.; Shimada, F.; Takaku, H. In vitro and in vivo transport and delivery of phosphorothioate oligonucleotides with cationic liposomes. *Antiviral Chemistry & Chemotherapy* **2004,** *15*, 93-100.

110. Chang, H.-I.; Yeh, M.-K. Clinical development of liposome-based drugs: formulation, characterization, and therapeutic efficacy. *International Journal of Nanomedicine* **2012,** *7*, 49-60.

111. Mufamadi, M.; Pillay, V.; Choonara, Y.; Du Toit, L.; Modi, G.; Naidoo, D.; Ndesendo, V. A review on composite liposomal technologies for specialized drug delivery. *Journal of Drug Delivery* **2011,** *2011*, 939851.

CHAPTER 2

Design and Synthesis of Proline/Hydroxy-proline Derived Monomers, Peptides and Their Biological Evaluation

Literature reported (R-Ahx-R)₄ peptide

Modifications

Section A
Constrained Lys/Arg analogue

Section B
Constrained spacer analogue
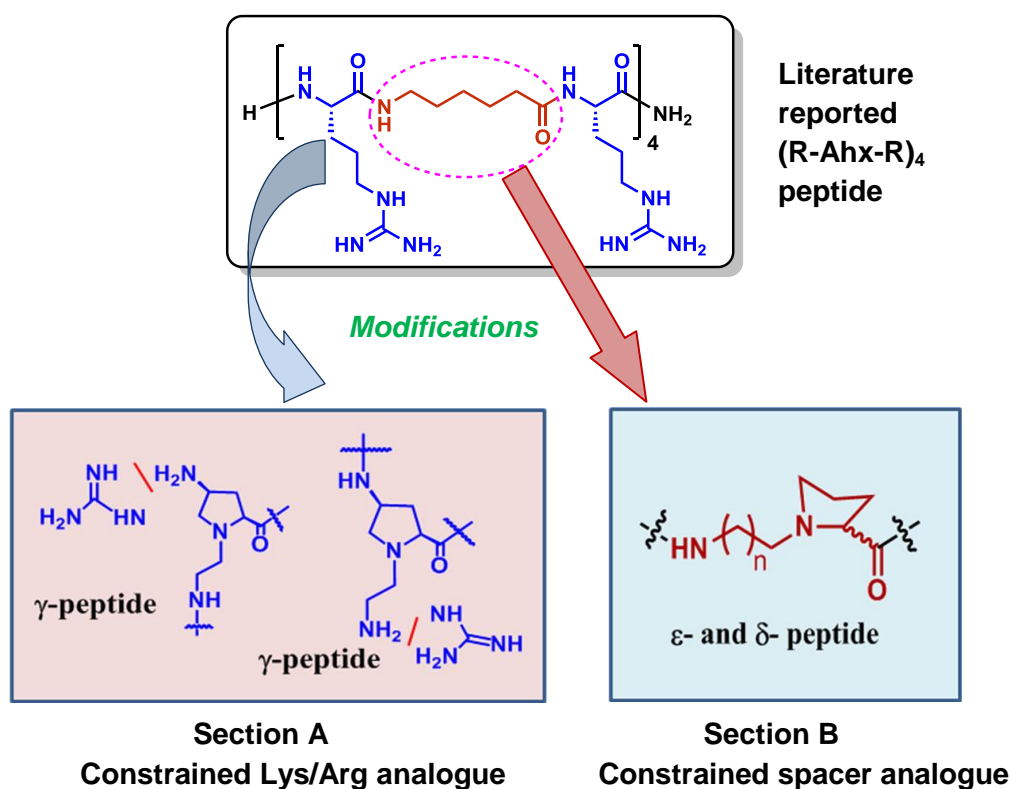
Proline-rich cell penetrating peptides (CPPs) were found to be useful in drug delivery applications. Many scaffolds of proline and 4-hydroxy proline containing peptides have been synthesized in literature. In Section A of this chapter, we have designed and synthesized a novel amino acid analogue derived from trans-4-hydroxy-L-proline with the synergistic property of proline/lysine or proline/arginine units. This analogue was included in peptides and a cell uptake property of synthesized peptides was studied in cells by FACS analysis. In section B, we have designed, synthesized and shown the applicability of chiral N-aminoalkyl proline-derived spacers in polycationic (R-X-R)-motif CPPs. Their cellular uptake property was studied by FACS and confocal microscopy analysis and pDNA delivery to cells was investigated.

Section 2A: Synthesis of *trans*-4-hydroxy-L-proline-derived orthogonally protected monomer, peptides and their cell uptake studies

2A.1 Introduction

In the past several years, numerous Cell-Penetrating Oligomers (CPOs) have been identified and evaluated as successful drug delivery agents, including Cell-Penetrating Peptides (CPPs). CPOs are proposed to be non-toxic and efficient drug delivery agents and proved to be alternatives to other approaches such as viral vectors,[1] electroporation,[2] metal-nanoparticle formulation,[3] liposomes,[4] polymeric encapsulation of drugs,[5] etc. These other approaches have a number of limitations such as inefficient drug delivery, high variability of drug expression among target cells, cellular damage and toxicity, and restrictions based upon drug and cell type.[6] Among the well-studied and applied CPPs, tat, Penetratin, oligoarginine, oligolysine, (R-X-R)-type (where 'R' is arginine and 'X' is natural or unnatural spacer amino acid) peptides and proline-rich peptides have exhibited good cell uptake properties.

CPPs containing natural amino acids are prone to proteolytic cleavage and thus have limitations for *in vivo* application. Several efforts have been made to overcome this drawback such as use of non-natural analogues of amino acids (e.g., D-amino acids) in the synthesis of oligomers,[7] incorporation of unnatural or modified amino acids or even replacement of peptide bonds by other linkages.

In the year 2000, Park and co-workers demonstrated that the proline hinge was responsible for the cell-penetrating ability of buforin II, a 21-amino acid-containing potent antimicrobial peptide.[8] Later, in 2002, Tama and co-workers showed that a 10-residue proline-rich peptide with two arginine residues was capable of delivering a noncovalent complex with protein into cells. Thus, the proline-rich peptides were found to be a potentially new class of cell-permeant peptides for intracellular delivery of protein cargo.[9] Farrera-Sinfreu *et al*. reported a synthetic method for the preparation of new class of foldamers containing conformationally constrained γ-peptides derived from γ-amino-L-proline.[10] Giralt and co-workers later designed and synthesized a new family of peptides based on the amphipathic proline-rich sequence (VXLPPP)*n*, where *n*=1−3 and X=His, Lys, or Arg, and showed their potential application as drug

carriers.[11] A family of peptide dendrimers based on polyproline helices and *cis*-4-amino-L-proline as a branching unit has also been reported by Giralt and co-workers, which showed the capability to enter rat kidney cells.[12]
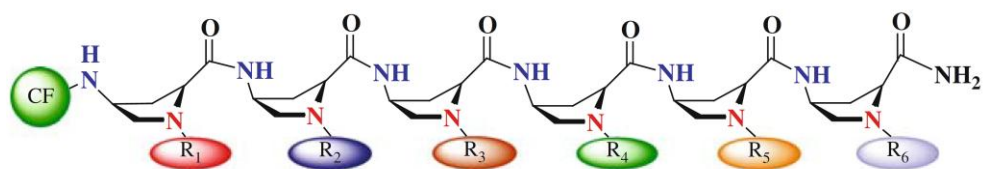
Figure 2.1 General structure of reported *cis*-γ-amino-L-proline oligomers where, R_1-R_6 are H atom, alkyl or guanidine groups.[13]

One of the most important advantages of proline-rich peptides enabling their application in biological systems is their solubility in water. Non-natural proline-derived γ-peptide, from *cis*- γ-amino-L-proline, was found to adopt a secondary structure in solution.[10] In 2005, Farrera-Sinfreu *et al.* reported the synthesis of three different γ-peptide families, N^α-acyl-γ-peptides (polyamides on the side chains), N^α-alkyl-γ-peptides (polyamines on the side chains), and N^α-guanidinylated-γ-peptides (Figure 2.1). They also reported polyethylene glycol-attached γ-peptides to monitor their amphipathicity and water solubility. In addition, these peptides were designed to have differences in amphipathicity by variations in the side-chain at the nitrogen atom of the pyrrolidine ring. Further, these peptides were evaluated for cell-uptake studies in COS-1 and HeLa cells, and these unnatural short length peptides were found to be advantageous over the well-known cell-penetrating 'tat' peptide in being less toxic and more protease-resistant.[13] Subsequently, many literature reports showed the importance of proline and its analogues in oligomers for drug delivery applications.[14]

In 2002, Ishiguro and co-workers synthesized (2*S*, 4*S*)- and (2*S*,4*R*)-4-(2′-guanidinoethyl)proline as a conformationally restricted arginine (Figure 2.2). Their backbones fit the i + 1 position in a turn, and the side chains are restricted compared to that of arginine. Later, these analogues were incorporated into mini atrial natriuretic polypeptide, which has an important turn-like conformation at Gly6-Arg7-Met8-Asp9 (number shows position of amino acid). Structural analysis revealed that the size of the conformational space of Arg7 on binding to the receptor was approximately one-third of

the entire conformational space. However, these monomers or monomer-containing peptides have not been used in cell uptake studies.[15]
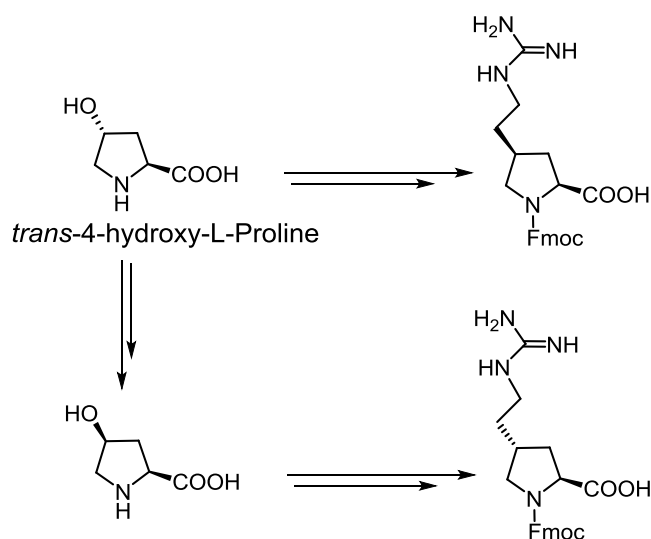
Figure 2.2 Literature reported *trans*-4-hydroxy-L-proline derived modified amino acid.

2A.2 Rationale, design and objectives of the present work

Synthetic peptides such as polyarginine, polylysine and polyproline, have shown potential cell-penetrating ability and are finding large application as delivery systems of biologically relevant cargo. Such peptides rich in basic residues such as lysine and/or arginine are able to efficiently condense DNA into small, compact particles that can be stabilized in serum. Oligoarginine containing non-α-aminoacids have proven superior to oligoarginine alone, and were developed to overcome the problem of endosomal entrapment. CPPs containing 6-aminohexanoic acid (X), β-alanine (B) or unnatural amino acid spacers were more stable in human serum than tat or oligoarginine peptides and efficient in cargo dellivery.[16] Recently, (RX)-type or (R-X-R)-type of CPPs[17] were found to be good candidates to cargo across cell membranes and significantly avoid the problem of endosomal entrapment, releasing the cargo in the cytoplasm. Moreover, these peptides were less cytotoxic compared to their parent polyarginine derivatives.

In this section, our aim was to design and synthesize a *trans*-4-hydroxy-L-proline-derived-monomer, as a conformationally restricted analogue of lysine or arginine. Due to the presence of the pyrrolidinyl ring and the flexible side-chain at the ring nitrogen atom in designed monomer, it might be possible to optimize the flexibility

and conformational restriction of the resulting peptides. We envisioned the synergistic properties of lysine/proline and arginine/proline units in designed orthogonally protected monomer (Figure 2.3). This monomer has a flexible aminoethyl group attached through the secondary nitrogen atom of the pyrrolidine ring. This secondary nitrogen atom may help to maintain hydrophobic/hydrophilic balanced in the peptide chain. This increased cationic charge could help to improve the cellular uptake efficiency. This monomer unit has two amino functionalities capable of peptide bond formation, which are protected orthogonally (Boc and Fmoc). This monomer thus has potential to be used in solid phase peptide synthesis employing either chemistry (Figure 2.3) to construct a library of novel CPPs.
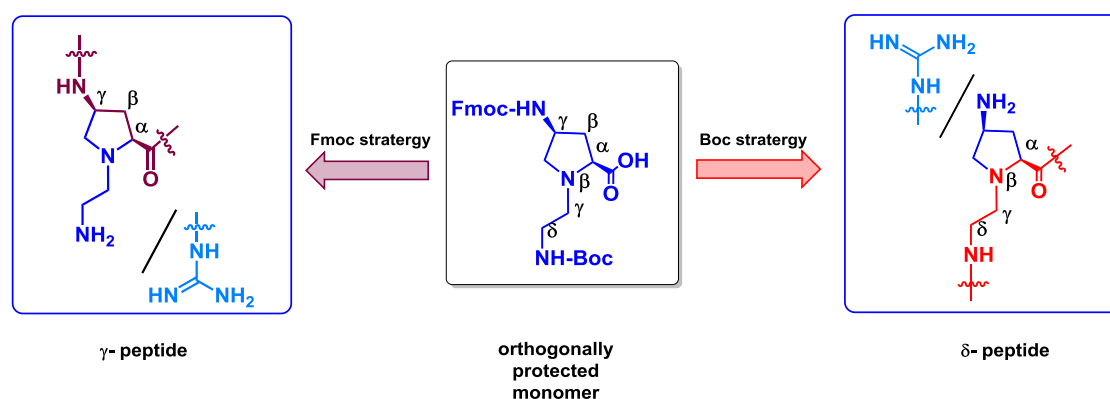
Figure 2.3 Schematic presentation of γ- and δ-peptides derived from single orthogonally protected monomer unit.

We further planned to incorporate the designed monomer in desired peptide sequences with and without spacer moiety. According to literature reports, peptides containing 6-8 amino or guanidino functional groups are optimal and exhibit good cellular uptake. Incorporation of spacer moieties such as 6-amino hexanoic acid could further improve their cell uptake efficiency.[18] Accordingly, we synthesized a heptapeptide (without spacer moiety) and 13-mer peptide (including spacers) sequences containing our newly designed monomer units. These peptides have free pendant amino functionalities attached on either flexible side chain of carbon or positioned on the pyrrolidinyl ring of the designed monomer (Figure 2.3). Further conversion of these pendant amino groups to guanidino groups could be achieved on the solid support itself, to get guanidinylated peptides. The synthesized peptide sequences could be end-labeled

(*N*-terminal) with carboxyfluorescein (*cf*) as a fluorescence tag to study their cellular uptake efficiency.

The planned peptides were designed to compare the impact of amino or guanidino functionality on the cell uptake efficiency. At the same time, the effect of the position where these functionalities are attached to the pyrrolidinyl ring (on flexible side chain or directly to pyrrolidinyl ring) would also be examined. Incorporation of 6-aminohexanoic acid as a spacer moiety was planned to modulate the space between adjacent amino or guanidino functionalities and to amend the amphipathcity in designed peptides.

The control heptapeptide made up of α-L-arginine was also synthesized to compare with the newly synthesized γ-peptide (by Fmoc strategy synthesis without spacer moiety), δ-peptide (by Boc strategy synthesis without spacer moiety), γ, ε-peptide (by Fmoc strategy synthesis with spacer moiety), and δ, ε -peptide (by Boc strategy synthesis with spacer moiety).

2A.3 Synthesis, results and discussion

2A.3.1 Synthesis of monomer

The synthesis of desired monomer unit started from commercially available *trans*-4-hydroxy proline and using the synthesis strategy depicted in Scheme 2.1. Accordingly, the carboxylic acid group in the *trans*-4-hydroxy-L-proline **1** was converted to its corresponding methyl ester **2**, by refluxing with thionyl chloride in methanol. Compound **3** was derived from 2-amino ethanol **3a** in two steps- initially *N*-Boc protection to get compound **3b** and subsequently mesylation of free hydroxyl group in **3b** by using mesyl chloride in the presence of pyridine. The *N*-alkylation of compound **2** was carried out using synthesized *N*-Boc-*O*-mesyl derivative of amino ethanol **3** in the presence of triethyl amine and catalytic amount of DMAP. This reaction mixture was heated at 70°C for 6 h to obtain *N*-alkylated compound **4.**
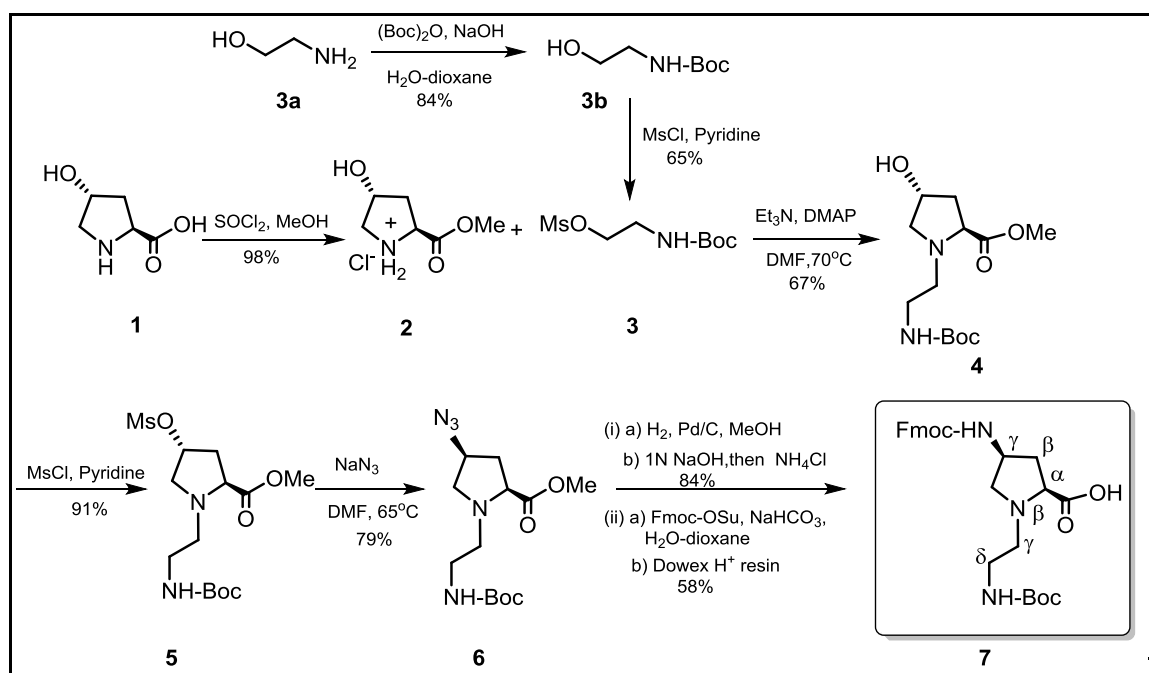
Scheme 2.1 Synthesis of orthogonally protected amino acid monomer.

The hydroxyl group at 4-position in compound **4** was converted to its mesylate by using mesyl chloride in pyridine. Further S_N2 displacement of the mesyl group was carried out by treatment of compound **5** with sodium azide in DMF, to get azido compound **6** with inverted stereochemistry at C-4 position. The azide group was further reduced to amine by hydrogenation in presence of Pd/C in methanol at 65psi hydrogen pressure. Subsequent hydrolysis of the resulting amino ester by treatment with 1N NaOH and neutralization by ammonium chloride furnish the corresponding amino acid. Further Fmoc-protection of the free amine was carried out using Fmoc-succinimide and NaHCO$_3$. Further acidification of the sodium salt of carboxylic acid by treatment with Dowex H$^+$ resin provided the orthogonally protected monomer **7**.

The monomer **7** was used in solid phase peptide synthesis using either Boc- or Fmoc-chemistry protocol to synthesize a library of designed novel cell-penetrating peptides.

2A.3.2 Solid phase peptide synthesis

2A.3.2a General principles of solid phase synthesis

In contrast to the solution phase method, the solid phase peptide synthesis (SPPS) strategy devised by Merrifield,[19] offers great advantages. In this method, the *C*-terminal amino acid is linked to an insoluble matrix such as polystyrene beads having reactive functional groups, which also act as a permanent protection for the carboxylic acid (Figure 2.4). The next N^{α}-protected amino acid can couple to the resin-bound amino acid either by using an active pentafluorophenyl (pfp) or 3-hydroxy-2, 3-dihydro-4-oxobenzotriazole (Dhbt) ester or by an *in situ* activation with available peptide coupling reagents along with HOBt and organic base such as DIPEA. Excess of all reagents along with protected amino acids is generally used to drive the reaction to completion (>95%). The unreacted reagents are then washed out and the deprotection, coupling reactions and washing cycles are repeated until the desired peptide is achieved. Hence the need of purification step after every amino acid attachment step is eliminated. Finally, the resin-bound peptide and the side chain protecting groups can be cleaved in a single step. Further, the resultant crude peptide can be purified to get the desired peptide.
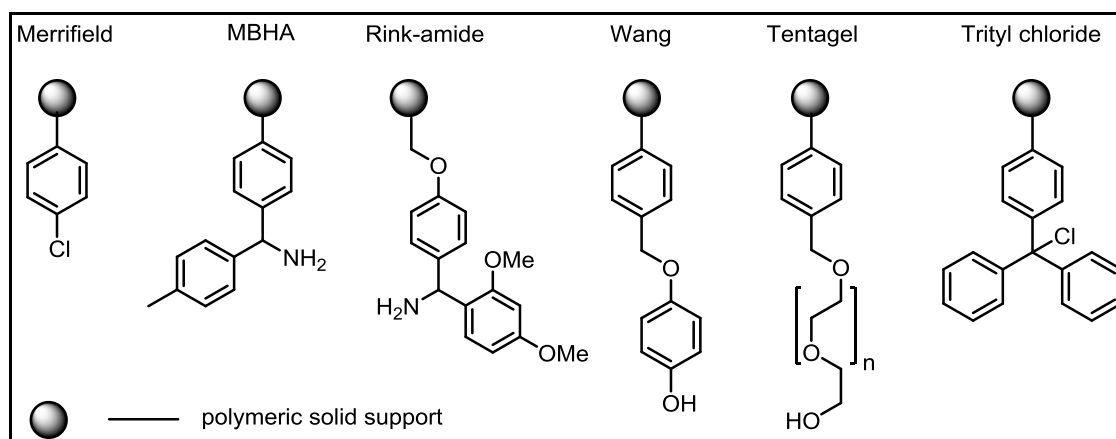
Figure 2.4 Few representative structures of functionalized resins used in SPPS.

       The advantages of solid phase synthesis are: (i) All the reactions are performed in a single vessel and will minimize the loss due to transfer, (ii) Large excess of carboxylic acid monomer and coupling reagents can be used to get high coupling

efficiency, (iii) Excess of reagents can be removed by simple filtration and washing steps and (iv) The method is amenable to automation and semi micro manipulation.

2A.3.2b Solid phase peptide synthesis of novel CPPs

All the peptide sequences (Table 2.1) were synthesized (Scheme 2.2 shows SPPS following the Boc- chemistry protocol) using standard Boc- or Fmoc- chemistry protocol and MBHA (4-methyl-benzyhdrylamine) resin as the solid support. Synthesis was carried out on 50μmol scale either manually or on an automated synthesizer (ABI 433A). Deprotection of the Boc- group was carried out in 50% TFA in CH_2Cl_2 followed by neutralization using 5% DIPEA in CH_2Cl_2. In case of Fmoc- chemistry protocol, the Fmoc group was removed in the presence of 20% piperidine in DMF. Further, coupling reactions were performed by use of three equivalents each of monomer amino acid, TBTU, HOBt and DIPEA in DMF for 6h. Successive deprotection, coupling and washing steps were carried out as iterative cycles (Scheme 2.2) until the desired length of peptide was synthesized. Deprotection and coupling reactions were monitored by the Kaiser test. To synthesize carboxyfluorescein-attached peptides, the final coupling was carried out in the presence of ten equivalents of 5(6)-carboxyfluorescein, HOBt, DIPCDI (Diisopropyl carbodiimide) in DMF overnight.
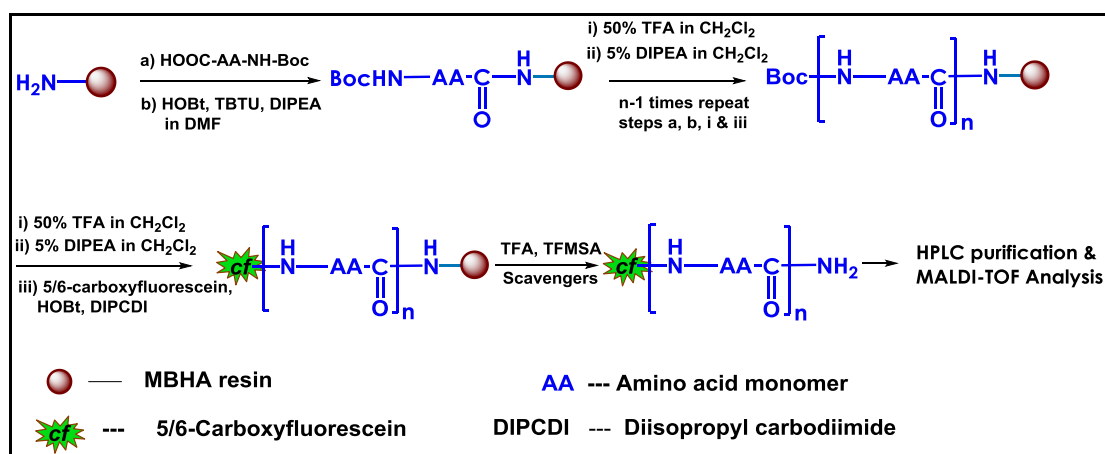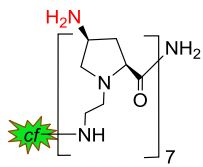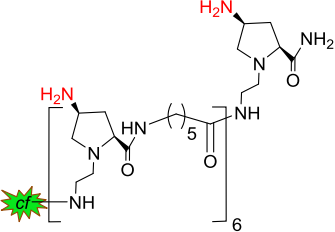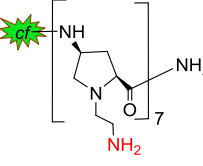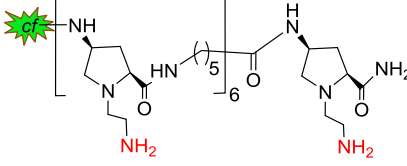
Scheme 2.2: SPPS by Boc-chemistry protocol.

2A.3.2c Cleavage and purification of resin bound peptide

After synthesis of the desired peptide sequences (Table 2.1), they were cleaved from the solid support by TFA-TFMSA cleavage protocol. In detail, 5 mg of dry peptide-bound resin was taken in glass sample vial (in the case of peptide sequences containing Fmoc as side chain protecting group, deprotection was done using 20% piperidine in DMF prior to peptide cleavage reaction). Scavengers, thioanisole (10 µL) and 1, 2-dithian (4 µL) were added to it. After 5 min., to the ice-cooled sample vial, 80 µL of TFA was added. After another 10 min., 8 µL of TFMSA was added with slow shaking and the resultant reaction mixture was kept for next 2 h to ensure removal of all the side chain-protecting groups and complete detachment of the peptide from the resin support. After 2h, the reaction mixture was filtered off through a sintered funnel and washed thrice with neat TFA, the collected filtrate in a pear-shaped flask was then evaporated on a rotary evaporator and cold ether was added to it. The formed precipitate was then separated by centrifugation and an appropriate amount of DI water was added to it. This crude peptide dissolved in DI water was further purified through C-18 column by RP-HPLC.

Table 2.1 Structure and code of synthesized peptides.[a]

Structure and Code	Structure and Code
[*cf*-(aePNH₂)₇ -NH₂] (**P1**)	[*cf*-(aePNH₂-Ahx)₆-Aaep-NH₂] (**P2**)
[*cf*-(AEPNH₂)₇ -NH₂] (**P3**)	[*cf*-(AEPNH₂-Ahx)₆ -AEPNH₂-NH₂] (**P4**)
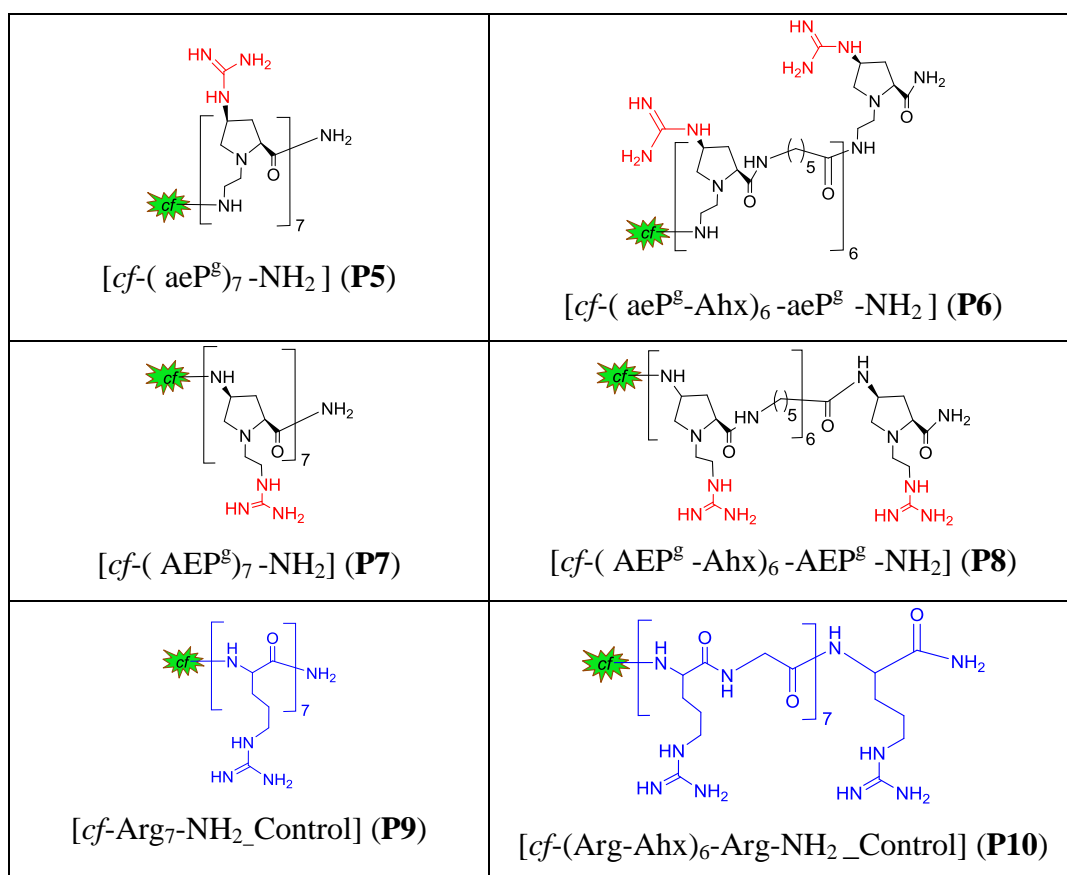
$[cf\text{-}(aeP^g)_7\text{-}NH_2]$ (**P5**)

$[cf\text{-}(aeP^g\text{-}Ahx)_6\text{-}aeP^g\text{-}NH_2]$ (**P6**)

$[cf\text{-}(AEP^g)_7\text{-}NH_2]$ (**P7**)

$[cf\text{-}(AEP^g\text{-}Ahx)_6\text{-}AEP^g\text{-}NH_2]$ (**P8**)

$[cf\text{-}Arg_7\text{-}NH_2\_Control]$ (**P9**)

$[cf\text{-}(Arg\text{-}Ahx)_6\text{-}Arg\text{-}NH_2\_Control]$ (**P10**)

[a]cf = 5(6)-carboxyfluorescein; Ahx = 6-aminohexanoic acid; Arg = L-Arginine; aeP^{NH_2} = (4-amino-(N-2-aminoethyl)prolyl); aeP^g = (4-guanidino-(N-2-aminoethyl)prolyl); AEP^{NH_2} = (N-2-aminoethyl)-4-aminoprolyl; AEP^g = (N-2-guanidinoethyl)-4-aminoprolyl)

aeP^NH2   **aeP^g**   **AEP^NH2**   **AEP^g**
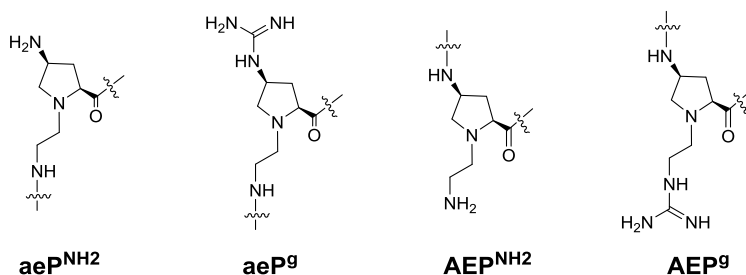
2A.3.3 Guanidinylation of pendant amines on solid and in solution phase

Global gunidinylation of pendant amino functionality in *cf*-labeled peptide sequences containing **aeP^NH2** ((4-amino-(*N*-2-aminoethyl)prolyl) and **AEP^NH2** ((*N*-2-aminoethyl)-4-aminoprolyl) moieties without and with spacer (**P1, P2** and **P3, P4** respectively) was attempted by reported procedure[20] and also by the procedure used in our laboratory for

the synthesis of guanidinylated Peptide Nucleic Acids (PNA).[21] In details, on the solid support, after desired length of peptide (**P1**, **P2**, **P3** and **P4**) synthesis, side chain amine protecting groups (Fmoc in case of **aeP^{NH2}** and Boc in case of **AEP^{NH2}**) were removed. Then the global guanidinylation of free amines was performed by using 10 equivalents of 1-*H*-pyrazole-1-carboxamidine hydrochloride reagent and 20 equivalents DIPEA (corresponding to each amino group) in DMF: THF (50:50 v/v) overnight. Further, the resin bound peptides were cleaved by TFA-TFMSA cleavage protocol. The fractions were collected from HPLC analysis and their masses were characterized by MALDI–TOF analysis. However, in our case, from MALDI analysis (showed in Table 2.2 **P5**, **P6**, **P7** and **P8**), the guanidinylation reaction was found incomplete.

Table 2.2 Synthesized peptides of study and their MALDI-TOF analysis.

Code	Sequence	Mass (MALDI-TOF)	
		Calcd.	Obsd.
P1	*cf*-(aeP^{NH2})$_7$-NH$_2$	1461.7	1461.7
P2	*cf*-(aeP^{NH2}-Ahx)$_6$-Aaep-NH$_2$	2139.3	2140.0, 2161.8
P3	*cf*-(AEP^{NH2})$_7$-NH$_2$	1461.7	1481.2
P4	*cf*-(AEP^{NH2}-Ahx)$_6$- AEP^{NH2}-NH$_2$	2139.3	2141.5
P5	*cf*-(aeP^g)$_7$-NH$_2$	1755.9	1767.9, 1710.02
P6	*cf*-(aeP^g-Ahx)$_6$ -aeP^g -NH$_2$	2433.4	2370.1, 2354.7
P7	*cf*-(AEP^g)$_7$ -NH$_2$	1755.9	1716.4, 1561.8
P8	*cf*-(AEP^g -Ahx)$_6$ -AEP^g -NH$_2$	2433.4	2238.7
P9	*Ccf*-(R)$_7$-NH$_2$_Control	1468.6	1469.9
P10	*cf*-(Arg-Ahx)$_6$-Arg-NH$_2$ _Control	2147.6	2145.2

[a]*cf* = 5(6)-carboxyfluorescein; Ahx = 6-aminohexanoic acid; Arg = L-Arginine; aeP^{NH2} = (4-amino-(*N*-2-aminoethyl)prolyl); aeP^g = (4-guanidino-(*N*-2-aminoethyl)prolyl); AEP^{NH2} = (*N*-2-aminoethyl)-4-aminoprolyl; AEP^g = (*N*-2-guanidinoethyl)-4-aminoprolyl).

In another attempt, solution phase guanidinylation was undertaken. In details, *cf*-labeled peptide sequences containing **aeP^{NH2}** ((4-amino-(*N*-2-aminoethyl)prolyl) and **AEP^{NH2}** ((*N*-2-aminoethyl)-4-aminoprolyl) moieties without and with spacers (**P1**, **P2** and **P3**, **P4** respectively) were cleaved from the resin and purified by HPLC and characterized by MALDI. The purified dry samples, of known concentration, of these peptides was resuspended in water: MeOH (20: 80 v/v) and to that DIPEA (20 equi./free amino group) was added, after stirring for 15min. the 1-*H*-pyrazole-1-carboxamidine hydrochloride reagent (10 equi./ free amino group) was added and stirred the reaction mixture overnight. The reaction mixture was further purified by HPLC and the separated fractions were characterized by MALDI-TOF analysis. Unfortunately, in this case also we observed partially guanidinylated peptides, their MALDI-TOF characterization is summarized in Table 2.2.

In the present case, the reason for incomplete guanidinylation was not fully understood, but it may be the conformational restriction added by pyrrolidinyl ring in designed monomer unit and hence the reactive free amines were not fully exposed to react with the guanidinylating reagent used. It was concluded that the different guanidinylating reagent and different reaction conditions may needed to achieve complete guanidinylation of synthesized peptides.

2A.3.4 Fluorescence-Activated Cell Sorting (FACS) analysis

2A.3.4a General principle of FACS analysis

Fluorescence-activated cell sorting (FACS) is a specialized type of flow cytometry. It provides a method for sorting a heterogeneous mixture of biological cells into two or more containers, one cell at a time, based upon the specific light scattering and fluorescence characteristics of each cell. It is a useful scientific instrument, as it provides fast, objective and quantitative recording of fluorescence signals from individual cells as well as physical separation of cells of particular interest.

The cell suspension is entrained in the center of a narrow, rapidly flowing stream of liquid. The flow is arranged so that there is a large separation between cells relative to their diameter. A vibrating mechanism causes the stream of cells to break into individual droplets. The system is adjusted so that there is a low probability of more

than one cell per droplet. Just before the stream breaks into droplets, the flow passes through a fluorescence measuring station where the fluorescence character of interest of each cell is measured. An electrical charging ring is placed just at the point where the stream breaks into droplets. A charge is placed on the ring based on the immediately prior fluorescence intensity measurement in the form of light signal, and the opposite charge is trapped on the droplet as it breaks from the stream. The charged droplets then fall through an electrostatic deflection system that diverts droplets into containers based upon their charge (Figure 2.5).
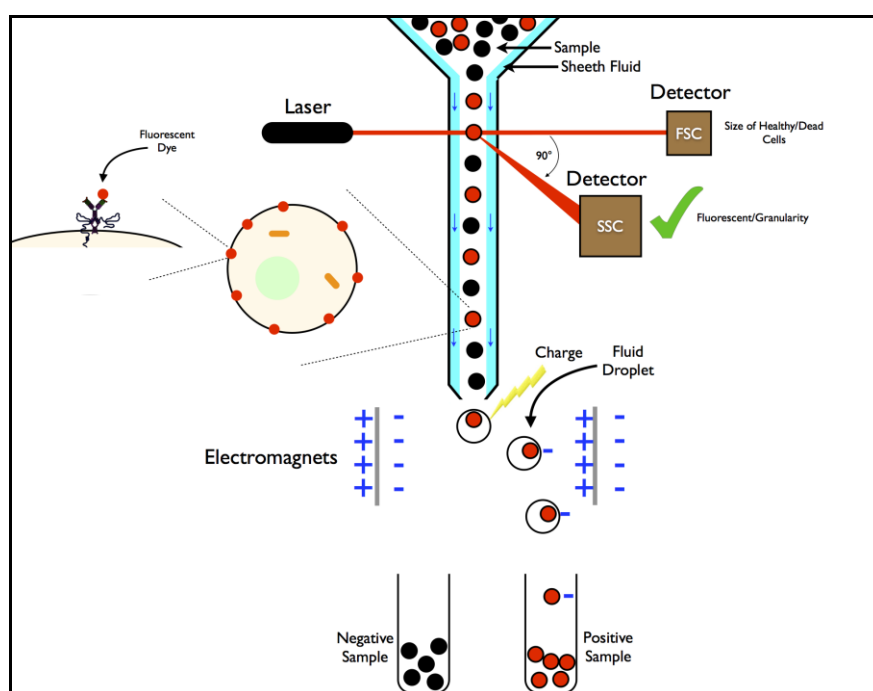
Figure 2.5 Principle of FACS (adopted from Wikipedia).

Once light signals have been converted to electronic pulses and then converted to channel numbers by the Analog-to-Digital Converter (ADC), data is stored according to a standard format, the flow cytometry standard (FCS) format. According to the FCS standard, a data storage file includes a description of the sample acquired, the instrument on which the data was collected, the data set, and the results of data analysis. Multiple (approximately 10,000 events) are collected for a single sample. Once a data file has been saved, cell populations can be displayed in several different formats. A single parameter such as FSC or FITC (FL1) can be displayed as a single parameter

histogram, where the horizontal axis represents the parameter's signal value in channel numbers and the vertical axis represents the number of events per channel number. Each event is placed in the channel that corresponds to its signal value. Signals with identical intensities accumulate in the same channel. Brighter signals are displayed in channels to the right of the dimmer signals.

Two parameters can be displayed simultaneously in a plot. One parameter is displayed on the x-axis and the other parameter is displayed on the y-axis. Three-dimensional data can also be viewed where the x- and y-axes represent parameters and the z-axis displays the number of events per channel.

2A.3.4b FACS analysis of *cf*-labeled peptides (P1-P10)

All the synthesized *cf*-labeled peptides were tested for cellular uptake studies by FACS analysis. Unmodified α-peptide **P9** containing seven arginine residues (R-type) was used as a control in these experiments. Peptides **P1**, **P3/P5**, **P7** contain conformationally constrained lysine/arginine analogues. Peptide **P10** is the arginine control peptide in which the arginine residues are separated by a 6-aminohexanoic acid spacer moiety. The peptides **P2**, **P4/P6**, **P8** contain constrained lysine/arginine analogue residues separated by 6-aminohexanoic acid, $(RX)_n$-type peptides. Cellular uptake studies were carried out in CHO (Chinese Hamster Ovary) cell line at 37°C for 4h incubation of 7μM peptides. The flow cytometry analysis is shown in Figure 2.6. As seen in the Figure 2.6; panel A, peptide **P7** (blue colour, Figure 2.6A) showed comparable cellular uptake to the control peptide **P9** (purple colour, Figure 2.6A) of poly-lysine/arginine-type peptides. As seen in the Figure 2.6; panel B, in the case of RX-type peptides peptide **P8** (blue colour, Figure 2.6B) showed comparable cellular uptake to the control peptide **P10** (purple colour, Figure 2.6B). These results confirm that the guanidinylated peptides can indeed enter the cells better than the amino functionalized peptides as studied earlier. Also the amphipathicity of the peptide (in peptide such as **P6** and **P8** with Ahx units allows better cellular uptake compared to other designed peptides.
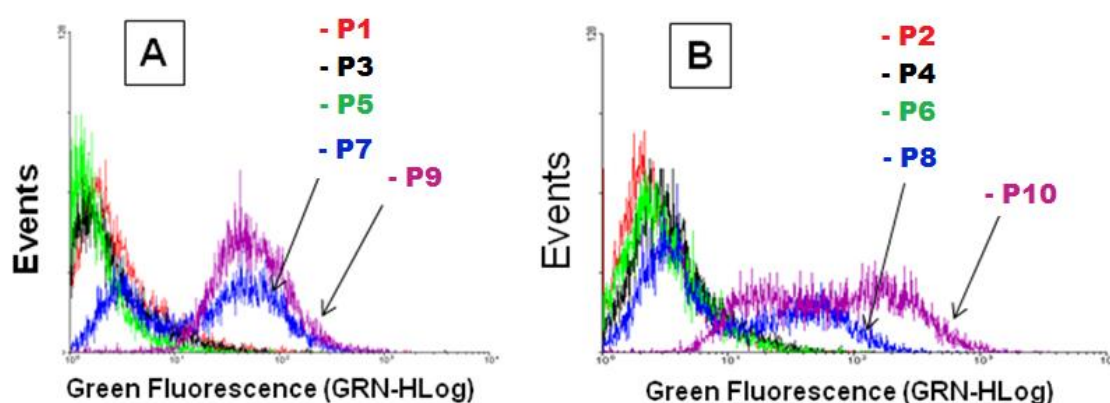
Figure 2.6 FACS analysis of peptides **P1-P10** in CHO cells at 37°C.

2A.4 Summary and conclusion

- We have synthesized novel conformationally constrained monomeric units, derived from easily available starting material- *trans*-4-hydroxy-L-proline, by simple chemical transformations.

- The flexibility of the aminoacid was constrained by use of pyrrolidinyl ring in hydroxyproline unit and the additional spacer hydrocarbon chain was also attached at ring nitrogen atom.

- The monomer unit was designed to get synergistic properties due to conformational strain, hydrophobicity from pyrrolidinyl ring and attached amino or guanidino pendant groups.

- The synthesis using Fmoc and Boc strategies lead to two different peptides and this is used to synthesize a small library of novel CPPs.

- The cell uptake studies of carboxyfluorescein-labeled peptides were carried out by FACS in CHO cells at 7μM concentration of peptides.

- FACS results shown in Figure 2.6; panel A (peptides without spacer) suggested guanidinylated peptides were superior over free amine-containing peptides. The peptides in which guanidines are attached through flexible hydrocarbon chain were found to be more active in cell uptake than when the guanidines are

attached directly to the constrained pyrrolidinyl ring. Similar results (Figure 2.6; panel B) were observed in case of 6-aminohexanoic acid-spaced containing oilgomers, but overall addition of spacer moieties to peptides showed little improvement in the cell uptake properties.

- To improve cell uptake efficiency of CPPs, guanidine groups are thus, superior to amines and significant when attached through flexible linker. Spacing between adjacent amines or guanidines also has a role in cell uptake efficiency.

Section B: Synthesis of L/D-Proline-derived monomers, peptides and their cell uptake studies

2B.1 Introduction

The (R-X-R)$_4$-motif peptides,[18] where X is the unnatural 6-aminohexanoic acid (Ahx) or 4-aminobutanoic acid spacer moiety, are the leading cell-penetrating peptides used in many studies and these type of peptides have been evaluated in various clinical trials.[22] However, the efficacy of this type of peptides can be increased by chemical modifications to achieve high therapeutic effect of attached drug molecules. As discussed in Section A, significant number of literature reports suggested that cationic proline-rich and modified proline-containing peptides are advantageous in cell uptake and have also been evaluated for cargo delivery applications.[14b]

2B.2 Rationale, design and objectives of the present work

In Section A of this chapter, we presented CPPs, where we replaced cationic amino acid (arginine or lysine) in known CPPs by our newly synthesized conformationally restricted analogue derived from *trans*-4-hydroxy-L-proline and studied the effect on cellular uptake properties. In this section, we evaluate the effects of conformational rigidity and configurational identity in designed (R-X-R)$_4$-motif peptides, where R is L-arginine and -X- is the designed spacer amino acid of the study, derived from *N*-alkylation of L- or D-proline. The designed spacer aminoacid (-X-) bears a positively charged tertiary *N*-atom, which can counterbalance the hydrophobicity in the alkyl chain. To optimize the spacing and flexibility between two arginine (R) units, the use of either *N*-aminoethyl or *N*-aminopropyl units with L/D-proline was planned to arrive at four different spacer units (Figure 2.7). The chirality of D/L-proline units allows a study of the effect of stereochemistry in the designed monomers. The 5-membered ring structure of proline would also restrict the conformational freedom in (-X-) as spacers. Thus, we can examine the effect of ring constraint endowed by proline-derived spacer moieties interspersed in polyarginine. The designed spacer (-X-) units are shown in Figure 2.7.
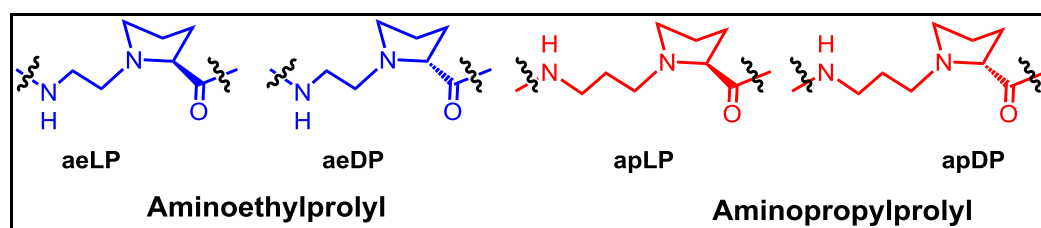
Figure 2.7 The designed spacer (-X-) units in (R-X-R)$_4$ peptides.

2B.3 Synthesis, results and discussion

2B.3.1 Synthesis of proline-derived conformationally restricted spacer units

The four *N*-alkyl-prolinyl spacers (-X-) differ in the stereochemistry at C-2 position, being derived from either L-proline (LP) or D-proline (DP) and in the length of the spacer using aminoethyl (ae) or aminopropyl (ap) alkyl groups. The synthesis of the four-monomers, amenable for solid phase peptide synthesis using Boc chemistry, was accomplished as shown in Scheme 2.3.
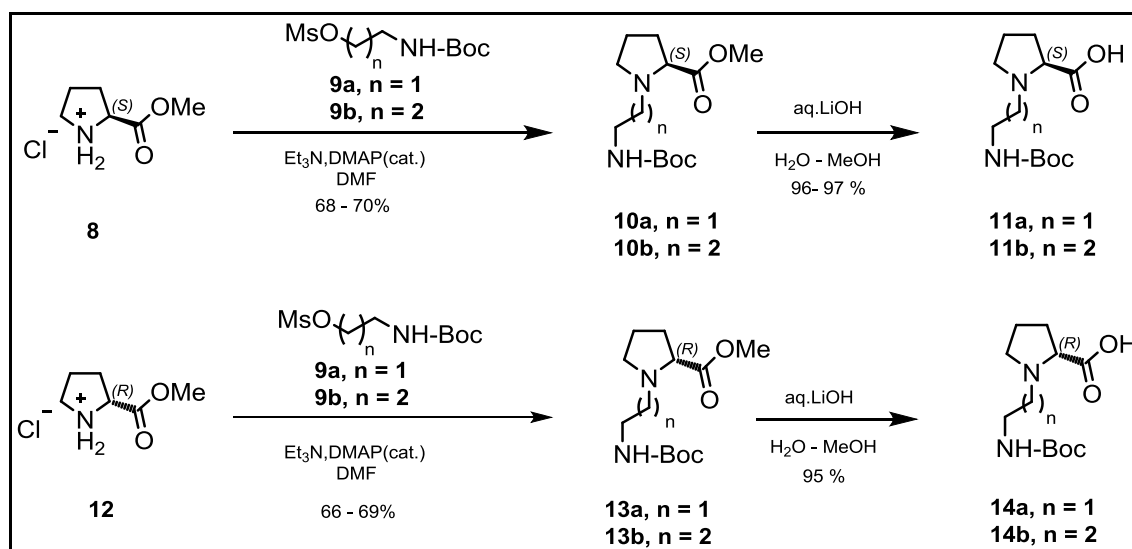
Scheme 2.3 Synthesis of aeLP, aeDP, apLP and apDP spacer monomers.

    N-alkylation of L/D-proline was achieved by displacement of the *O*-mesyl group in ω-*N*-Boc-*O*-mesyl-aminoethanol/aminopropanol in the presence of triethylamine in DMF at 60°C. Subsequent ester hydrolysis by LiOH followed by neutralization with Dowex H$^+$ resin provided the four different *N*-Boc protected amino acids, suitable for

use in the solid phase peptide synthesis as spacers (-X-) in designed (R-X-R)-motif CPPs.

2B.3.2 Solid phase peptide synthesis

The synthesized spacer moieties were incorporated at appropriate positions in the desired (R-X-R)$_4$-type peptide sequences (Figure 2.8) on solid support (MBHA resin) using Boc-chemistry protocol by following repetitive cycles of deprotection, neutralization and coupling. For FACS analysis and confocal microscopy studies, a portion of the synthesized CPP was labeled by coupling 5/6-carboxyfluorescein (*cf*) in the presence of *N,N′*-diisopropylcarbodiimide (DIPCDI) and HOBt in DMF at the *N*-terminal (as shown in section A scheme 2.2).

cf-(R-aeLP-R)$_4$-NH$_2$ (*cf*P11)

cf-(R-aeDP-R)$_4$-NH$_2$ (*cf*P12)

cf-(R-Ahx-R)$_4$-NH$_2$
control peptide (*cf*P15)

cf-(R-apLP-R)$_4$-NH$_2$ (*cf*P13)

cf-(R-apDP-R)$_4$-NH$_2$ (*cf*P14)
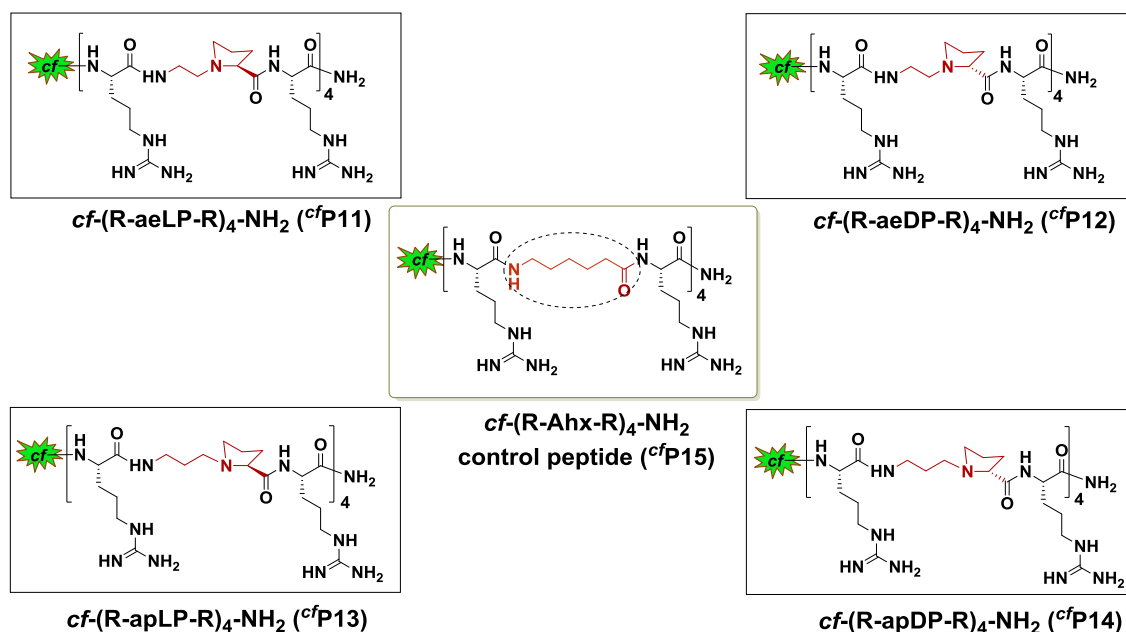
Figure 2.8 Structural comparison of *cf* labeled (R-X-R)$_4$-motif where '-X-' is a flexible spacer (Ahx in the control, and the designed constrained moieties in peptides of the study).

For the cargo delivery studies, unlabeled CPPs were used. In the absence of *cf*, phenylalanine (Phe) residue was coupled at the *N*-terminal to facilitate concentration calculation by UV-absorbance and further free amine at *N*-terminal was acylated using acetic anhydride and DIPEA in CH$_2$Cl$_2$ (Figure 2.9).
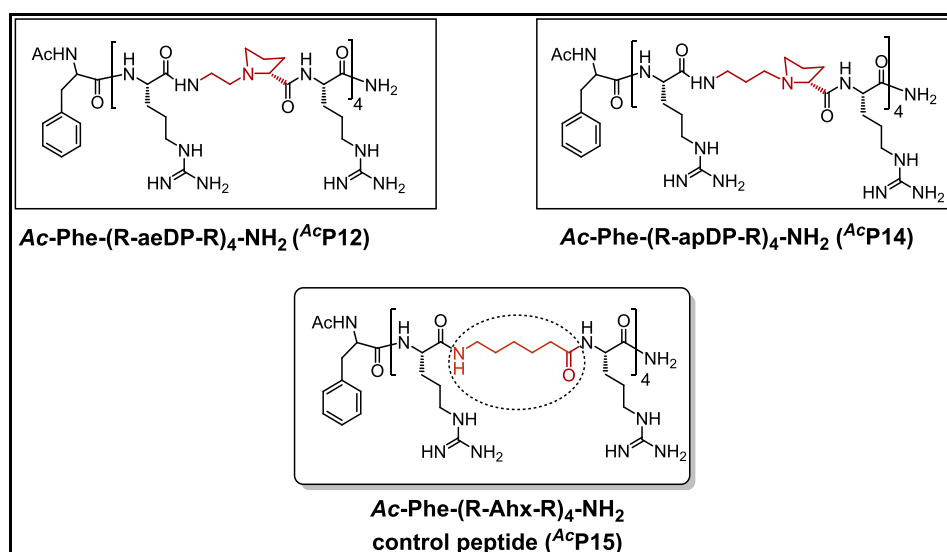
Figure 2.9: Structural comparison of unlabeled (R-X-R)$_4$-motif.

After synthesis of the desired sequence and length of peptides, the peptides were cleaved from the solid support using TFA-TFMSA cleavage protocol as discussed in section A of this chapter. The crude peptides were purified by RP-HPLC and then characterized by MALDI-TOF mass spectroscopic analysis, after re-checking their purity by analytical RP-HPLC on a C18 column. The synthesized CPPs are listed in Table 2.3.

Table 2.3 Synthesized peptides of the study.[a]

Code	Sequences	Mass (MALDI-TOF)	
		Calcd.	Obsd.
[cf]**P11**	*cf*-(R-aeLP-R)$_4$-NH$_2$	2184.26	2185.02
[cf]**P12**	*cf*-(R-aeDP-R)$_4$-NH$_2$	2184.26	2184.79
[cf]**P13**	*cf*-(R-apLP-R)$_4$-NH$_2$	2240.32	2241.69
[cf]**P14**	*cf*-(R-apDP-R)$_4$-NH$_2$	2240.32	2241.60
[cf]**P15**	*cf*-(R-Ahx-R)$_4$-NH$_2$ control	2077.48	2078.07
[Ac]**P12**	*Ac*-Phe-(R-aeDP-R)$_4$-NH$_2$	2016.50	2020.86
[Ac]**P14**	*Ac*-Phe-(R-apDP-R)$_4$-NH$_2$	2072.61	2076.71
[Ac]**P15**	*Ac*-Phe-(R-Ahx-R)$_4$-NH$_2$ control	1907.25	1907.33

[a] *cf* denotes carboxyfluorescein and *Ac* denotes *N*-terminal acetate

2B.3.3 Circular Dichroism analysis of synthesized peptides

The structural features of synthesized *cf*-labeled peptides were analyzed using circular dichroism (CD) spectroscopy to examine the structural features induced by the chiral proline-based spacers in the (R-X-R)-motif CPPs.
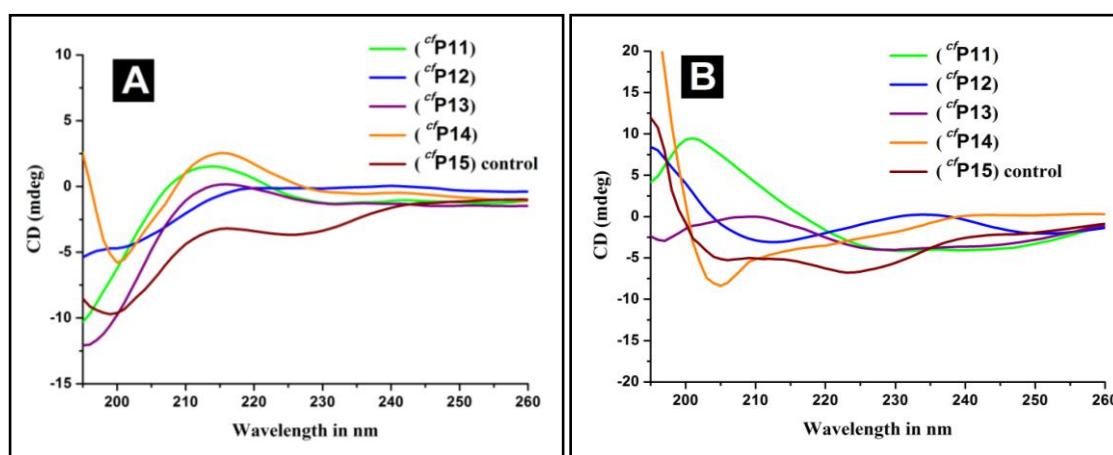
Figure 2.10. CD spectra of peptides ^{cf}**P11-**^{cf}**15** in water and TFE at 10 μM peptide concentration.

CD spectra were recorded in water as well as in the structure-inducing solvent, trifluoroethanol (TFE). In water, all four CPPs showed approximately similar CD spectra (Figure 2.10; panel A), with a maximum at ~215nm. These spectra are indicative of a random coil structure in the case of α-peptides. Thus, the differing chirality of the spacer and conformational restrictions due to ring structures seem to have a very less effect on the CPP secondary structure at concentration studied. In TFE also, there was very less difference in the CD spectra which may be related to the stereochemistry in the four different spacer moieties but the graph did not reveal any significant structural feature (Figure 2.10; panel B).

2B.3.4 FACS analysis of synthesized peptides

Quantitative cell uptake studies of CPPs ^{cf}**P11**-^{cf}**15** were carried out by FACS analysis in CHO-K1 cells at 37°C. At 37°C all the peptides ^{cf}**P11**-^{cf}**14** showed enhanced uptake in almost all cells (~95% cells) compared to control peptide ^{cf}**P15** (70% cells) (Figure 3), with high mean fluorescence (~74a.u.) as compared with the control peptide (31a.u.). In order to gain insight into the mechanism of cell uptake, FACS analysis was carried out at 4°C. Cellular uptake was found to be hampered by lowering the temperature (4°C) in case of all the synthesized peptides including the (R-Ahx-R)$_4$ control. The peptides with D-stereochemistry of the proline (^{cf}**P12** and ^{cf}**P14**) retained their ability to enter cells at least in part, even at lower temperature. The L-proline-containing peptides were only as good as control ^{cf}**P15**, which is known to follow an energy-dependent cellular internalization. For the peptides ^{cf}**P12** and ^{cf}**P14** additional mechanisms could be possibly operating along with the energy-dependent mechanism of uptake. Out of the four new CPPs described herein, *cf*-(R-apDP-R)$_4$-NH$_2$ (^{cf}**P14**) showed the best cellular uptake. The D-stereochemistry in the spacer (-X-) of peptides ^{cf}**P12** and ^{cf}**P14** seems to have a favorable effect, causing them to enter the cells better, even at lower temperature. The additional CH$_2$ group in the spacer chain of peptide ^{cf}**P14** could endow increased hydrophobicity and flexibility, towards the optimum, leading to the increased cell-penetrating ability of this peptide. These results thus draw attention to the importance of different parameters that optimize the CPPs for better Cell-Penetrating properties (Figure 2.11).
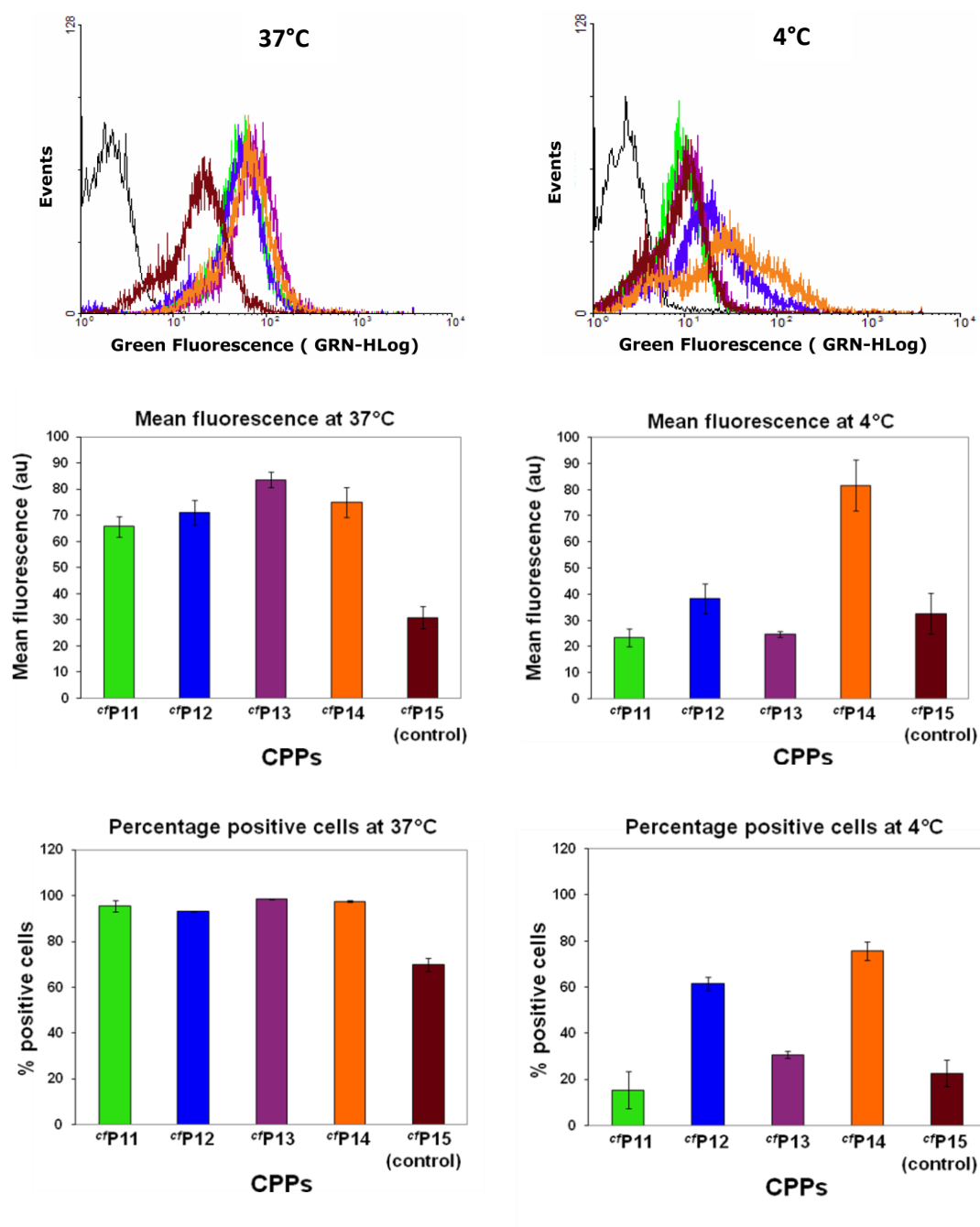
Figure 2.11 FACS analysis of peptides ^{cf}**P11**-^{cf}**15** in CHO-K1 cells at 37°C and 4°C, at 10 μM concentration and after 4h incubation time.

2B.3.5 confocal microscopy analysis

2B.3.5a Principle of confocal microscopy

The confocal microscope has its name from the arrangement of the light path. In a confocal microscope, the illumination and detection light paths share a common focal plane, which is achieved by 2 pinholes that are equidistant to the specimen (Figure 2.12). Commonly, Krypton/Argon and Helium/Neon mixed gas lasers are used that give you a range of different distinct wavelengths. This light is sent through a pinhole and reflected by a beamsplitter to the objective and specimen. The beamsplitter is a dichroic filter that acts as a mirror for the excitation wavelengths and is transparent to all other wavelengths.
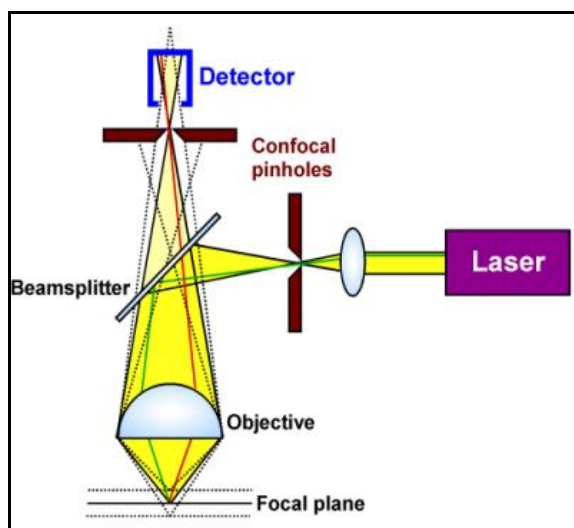
Figure 2.12 principle of confocal microscopy.[23]

Therefore, the emitted light from the specimen (which has a wavelength spectrum above the excitation wavelength) can go through the beamsplitter to the detection pinhole and the detector (actually the beamsplitter now has been replaced by an acousto-optical device). As a consequence of the pinhole arrangement, light arriving at the detector comes predominantly from a narrow focal plane, which improves the z-resolution significantly compared to conventional microscopy. At the high end, it is possible to achieve axial resolution in the submicron range.[23]

2B.3.5b Confocal microscopic analysis of synthesized peptides

Further, in order to determine the intracellular localization of the CPPs, confocal microscopic analysis was carried out at 37°C by incubating labeled CPPs (^{cf}**P11-**^{cf}**15**) for 4h with CHO-K1 cells. All the newly synthesized CPPs showed cytoplasmic entry and preferentially accumulated near the nuclear membrane (Figure 2.13).
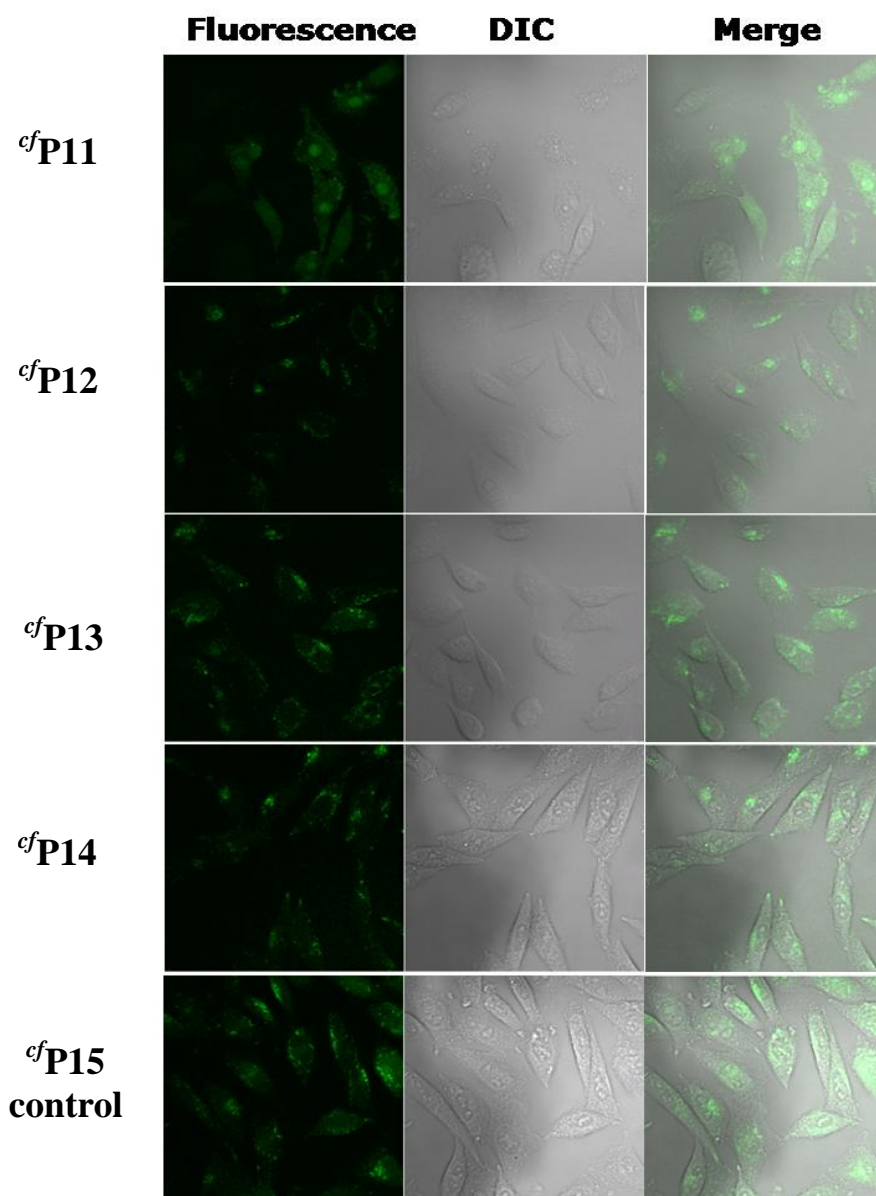
Figure 2.13 Confocal microscopy images of CHO-K1 cells after 4h incubation at 37°C with the peptide ^{cf}**P11-**^{cf}**P15** (10 μM) Scale bar: 20 μm.

2B.3.6 pDNA delivery to cells by unlabeled peptides

The efficiency of selected CPPs at cargo delivery in CHO-K1, HaCaT and WM melanoma cells was tested using pMIR-Report Luciferase plasmid DNA as the cargo. The ability of the CPPs to form charge complexes with the pMIR-Report[TM] Luciferase plasmid was evaluated by mixing the CPPs and plasmid at different charge ratios. The resulting complexes were examined by agarose gel electrophoresis (Figure 2.14).
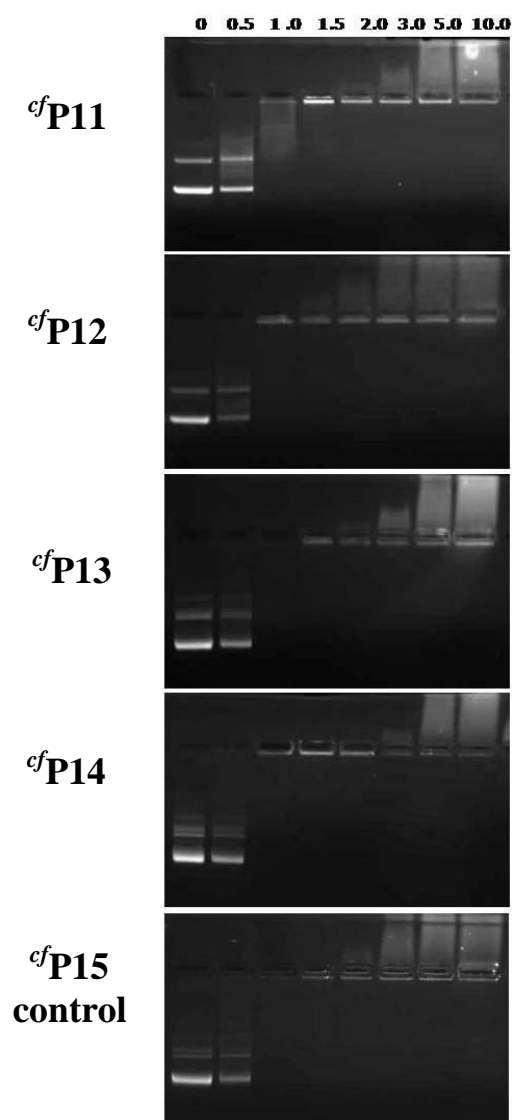
Figure 2.14 Agarose gel electrophoresis images of complexes between plasmid DNA and peptides at different charge ratios; gel stained with ethidium bromide.

Each of the newly-synthesized CPPs was able to form a neutral complex at 1:1 charge ratio of pDNA:CPP. The ability of the CPPs to transport the pMIR-Report Luciferase plasmid into cells was assessed by measuring the luciferase activity. For this study, the two unlabeled CPPs containing *N*-alkyl-D-proline spacers (peptide ^{Ac}**P12** and ^{Ac}**P14**) were chosen, since they were shown to have superior cell-penetration properties as seen by the FACS analysis. As seen in Figure 2.15, both these CPPs were able to transport the plasmid into CHO-K1 and WM melanoma cells better than the control peptide (^{Ac}**P15**). Specifically, a 3-fold and 2-fold increase in transfection efficiency was observed with peptides ^{Ac}**P12** and ^{Ac}**P14** respectively. In WM melanoma cells too, the peptides ^{Ac}**P12** and ^{Ac}**P14** showed higher transfection efficiency, displaying a 6-fold and 37-fold increase respectively. However, this increase in transfection efficiency was not observed in HaCaT cells. The reasons for this differential transfection are not yet fully understood.
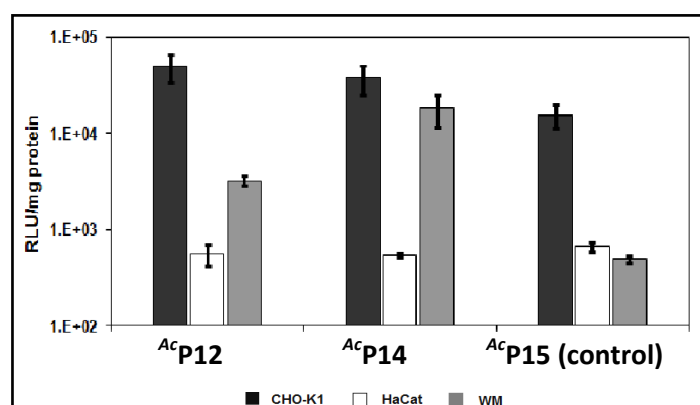
Figure 2.15 Transfection of CHO-K1 cells by pMIR-Report luciferase with peptides ^{Ac}**P12**, ^{Ac}**P14** and ^{Ac}**P15**.

2B.3.7 Cytotoxicity analysis of synthesized peptides

The cytotoxicity of the synthesized CPPs was estimated in CHO-K1 and HeLa cells. Accordingly, the synthesized CPPs were incubated with CHO-K1 or HeLa cells separately at concentrations of 5μM and 10μM for 4h and their cytotoxity was assessed by Cell Titer Glo Luminescent Cell Viability assay. All the synthesized CPPs ^{cf}**P12-**^{cf}**P14** except *cf*-(R-aeLP-R)$_4$-NH$_2$ (^{cf}**P11**) were found to be almost non-toxic to both cell

types studied (Figure 2.16). The reason for the observed higher cytoxicity of CPP ^{cf}**P11** is not clear at present.

The cytotoxicity of the pDNA:CPP polyplexes was assessed after 4h and 24h incubation with HaCaT and WM melanoma cells (Figures 2.17). The polyplexes of peptides ^{Ac}**P12,** ^{Ac}**P14** and ^{Ac}**P15** were found to be relatively non-toxic in comparison to lipofectamine, which displayed a marked decrease in cell viability after 24h.
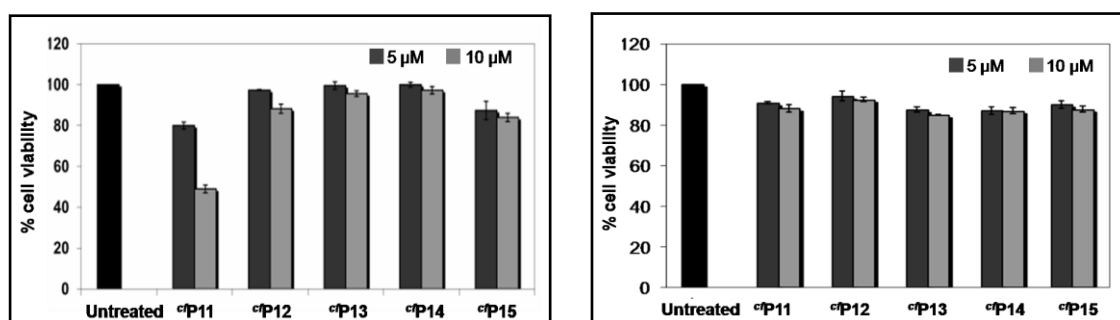
Figure 2.16 Cytotoxicity profile in CHO-K1(left panel) and HeLa (right panel) cells after 4h incubation with 5μM or 10μM concentration of peptides ^{cf}**P11-**^{cf}**15.**
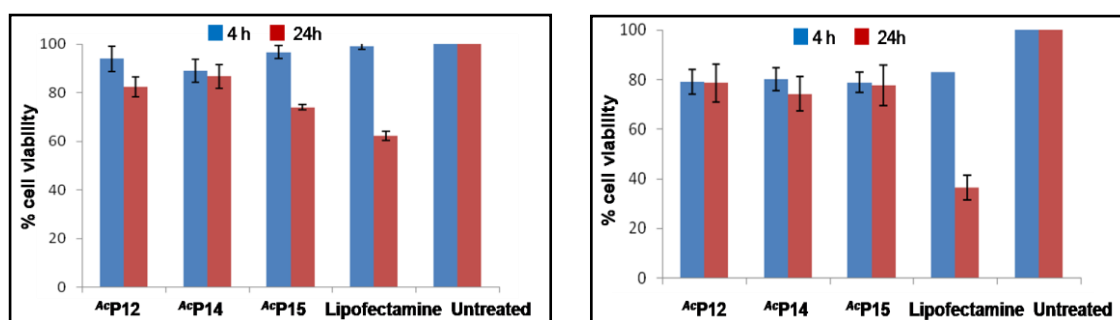
Figure 2.17 Cytotoxicity profile in HaCaT and WM melanoma cells after 4h and 24h incubation with peptide (^{Ac}**P12,** ^{Ac}**P14** ^{Ac}**P15**)-pDNA polyplexes.

2B.4 Summary and conclusion

- We designed and synthesized novel conformationally restricted spacer moieties from proline and incorporated them in polyarginines.

- The synthesized monomers differed in either stereochemistry at α-carbon or hydrocarbon chain length attached at pyrrolidinyl *N*-atom.

- The *N*-terminal carboxyfluorescein-labeled or acetylated $(R-X-R)_4$-type of peptides were synthesized by solid phase peptide synthesis.

- The *cf*-labeled peptides were tested in CHO-K1 cells for cell uptake studies at 37°C and 4°C by FACS analysis (Figure 2.11) and their intracellular localization was assessed by confocal microscopy (Figure 2.13).

- FACS analysis results revealed that the N-aminopropyl-containing spacer, combined with the D-stereochemistry at the α-carbon (apDP) endowed the peptide (*cf*P14) with properties making it most effective in cell uptake.

- Lower cell uptake efficiency was observed for all the labeled peptides (*cf*P11-*cf*P15) at low temperature (4°C), suggesting an energy-dependent mechanism in operation for cell entry (Figure 2.11).

- Confocal microscopy images revealed that the labeled peptides accumulated in the cytosol preferably and near the nuclear membrane (Figure 2.13).

- pDNA delivery to CHO-K1, HaCat and WM melanoma cells was studied with unlabeled peptides *Ac*P12 and *Ac*P14 in comparison to control peptide *Ac*P15 by non-covalent, charge complex formation strategy. The results showed the modified peptides *Ac*P12 and *Ac*P14 to be more efficient than the control peptide *Ac*P15 (Figure 1.15).

- Cytotoxicity of labeled peptides was studied in CHO-K1 and HeLa cells at 5μM and 10μM concentration after 4h incubation time, except peptide *cf*P11 other peptides were found non-toxic to cells to the concentration studied (Figure 2.16).

- Cytotoxicity of unlabeled peptide: pDNA complexes were studied in skin cells (HaCat and WM melanoma) and found nontoxic to cells at the concentrations studied, where the control transfecting reagent Lipofectamine was found toxic to the cells (Figure 2.17).

2.1 Experimental

2.1.1 Synthesis of compounds/monomer

General Information: Most of the reagents were purchased from Sigma-Aldrich and used without further purification. DMF, CH_2Cl_2, pyridine were dried over P_2O_5, CaH_2, KOH respectively. DMF, CH_2Cl_2 were stored by adding 4 Å molecular sieves and pyridine by adding KOH. THF was passed over basic alumina and dried by distillation over sodium. Column chromatography was performed for purification of compounds on silica gel (100- 200 mesh or 60-120 mesh, Merck). TLCs were performed on pre-coated with silicagel 60 F254 (Merck) aluminium sheets. TLCs were performed using petroleum ether-ethyl acetate and ethyl acetate-methanol solvent systems. TLCs were visualised after spraying with ninhydrin reagent and heating. ^{1}H and ^{13}C NMR spectra were recorded on a Bruker AV 200 or AV 400 or AV 500 spectrometer fitted with an Aspect 3000 computer and all the chemical shifts (ppm) are referred to internal TMS, D_2O or chloroform-d for for ^{1}H and/or ^{13}C NMR. ^{1}H NMR data are reported in the order of chemical shift, multiplicity (s, singlet; d, doublet; t, triplet; q, quartet; br, broad; br s, broad singlet; m, multiplet and/ or multiple resonance), number of protons. HRMS mass spectra were recorded on a Thermo Scientific Q-Exactive, Accela 1250 pump MALDI-TOF spectra were obtained from a Voyager-De-STR (Applied Biosystems) and CHCA (α-Cyano-4- hydroxycinnamic acid) matrix was used to analyze MALDI-TOF samples. UV absorbance was performed on a Varian Cary 300 UV-VIS spectrophotometer. Circular Dichroism (CD) analysis was performed on a JASCO J-715 and J-815 spectrophotometer using a cell of 10mm pathlength. CD spectra were recorded as accumulations of 5 scans using a scan speed of 200nm/min, resolution of 1.0 nm, band-width 1.0 nm and a response of 1 sec. The spectra were smoothened and plotted using OriginPro 6.1. Flow Cytometry measurements were carried out on Guava® EasyCyteTM System (Guava Technologies) using CytoSoftTM software and FACS-Aria IIIrd (Becton Dickinson). Imaging was done on an inverted LSM510 META laser scanning microscope (Carl Zeiss, Germany) using a Plan- Apochromat 63x 1.4 N.A. lens and the 488-nm line of an argon laser for carboxyfluorescein and 405 nm diode for Hoechst. The cytotoxicity of the synthesized peptides was determined by the CellTiter-Glo® Luminescent. Cell Viability Assay system (Promega). Luminescence was

measured by integration over 10s in Orion microplate luminometer (Berthold Detection System, Germany).

2.1.1a Experimental procedure and spectral data

(2S, 4R)-methyl-1-(2-(Boc-amino)ethyl)-4-hydroxypyrrolidine-2-carboxylate: (4)
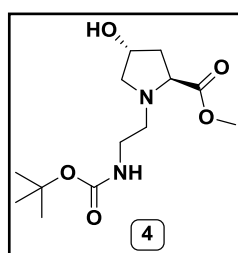
To a 250 mL round bottom flask containing of hydrochloride salt of *trans*-4-hyroxy-L-proline **2** (10 g, 55.0 mmol) dissolved in dry DMF (15 mL), triethylamine (19.2 mL, 137.0 mmol) and catalytic amount of DMAP were added to it. Stirred the above reaction mixture for 30 min at room temperature and 2-((Boc)amino)ethyl methanesulfonate **3** (14.4 g, 60.5 mmol) dissolved in dry DMF was added drop wise to it. The reaction was heated at 80-85°C for 6 h and monitored by TLC. Solvent evaporated in vacuo and re-suspend the crude reaction mixture in ethyl acetate (100 mL) and water (100 mL). The layers were separated, and the aqueous phase was extracted with ethyl acetate (3 x 100 mL). The combined organic extracts were washed with brine (100 mL), dried over Na_2SO_4. The solvent evaporate and crude residue was purified by column chromatography (35% EtOAc/Pet-ether) to give title compound **4** as a pale yellow gummy liquid (10.6 g, 67%).

Molecular Formula: $C_{13}H_{24}N_2O_5$; **Molecular weight:** 288.34

^{1}H NMR (200 MHz, CDCl$_3$) δ ppm: 5.25 (bs, 1H), 4.47 (bs, 1H), 3.72 (s, 3H), 3.62 (m, 1H), 3.40 (m, 1H), 3.17 (m, 2H), 2.78 (m, 2H), 2.55(m, 1H), 2.15 (m, 3H), 1.45 (s, 9H); DMF solvent traces: 8.09 (s), 2.96 (s), 2.89 (s)

^{13}C NMR (50 MHz, CDCl$_3$) δ ppm: 174.4, 156.1, 78.9, 70.1, 64.1, 61.1, 53.9, 51.7, 39.6, 39.1, 28.3; DMF solvent traces: 162.6, 36.5, and 31.4

^{13}C DEPT (50 MHz, CDCl$_3$) δ ppm: *positive peaks*: 70.1, 64.1, 51.7, 28.3; *Negative peaks*: 61.1, 53.9, 39.3, 39.0

HRMS (ESI): *m/z* calculate for $C_{13}H_{24}N_2O_5$: 289.1758, found: 289.1757

(2S,4R)-methyl-1-(2-(Boc-amino)ethyl)-4-((methylsulfonyl)oxy)pyrrolidine-2-carboxylate: (5)
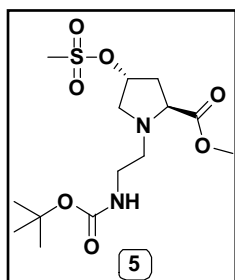
To a 250 mL round bottom flask containing *N*-alkyl hydroxyl compound **4** (7.0 g, 0.024 mol) dry pyridine (15 mL) was added to it as reagent as well as solvent. Stirred above reaction mixture for 30 min. and mesyl chloride (2.2 mL, 0.029 mol) was added drop wise by syringe and continued stirring for next 30 min at 0-5°C. Reaction monitored by TLC, upon completion of reaction, excess of CH_2Cl_2 and water (100 mL) was added to it. The layers were separated, and the aqueous phase was extracted with CH_2Cl_2 (3 x 100 mL). The combined organic extracts were washed with brine (100 mL), dried over Na_2SO_4. The solvent evaporated in vacuo and crude residue was purified by column chromatography (15% EtOAc/Pe-ether) to five the title compound **5** as a pale yellow gummy liquid (8.1 g, 91%).

Molecular Formula: $C_{14}H_{26}N_2O_7S$; **Molecular weight:** 366.43

^{1}H NMR (200 MHz, CDCl$_3$) δ ppm: 5.24 (m, 2H, CH), 3.74(s, 3H), 3.20 (q, 2H), 3.04 (s, 3H), 2.83 (m, 3H), 2.38 (m, 2H), 2.18 (s, 1H), 1.45 (s, 9H)

(2S,4S)-methyl-4-azido-1-(2-(Boc-amino)ethyl)pyrrolidine-2-carboxylate: (6)
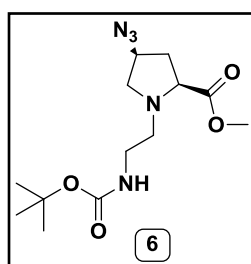
To a 100 mL round bottom flask containing mesyl compound **5** (2.5 g, 6.8 mol) was dissolved in dry DMF (10 mL) to that sodium azide (2.2 g, 0.034 mol) was added portion wise at room temperature with constant stirring. The reaction was heated at 55°C for next 6h, reaction was monitored by TLC. Upon completion of reaction, solvent was evaporated in vacuo and ethyl acetate (100 mL) and water (100 mL) was added to it. The layers were separated, and the aqueous phase was extracted with ethyl acetate (3 x 100 mL). The combined organic extracts were washed with brine (100 mL), dried over Na_2SO_4. The solvent evaporated and crude residue was purified by column chromatography (20% EtOAc/Pet-ether) to give the title compound **6** as a pale yellow solid (1.7 g, 79%).

Molecular formula: $C_{13}H_{23}N_5O_4$; **Molecular weight:** 313.36

¹H NMR (200 MHz, CDCl₃) δ ppm: 5.35 (bs, 1H, NH), 3.97 (m, 1H), 3.76 (s, 3H), 3.22 (m, 4H), 2.83 (p, 1H), 2.61 (m, 3H), 2.11 (m, 1H), 1.45(s, 9H)

¹³C NMR (50 MHz, CDCl₃) δ ppm: 173.44, 156.16, 78.97, 64.35, 58.77, 58.19, 53.51, 52.16, 39.03, 35.73, 28.40

MS (ESI): *m/z* calculated: 313.3; found: 336.07 (M+Na)

¹³C DEPT (50 MHz, CDCl₃) δ ppm: *positive peaks*: 64.3, 58.7, 52.1, 28.4; *negative peaks*: 58.1, 53.5, 39.0, 35.7

(2S,4S)-4-amino-1-(2-(Boc-amino)ethyl)pyrrolidine-2-carboxylic acid: (6a)
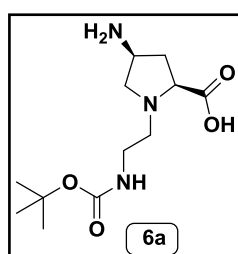
To a oven dried 100 mL round bottom flask solution of azido compound **6** (1.5 g, 4.7 mmol) dissolved in dry MeOH (25 mL), 10% palladium on charcoal (300 mg, 20% w/w) was added and the resulting reaction mixture stirred under hydrogen gas atmosphere pressure for 3h and reaction monitored by TLC. After filtration trough celite and DI water (10 mL) was added. 2N NaOH (15 mL) was further added to above resultant reaction mixtue and stirred for next 30 min. Methanol was evaporated under reduced pressure and the resulting reaction mixture was neutralised with dil. HCl. Evaporated solvents and resulting reaction mixture was re-suspend in methanol, filtered through whatman filter paper, collected supernatant was evaporated in vacuo and compound was dried in desiccator to give title amino acid compound **6a** (1.1 g, 84 %) over two steps.

Molecular formula: C₁₂H₂₃N₃O₄; **Molecular weight:** 273.17

¹H NMR (200 MHz, CDCl₃) δ ppm: 3.87 (m, 1H), 3.17 (m, 4H), 2.86 (m, 2H), 2.54 (m, 2H), 1.84 (m, 1H), 1.38 (s, 1H)

¹³C NMR (50 MHz, CDCl₃) δ ppm: 180.22, 158.11, 81.04, 67.56, 56.41, 52.69, 49.67, 38.41, 34.23, 27.58

¹³C DEPT (50 MHz, CDCl₃) δ ppm: *positive peaks*: 67.5, 49.6, 27.5; *negative peaks*: 56.4, 52.6, 38.4, 34.2

MS (ESI): *m/z* calculated 273.17; found: 274.39 (M+1)

(2S,4R)-4-Fmoc-1-(2-(Boc-amino)ethyl)pyrrolidine-2-carboxylic acid: (7)

To a oven dried 100 mL round bottom flask amino acid compound **6a** (1.0 g, 3.6 mmol) was dissolved in 1, 4-dioxane:water (20 mL: 20 mL), to which NaHCO$_3$ (3.0 g, 36 mmol) was added to maintain basic pH. The resulting reaction mixture was stirred at
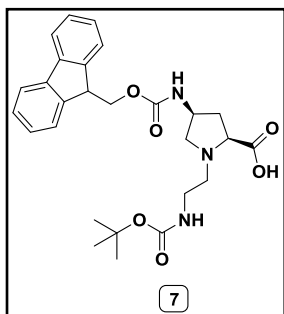
room temperature for 30 min. and Fmoc *N*-hydroxysuccinimide ester (6.1 g, 18 mmol) was added slowly to it and stirred the reaction mixture overnight at room temperature. The reaction was monitored by TLC. The resulting mixture was neutralized by Dowex H$^+$ resin and filtered through Whatman filter paper. The formed crude compound was extracted in ethyl acetate (3 x 25 mL). Solvent evaporated and formed solid was washed by Per-ether (2 x 20 mL) and diethyl ether (2 x 20 mL) to give title compound **7** (1.0 gm, 58%) as solid yellowish foam.

Molecular formula: C$_{27}$H$_{33}$N$_3$O$_6$; **Molecular weight:** 495.24

^{1}H NMR (200 MHz, CDCl$_3$) δ ppm: 7.66 (d, 2H), 7.51 (d, 2H), 7.20 (p, 4H), 4.04 (m, 5H), 3.48 (m, 2H), 3.16 (p, 4H), 2.51 (s, 1H), 1.86 (s, 2H), 1.28 (s, 9H)

^{13}C NMR (50 MHz, CDCl$_3$) δ ppm: 171.68, 156.46, 144.04, 141.37, 127.77, 127.19, 125.47, 120.03, 80.07, 69.53, 67.00, 60.08, 48.76, 47.27, 37.63, 35.80, 29.83, 28.55

^{13}C DEPT (50 MHz, CDCl$_3$) δ ppm: *positive peaks*: 127.7, 127.1, 125.4, 120.0, 69.5, 48.7, 47.2, 28.5; *negative peaks*: 67.6, 60.0, 55.5, 35.7, 29.8

MS (ESI): *m/z* calculated: 495.24; found: 495.48

General procedure for synthesis of compounds 10a, 10b, 13a and 13b:

In a dry 500 mL round bottom flask equipped with magnetic bar, the hydrochloride salt of L- or D-proline methyl ester (4.0 g, 24.1 mmol) was dissolved in dry DMF (25 mL) under argon atmosphere. To this, triethylamine (7.4 mL, 53.0 mmol) and DMAP (cat.) was added and the reaction mixture was stirred for 30 min at room temperature. 2-(Boc-

amino)ethyl methanesulfonate **9a** (6.3 g, 26.5 mmol) or 3-(Boc-amino)propyl methanesulfonate **9b** (6.6 g, 26.5 mmol) dissolved in dry DMF (15.0 mL) was added drop-wise to the above reaction mixture and the reaction mixture was heated at 60°C for 3h. The reaction was monitored by TLC. The solvents evaporated in vacuo and the crude compound was re-suspended in ethyl acetate, washed with water (3 x 200 mL), brine (200 mL) and dried over Na_2SO_4. The solvent evaporated in vacuo to give crude reaction mixture, shich was further purified by silica gel column chromatography (20-25% EtOAc/Pet-ether) to give the *N*-alkylated L- or D-proline methyl ester (**10a** or **10b** or **13a** or **13b**) as a yellowish gummy liquid in 66-70% yield.

(2-(Boc-amino)ethyl)-methyl-L-prolinate: (10a)
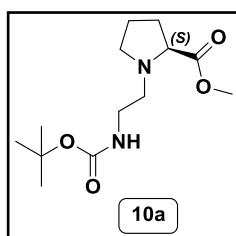
Gummy liquid (4.6 g, 70%); **Molecular formula:** $C_{13}H_{24}N_2O_4$;

Molecular weight: 272.35

^{1}H NMR (200 MHz, $CDCl_3$) δ ppm: 5.29 (br, 1H), 3.73 (s, 3H), 3.21 (m, 4H), 2.74 (m, 2H), 2.44 (m, 1H), 2.09 (m, 1H), 1.91 (m, 3H), 1.45 (s, 9H)

^{13}C NMR (50 MHz, $CDCl_3$) δ ppm: 174.5, 156.0, 78.8, 65.6, 53.9, 53.3, 51.8, 39.1, 29.3, 28.3, 23.2

^{13}C DEPT (50 MHz, $CDCl_3$) δ ppm: *positive peaks*: 65.5, 51.7, 28.3; *negative peaks*: 53.9, 53.3, 39.1, 29.2, 23.2

HRMS (ESI): *m/z* calculated for $C_{13}H_{25}O_4N_2$: 273.1807; found: 273.1809

[α]$^{27}_D$ = -20.3 (c = 2.0 in $CHCl_3$)

(2-(Boc-amino)ethyl)-methyl-D-prolinate: (10b)

Gummy liquid (4.5 g, 69%) **Molecular formula:** $C_{13}H_{24}N_2O_4$; **Molecular weight:** 272.35
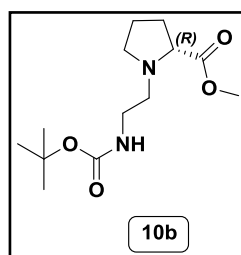
¹H NMR (200 MHz, CDCl₃) δ ppm: 5.26 (br, 1H), 3.72 (s, 3H), 3.21 (m, 4H), 2.70 (m, 2H), 2.39 (m, 1H), 2.11 (m, 1H), 1.88 (m, 3H), 1.45 (s, 9H)

¹³C NMR (125 MHz, CDCl₃) δ ppm: 174.7, 156.1, 78.9, 65.7, 54.0, 53.4, 51.8, 39.2, 29.6, 28.4, 23.4

¹³C DEPT (125 MHz, CDCl₃) δ ppm: *positive peaks*: 65.7, 51.8, 28.4; *negative peaks*: 54.4, 53.4, 39.2, 29.6, 23.4

HRMS (ESI): *m/z* calculated for $C_{13}H_{25}O_4N_2$: 273.1808, found: 273.1809

$[\alpha]^{27}_D$ = +20.3 (c = 2.0 in CHCl₃)

(3-(Boc-amino)propyl)-methyl-L-prolinate: (13a)
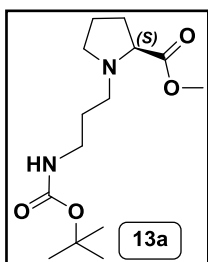
Gummy liquid (4.7 g, 68%); **Molecular formula:** $C_{14}H_{26}N_2O_4$; **Molecular weight:** 286.27

¹H NMR (200 MHz, CDCl₃) δ ppm: 5.34 (br, 1H), 3.74 (s, 3H), 3.18 (m, 4H), 2.80 (m, 1H), 2.43 (m, 2H), 2.12 (m, 1H), 1.87 (m, 3H), 1.65 (m, 2H), 1.44 (s, 9H)

¹³C NMR (50 MHz, CDCl₃) δ ppm: 174.3, 156.1, 78.7, 65.97, 52.9, 52.2, 51.8, 38.7, 29.1, 28.3, 28.0, 23.0

¹³C DEPT (50 MHz, CDCl₃) δ ppm: *positive peaks:* 65.9, 51.8, 28.3; *negative peaks:* 52.9, 52.2, 38.7, 29.1, 28.0, 23.0

HRMS (ESI): *m/z* calculated for $C_{14}H_{27}O_4N_2$: 287.1964, found: 287.1964

$[\alpha]^{27}_D$ = -29.2 (c = 2.0 in CHCl₃)

(3-(Boc-amino)propyl)-methyl-D-prolinate: (13b)

Gummy liquid (4.6 g, 66%); **Molecular formula:** $C_{14}H_{26}N_2O_4$; **Molecular weight:** 286.27
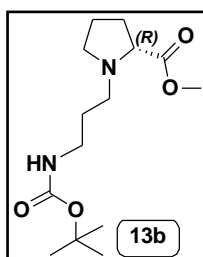
¹H NMR (200 MHz, CDCl₃) δ ppm: 5.36 (br, 1H), 3.73 (s, 3H), 3.19 (m, 4H), 2.73 (m, 1H), 2.41 (m,1H), 2.12 (m, 2H), 1.88 (m, 3H), 1.65 (m, 2H), 1.44 (s, 9H)

¹³C NMR (50 MHz, CDCl₃) δ ppm: 174.7, 156.1, 78.7, 66.1, 52.9, 52.4, 51.8, 38.8, 29.2, 28.4, 28.1, 23.2

¹³C DEPT (50 MHz, CDCl₃) δ ppm: *positive peaks*: 66.1, 51.8, 28.4; *negative peaks*: 52.9, 52.4, 38.8, 29.2, 28.1, 23.1

HRMS (ESI): *m/z* calculated for $C_{14}H_{27}O_4N_2$: 287.1964, found: 287.1965

$[\alpha]^{27}_D$ = +29.2 (c = 2.0 in CHCl₃)

General procedure for synthesis of compounds 11a, 11b, 14a and 14b:

The purified *N*-alkylated L- or D-proline methyl ester (1.0 g) was dissolved in minimum amount of methanol and then 1M LiOH was added drop-wise with constant stirring until complete consumption of starting material was observed on TLC. The solvents were evaporated in vacuo and the above-formed lithium salt of carboxylic acid was re-dissolved in de-ionized water. Dowex H⁺ resin was added with slow stirring until reaction mixture became slightly acidic (~pH 6.0). The solvent was evaporated and the residue was co-evaporated twice with methanol. Purification through neutral alumina by column chromatography (10-15% MeOH/EtOAc) afforded pure, hygroscopic yellowish foamy compound (**11a** or **11b** or **14a** or **14b**) in 95-97% yield, which was stored under desiccation.

(2-(Boc-amino)ethyl)-L-proline: (11a)
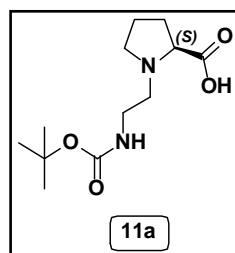
Yellowish foam (0.92 g, 97%); **Molecular formula:** $C_{12}H_{22}N_2O_4$; **Molecular weight:** 286.27

¹H NMR (500 MHz, D₂O) δ ppm: 3.94 (m, 1H), 3.80 (m, 1H), 3.42 (m, 1H), 3.34 (m, 2H), 3.26 (m, 2H), 2.42 (m, 1H), 2.09 (m, 2H), 1.94 (m, 1H), 1.40 (s, 9H)

^{13}C NMR (125 MHz, D_2O) δ ppm: 174.4, 159.0, 82.4, 70.5, 55.9, 55.8, 37.3, 29.5, 28.4, 23.90

^{13}C DEPT (125 MHz, D_2O) δ ppm: *positive peaks*: 70.5, 28.4; *negative peaks*: 50.9, 55.8, 37.3, 29.5, 23.9

HRMS (ESI): *m/z* calculated for $C_{12}H_{22}O_4N_2Na$: 281.1472, found: 281.1468

$[α]^{26}_D$ = -23.9 (c = 0.5 in MeOH)

(2-(Boc-amino)ethyl)-D-proline: (11b)
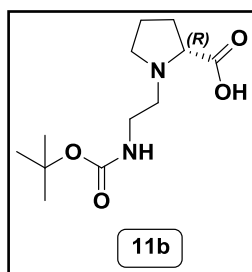
Yellowish foam (0.90 g, 95%); **Molecular formula:** $C_{12}H_{22}N_2O_4$; **Molecular weight:** 286.27

^{1}H NMR (500 MHz, D_2O) δ ppm: 3.93 (m, 1H), 3.80 (m, 1H), 3.45 (m, 1H), 3.38 (m, 2H), 3.25 (m, 1H), 3.10 (m, 1H), 2.43 (m, 1H), 2.10 (m, 3H), 1.43 (s, 9H)

^{13}C NMR (100 MHz, D_2O) δ ppm: 174.8, 159.0, 82.4, 70.5, 55.8, 55.7, 37.4, 29.5, 28.4, 23.8

^{13}C DEPT (100 MHz, D_2O) δ ppm: *positive peaks*: 70.5, 28.4; *negative peaks*: 55.9, 55.7, 37.4, 29.5, 23.8

HRMS (ESI): *m/z* calculated for $C_{12}H_{22}O_4N_2Na$: 281.1472, found: 281.1467

$[α]^{26}_D$ = +23.9 (c = 0.5 in MeOH)

(3-(Boc-amino)propyl)-L-proline: (14a)
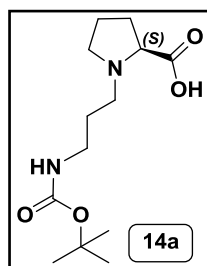
Yellowish foam (0.92 g, 96%); **Molecular formula:** $C_{13}H_{24}N_2O_4$; **Molecular weight:** 272.32

^{1}H NMR (500 MHz, D_2O) δ ppm: 3.91 (m, 1H), 3.74 (m, 1H), 3.16 (m, 5H), 2.44 (m, 1H), 2.09 (m, 2H), 1.84 (m, 3H), 1.40 (s, 9H)

^{13}C NMR (125 MHz, D_2O) δ ppm: 174.6, 158.9, 81.8, 69.8, 56.0, 53.7, 37.6, 29.7, 28.4, 26.5, 23.8

^{13}**C DEPT** (125 MHz, D$_2$O) δ ppm: *positive peak*: 70.5, 28.4; *negative peaks*: 55.9, 55.7, 37.4, 29.5, 23.8

HRMS (ESI): *m/z* calculated for C$_{13}$H$_{24}$O$_4$N$_2$Na: 295.1628, found: 295.1627

$[α]^{26}_D$ = -33.1 (c = 0.5 in MeOH)

(3-(Boc-amino)propyl)-D-proline: (14b)
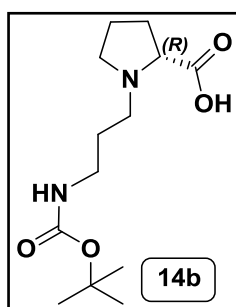
Yellowish foam (0.91 g, 95%); **Molecular formula:** C$_{13}$H$_{24}$N$_2$O$_4$; **Molecular weight:** 272.32

^{1}**H NMR** (500 MHz, D$_2$O) δ ppm: 3.87 (m, 1H), 3.70 (m, 1H), 3.10 (m, 5H), 2.38 (m, 1H, CH), 2.03 (m, 2H), 1.80 (m, 3H), 1.35 (s, 9H)

^{13}**C NMR** (125 MHz, D$_2$O) δ ppm: 174.6, 158.9, 81.8, 69.8, 56.0, 53.7, 37.6, 29.7, 28.4, 26.5, 23.8

^{13}**C DEPT** (125 MHz, D$_2$O) δ ppm: *positive peaks*: 69.7, 28.4; *negative peaks*: 56.0, 53.7, 37.6, 29.7, 26.5, 23.8

HRMS (ESI): *m/z* calculated for C$_{13}$H$_{24}$O$_4$N$_2$Na: 295.1628, found: 295.1626

$[α]^{26}_D$ = +33.1 (c = 0.5 in MeOH)

2.1.2 Procedures for Cell uptake studies (FACS, confocal microscopy) and Cytotoxicity studies

Cellular uptake studies using FACS: CHO-K1 were seeded in 24-well plates at a density of 50,000 cells/well and incubated for 24h. The fluorescently tagged peptides were added to the cells at concentrations of 10 μM in 300 μL of serum-free medium. After 4h of incubation at 37°C or 4°C, cells were washed with PBS containing heparin (1 mg/mL) and with trypan blue in PBS. Cells were then collected by trypsinization and resuspended in PBS and placed on ice. Flow Cytometry measurements were carried out on Guava® EasyCyte^{TM} System (Guava Technologies) using CytoSoft^{TM} software. 10,000 live cells were used for each analysis at room temperature. FACS measurements

at 4°C or 37°C, subsequent to treating the cells with peptides at the same temperature were carried out using the same protocols as mentioned above, but on a FACS-Aria IIIrd (Becton Dickinson) instrument, while maintaining the temperature at 4°C or 37°C respectively. The uptake experiments were repeated to include an acid wash step (0.2 mol/l acetic acid and 0.2 mol/l NaCl) that quenches fluorescence of carboxyfluorescein that is externally bound to the cell membrane.

2.1.3 Peptide-pDNA complex formation determined by agarose gel electrophoresis

Complexes of peptide and plasmid DNA (termed polyplexes) were prepared at defined charge ratios, calculated theoretically considering the peptide guanidines (positive charges) per pDNA phosphate (negative charge), Z (+/−). Briefly, the plasmid DNA was added drop-wise to an equal volume of the appropriate peptide dilution while vortexing. The polyplexes at different charge ratios were incubated for 30 min at room temperature. 20 µL of the polyplex having 200 ng total DNA was loaded in each case onto 1% agarose gel containing ethidium bromide. Electrophoresis was carried out at 100V in 1× TAE buffer (pH 7.4) for 30 min. Gel images were obtained using Syngene G:Box gel documentation system.

2.1.4 pDNA Transfection assay

Cells were seeded in a 24-well plate in complete media 24h before transfection. Polyplexes were prepared at Z (+/−) 10 with final DNA concentration of 40 ng/µL (4.98 nM) (pMIR-Report™ Luciferase) and incubated for 1h at room temperature. 100 µL of polyplex per well was added to cells (final DNA conc. = 1.25 nM and peptide conc.= 21 µM) (~70% confluency) in serum free media (OptiMEM, Invitrogen). In case of LipofectamineTM 2000 (Invitrogen, USA), the complexes were formed according to the manufacturer's protocol. After 5 h of incubation at 37°C, the media was aspirated; cells were washed and supplemented with 500 µL complete medium. After 24h, cells were washed with PBS and lysed with 100 µL of cell culture lysis buffer (1× CCLR, Promega). Luciferase expression was measured in 50 µL of cell lysate supernatant using 50 µL luciferase assay substrate (Promega). Luminescence was measured by integration over 10s in an Orion microplate luminometer (Berthold Detection System, Germany).

Luciferase activity was normalized with total protein content of the cell lysate estimated using BCA protein assay (Pierce).

2.1.5 Confocal microscopy

Cells were seeded at a density of 1.2 x 10^5 in 35 mm µ-dishes (ibidi, Germany) and incubated for 24h. Labeled peptides (10 µM) were added to the cells in serum-free media and incubated at 37°C for 4h. Cells were washed thrice with ice cold PBS(+) containing heparin (1mg/mL). Imaging was done at room temperature on an inverted LSM510 META laser scanning microscope (Carl Zeiss, Germany) using a Plan-Apochromat 63 x 1.4 N.A. lens and the 488nm line of an argon laser for carboxyfluorescein.

2.1.6 Cytotoxicity studies

The toxicity of the synthesized peptides was determined by the CellTiter-Glo® Luminescent Cell Viability Assay system (Promega). Cells were seeded in 96-well plates 1 day before treatment. Cells were then treated with different concentrations of the peptide for 4h in serum-free media, and the cell viability was assayed according to the manufacturer's protocol. Alternatively, cells were replenished with complete media, and the cell viability was assayed after 24h. For estimating the cytotoxicity of the complexes cells were treated with a 20 µL of polyplexes at charge ratio 10 in serum-free media for 5h, the media was aspirated and supplemented with 100 µL complete growth medium. After 24h viability was evaluated.

2.1.7 Peptide synthesis

All the peptide sequences were synthesized using MBHA resin (loading value 0.5 mmol/g) as solid support by standard Boc- or Fmoc- protection strategy. Peptides were synthesized on a 50 µmol scale. Removal of Boc- group was carried out by 50% TFA in CH_2Cl_2 followed by neutralization by 5% DIPEA in CH_2Cl_2. Removal of Fmoc-group was carried out by 20% piperidine in DMF. All coupling reactions were performed using three equivalents each of Boc- protected monomer, HOBt, TBTU and DIPEA in DMF for 4h at room temperature. Successive deprotection, neutralization and coupling steps were carried out as iterative cycles until the desired length of peptides

were synthesized. Deprotection and coupling reactions were monitored by the Kaiser test. For *cf*-labeled peptide, the final coupling was done by using ten equivalents each of 5(6)-carboxyfluorescein (*cf*), HOBt, DIPCDI (di-isopropyl carbodiimide) in DMF overnight to yield the *cf*-labeled peptide. For peptides (^{Ac}**P12**, ^{Ac}**P14** and ^{Ac}**P15**) synthesis, a portion of resin-supported BocNH-(R-aeDP-R)$_4$-NH$_2$, BocNH-(R-apDP-R)$_4$-NH$_2$, BocNH-(R-Ahx-R)$_4$-NH$_2$ peptides were extended further after removal of *N*-terminal Boc group and successive coupling of phenylalanine using three equivalents each of Boc-phenylalanine, TBTU, HOBt and DIPEA in DMF. Finally, the terminal amine was capped after Boc deprotection by using ten equivalents of Ac$_2$O and DIPEA in DMF to yield peptides ^{Ac}**P12**, ^{Ac}**P14** and ^{Ac}**P15**.

2.1.8 Cleavage of peptides from the solid support and purification by HPLC

All the peptides were cleaved from the MBHA solid support using TFA-TFMSA cleavage protocol in the presence of 1, 2-ethanedithiol and thioanisole as scavengers to yield *C*-terminal amide containing peptides. The purity of the peptides was assessed by RP-HPLC, followed by purification. Pure peptides were obtained after RP-HPLC on a C18 column with a water/acetonitrile gradient containing 0.1%TFA. The fractions of pure peptides were concentrated by lyophilization, their identity confirmed by MALDI-TOF mass spectrometry and their concentration determined from their absorbance, using the molar absorption co-efficient of *cf* at 490 nm for carboxyfluorescein-labeled peptides and at 259 nm for phenylalanine-labeled peptide.

2.2 Appendix A

Compound and characterization	Page No.
Compound 4: ^{1}H, ^{13}C NMR, ^{13}C DEPT	89-90
Compound 5: ^{1}H	90
Compound 6: ^{1}H, ^{13}C NMR, ^{13}C DEPT, IR	91-92
Compound 6a: ^{1}H, ^{13}C NMR, ^{13}C DEPT	93-94
Compound 7: ^{1}H, ^{13}C NMR, ^{13}C DEPT, MS	94-96
Compound 10a: ^{1}H, ^{13}C NMR, ^{13}C DEPT, HRMS	96-98
Compound 10b: ^{1}H, ^{13}C NMR, ^{13}C DEPT, HRMS	98-100
Compound 13a: ^{1}H, ^{13}C NMR, ^{13}C DEPT, HRMS	100-102
Compound 13b: ^{1}H, ^{13}C NMR, ^{13}C DEPT, HRMS	102-104
Compound 11a: ^{1}H, ^{13}C NMR, ^{13}C DEPT, HRMS	104-106
Compound 11b: ^{1}H, ^{13}C NMR, ^{13}C DEPT, HRMS	106-108
Compound 14a: ^{1}H, ^{13}C NMR, ^{13}C DEPT, HRMS	108-110
Compound 14b: ^{1}H, ^{13}C NMR, ^{13}C DEPT, HRMS	110-112
MALDI-TOF spectra of peptides	112-120

¹H NMR (200 MHz; CDCl₃) spectra of compound **4**:
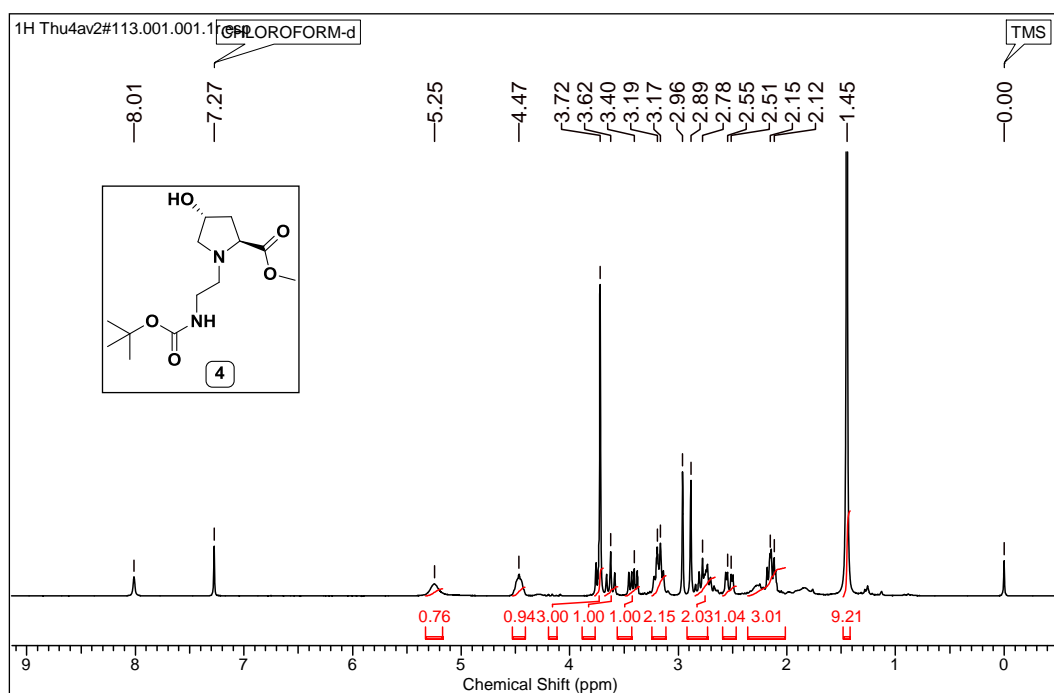
¹³C NMR (50 MHz; CDCl₃) spectra of compound **4**:
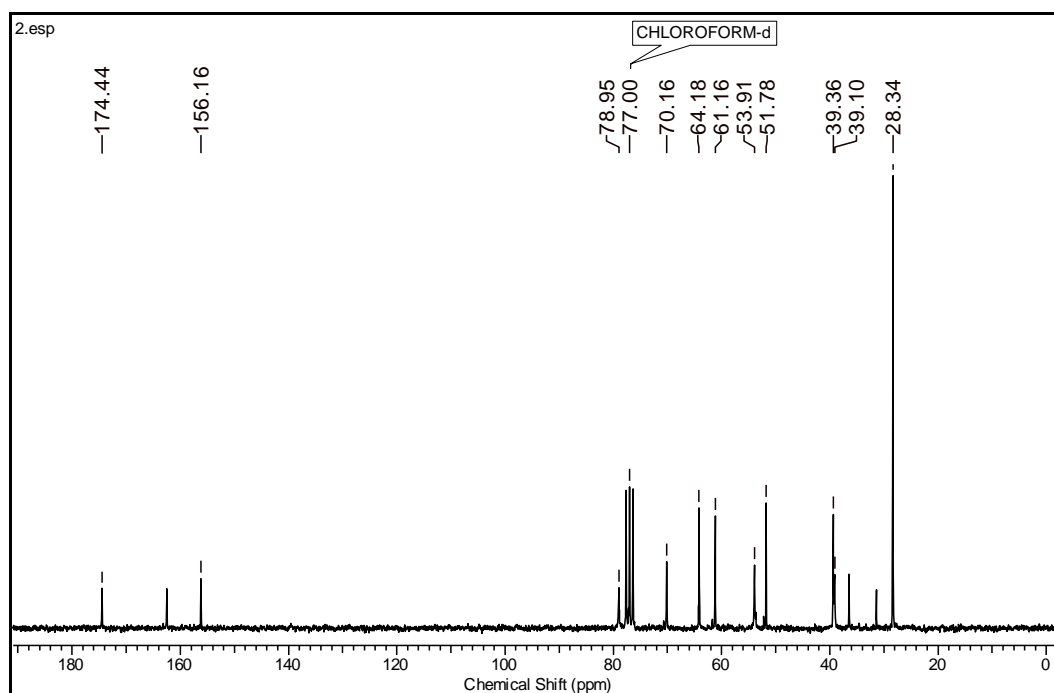
^{13}C DEPT (50 MHz; CDCl$_3$) spectra of compound **4**:
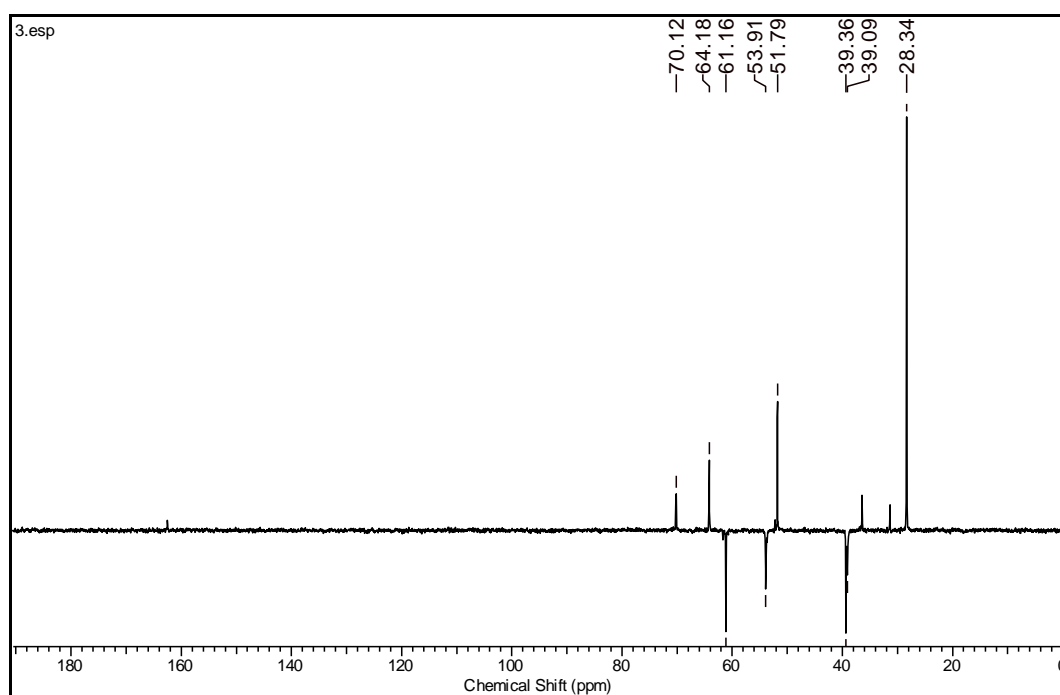
^{1}H NMR (200 MHz; CDCl$_3$) spectra of compound **5**:
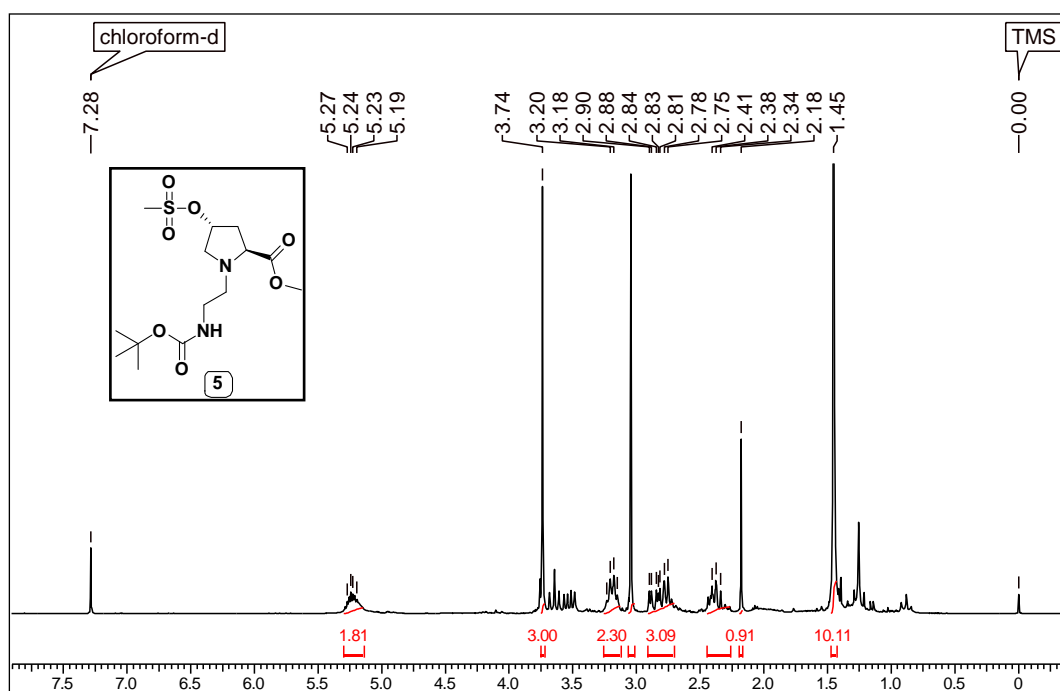
^{1}H NMR (200 MHz; CDCl$_3$) spectra of compound **6**:
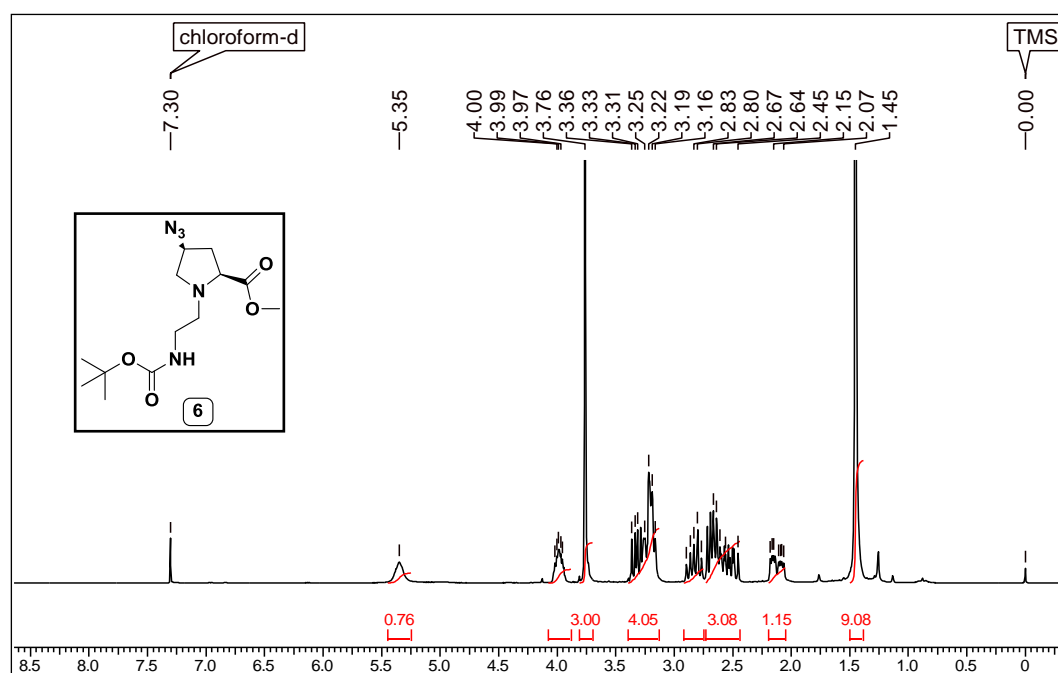
^{13}C NMR (50 MHz; CDCl$_3$) spectra of compound **6**:
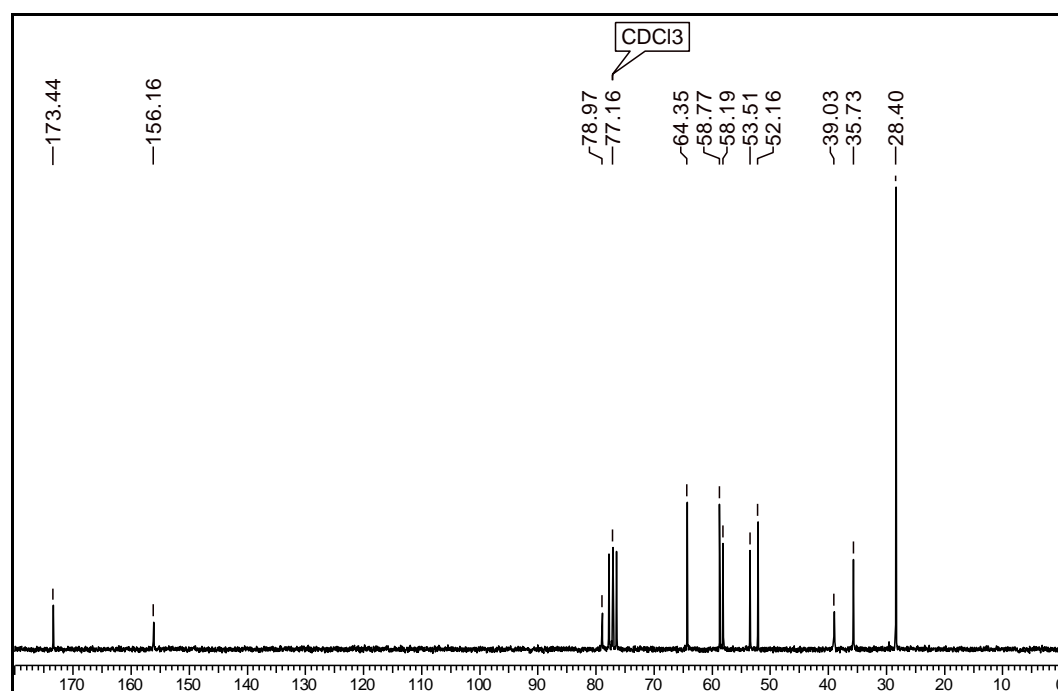
^{13}C DEPT (50 MHz; CDCl$_3$) spectra of compound **6**:
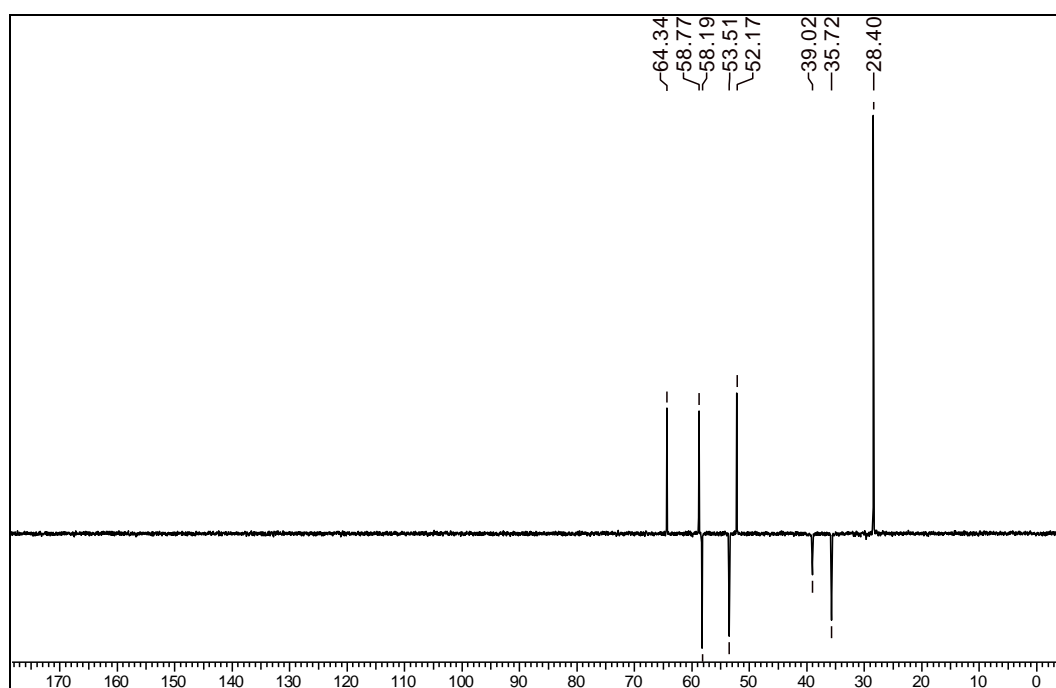
IR spectra of compound **6**:
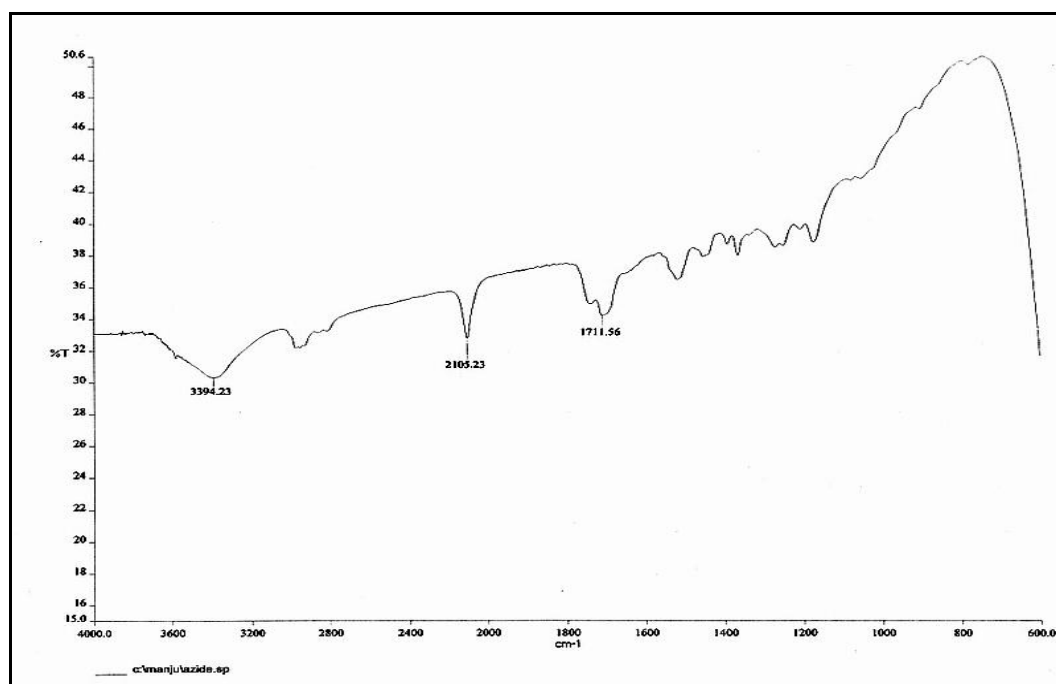
^{1}H NMR (200 MHz; CDCl[3]) spectra of compound **6a**:
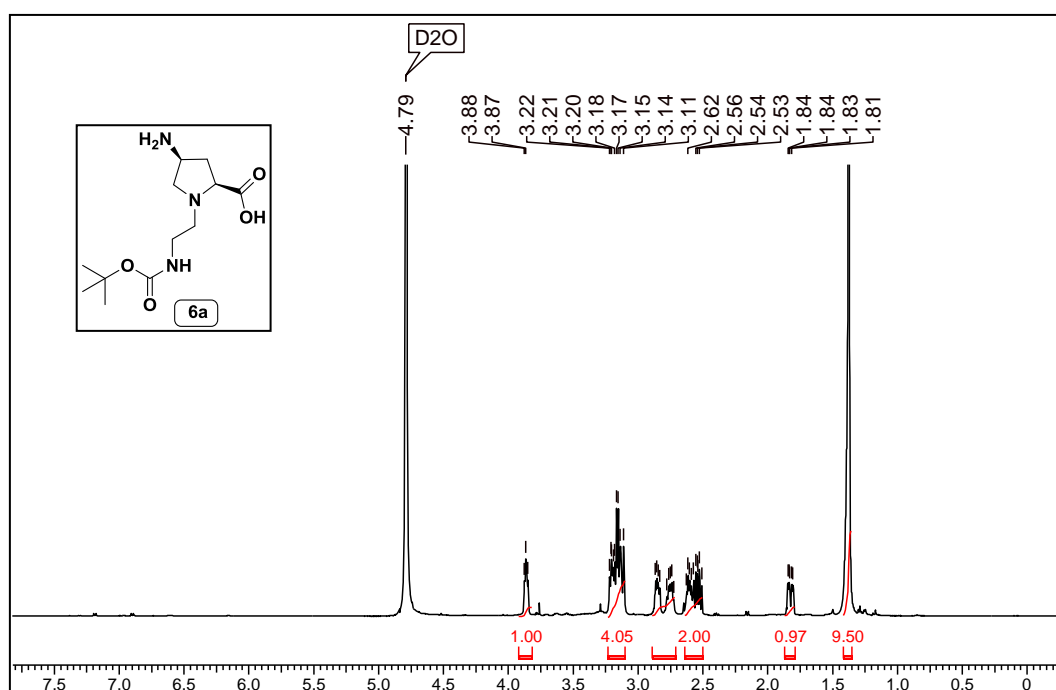
^{13}C NMR (50 MHz; CDCl[3]) spectra of compound **6a**:
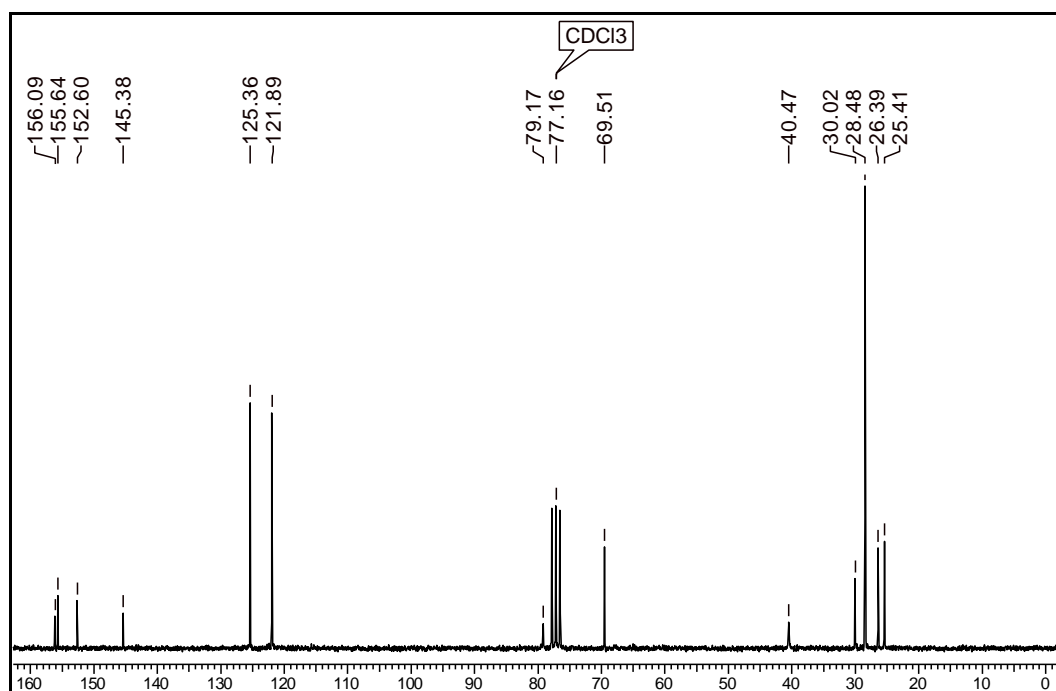
^{13}C DEPT (50 MHz; CDCl$_3$) spectra of compound **6a**:
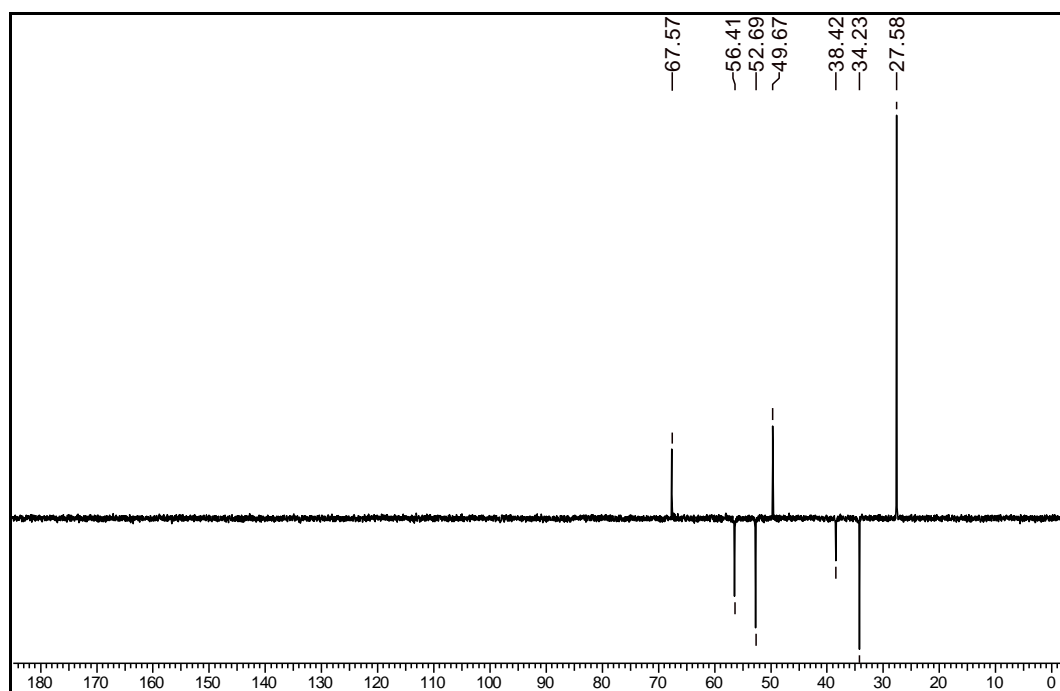
^{1}H NMR (200 MHz; CDCl$_3$) spectra of compound **7**:
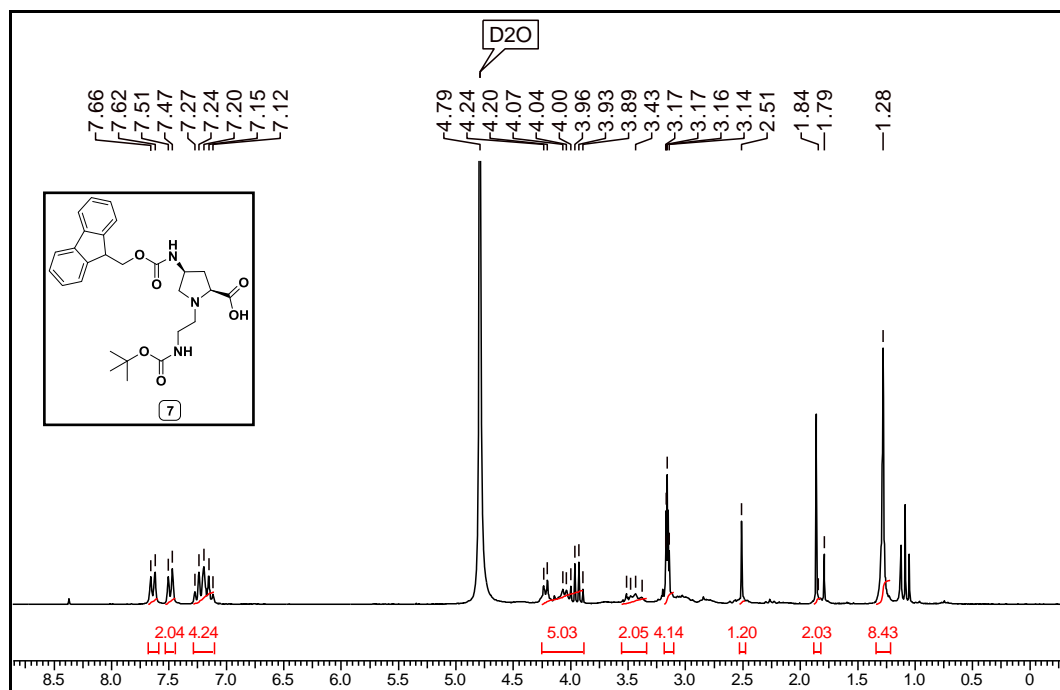
^{13}C NMR (50 MHz; CDCl$_3$) spectra of compound **7**:
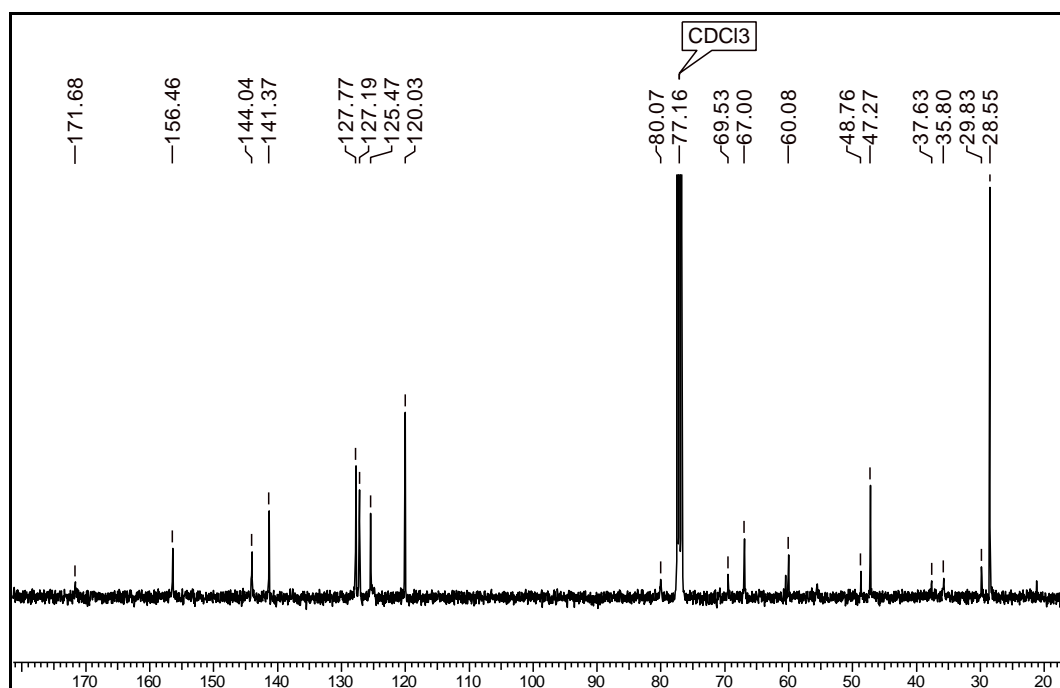
^{13}C DEPT (50 MHz; CDCl$_3$) spectra of compound **7**:
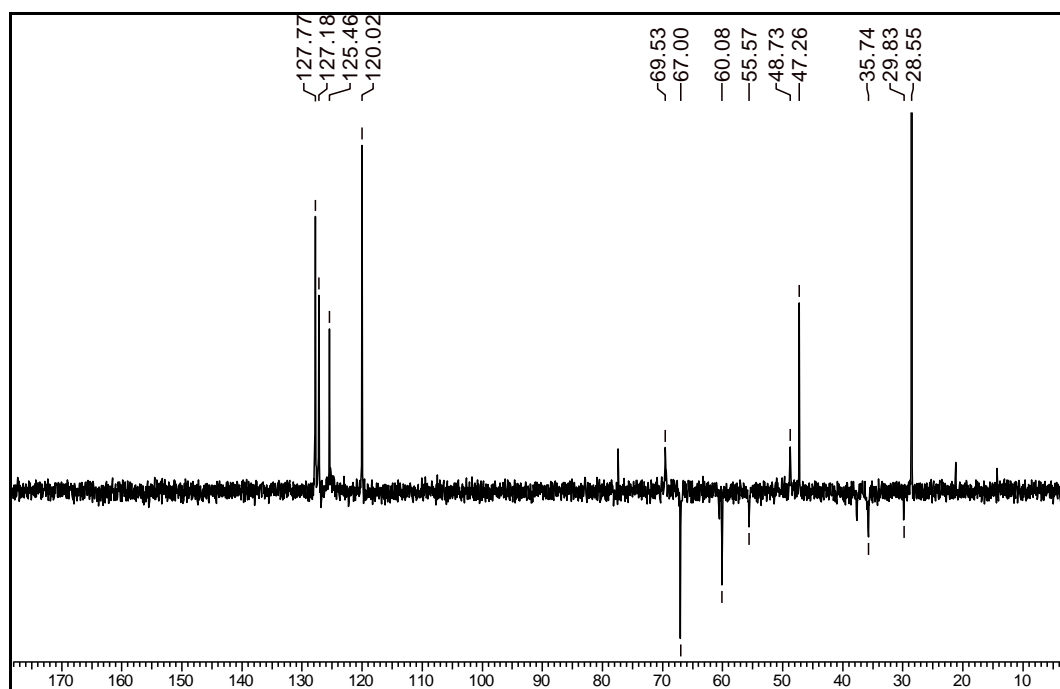
Mass (ESI) spectra of compound **7**:
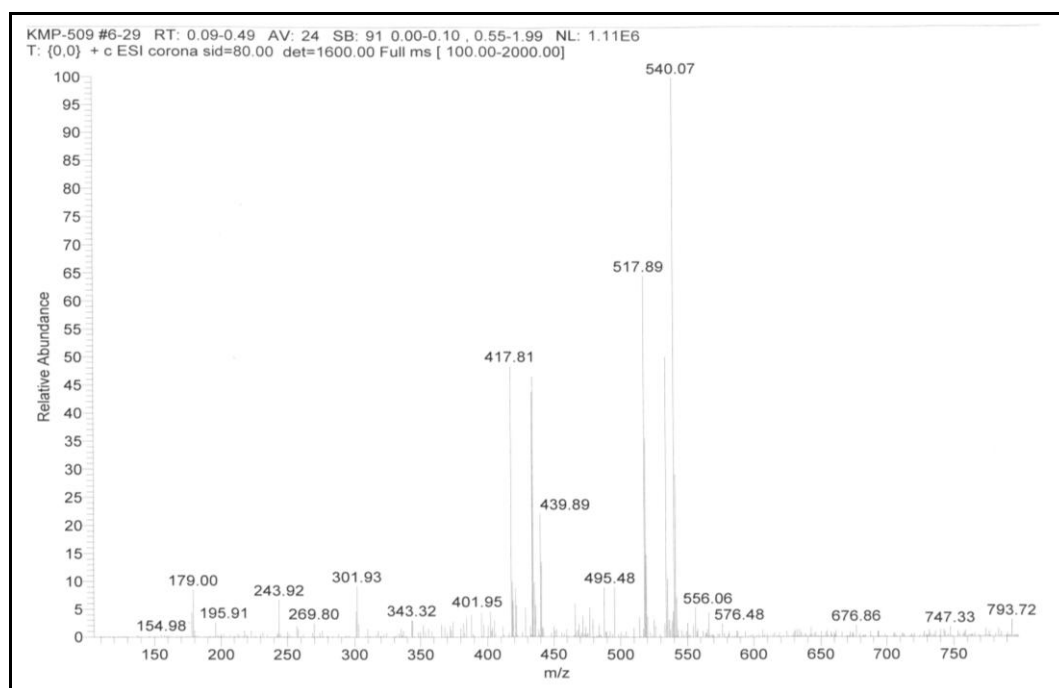
^{1}H NMR (200 MHz; CDCl$_3$) spectra of compound **10a**:
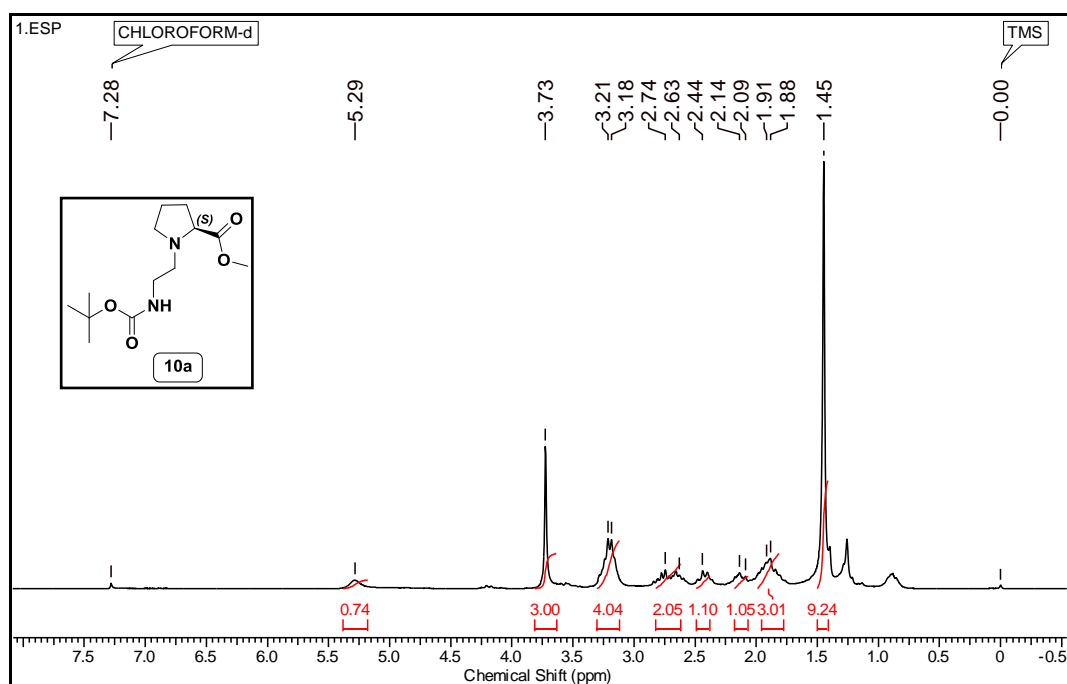
^{13}C NMR (50 MHz; CDCl$_3$) spectra of compound **10a**:
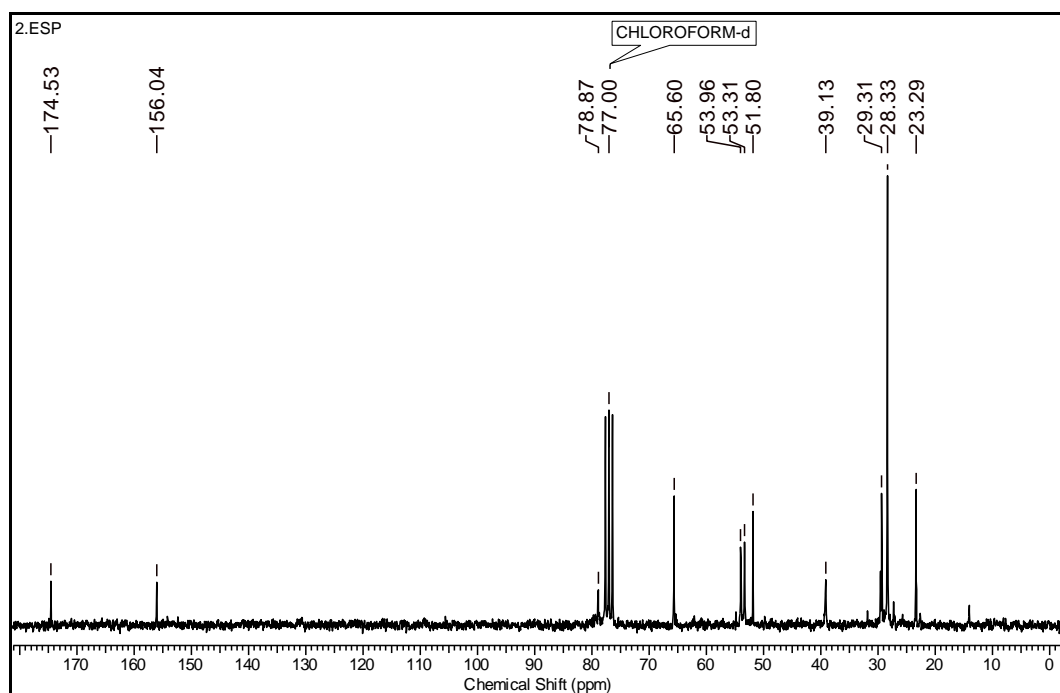
^{13}C DEPT (50 MHz; CDCl$_3$) spectra of compound **10a**:
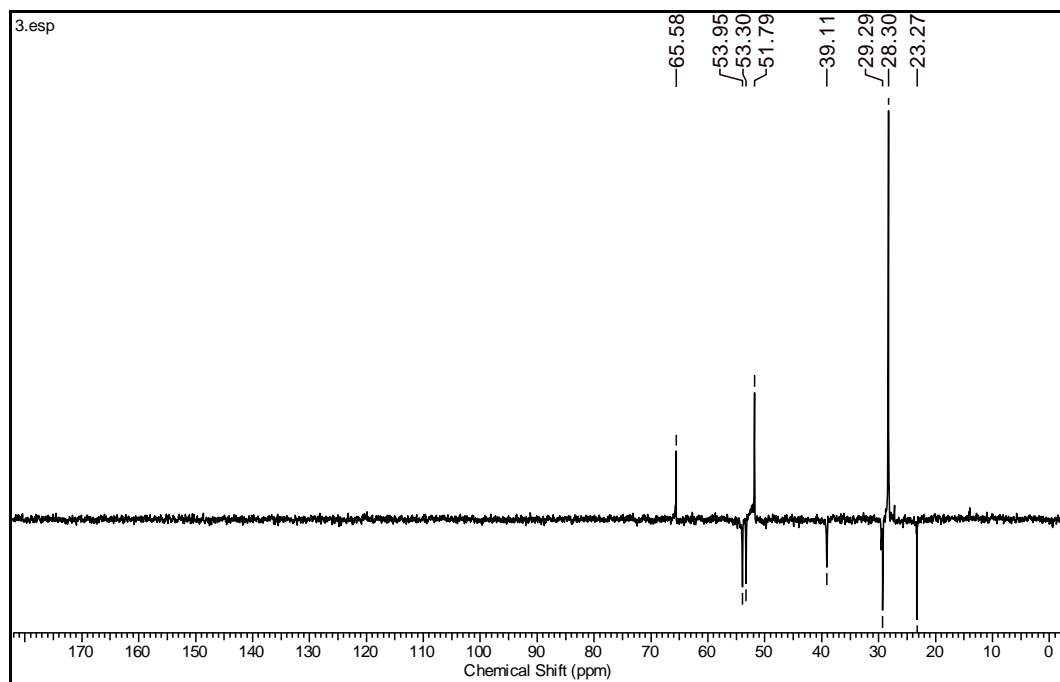
HRMS (ESI) spectra of compound **10a:**
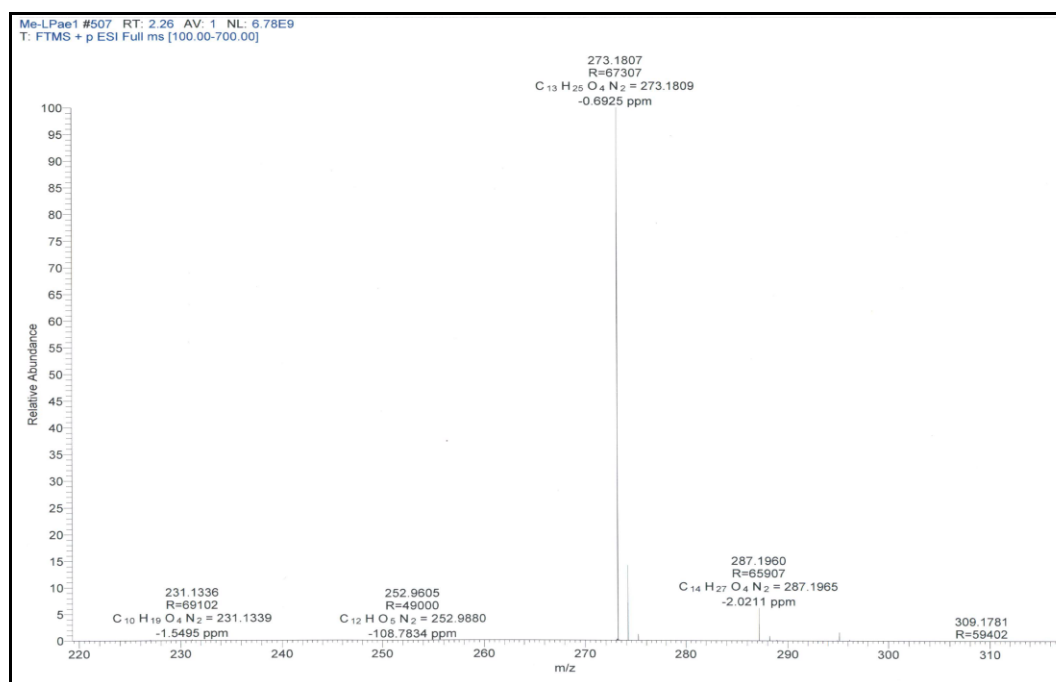
^{1}H NMR (200 MHz; CDCl$_3$) spectra of compound **10b**:
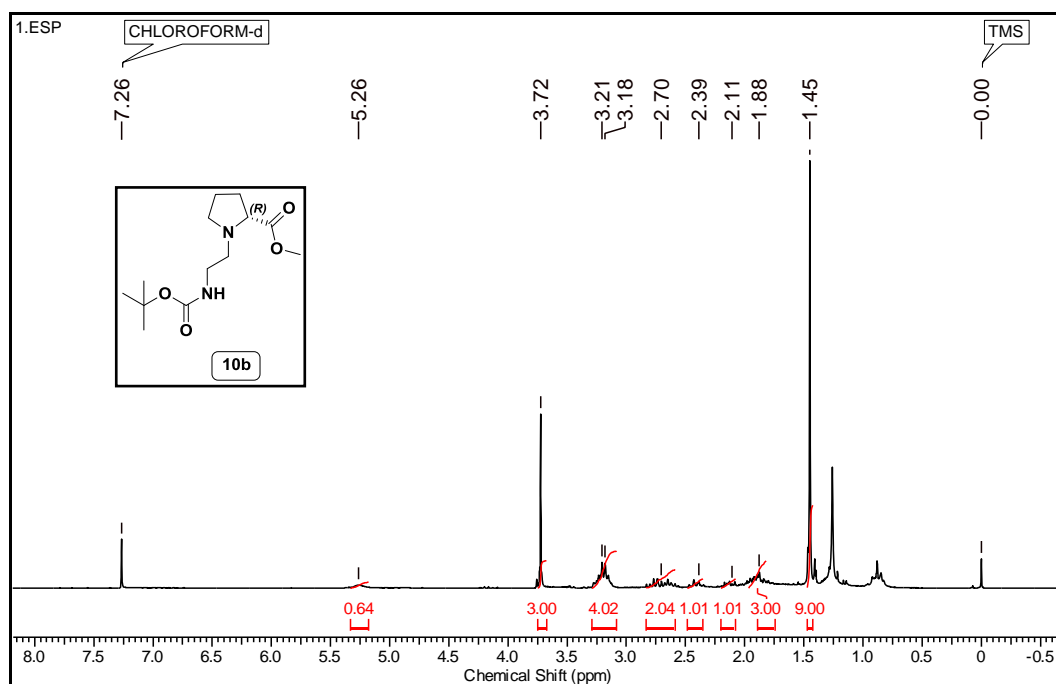
^{13}C NMR (125 MHz; CDCl$_3$) spectra of compound **10b**:
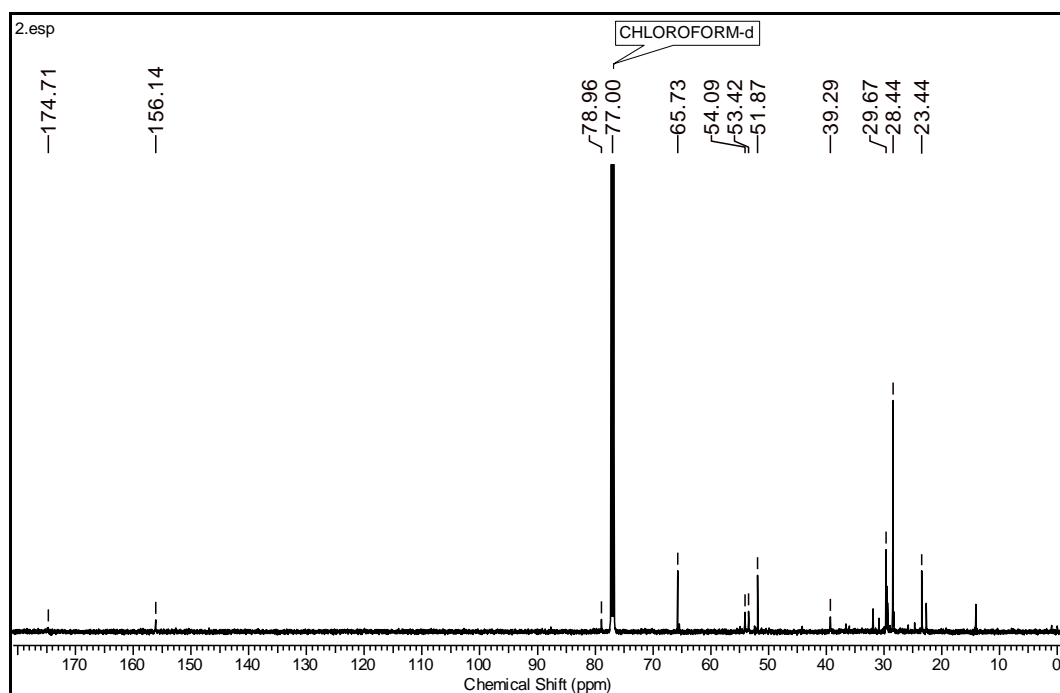
^{13}C DEPT (125 MHz; CDCl$_3$) spectra of compound **10b**:
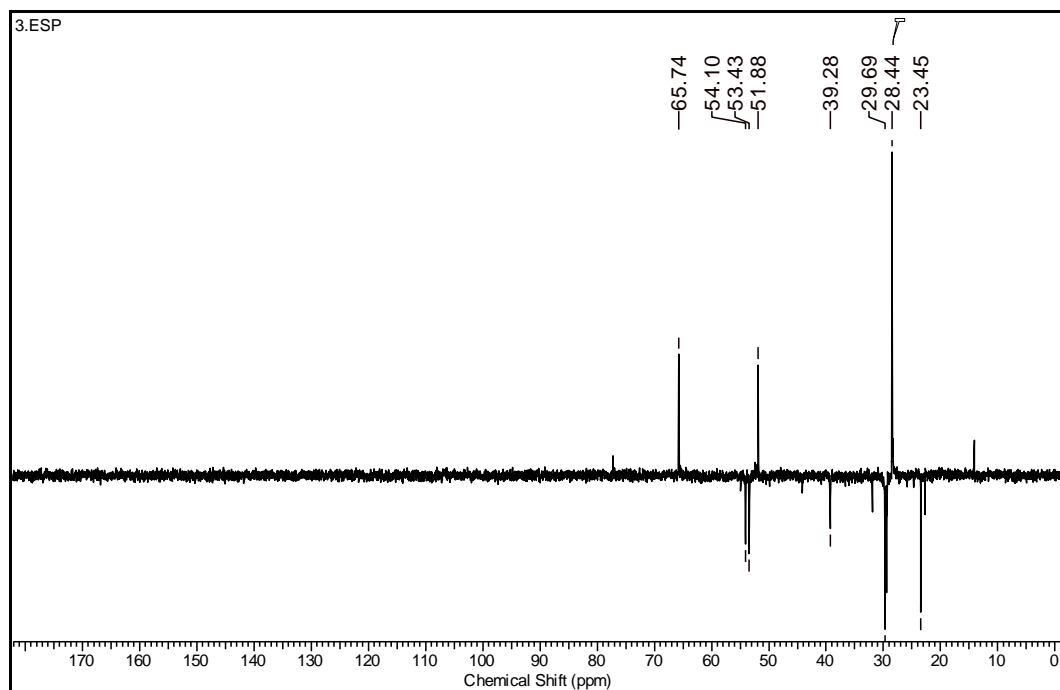
HRMS (ESI) spectra of compound **10b:**
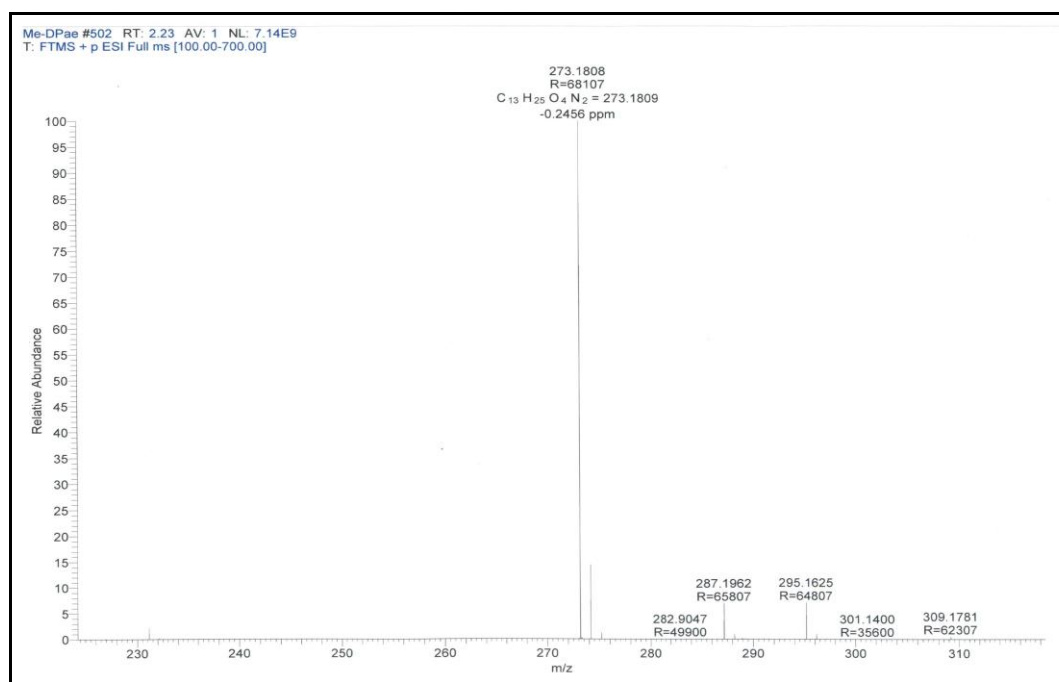
¹H NMR (200 MHz; CDCl₃) spectra of compound **13a**:
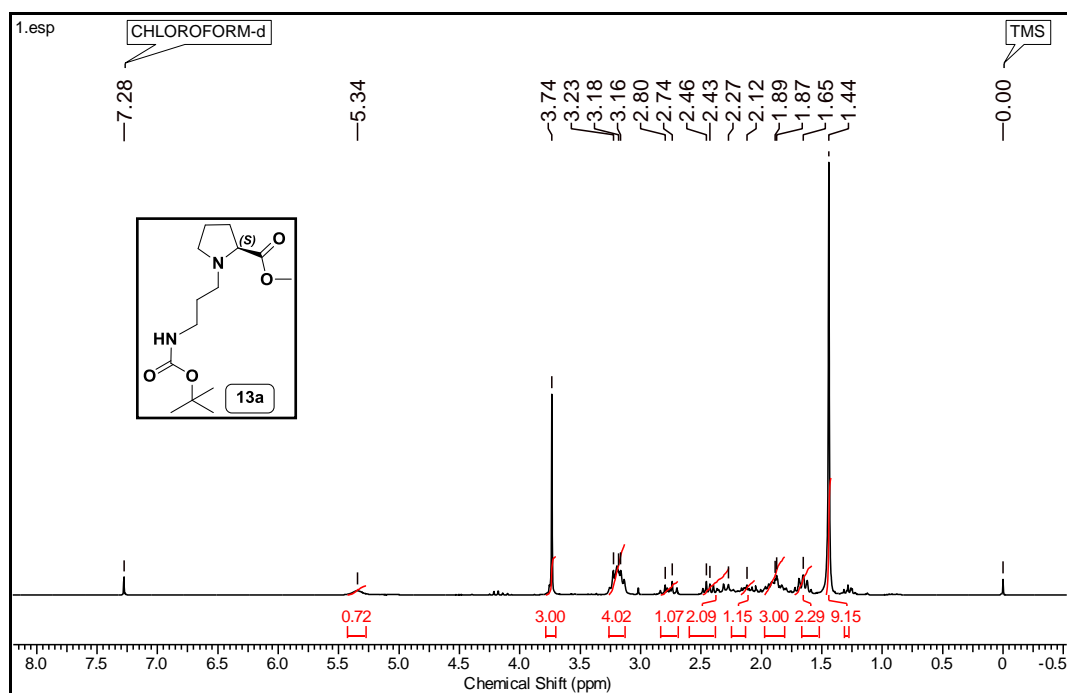
^{13}C NMR (50 MHz; CDCl$_3$) spectra of compound **13a**:
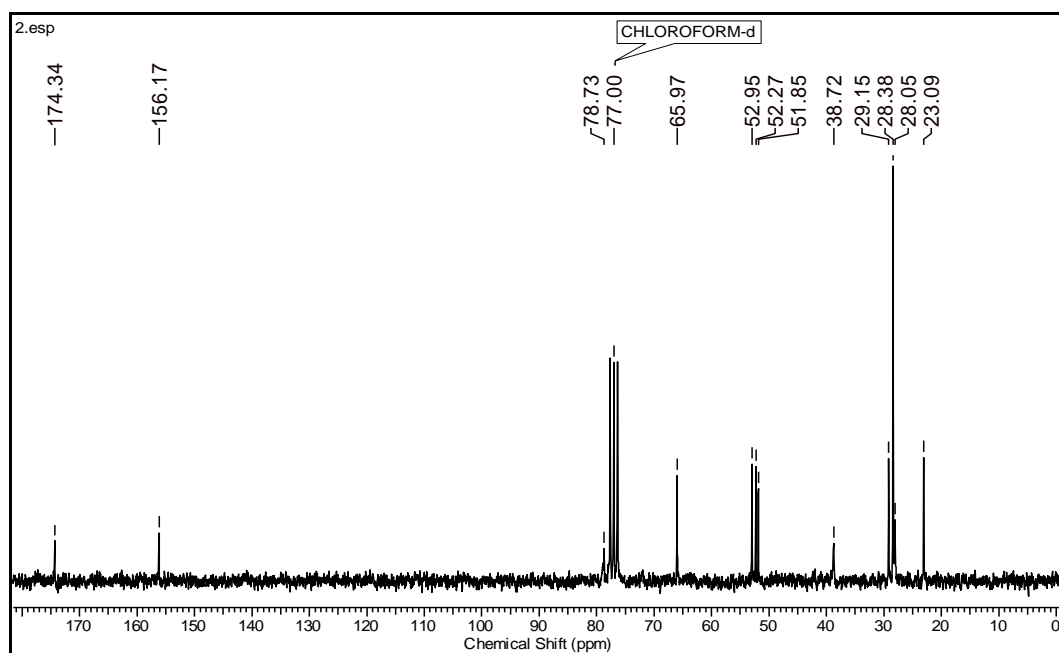
^{13}C DEPT (50 MHz; CDCl$_3$) spectra of compound **13a**:
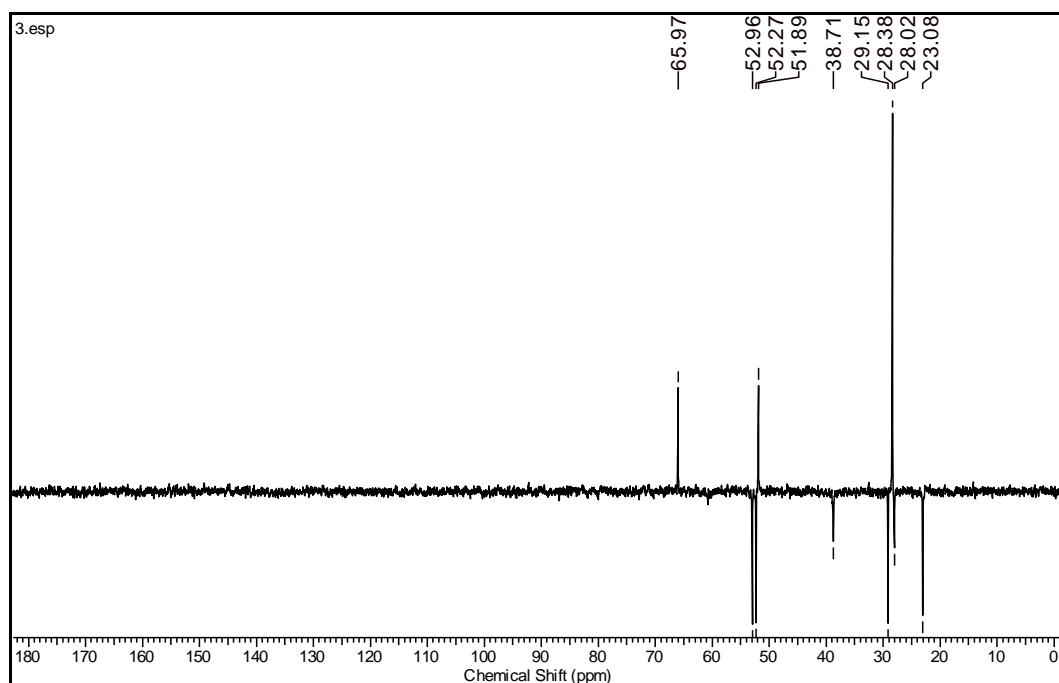
HRMS (ESI) spectra of compound **13a**:
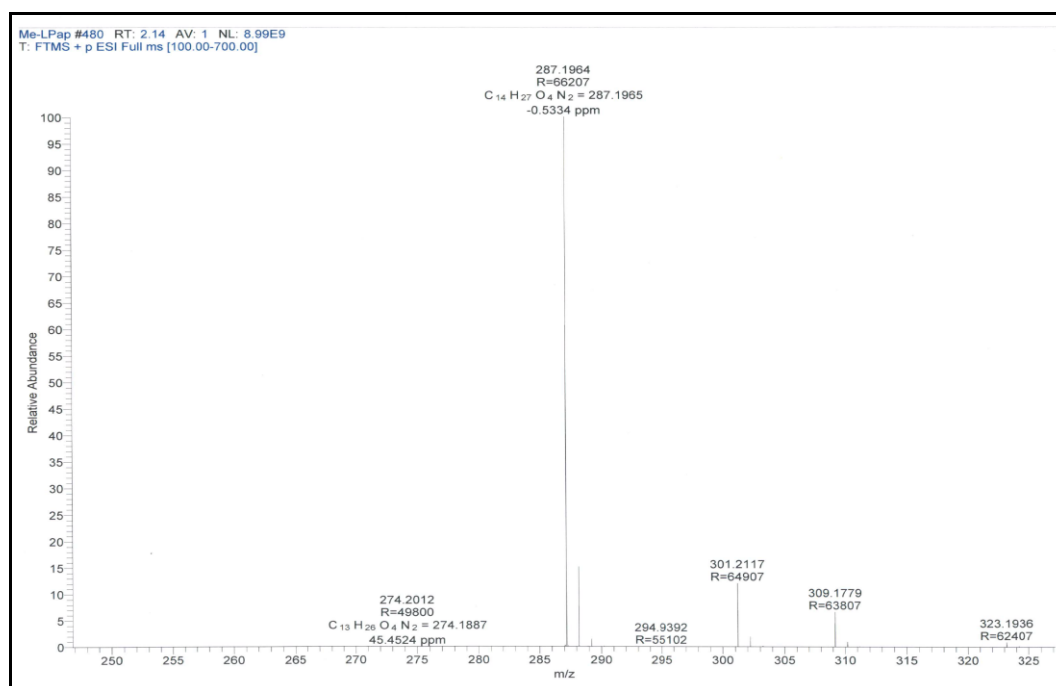
^{1}H NMR (200 MHz; CDCl$_3$) spectra of compound **13b**:
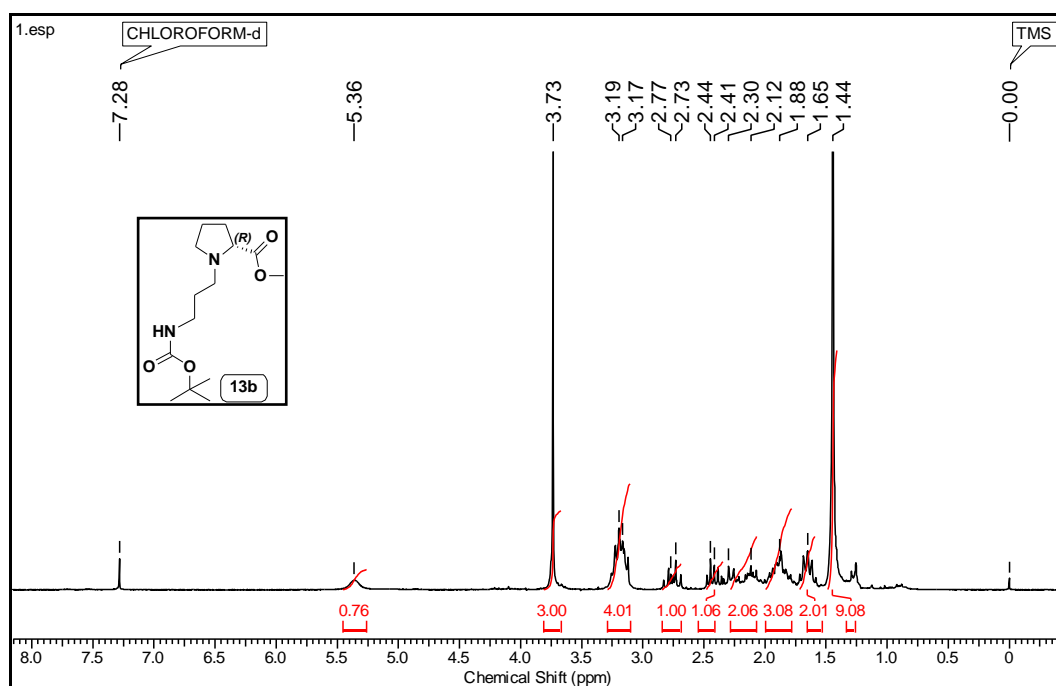
^{13}C NMR (50 MHz; CDCl$_3$) spectra of compound **13b**:
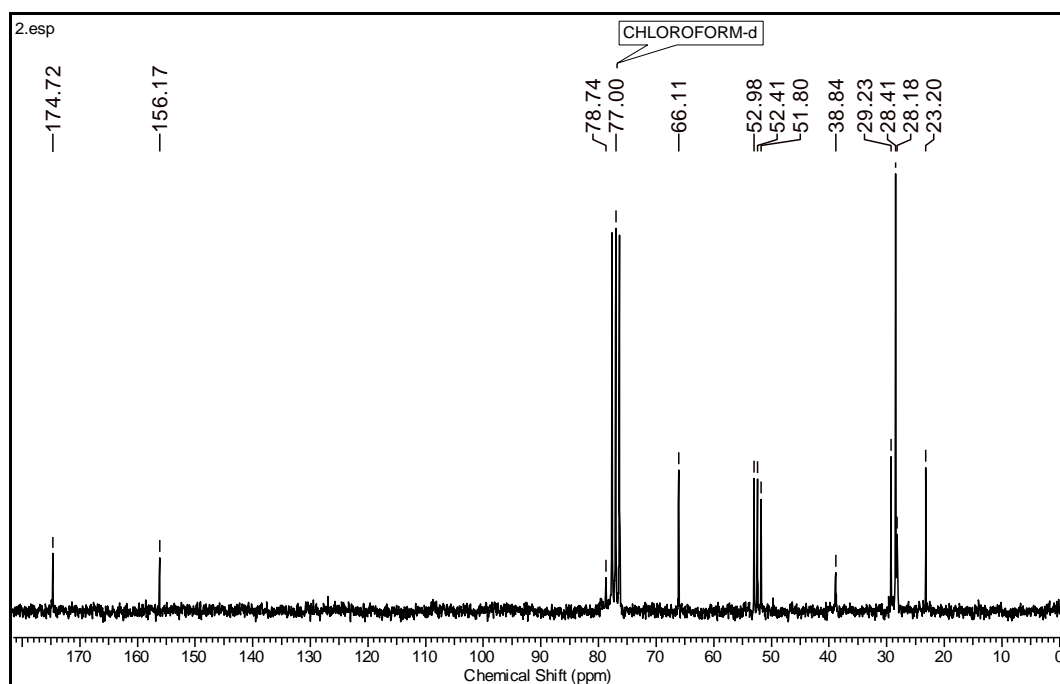
^{13}C DEPT (50 MHz; CDCl$_3$) spectra of compound **13b**:
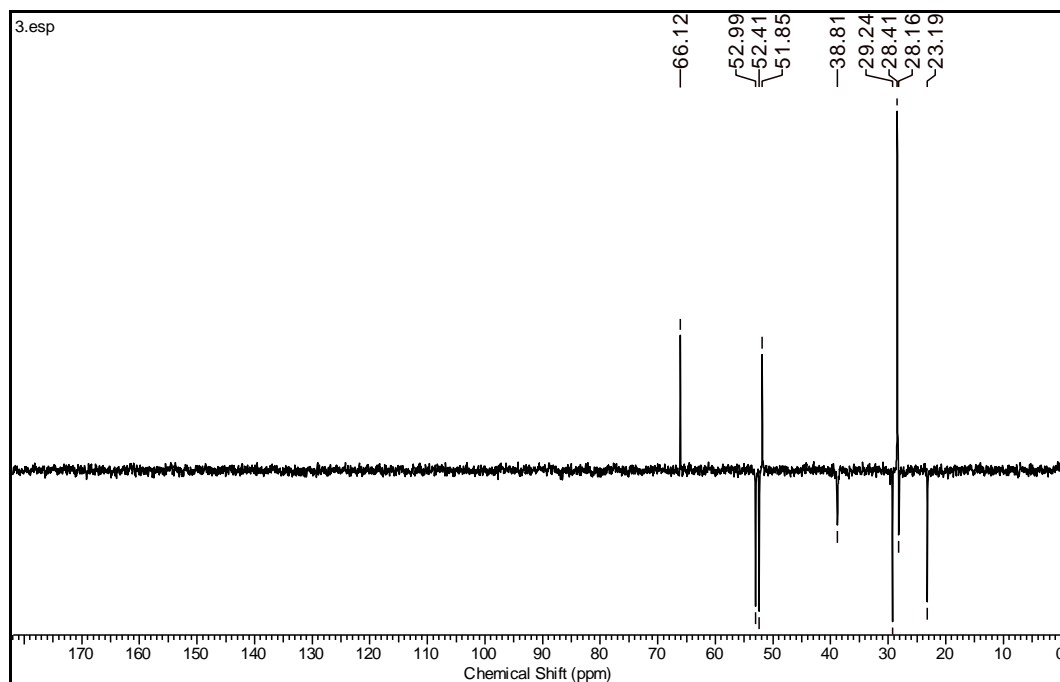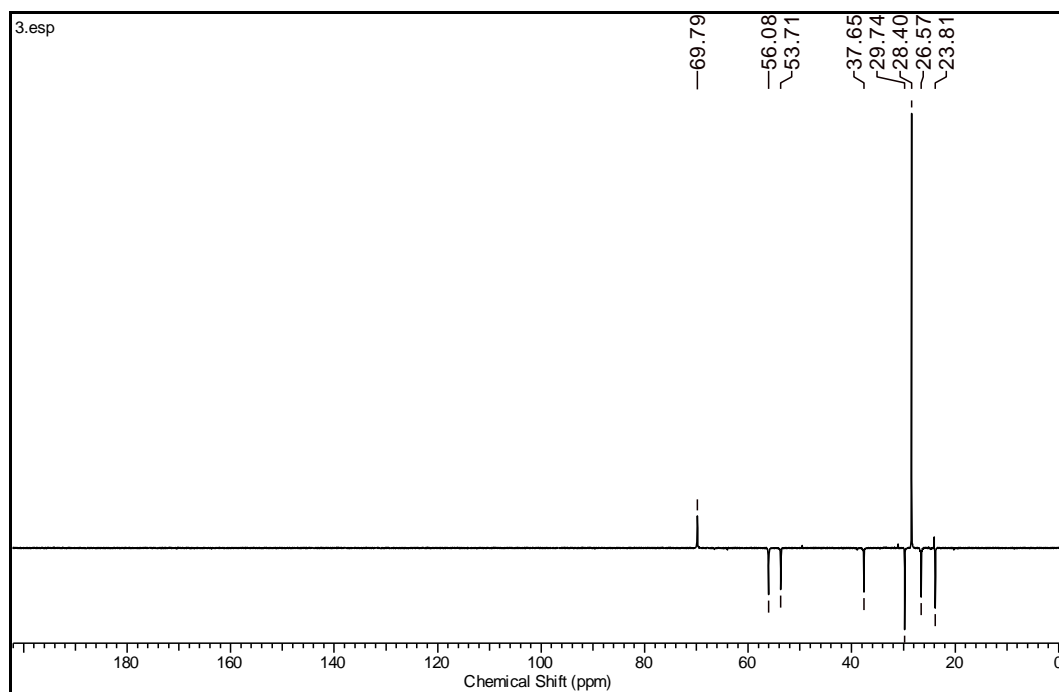
HRMS (ESI) spectra of compound **13b**:
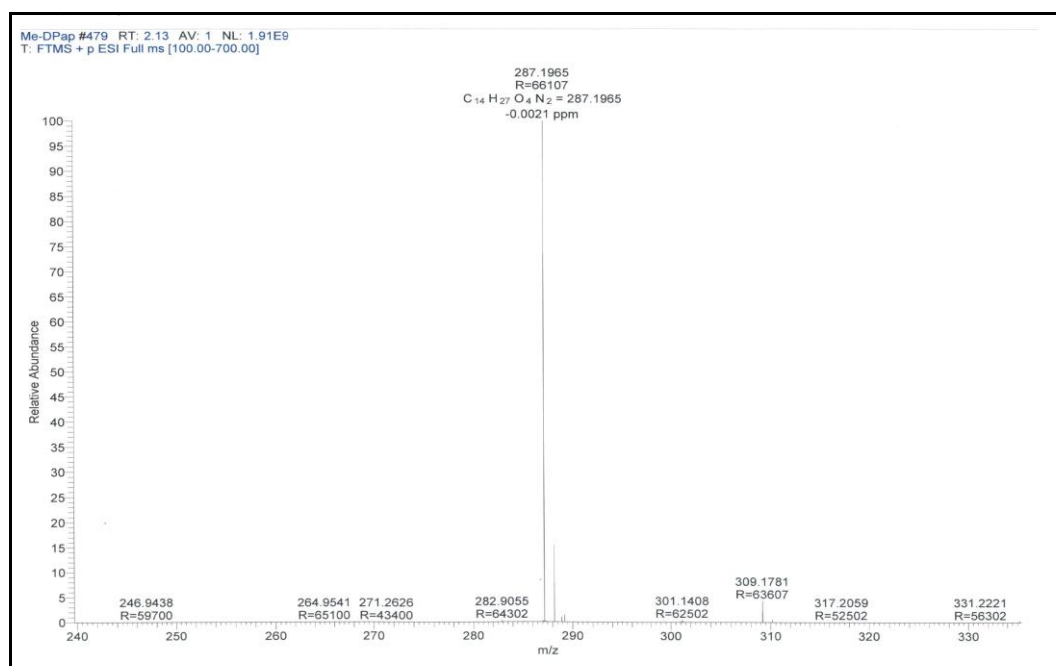
^{1}H NMR (500 MHz; D$_2$O) spectra of compound **11a**:
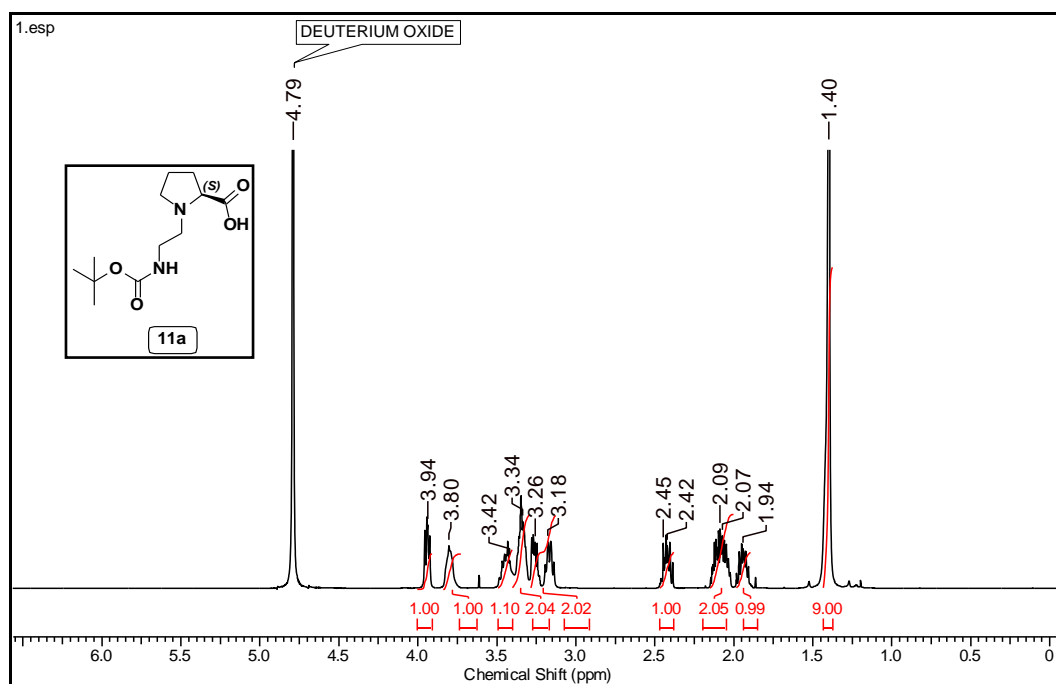
^{13}C NMR (125 MHz; D$_2$O) spectra of compound **11a**:
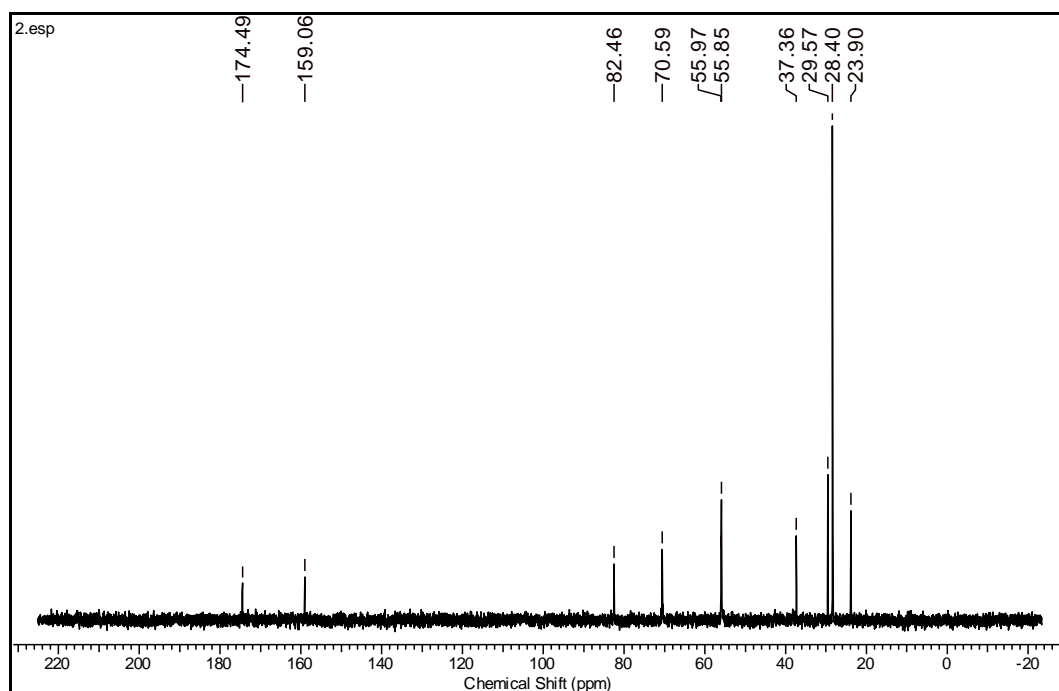
^{13}C DEPT (125 MHz; D$_2$O) spectra of compound **11a**:
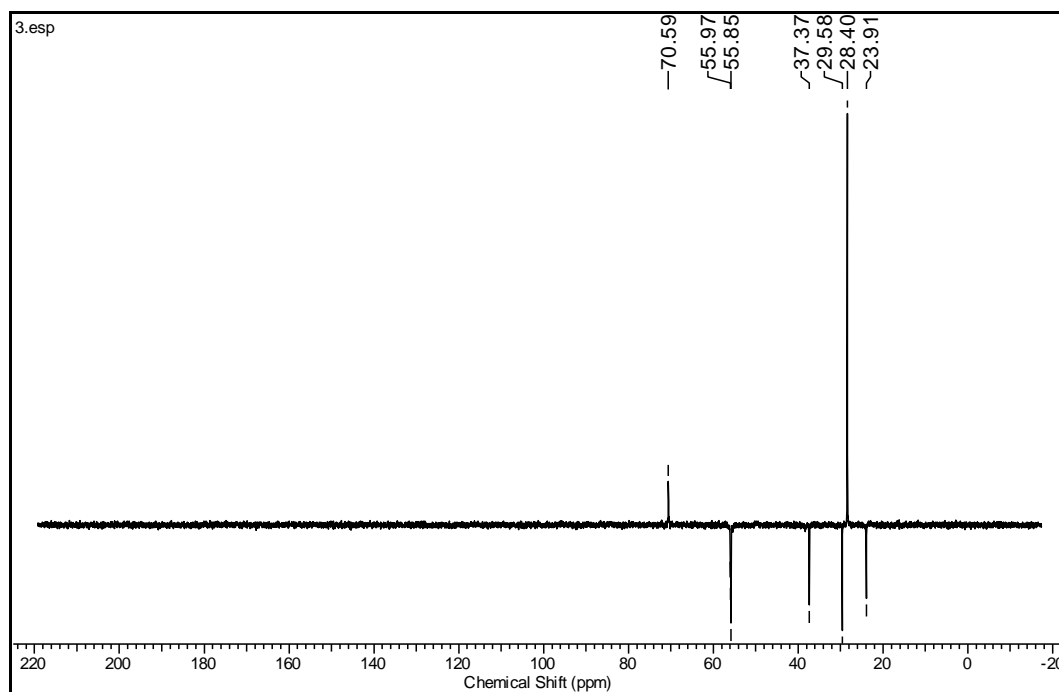
HRMS (ESI) spectra of compound **11a**:
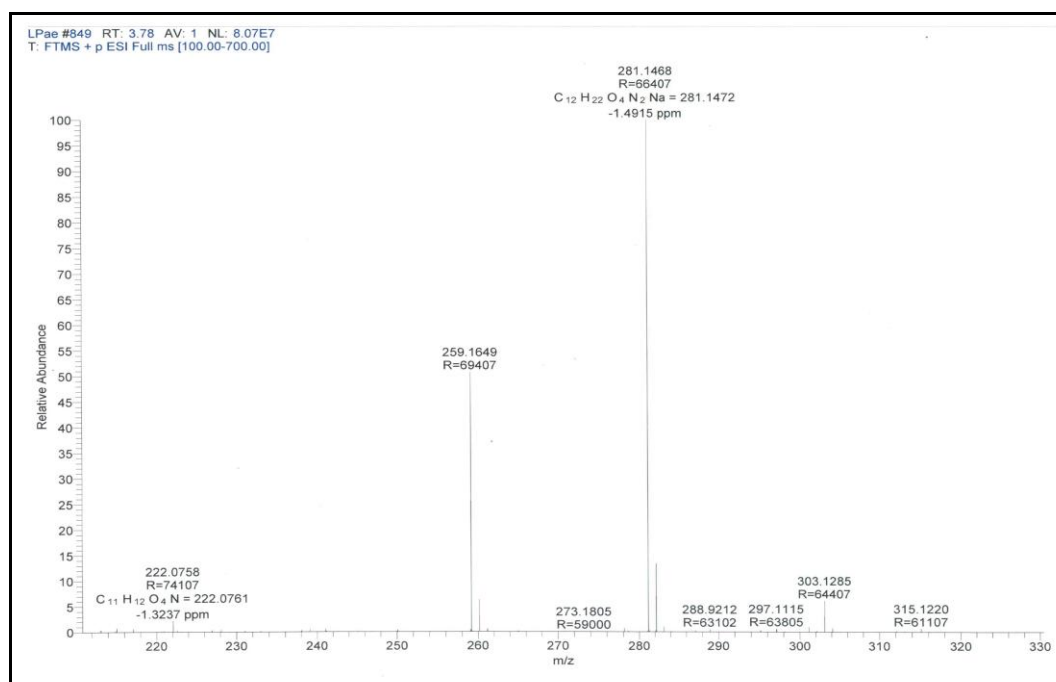
^{1} H NMR (400 MHz; D$_2$O) spectra of compound **11b**:
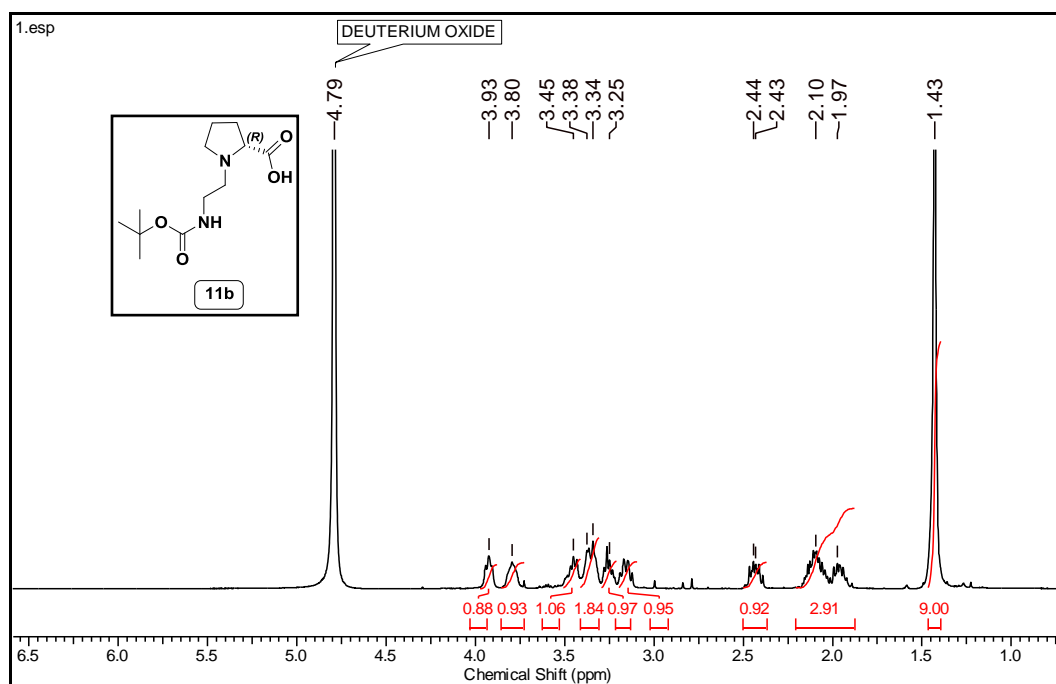
^{13}C NMR (100 MHz; D$_2$O) spectra of compound **11b**:
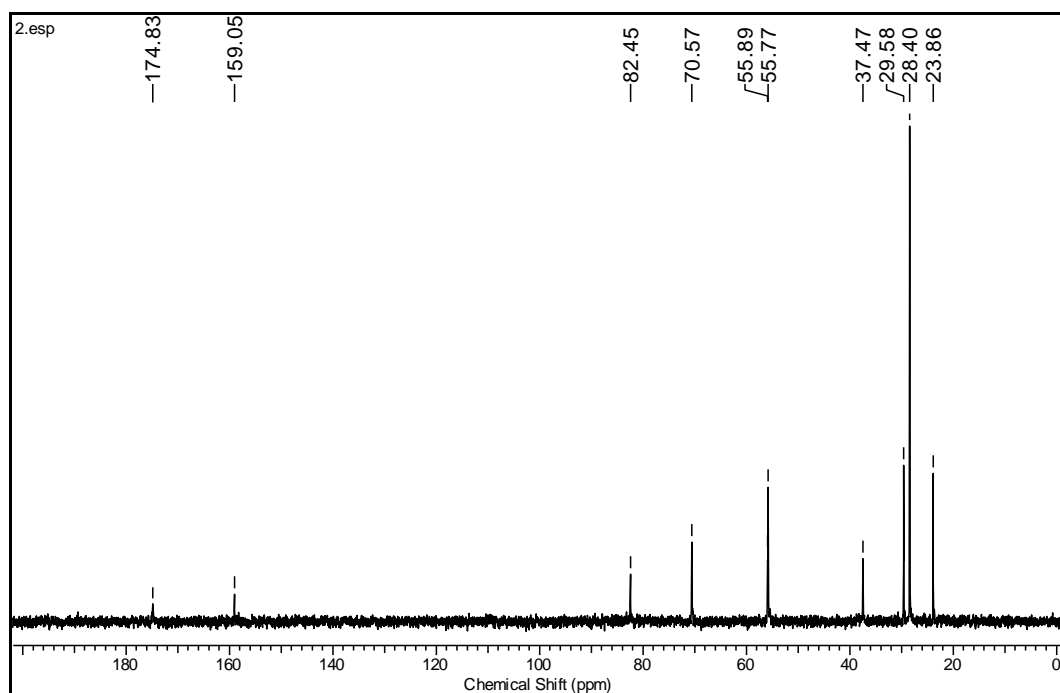
^{13}C DEPT (100 MHz; D$_2$O) spectra of compound **11b**:
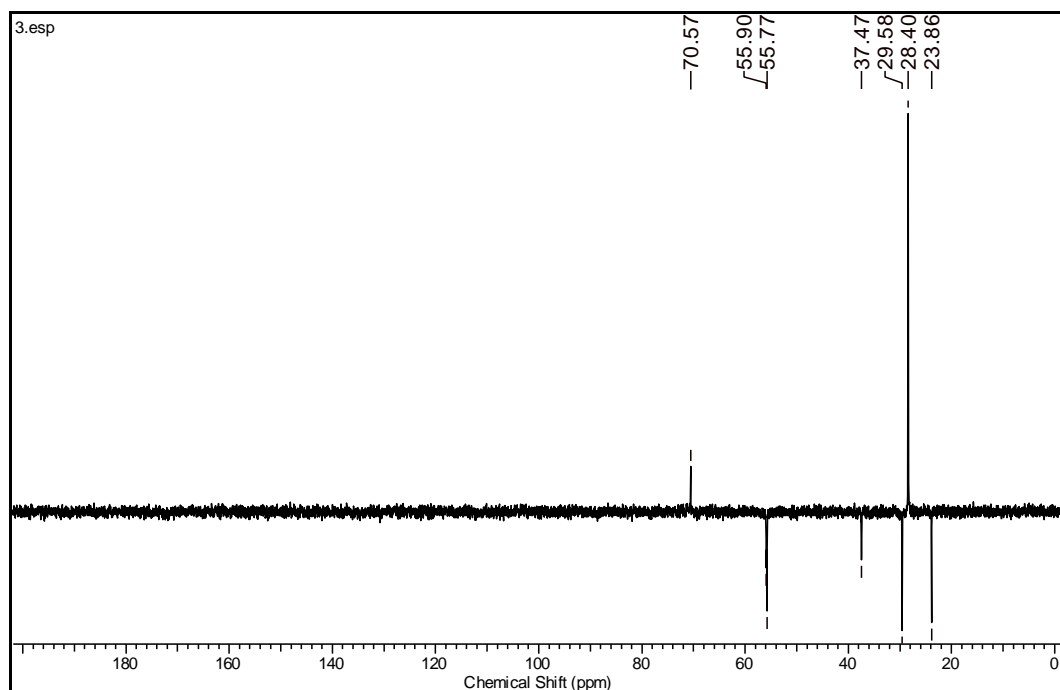
HRMS (ESI) spectra of compound **11b**:
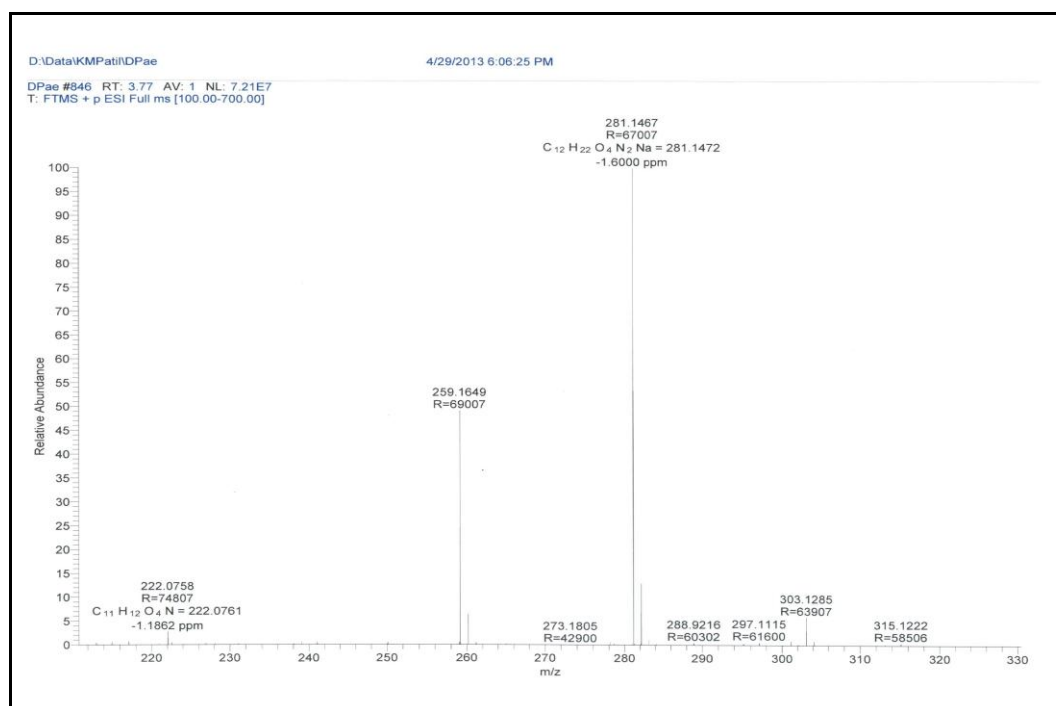
^{1}H NMR (500 MHz; D$_2$O) spectra of compound **14a**:
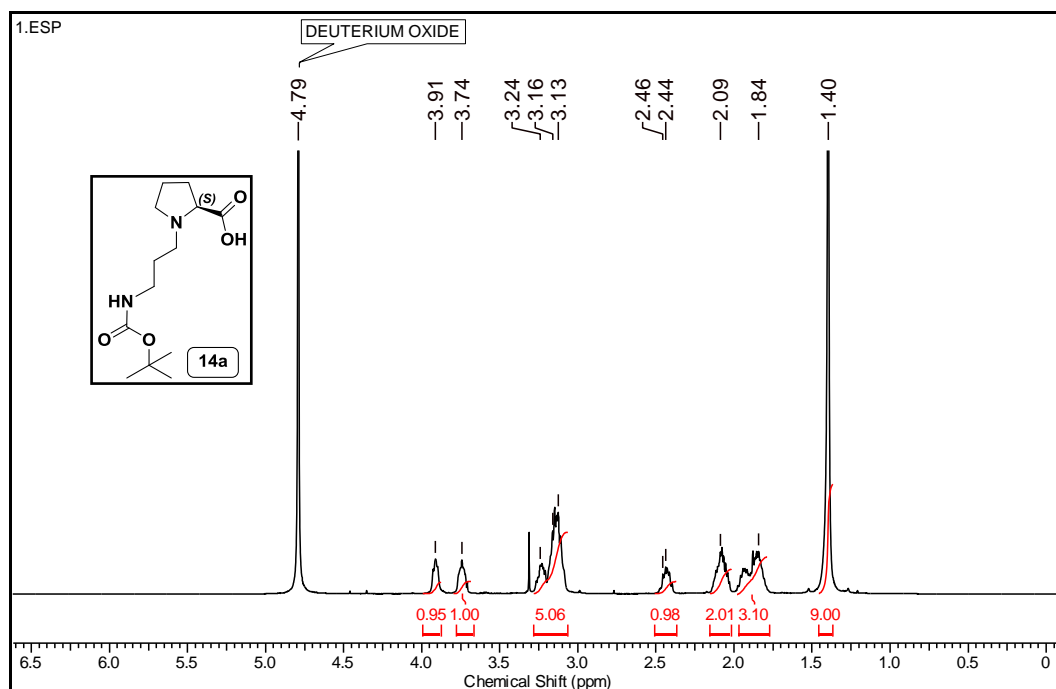
^{13}C NMR (125 MHz; D$_2$O) spectra of compound **14a**:
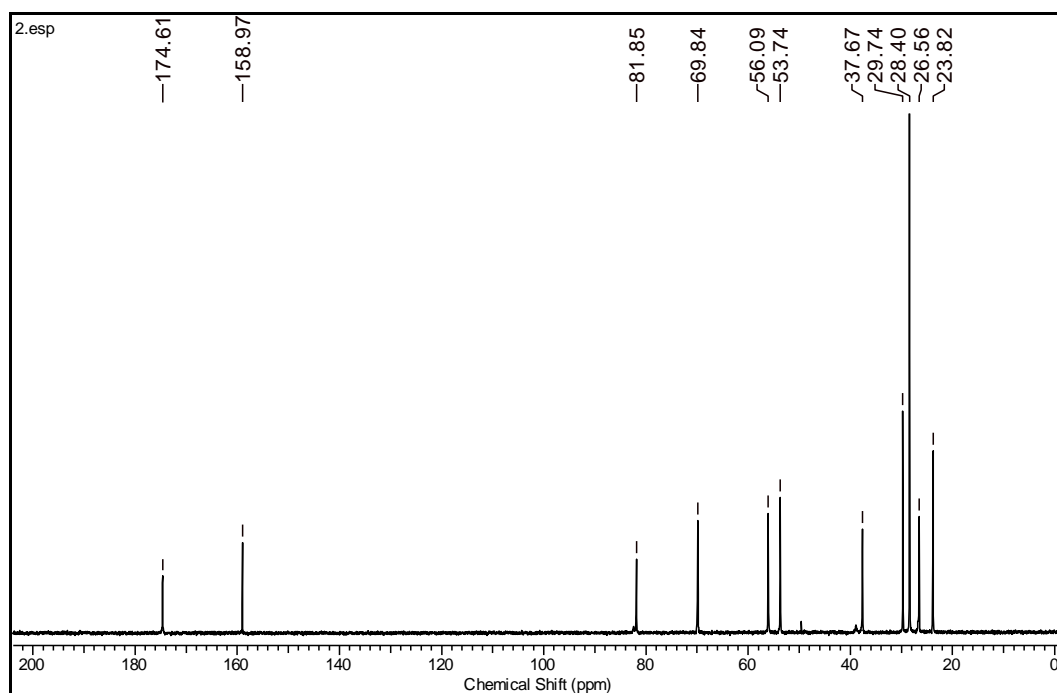
^{13}C DEPT (125 MHz; D$_2$O) spectra of compound **14a**:
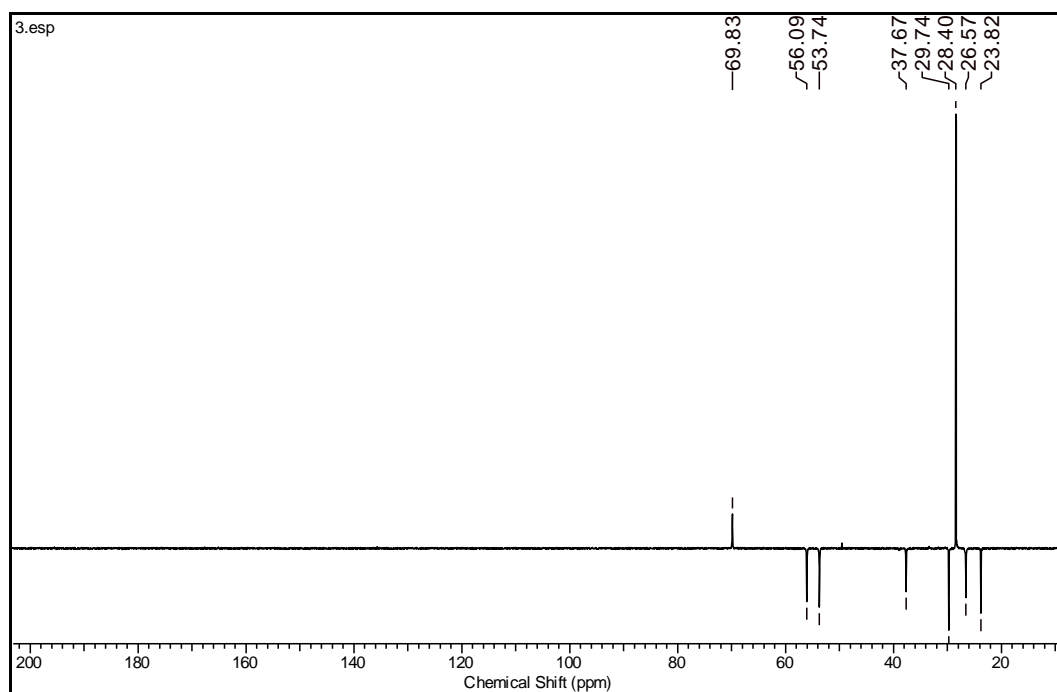
HRMS (ESI) spectra of compound **14a**:
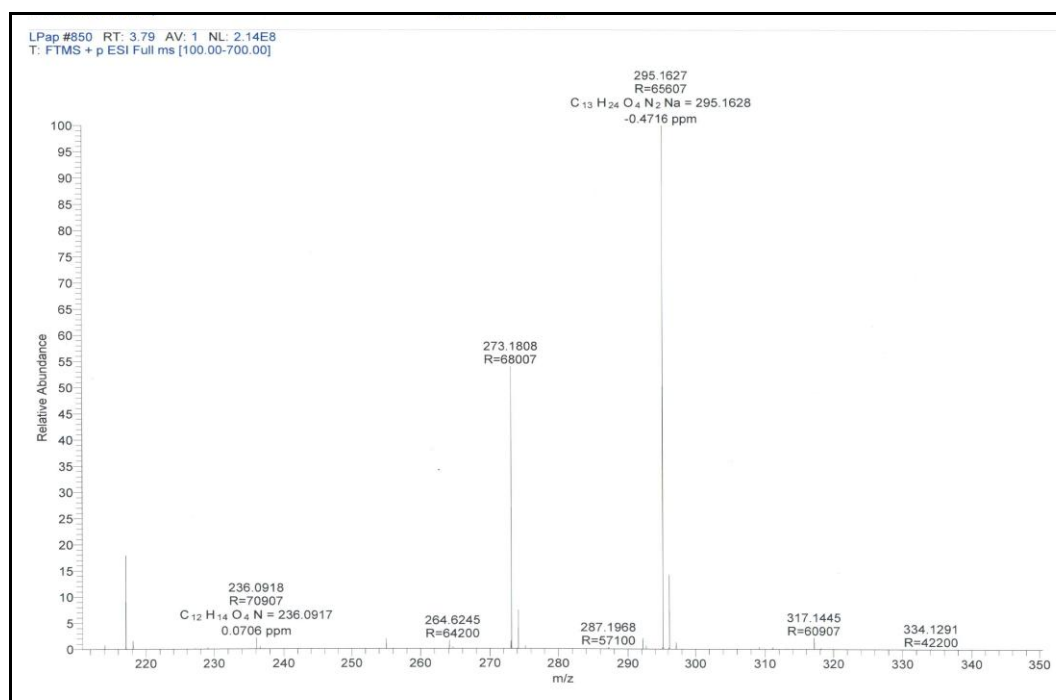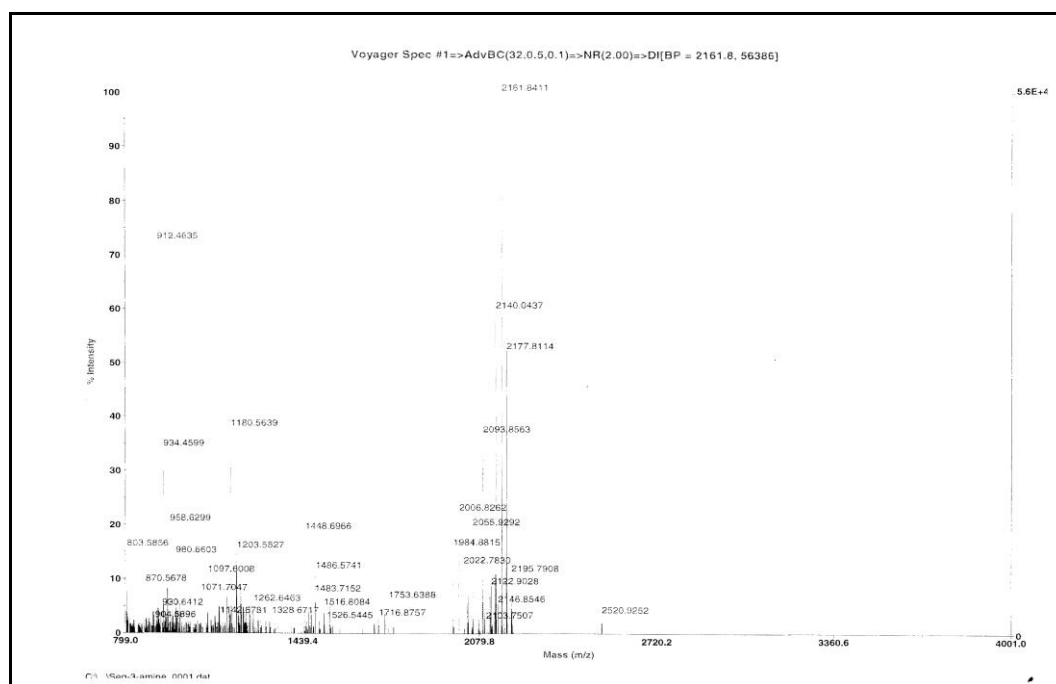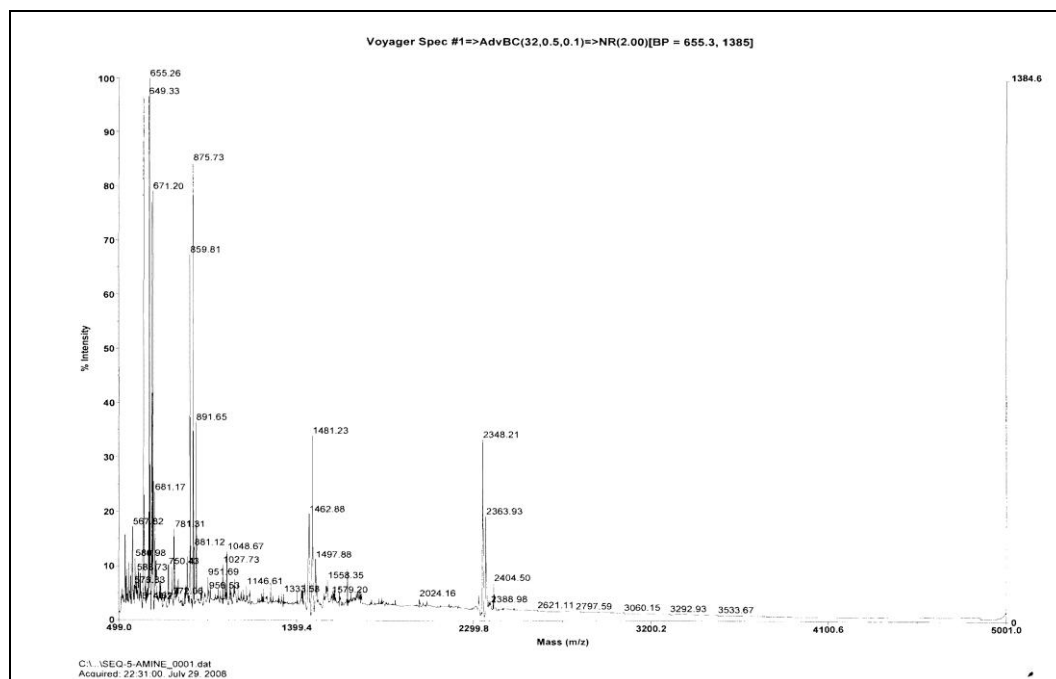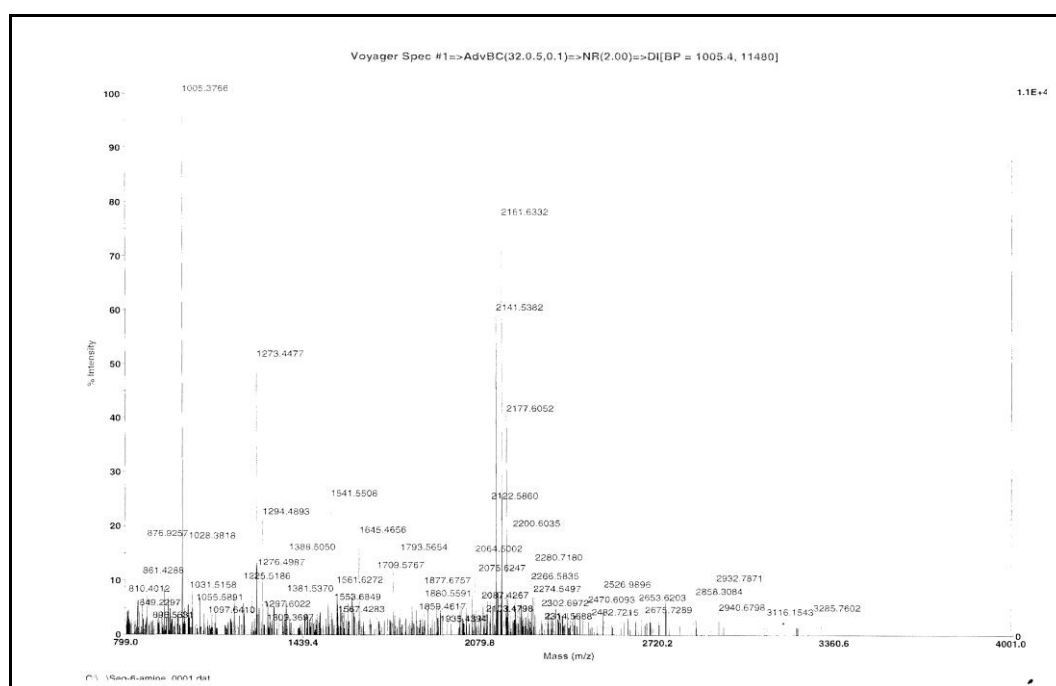

^{1}H NMR (125 MHz; D$_2$O) spectra of compound **14b**:
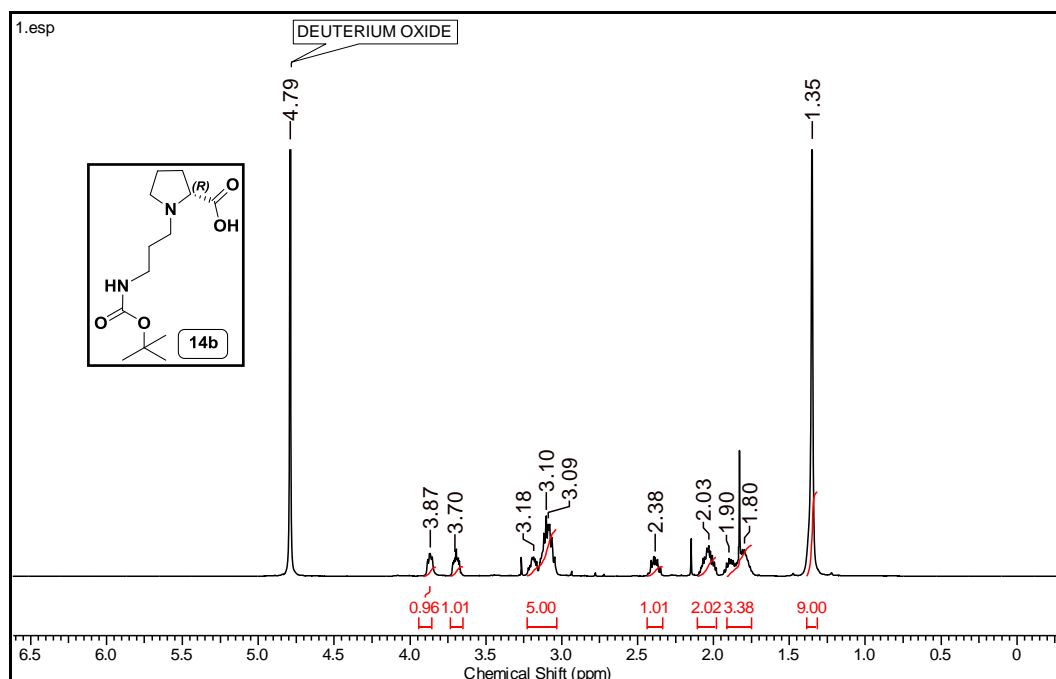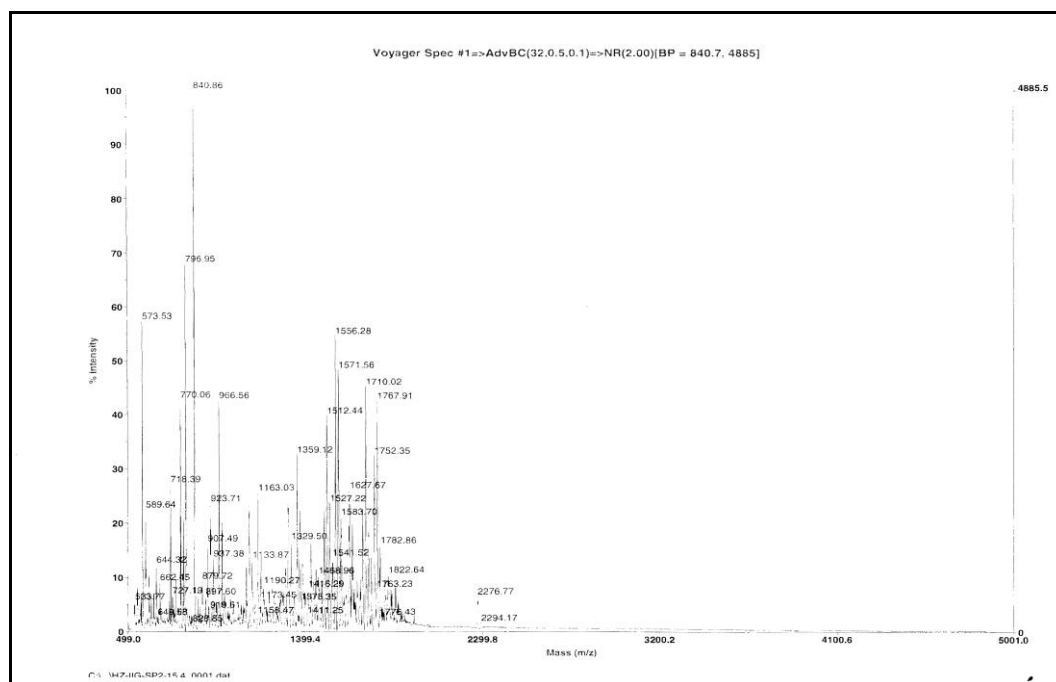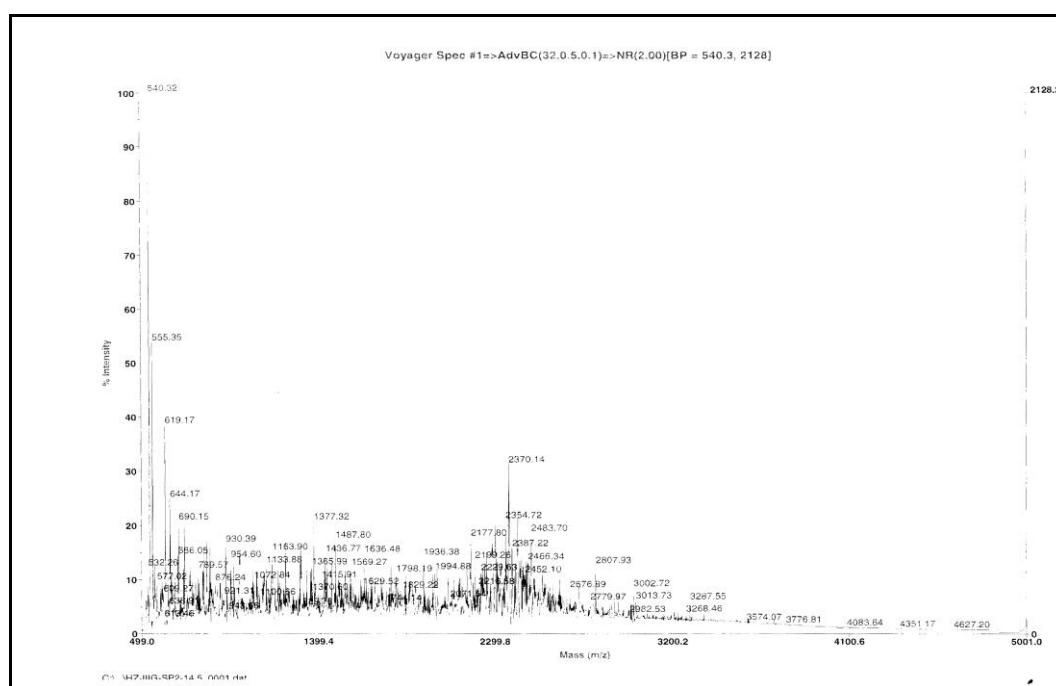
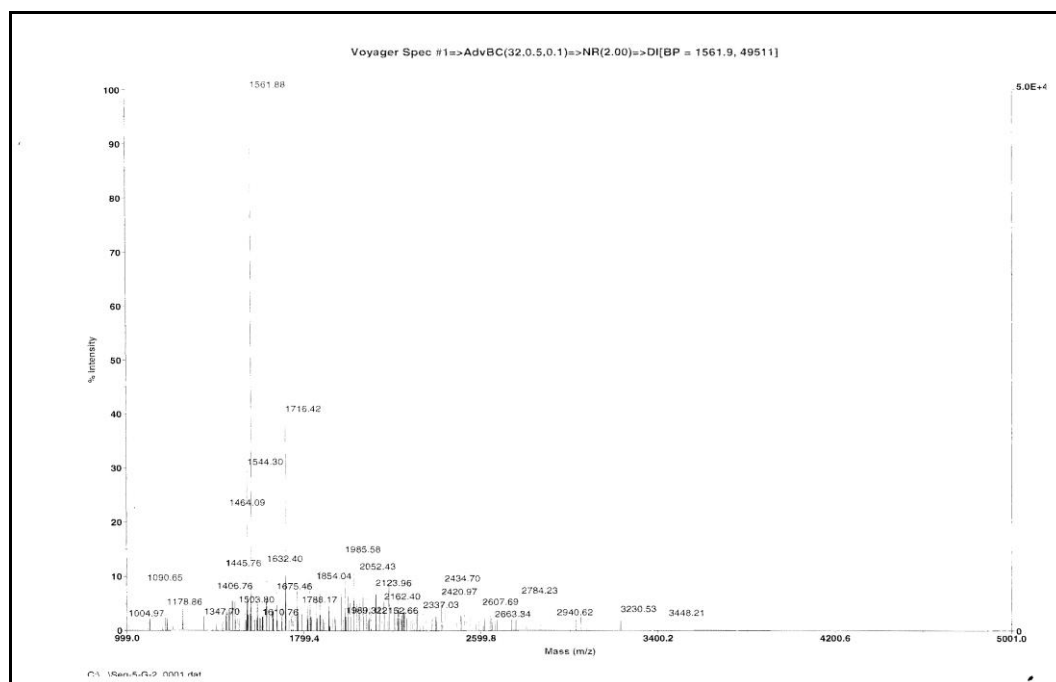^{13}C NMR (125 MHz; D$_2$O) spectra of compound **14b**:
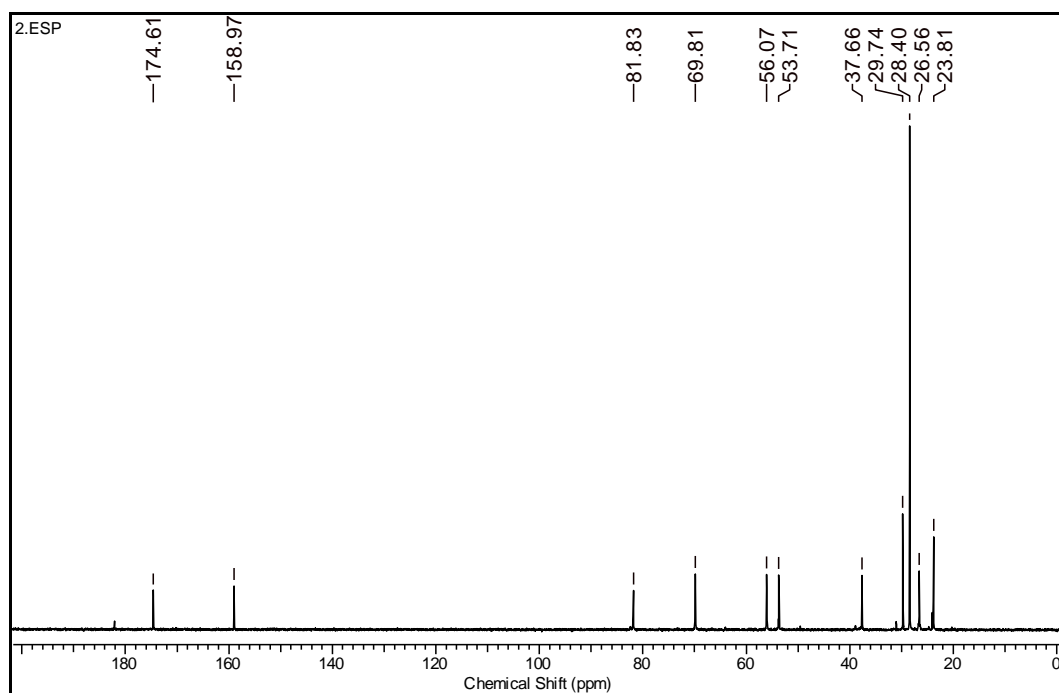
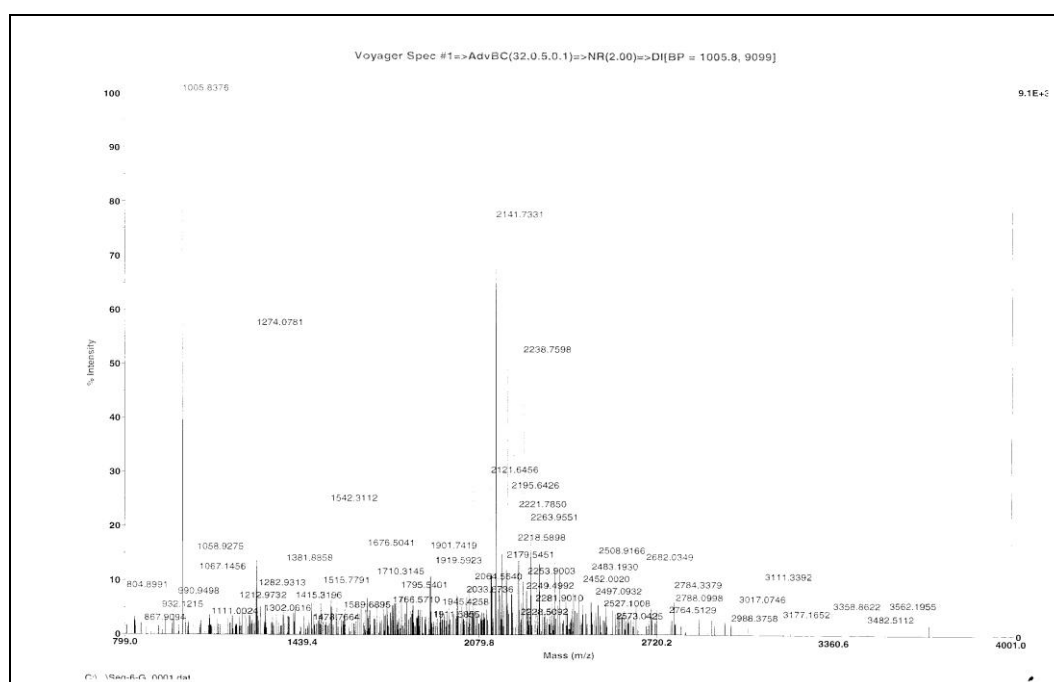^{13}C DEPT (125 MHz; D$_2$O) spectra of compound **14b**:

HRMS (ESI) spectra of compound **14b**:
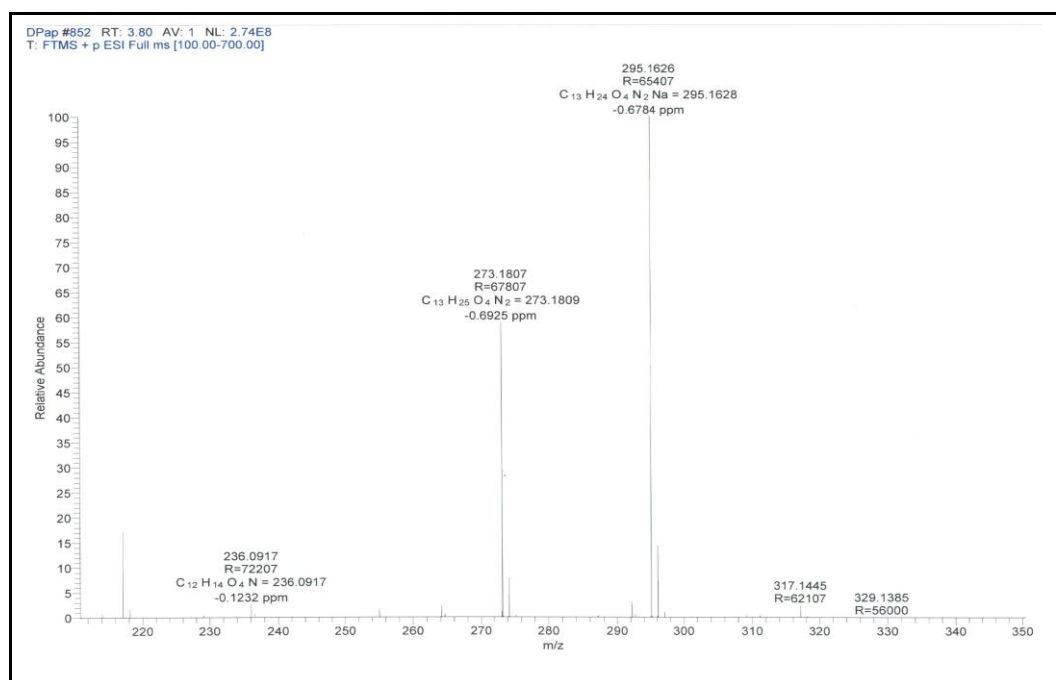
MALDI-TOF spectrum of **P1**:
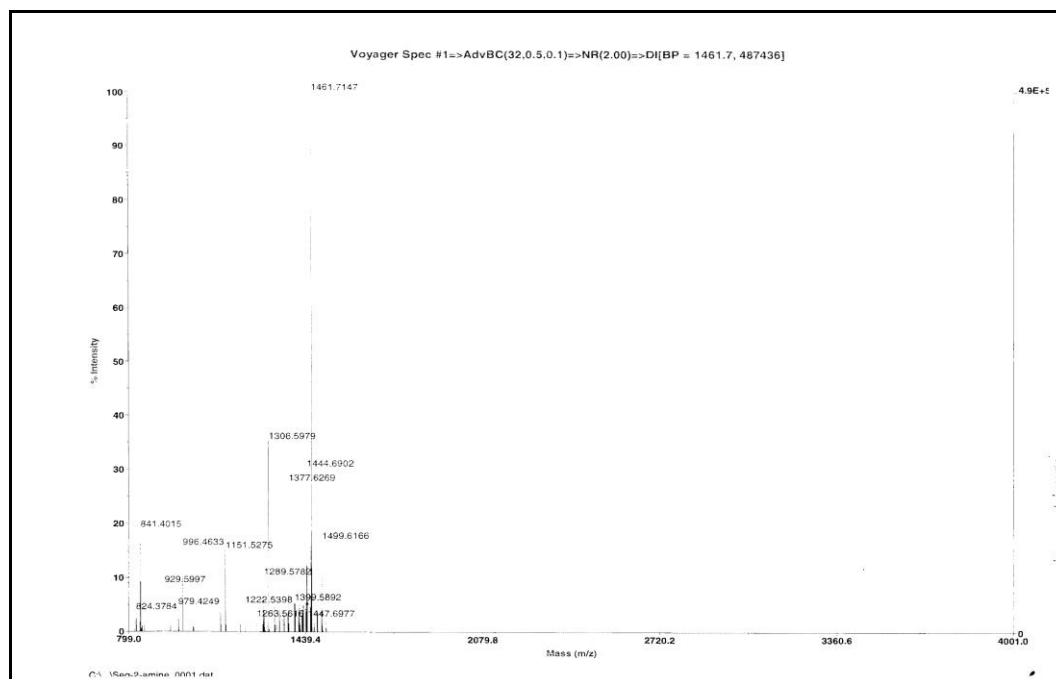
MALDI-TOF spectrum of **P2**:

MALDI-TOF spectrum of **P3**:

MALDI-TOF spectrum of **P4**:

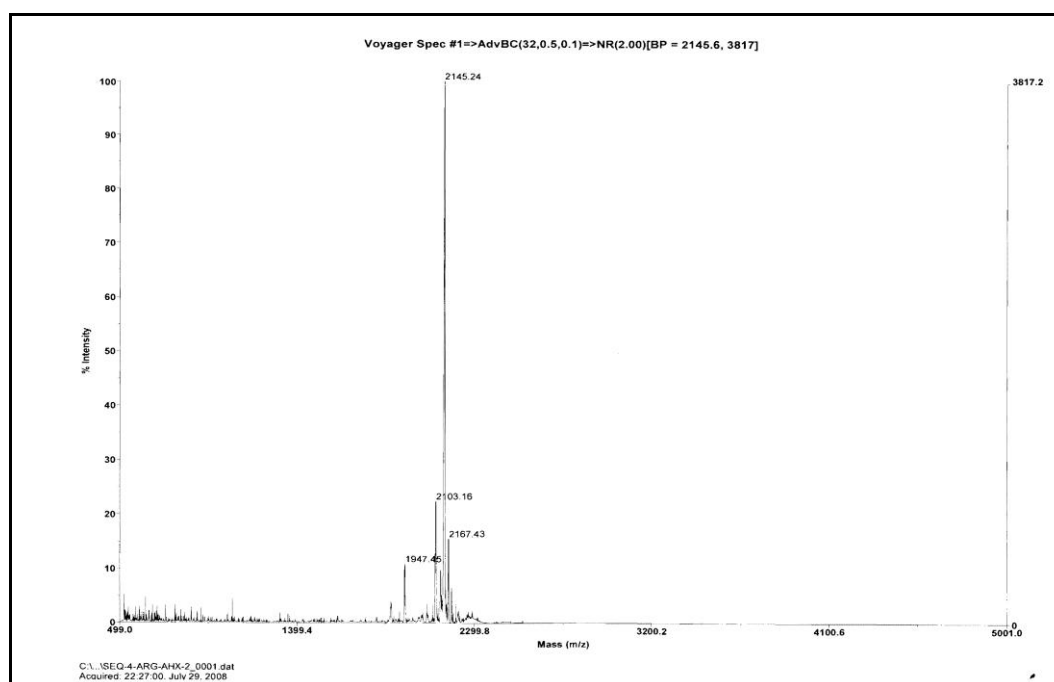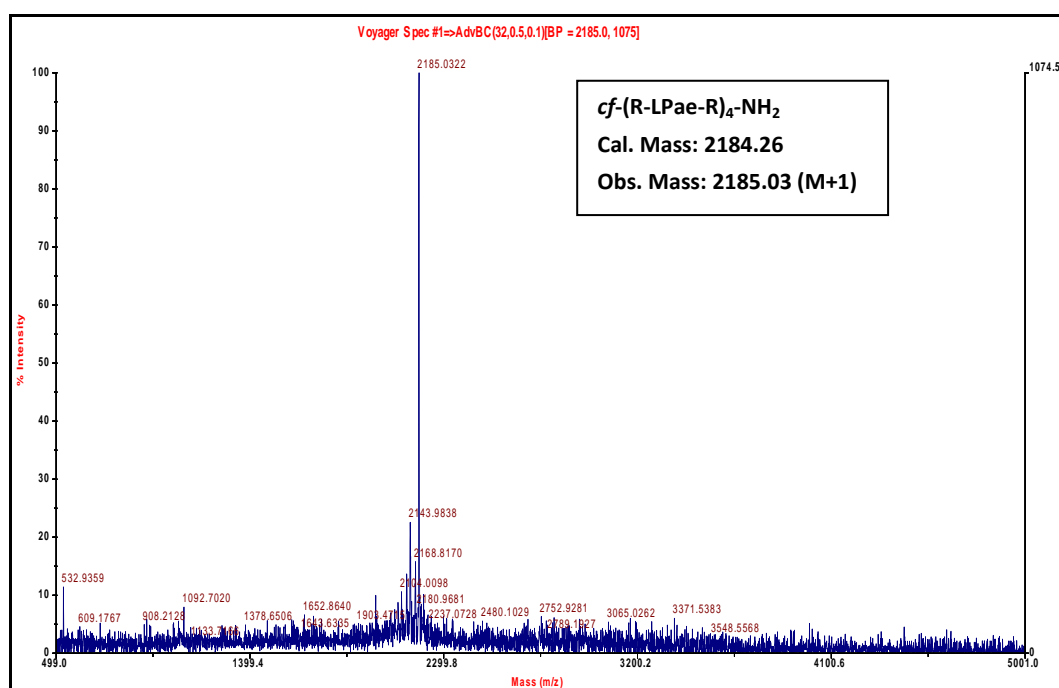MALDI-TOF spectrum of **P5**:

MALDI-TOF spectrum of **P6**:

MALDI-TOF spectrum of **P7**:

MALDI-TOF spectrum of **P8**:

MALDI-TOF spectrum of **P10**:

MALDI-TOF spectrum of ^{cf}**P11**:

MALDI-TOF spectrum of ^{cf}**P12**:
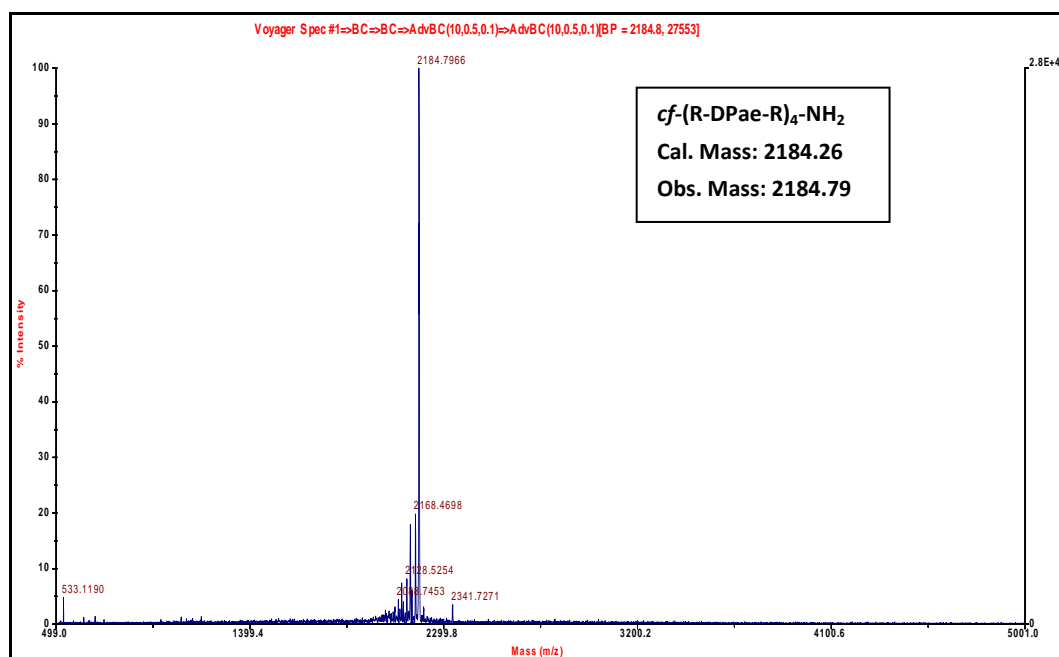
MALDI-TOF spectrum of ^{cf}**P13**:
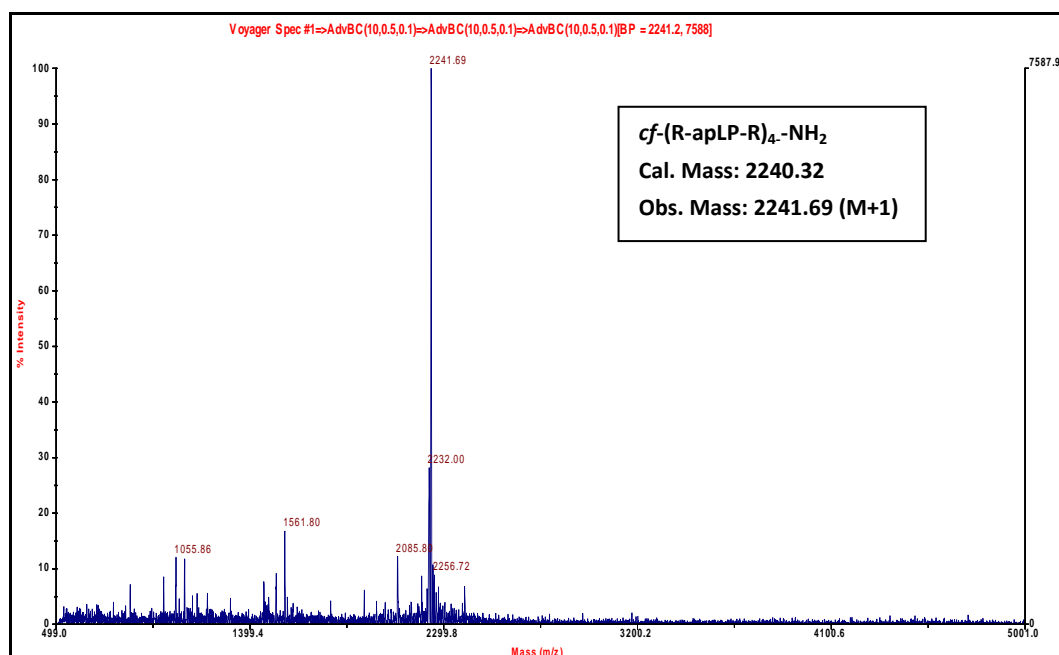
MALDI-TOF spectrum of ^{cf}**P14**:
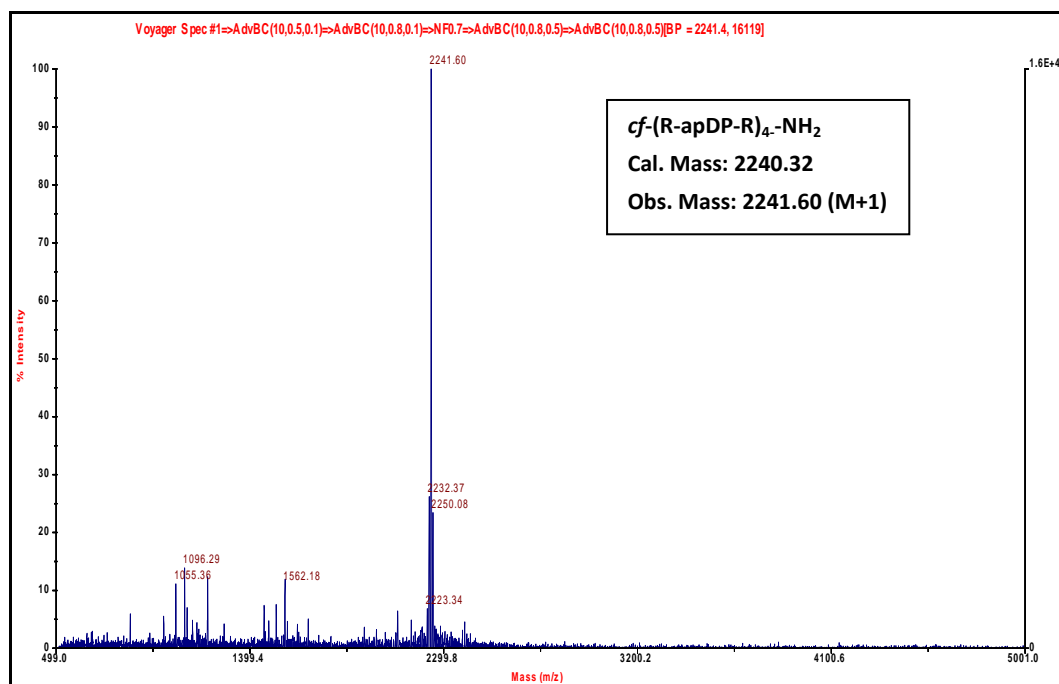
MALDI-TOF spectrum of ^{cf}**P15**:
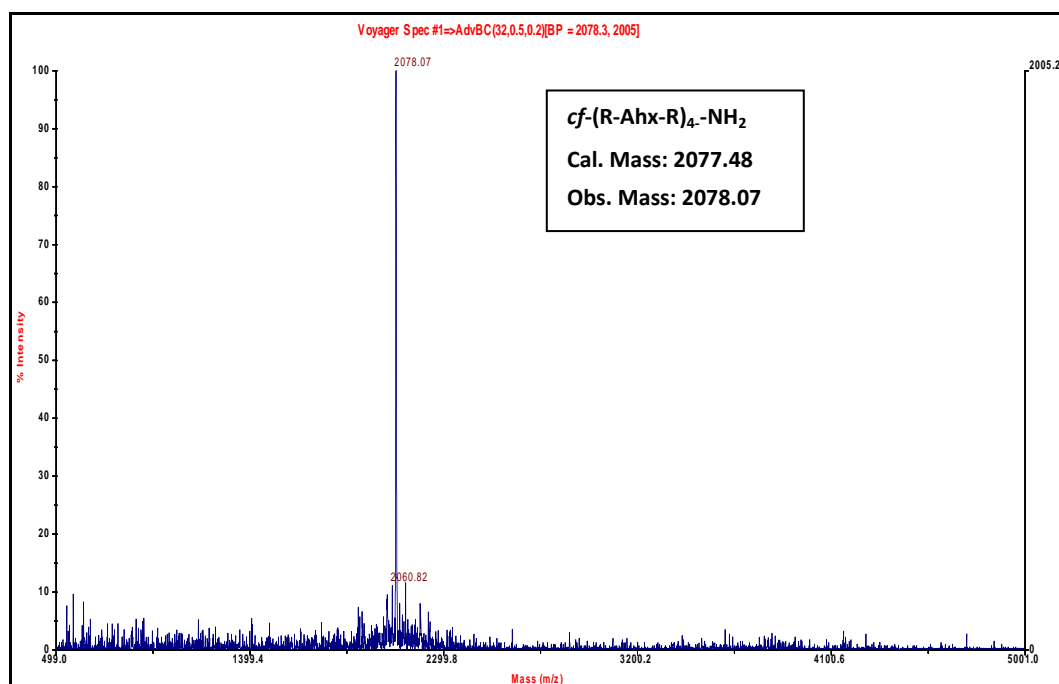
MALDI-TOF spectrum of ^{Ac}**P12**:
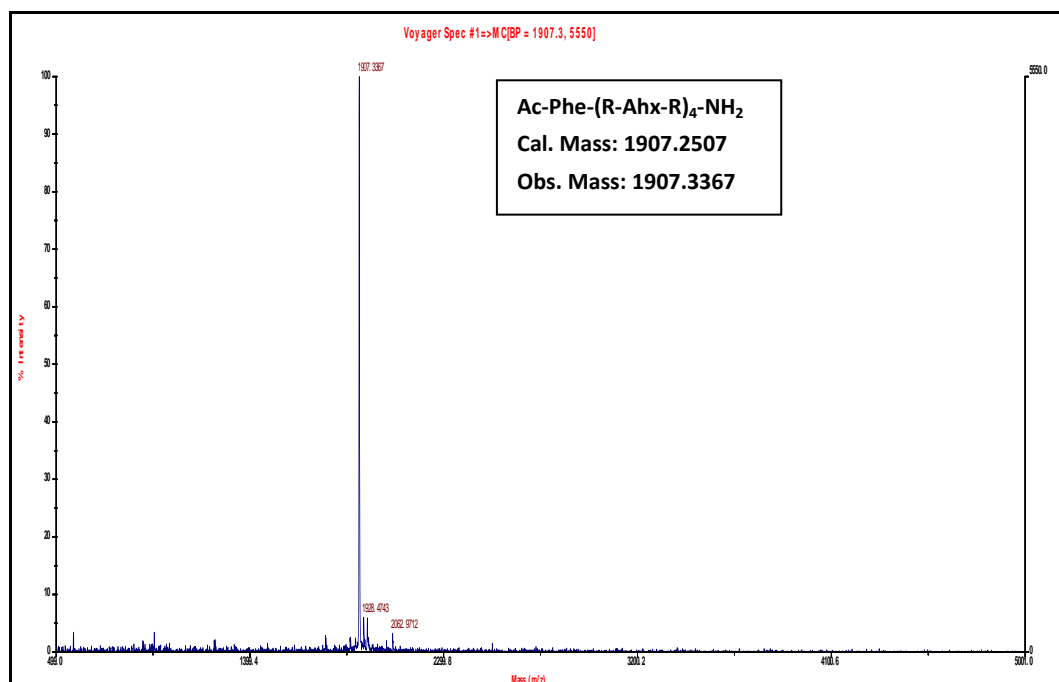
MALDI-TOF spectrum of ^{Ac}P14:

Ac-Phe-(R-apDP-R)$_4$-NH$_2$
Cal. Mass: 2072.61
Obs. Mass: 2076.71 (M+4)

MALDI-TOF spectrum of ^{Ac}P15:

Ac-Phe-(R-Ahx-R)$_4$-NH$_2$
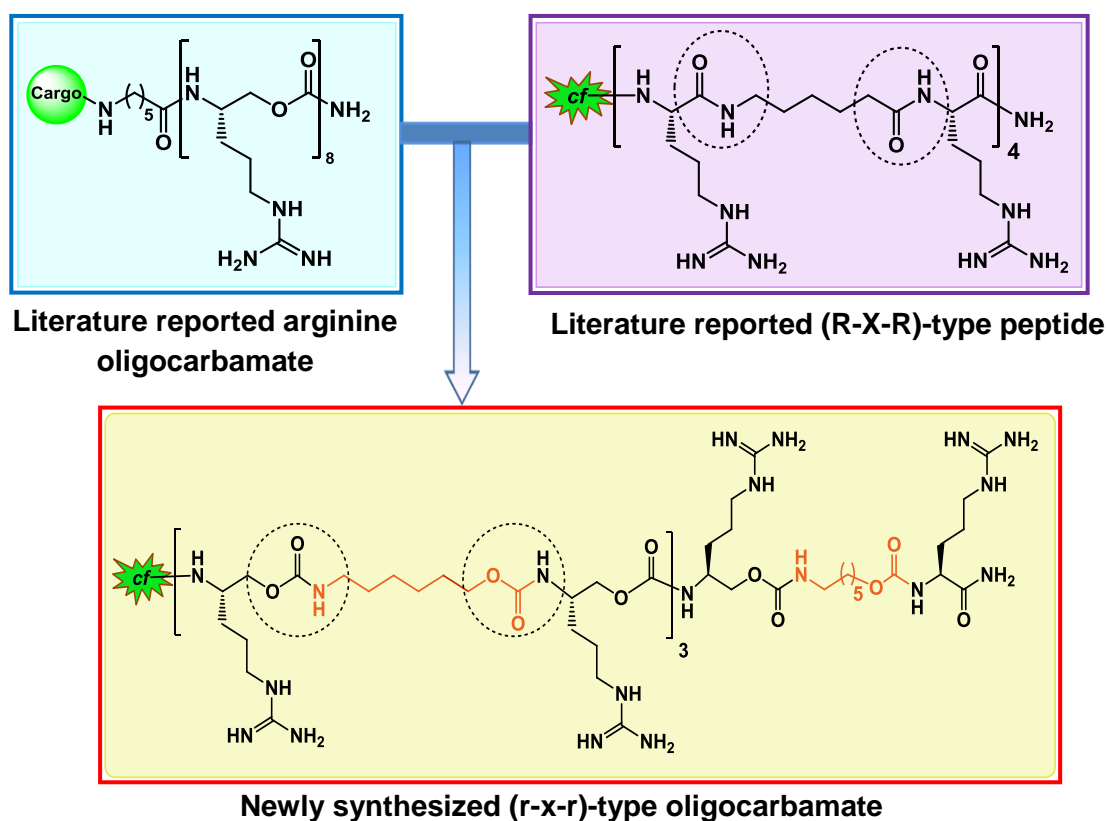Cal. Mass: 1907.2507
Obs. Mass: 1907.3367
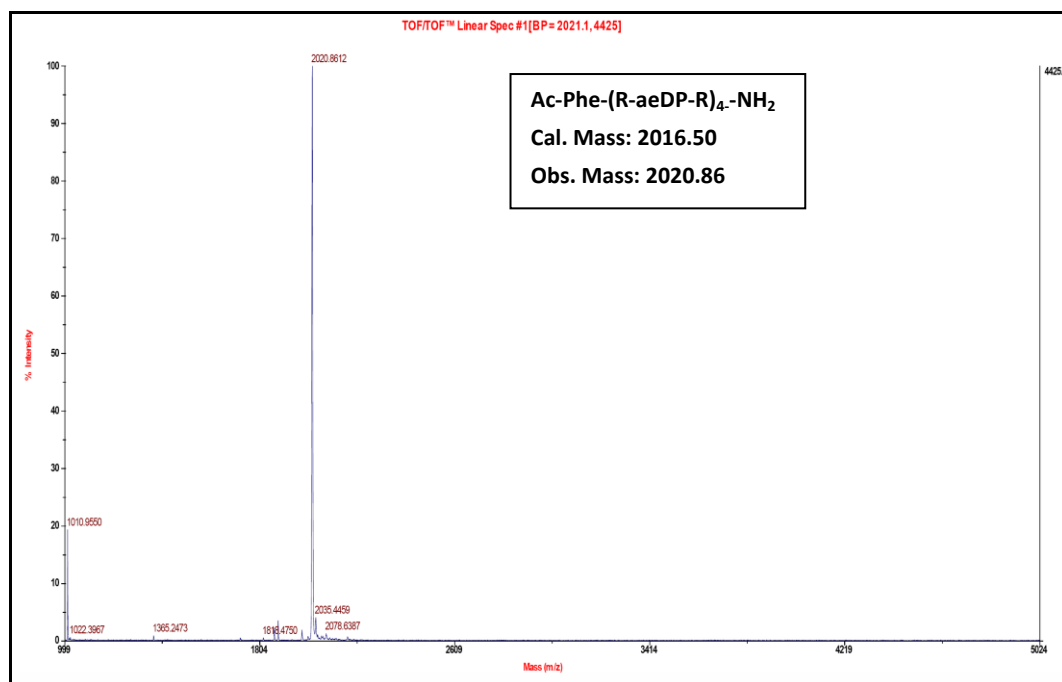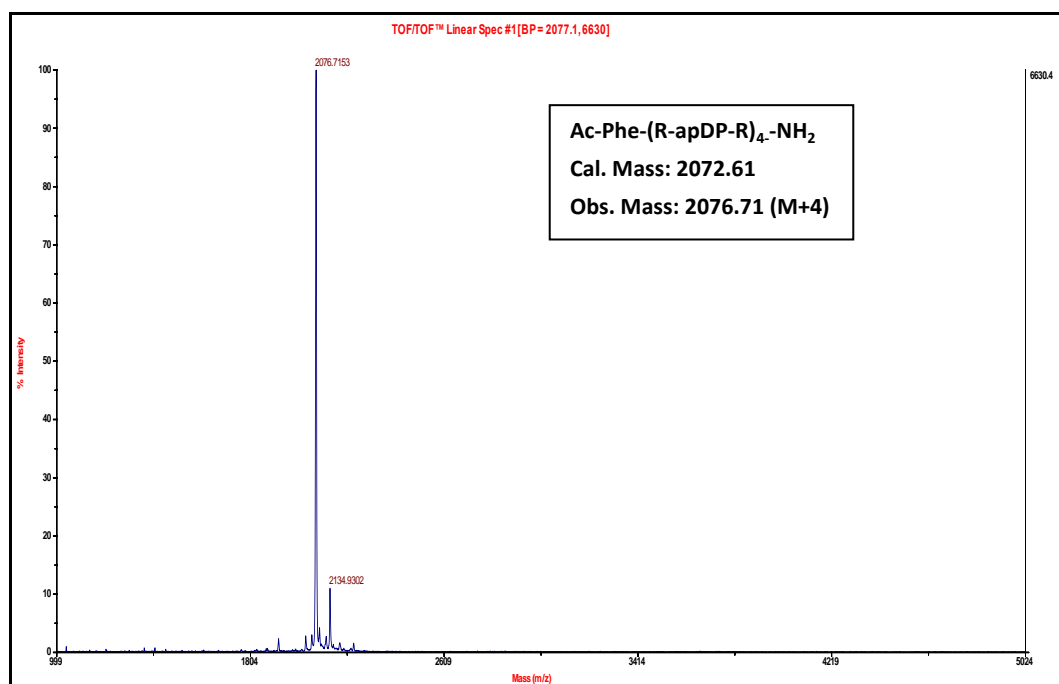
2.3 References

1. (a) Thomas, C.; Ehrhardt, A.; Kay, M. Progress and problems with the use of viral vectors for gene therapy. *Nature Reviews.Genetics* **2003,** *4*, 346-358. (b) Lentz, T. B.; Gray, S. J.; Samulski, R. J. Viral vectors for gene delivery to the central nervous system. *Neurobiology of Disease* **2012,** *48*, 179-188.

2. Geng, T.; Lu, C. Microfluidic electroporation for cellular analysis and delivery. *Lab on a Chip* **2013**, *13*, 3803-3821

3. De Jong, W.; Borm, P. Drug delivery and nanoparticles:applications and hazards. *International Journal of Nanomedicine* **2008,** *3*, 133-149.

4. Foldvari, M.; Mezei, C.; Mezei, M. Intracellular delivery of drugs by liposomes containing Po glycoprotein from peripheral nerve myelin into human M21 melanoma cells. *Journal of Pharmaceutical Sciences* **1991,** *80*, 1020-1028.

5. Gentile, F. T.; Doherty, E. J.; Rein, D. H.; Shoichet, M. S.; Winn, S. R. Polymer science for macroencapsulation of cells for central nervous system transplantation. *Reactive Polymers* **1995,** *25*, 207-227.

6. Schmidt, N.; Mishra, A.; Lai, G. H.; Wong, G. C. L. Arginine-rich cell-penetrating peptides. *FEBS Letters* **2010,** *584*, 1806-1813.

7. (a) Singh, D.; Kiarash, R.; Kawamura, K.; LaCasse, E. C.; Gariépy, J. Penetration and Intracellular Routing of Nucleus-Directed Peptide-Based Shuttles (Loligomers) in Eukaryotic Cells. *Biochemistry* **1998,** *37*, 5798-5809. (b) Brokx, R. D.; Bisland, S. K.; Gariépy, J. Designing peptide-based scaffolds as drug delivery vehicles. *Journal of Controlled Release* **2002,** *78*, 115-123.

8. Park, C. B.; Yi, K.-S.; Matsuzaki, K.; Kim, M. S.; Kim, S. C. Structure–activity analysis of buforin II, a histone H2A-derived antimicrobial peptide: The proline hinge is responsible for the cell-penetrating ability of buforin II. *Proceedings of the National Academy of Sciences* **2000,** *97*, 8245-8250.

9. Sadler, K.; Eom, K.; Yang, J.-L.; Dimitrova, Y.; Tam, J. Translocating proline-rich peptides from the antimicrobial peptide bactenecin 7. *Biochemistry* **2002,** *41*, 14150-14157.

10. Farrera-Sinfreu, J.; Zaccaro, L.; Vidal, D.; Salvatella, X.; Giralt, E.; Pons, M.; Albericio, F.; Royo, M. A New Class of Foldamers Based on cis-γ-Amino-l-proline1,2. *Journal of the American Chemical Society* **2004,** *126*, 6048-6057.

11. Fernández-Carneado, J.; Kogan, M. J.; Castel, S.; Giralt, E. Potential Peptide Carriers: Amphipathic Proline-Rich Peptides Derived from the N-Terminal Domain of γ-Zein. *Angewandte Chemie International Edition* **2004,** *43*, 1811-1814.

12. Crespo, L.; Sanclimens, G.; Montaner, B.; Pérez-Tomás, R.; Royo, M.; Pons, M.; Albericio, F.; Giralt, E. Peptide Dendrimers Based on Polyproline Helices. *Journal of the American Chemical Society* **2002,** *124*, 8876-8883.

13. Farrera-Sinfreu, J.; Giralt, E.; Castel, S.; Albericio, F.; Royo, M. Cell-Penetrating cis-γ-Amino-l-Proline-Derived Peptides. *Journal of the American Chemical Society* **2005,** *127*, 9459-9468.

14. (a) Brandsch, M. Transport of L-proline, L-proline-containing peptides and related drugs at mammalian epithelial cell membranes. *Amino Acids* **2006,** *31*, 119-136. (b) Pujals, S.; Giralt, E. Proline-rich, amphipathic cell-penetrating peptides. *Advanced drug delivery reviews* **2008,** *60*, 473-484. (c) Cavalli, S.; Carbajo, D.; Acosta, M.; Lope-Piedrafita, S.; Candiota, A.; Arús, C.; Royo, M.; Albericio, F. Efficient γ-amino-proline-derived cell penetrating peptide-superparamagnetic iron oxide nanoparticle conjugates via aniline-catalyzed oxime chemistry as bimodal imaging nanoagents. *Chemical Communications (Cambridge, England)* **2012,** *48*, 5322-5324. (d) Gorrea, E.; Carbajo, D.; Gutiérrez-Abad, R.; Illa, O.; Branchadell, V.; Royo, M.; Ortuño, R. Searching for new cell-penetrating agents: hybrid cyclobutane-proline γ,γ-peptides. *Organic & Biomolecular Chemistry* **2012,** *10*, 4050-4057.

15. Sugase, K.; Horikawa, M.; Sugiyama, M.; Ishiguro, M. Restriction of a Peptide Turn Conformation and Conformational Analysis of Guanidino Group Using Arginine-Proline Fused Amino Acids: Application to Mini Atrial Natriuretic Peptide on Binding to the Receptor. *Journal of Medicinal Chemistry* **2003,** *47*, 489-492.

16. (a) Amantana, A.; Moulton, H. M.; Cate, M. L.; Reddy, M. T.; Whitehead, T.; Hassinger, J. N.; Youngblood, D. S.; Iversen, P. L. Pharmacokinetics, Biodistribution, Stability and Toxicity of a Cell-Penetrating Peptide−Morpholino Oligomer Conjugate. *Bioconjugate Chemistry* **2007,** *18*, 1325-1331. (b) Youngblood,

D. S.; Hatlevig, S. A.; Hassinger, J. N.; Iversen, P. L.; Moulton, H. M. Stability of Cell-Penetrating Peptide−Morpholino Oligomer Conjugates in Human Serum and in Cells. *Bioconjugate Chemistry* **2006,** *18*, 50-60. (c) Abes, S.; Moulton, H. M.; Clair, P.; Prevot, P.; Youngblood, D. S.; Wu, R. P.; Iversen, P. L.; Lebleu, B. Vectorization of morpholino oligomers by the (R-Ahx-R)₄ peptide allows efficient splicing correction in the absence of endosomolytic agents. *Journal of Controlled Release* **2006,** *116*, 304-313.

17. Abes, R.; Arzumanov, A.; Moulton, H.; Abes, S.; Ivanova, G.; Gait, M. J.; Iversen, P.; Lebleu, B. Arginine-rich cell penetrating peptides: Design, structure–activity, and applications to alter pre-mRNA splicing by steric-block oligonucleotides. *Journal of Peptide Science* **2008,** *14*, 455-460.

18. Rothbard, J.; Kreider, E.; VanDeusen, C.; Wright, L.; Wylie, B.; Wender, P. Arginine-rich molecular transporters for drug delivery: role of backbone spacing in cellular uptake. *Journal of Medicinal Chemistry* **2002,** *45*, 3612-3618.

19. Merrifield, R. B. Solid Phase Peptide Synthesis. I. The Synthesis of a Tetrapeptide. *Journal of the American Chemical Society* **1963,** *85*, 2149-2154.

20. Bernatowicz, M. S.; Wu, Y.; Matsueda, G. R. 1H-Pyrazole-1-carboxamidine hydrochloride an attractive reagent for guanylation of amines and its application to peptide synthesis. *The Journal of Organic Chemistry* **1992,** *57*, 2497-2502.

21. Gokhale, S. S.; Kumar, V. A. Amino/guanidino-functionalized *N*-(pyrrolidin-2-ethyl)glycine-based pet-PNA: Design, synthesis and binding with DNA/RNA. *Organic & Biomolecular Chemistry* **2010,** *8*, 3742-3750.

22. Koren, E.; Torchilin, V. Cell-penetrating peptides: breaking through to the other side. *Trends in Molecular Medicine* **2012,** *18*, 385-393.

23. JB, P. Handbook of Biological Confocal Microscopy *second Edition. New York, London: Plenum Press* **1995**.

CHAPTER 3

Design and Synthesis of (R-X-R)-type Oligocarbamate Transporters for Cellular Delivery *via*: Non-covalent Complexation and Covalent Conjugation Strategies

Literature reported arginine oligocarbamate

Literature reported (R-X-R)-type peptide

Newly synthesized (r-x-r)-type oligocarbamate

The (R-X-R) motif-containing arginine-rich peptides are among the most effective Cell-Penetrating Peptides. In this chapter we replaced amide linkages in the (R-X-R) motif by carbamate linkages as in (r-ahx-r)$_4$ or (r-ahx-rr- apr-r)$_2$. Circular Dichroism analysis and partitioning experiments shows newly synthesized oligocarbamates were less structured and amphipathic in nature. FACS analysis showed enhanced cellular uptake over control oligoamide. Confocal analysis revealed, these oligomers were interspersed in cytosol as well as in nucleus. Internalization of these oligomers in mammalian cell lines probably occurs by an energy-independent process. These oligomers show efficient delivery of biologically active plasmid DNA, siRNA and Tripeptide into CHO-K1 cells. Attachment of PMO and Daunomycin by covalent conjugation was also been discussed in this chapter.

3.1 Introduction

Numerous naturally occurring as well as synthetically modified Cell-Penetrating Peptides (CPPs) or Cell-Penetrating Oligomers (CPOs) were explored for cellular delivery applications.[1] However, their proteolytic degradation and serum instability limit their use *in vivo*. For this reason replacement of the amide backbone present in natural or synthetic modified CPPs is one of the key factors which makes oligomers suitable to use *in vivo*. Additionally these replacements sometimes were found to be beneficial as their structural and functional properties were different from their oligoamide counterpart.

The arginines (R) separated by ω-amino acids (-X-) with variable chain lengths as in the (R-X-R) motif peptide, were shown to be far better than the natural α-amino acid-containing peptides (polyarginines or polylysines), probably due to the preferred spatial arrangement of guanidines and their amphipathic nature.[2] The arginine peptides interspersed with ε-aminohexanoic acid (Ahx) and γ-aminopropionic acid (Apr) were found to be among the most effective synthetic CPPs for highly efficient cargo transportation.[3] The mechanism of uptake of CPPs is still under debate, and it is postulated that it could be operating by multiple pathways.[4] The (R-X-R)-type of peptides were found to be stable to peptidases than the natural α-amino acid-containing peptides.[3a] In case of (R-X-R)$_4$ peptides, the peptide linkages between subsequent arginine units are still amenable for enzymatic cleavage and can cause the toxicity. To overcome this problem, peptidomimetics such as peptoids,[5] oligoureas,[6] oligocarbonates,[7] and oligocarbamates[8] as transporters have been explored with an aim to increase the stability of the oligomers *in vivo*. Among the carbamate analogues, the oligoarginines, linked through carbamate linkages were synthesized and explored for cell uptake studies and were found to exhibit enhanced uptake properties.[8]

3.2 Rational, design and objective of present work

In this section, we designed, synthesized, and evaluated the uptake properties of carbamate-linked (r-x-r)-motif oligomers based on their (R-X-R)-type amide-linked counterpart ['-R-X-R-R-X-R-R-X-R-R-X-R-' (where 'R' is arginine and 'X' is 6-aminohexanoic acid or 3-aminopropanoic acid)]. It was envisaged that the carbamate-

linked (r-x-r)-motif would exhibit synergistic properties when carbamate linker is used in tandem with appropriate spacer (-x-) for optimizing the interaction of two consecutive guanidine groups as in '-r-x-r-r-x-r-r-x-r-r-x-r-' (where 'r' represents the carbamate analogue of L-arginine and '-x-' represents the carbamate analogue of 6-aminohexanoic- or 3-aminopropanoic- acid) with the cell membrane, which may lead to favourable uptake and enzymatic stability.

The carbamate linkage adds O−CH$_2$ to the amide NH−CO, thus adding flexibility and hydrophobicity and reducing the possibility of hydrogen-bonded secondary structures.[9] This would probably leave the oligomers more amenable for adopting structural features better suited to interact with lipid membranes. Aminohexanol (ahx) and aminopropanol (apr) linkers were used to separate selected adjacent guanidine functionalities and to optimize the effect of chain lengths on guanidinium display. Initially their structural feature and amphipathicity was studied by Circular Dichroism (CD) and water-octanol partitioning experiments. The reversed phase HPLC analysis of synthesized oligomers confirmed their balanced hydrophilicity/hydrophobicity in comparison to control oligoamide counterpart. Further FACS, confocal analysis and cargo delivery applications were studied to evaluate cellular uptake and applicability of synthesized oligomer. Cell viability assay was performed to evaluate their cytotoxicity profile.

## 3.3 Synthesis, result and discussion

3.3.1 Synthesis of *p*-nitrophenyl activated monomers

To synthesize carbamate-linked (r-x-r)-motif oligomers, *N*-protected aminocarbonates were synthesized according to Scheme 3.1. Initially the carboxylic acid functionality in N^α-Boc-L-Arg(Mts)-OH was converted to its methyl ester **16** by use of dimethylsulphate in the presence of potassium carbonate as a base in methanol. The ester function in **16** was reduced by in situ generated LiBH$_4$ to yield the corresponding alcohol **17**.

Similarly, conversion of 6-aminohexanoic acid **19** to its methyl ester **20** using thionyl chloride, Boc-protection of free amine by using Boc-anhydride to get compound

21 and subsequent reduction of methyl ester to free alcohol compound by *in situ* generated LiBH$_4$ afforded *N*-Boc protected 6-aminohexanol **22**.

The hydroxyl groups in **17**, *N*-Boc-6-aminohexanol **22**, and *N*-Boc-3-aminopropanol **24** were each activated as their *p*-nitrophenyl carbonates by treating with *p*-nitrophenyl chloroformate in pyridine and dichloromethane to get the *N*-Boc-protected monomers **18**, **23** and **25** respectively, suitable to use for solid-phase carbamate synthesis (Scheme 3.1a-c).
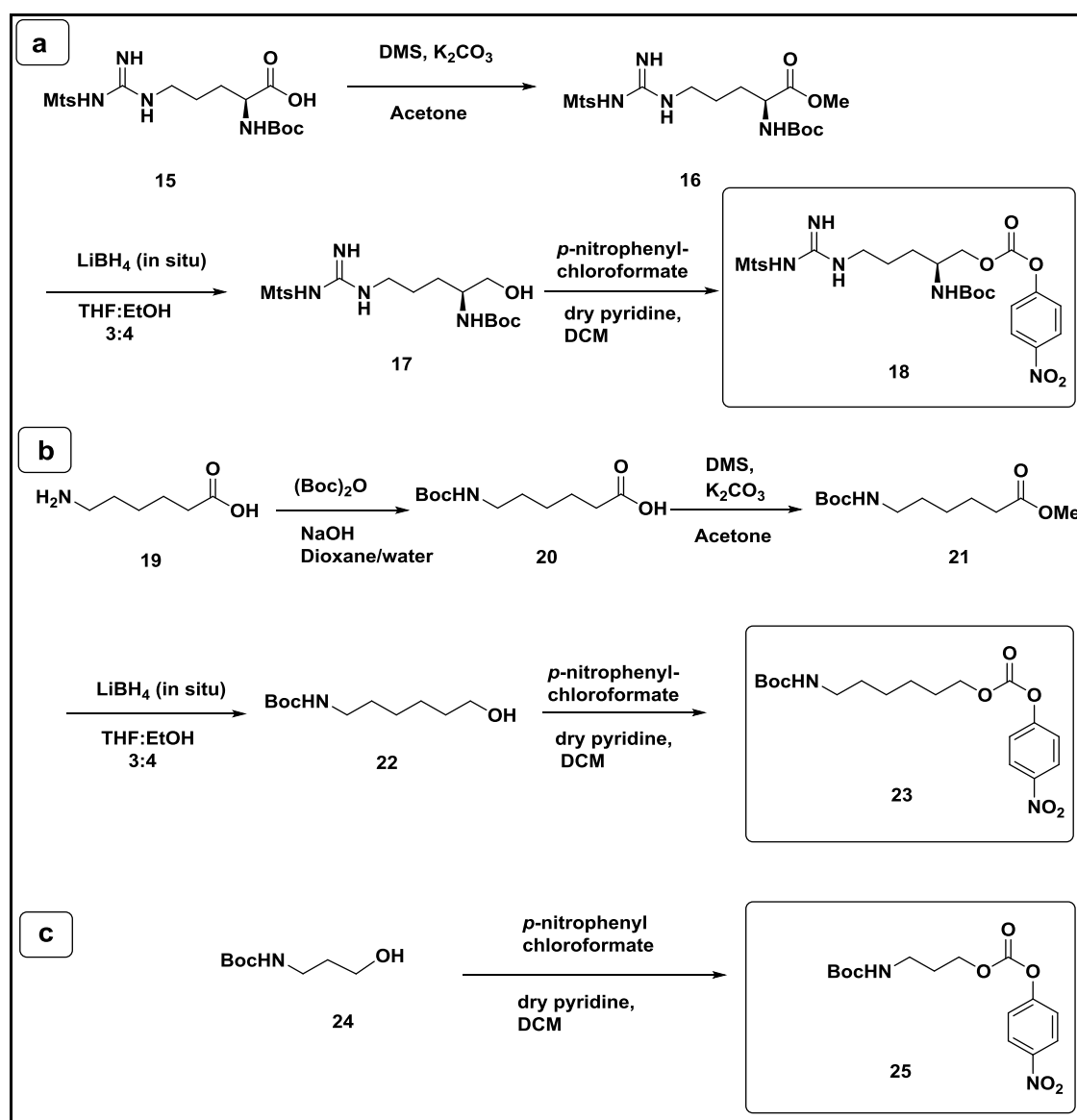
Scheme 3.1 Synthesis of *p*-nitrophenyl-activated monomers units for oligocarbamate synthesis.

3.3.2 Solid phase peptide and oligocarbamates synthesis

3.3.2a General solid phase carbamate synthesis

General synthetic approaches for the formation of the carbamate linkage are mostly derived from active ester method used for peptide synthesis. A carbamate linkage can be synthesized by first converting the primary hydroxyl component of one unit to activated carbonate or carbamate, which is then condensed with the primary/secondary amine of the second unit (Figure 3.1).
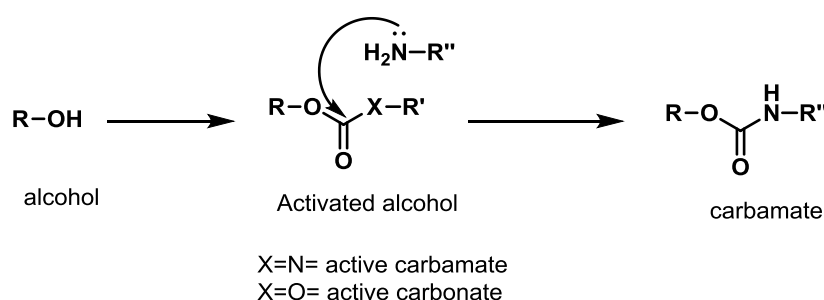

X=N= active carbamate
X=O= active carbonate

Figure 3.1 Schematic representation of carbamate synthesis by active carbamate and active carbonate methods.

A reactive carbamate can be prepared by treating the alcohol with 1,1'-carbonyldi imidazole (CDI) while reagents such as *p*-nitrophenylchloroformate, bis (*p*-nitrophenyloxy) carbonyl or dihydroxybenzotriazolyl carbonate (DBTC) can readily convert the alcohol to the active carbonate (Figure 3.2).

Cho *et al.*[10] in year 1993 reported the highly efficient solid-phase synthesis of oligocarbamates from a pool of chiral aminocarbonates derived from amino acids and screened a library of oligocarbamates for their ability to bind to a monoclonal antibody. In the year 1998 first cyclic oligocarbamate synthesis on solid phase from aminoalcohols of proteinogenic amino acids was demonstrated by Warrass *et al.*[11] In the case of carbamate linked oligonucleotides; Gait *et al.*[12] reported the first synthesis of a 3'-*O*-5'-*N*-carbamate-linked dimer of thymidine, in 1974 using CDI as coupling reagent in 44% yield. Using the same strategy, later in 1987, Coull *et al.*,[13] reported synthesis and characterization of a carbamate-linked oligonucleoside. In 1977, Mungall and Kaiser[14] described the synthesis of a trimer where 3'-*O*-tritylthymidine was activated with *p*-nitrophenylchloroformate followed by coupling with 5'-amino-5'-

deoxythymidine. Further activation of the dimer and repeat of condensation gave the trimer. Warrass and Jung[15] used dihydroxybenzotriazolylcarbonate (DBTC) as an activating reagent, which gave excellent yields for the preparation cyclic oligocarbamates on solid support. Our group reported synthesis of polycarbamate nucleic acids based on L/D-Serine using *p*-nitrophenyl carbonate as an activator.[16]
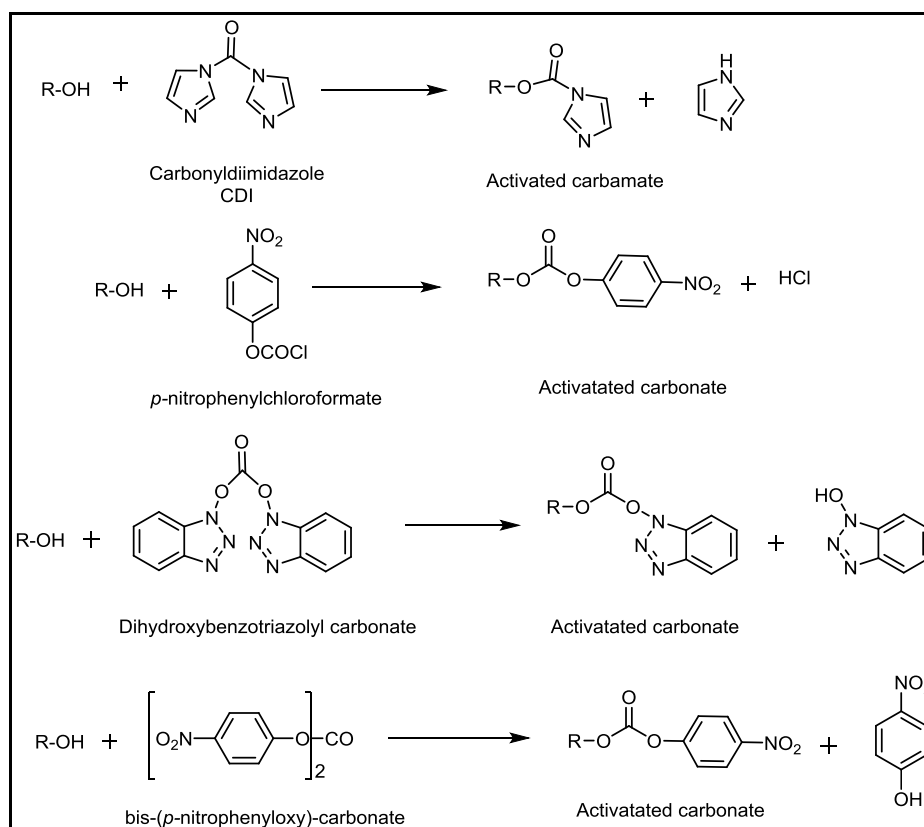

Figure 3.2 Reagents for activation of alcohols to its carbamates or carbonates.

The advantage of solid phase synthesis of oligocarbamates over regular solid phase peptide synthesis is that the (a) oligocarbamate synthesis does not involve any expensive coupling reagents (b) excessively used un-reacted monomers can be recovered, as they are not contaminated with any other reagents (Figure 3.3).
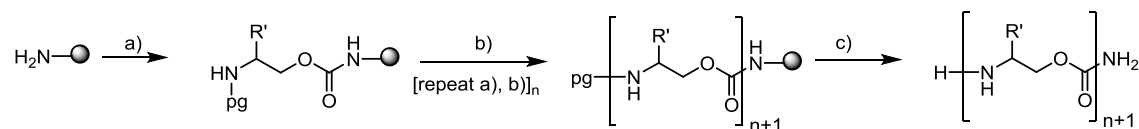
Figure 3.3 General strategy for synthesis of oligocarbamate: a) *p*-nitophenyl activated monomer, DIPEA in solvent (b) *N*-deprotecting reagent, (c) cleavage from solid support and purification. Where, pg is nitrogen-protecting group either Boc or Fmoc.

3.3.2b Synthesis of oligocarbamates on solid support by *N*-Boc chemistry

The synthesized *N*-Boc-protected *p*-nitophenyl activated carbonate monomers (**18**, **23** and **25**) were incorporated at appropriate positions in the desired (r-x-r)-type oligocarbamate sequences on solid support (MBHA resin) using Boc chemistry protocol, following repetitive cycles of deprotection, neutralization and coupling. In the same way desired control (R-Ahx-R)$_4$ peptide sequences were also synthesized by solid phase peptide synthesis using TBTU, HOBt and DIPEA as a coupling reagents. The difference between solid phase oligocarbamate and oligoamide synthesis is in the attachment or coupling step. In the case of oligocarbamate synthesis, the monomer is in the form of pre-activated carbonates where as in oligoamide synthesis, activation is required by an addition of external peptide coupling reagents.
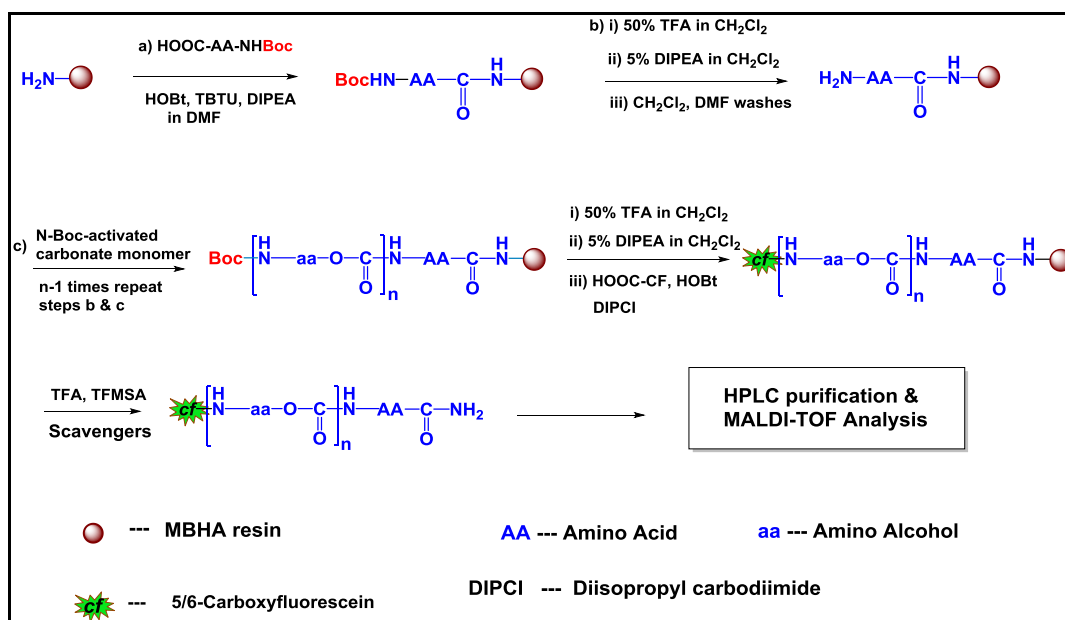
Scheme 3.2 Schematic presentation of solid phase oligocarbamate synthesis of *cf*-labeled oligocarbamates employs Boc-chemistry protocol.

For Fluorescence Activated Cell Sorting (FACS) analysis and confocal microscopy studies, a portion of the synthesized oligomer was labeled by coupling 5/6-carboxyfluorescein (*cf*) in the presence of *N,N'*-diisopropylcarbodiimide (DIPCDI) and HOBt in DMF at the *N*-terminal. For cargo delivery studies, unlabeled oligocarbamates and control oligoamide were used. In the absence of *cf*, phenylalanine (Phe) residue was coupled at the *N*-terminal to allow concentration calculation by UV-absorbance.

3.3.2c Cleavage of oligomers from solid support

The synthesized oligocarbamates (coded with alphabet '**C'**) as well as peptides (coded with alphabet '**P**') were cleaved from the solid support using TFA-TFMSA cleavage protocol, purified by RP-HPLC and then characterized by MALDI-TOF mass spectroscopic analysis, after re-checking their purity by analytical RP-HPLC on a C18 column. The synthesized *cf*-labeled oligocarbamates and control amide sequences and *N*-terminal phenylalanine attached oligomers are listed in Table 3.1.

Table 3.1 Synthesized oligomers of study.[a]

Code	Sequence	Mass (MALDI-TOF)	
		Calcd.	Obsd.
[cf]**P15**	*cf*-(R-Ahx-R)$_4$ -NH$_2$ control	2077.48	2078.07
[cf]**C1**	*cf*-(r-ahx-r)$_4$-NH$_2$	2406.33	2408.40
[cf]**C2**	*cf*-(r-ahx-r-r-apr-r)$_2$ -NH$_2$	2322.24	2324.81
[cf]**C3**	*cf*-(r)$_8$ –NH$_2$ control	1833.95	1834.49
[Ac]**P15**	*Ac*-Phe-(R-Ahx-R)$_4$ -NH$_2$ control	1907.25	1907.33
[Ac]**C1**	*Ac*-Phe-(r-ahx-r)$_4$ -NH$_2$	2237.36	2238.33
[Ac]**C3**	*Ac*-Phe-(r)$_8$ -NH$_2$ control	1664.98	1666.71

[a] The upper case R and Ahx denote amino acid residues; the lower case r, ahx, and apr denote amino alcohol residues; *cf* denotes carboxyfluorescein and *Ac* denotes *N*-terminal acetate

3.3.3 Bio-physical evaluation of synthesized oligomers

3.3.3a Comparative HPLC analysis of synthesized oligomers

Amphipathic nature of synthesized and purified oligomers was compared by their analytical HPLC analysis. MALDI characterized pure sample of oligomer was dissolved in water, injected to HPLC, passed through the C18 analytical column and recorded chromatograms were plotted are as shown in Figure 3.4. For comparison in retention time (t_R) differences between oligomers ^{cf}**P15** (control)**, ^{cf}C1 and ^{cf}C2**; all three oligomers were premixed in approximately same quantity in water and injected through HPLC and they were separated through C18 HPLC column and the chromatograms are shown in Figure 3.4 and 3.5.
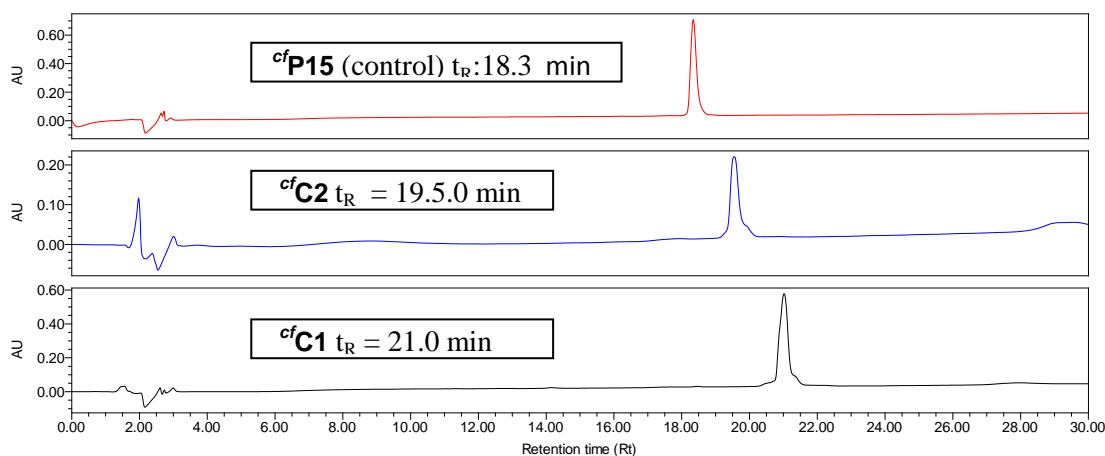

Figure 3.4 Overlaid HPLC chromatogram of ^{cf}**P15** (control) t_R = 18.3 min (Red color); ^{cf}**C2** t_R = 19.5 min (Blue color) and ^{cf}**C1** t_R = 21.0 min (black color).
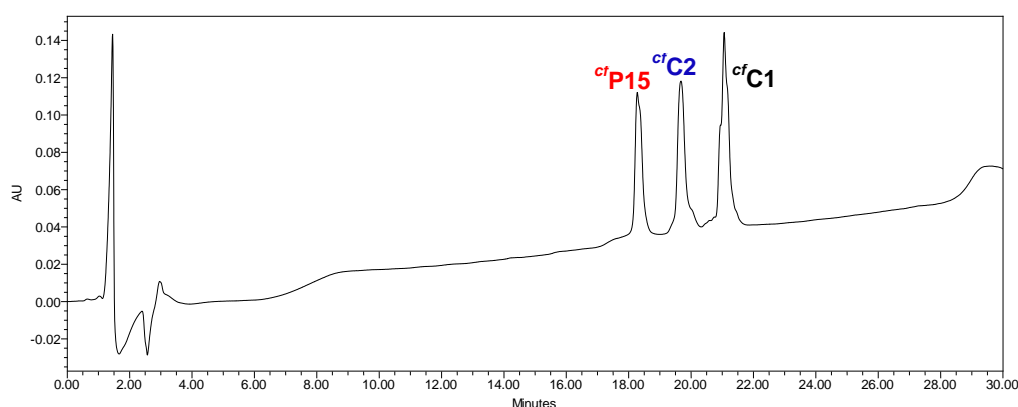

Figure 3.5 HPLC chromatogram of a co-injection of oligomers, ^{cf}**P15** (control); t_R = 18.3 min, ^{cf}**C2**; t_R = 19.5 min and ^{cf}**C1**; t_R = 21.0 min.

HPLC analysis chromatograms clearly revealed that both the oligocarbamate sequences (^{cf}**C1** and ^{cf}**C2**) showed more retardation on HPLC column and hence they are more hydrophobic compared to oligoamide control. The oligocarbamate ^{cf}**C1** showed high retention time in comparison to oligocarbamate ^{cf}**C2**, indicating that the hydrocarbon-spacer has indeed an effect on hyrophobicity and amphipathicity of synthesized oligomer.

3.3.3b Octanol-water partitioning experiments

Partitioning experiment was carried out in octanol-water model system to estimate the affinity of the oligomers for the lipid membrane.[17] The partitioning of the oligoamide (^{cf}**P15**) and oligocarbamates (^{cf}**C1** and ^{cf}**C2**) was monitored using visual fluorescence of the *cf*-labeled oligomers. The oligomers were highly water-soluble and remained completely in the aqueous phase. Upon addition of sodium laurate, complete migration of oligoamide ^{cf}**P15** and oligocarbamate ^{cf}**C1** into the octanol phase was observed, whereas carbamate ^{cf}**C2** was found in aqueous as well as octanol phases. The observation is indicative of the fact that the linker length indeed affects an oligomer's affinity for water as well as lipid and consequently its amphipathic nature. This partitioning could be monitored visually and is shown in Figure 3.6. The *cf*-(r-apr-r)$_4$-NH$_2$ (^{cf}**C2**, where, -apr- is aminopropanol unit) was found to be less efficient in partitioning from water to octanol layer in comparison to *cf*-(r-ahx-r)$_4$-NH$_2$ (^{cf}**C1**, where –ahx- is aminohexanol derivative) and *cf*-(R-Ahx-R)$_4$-NH$_2$ (^{cf}**P15**, where –Ahx- is aminohexanoic acid).
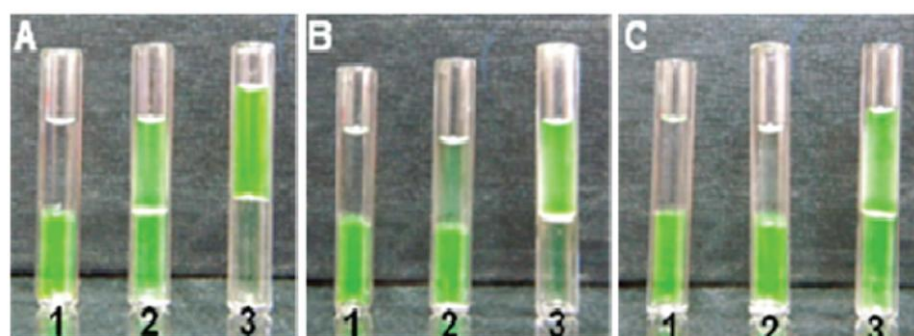
Figure 3.6 Partitioning of oligomers ^{cf}**P15** (A), ^{cf}**C1** (B), and ^{cf}**C2** (C) in water-octanol without added sodium laurate (1) and with 3.0 (2) and 6.0 equiv (3) of sodium laurate/guanidinium group.

3.3.3c Circular Dichroism (CD) analysis

CD spectroscopic studies were then carried out to study the presence of secondary structures in these oligomers (Figure 3.7). The oligoamide [cf]**P15** exhibited a significant CD pattern with prominent signals around 200 and 230 nm, indicating the presence of a random coil structure, whereas no CD pattern emerged for the oligocarbamates [cf]**C1** and [cf]**C2**, indicating no pattern. This is in tune with the literature reports where replacement of a relatively rigid amide bond by the more flexible carbamate linkages led to a loss of secondary structure.[9]
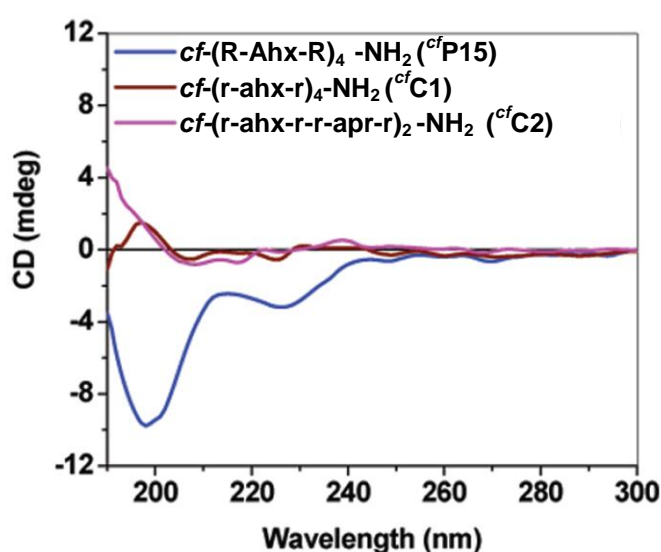

Figure 3.7 Circular dichroism analysis of synthesized oligomer in water.

Inference from HPLC analysis, water-octanol partitioning experiment and CD analysis shows that, as per the design expectations, the oligocarbamates [cf]**C1** and [cf]**C2** were shown to be more hydrophobic than oligoamide or amphipathic in nature similar to the oligoamide [cf]**P15**, but less structured. It would be interesting to see if these attributes could prove to be advantageous in the case of the oligocarbamates, enabling them to easily adopt a conformation suited for membrane interactions and cellular uptake as envisaged. The oligocarbamates, endowed with better amphipathic, unstructured backbones and eight guanidine functionalities, were evaluated in this study to gauge their ability to enter cells in comparison with the control oligoamides. *cf*-labeled oligomers [cf]**C1**- [cf]**C3** and [cf]**P15** were used in the cellular uptake experiments.

Oligomers ^{Ac}**C1**, ^{Ac}**C2**, and ^{Ac}**P15** were used for cargo delivery applications, in which AcNH-Phe replaces the *cf*-tag in ^{cf}**C1**, ^{cf}**C2**, and ^{cf}**P15**, respectively.

3.3.4 Biological evaluation of synthesized oligomers

3.3.4.1 Fluorescence Activated Cell Sorting (FACS) analysis

3.3.4.1a FACS study at 37 and 4°C temperatures

Cellular uptake was determined by fluorescence-activated cell sorting (FACS) analysis in CHO-K1 cells after incubation at 37°C for 1 h at 5 μM concentrations. *cf* itself did not enter cells in this assay. The uptake at 5 μM of ^{cf}**P15** and ^{cf}**C1** is depicted in Figure 3.8. The oligomer ^{cf}**C1** showed excellent uptake in nearly 100% of cells, compared to the 70% of cells showing uptake of control oligomer ^{cf}**P15**. The mean fluorescence intensity for oligomer ^{cf}**C1** was also about 9 times greater than that for the control oligoamide ^{cf}**P15**. The uptake of ^{cf}**C1** was also better than the known r$_8$-carbamate[8] ^{cf}**C3**. An additional experiment with mild acid wash, known to effectively quench cell membrane bound fluorescence,[18] was carried out to ensure that only the internalized fluorescence was assayed. The relative results of cellular uptake did not show any change; however, high cellular toxicity was observed due to the acid wash.
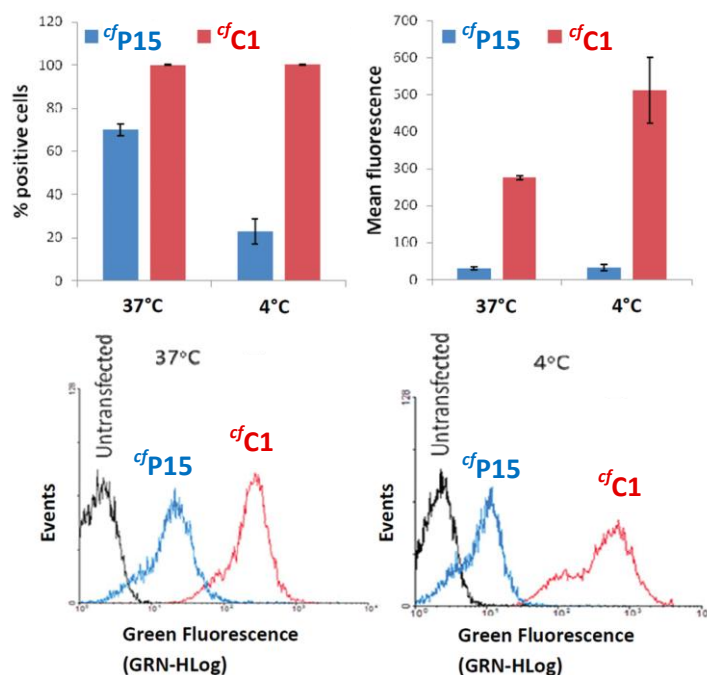

Figure 3.8 Cell uptake studies of ^{cf}**P15** and ^{cf}**C1** in CHO-K1 cells at 37 and 4°C by FACS analysis.

All energy-dependent pathways of cellular uptake such as endocytosis are known to be inhibited at low temperatures and due to pre-treatment of cells with sodium azide.[1b, 19] To study the effect of temperature, the cellular uptake of the oligomers ^{cf}**P15**, ^{cf}**C1** (Figure 3.8), and ^{cf}**C3** (Figure 3.11) was compared at 4 and 37°C using the same protocols as above. Surprisingly, the oligocarbamate ^{cf}**C1** was taken up by almost 100% of cells at 4 °C, whereas at the same temperature, amide I was taken up in only about 20% of cells. The ratio of mean fluorescence at 4 °C for ^{cf}**C1**:^{cf}**P15** was almost 16:1.

FACS analysis of oligoamide ^{cf}**P15** and oligocarbamate ^{cf}**C1** was also compared in HeLa cells by incubation of 5 μM oligomers at 37°C and 4°C. The FACS analysis results of HeLa cells showed almost similar trend of cellular uptake as seen in the case of CHO-K1 cells (Figure 3.9). From the FACS analysis at both the temperatures studied, oligocarbamate revealed to be advantageous in cell entry as well as in fluorescent intensity over its oligoamide counterpart.
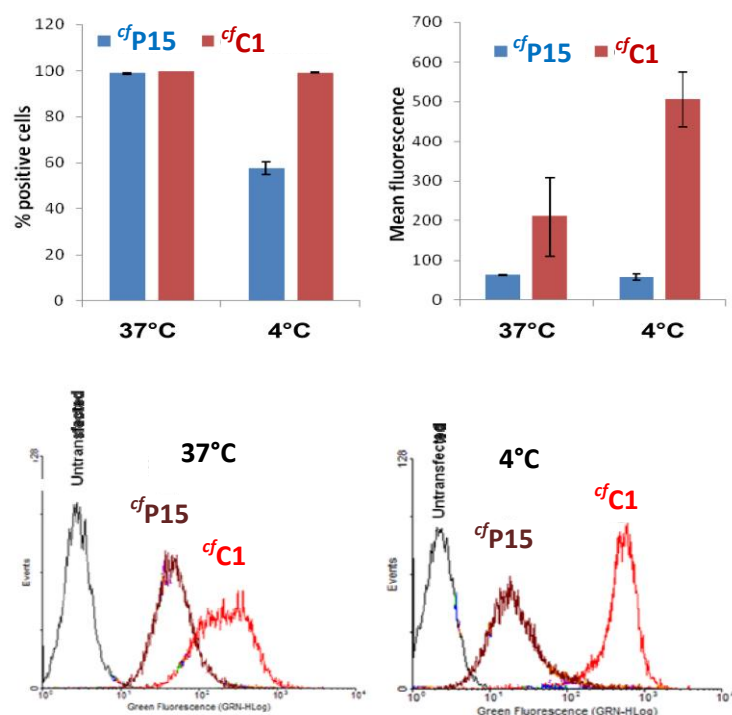

Figure 3.9 Cell uptake studies of ^{cf}**P15** and ^{cf}**C1** in HeLa cells at 37 and 4°C by FACS analysis.

3.3.4.1b FACS analysis of oligomers in the presence of serum

Excluding some rare cases, all the amide bonds between naturally occurring amino acids are susceptible for enzymatic degradation in serum. Therefore, the *in vivo* application of cell-penetrating peptides or oligomers containing these types of amide bonds sometimes acts as drawbacks and hence there is always a demand of serum stable drug delivering oligomers.

In order to test serum stability of our newly synthesized oligocarbamates (^{cf}**C1** and ^{cf}**C2**) in comparison with its oligoamide counterpart, FACS analysis of oligomers (^{cf}**P15**, ^{cf}**C1** and ^{cf}**C2**) in CHO-K1 cells at 37°C, 5µM oligomer concentration was carried out in cell medium containing 10% serum.
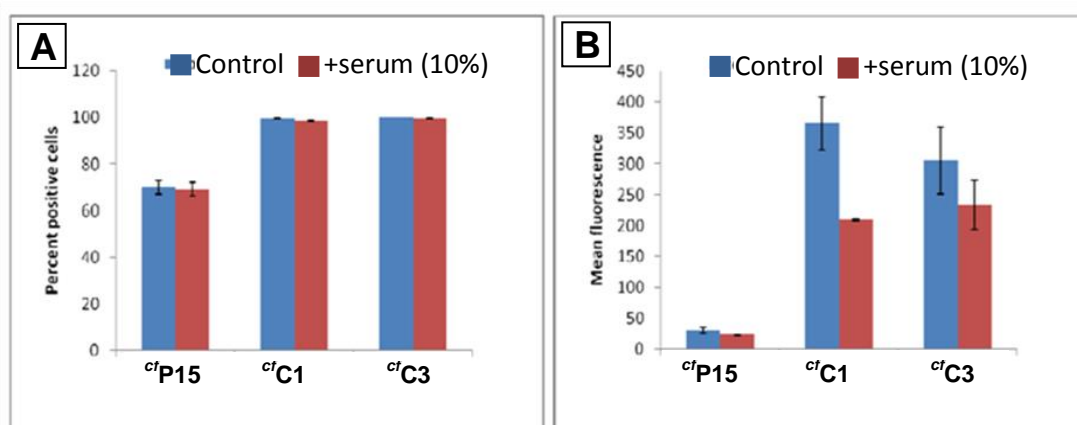

Figure 3.10 FACS analysis showing uptake of oligomer ^{cf}**P15**, ^{cf}**C1** and ^{cf}**C3** in CHO-K1 cells after 1h incubation at 37°C in presence of serum.

FACS analysis done in the presence and in the absence of serum clearly show that oligocarbamates entry in almost 100% cells whereas approx. only 70% cell entry in the case of oligoamide control (Figure 3.10; Panel A). The fluorescent intensity of (Panel B) cell-entered oligomers was also remarkably low in case of oligoamide control than oligocarbamates (Figure 3.10; Panel B). The difference in cellular uptake efficiency of oligocarbamates studies in the presence and in the absence of 10% serum was minute and hence it confirmed the stability of these oligomers in serum.

3.3.4.1c FACS analysis of oligocarbamates with and without spacer moiety

Octaarginine oligocarbamate analogue was already reported in literature by Wender *et al.*, and here we synthesized oligocarbamate analogue of (R-X-R)-motif which contains additional spacer moieties of different carbon chain. The addition of spacer moieties was incorporated in octaarginine oligocarbamate by envisioning getting additional flexibility and amphipathicity to oligomers, hence to improve cell uptake properties of oligocarbamate. To test the hypothesis, FACS analysis of newly synthesized spacer moiety containing oligomers was carried out by keeping octaarginine oligocarbamate as a control. The cell uptake studies was studied in CHO-K1 cells at 37°C and 4°C, at 5 µM oligomer concentration and incubated for 1h and results are shown in Figure 3.11.
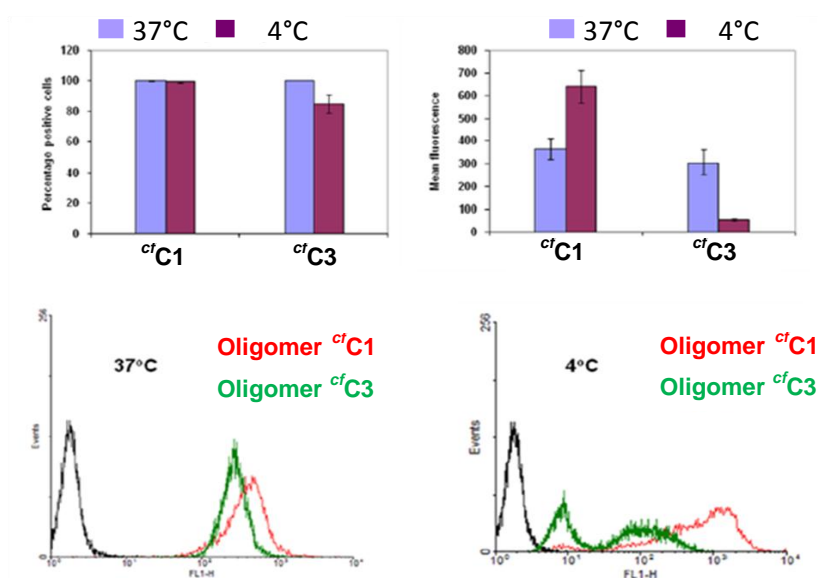

Figure 3.11 FACS analysis showing uptake of *cf*-(r-ahx-r)$_4$-NH$_2$ (*^{cf}C1*) in comparison to *cf*-(r)$_8$ –NH$_2$ (*^{cf}C3*) control in CHO-K1 cells at 37°C and 4°C after 1h incubation.

FACS results demonstrated that the newly synthesized spacer containing 12mer oligocarbamates was superior in cellular uptake property over reported octaarginine oligocarbamate analogue. The amount or intensity in large number of cells was found more in case of newly synthesized oligocarbamates *^{cf}C1*. Uptake of control oligomer *^{cf}C3* was found to be adversely affected at lower temperature (Figure 3.11) in our studies. Hence, the flexibility and amphipathicity has effective to tune the cell uptake property of oligomers.

3.3.4.2 Confocal microscopy analysis of synthesized oligomers

3.3.4.2a Incubation at 37°C with CHO-K1 and HeLa cells

Confocal microscopy studies were further undertaken in CHO-K1 (Figure 3.12) and HeLa (Figure 3.13) cells in order to see the intracellular distribution of the synthesized oligomers. In case of CHO-K1 cells, the oligomer ^{cf}C1 (at 5 μM) exhibited strong fluorescence, with predominantly cytosolic localization. The fluorescence for the control oligoamide ^{cf}P15 was observed only at higher concentration (10 μM) and was found in cytosol as well as near/within the nucleus.
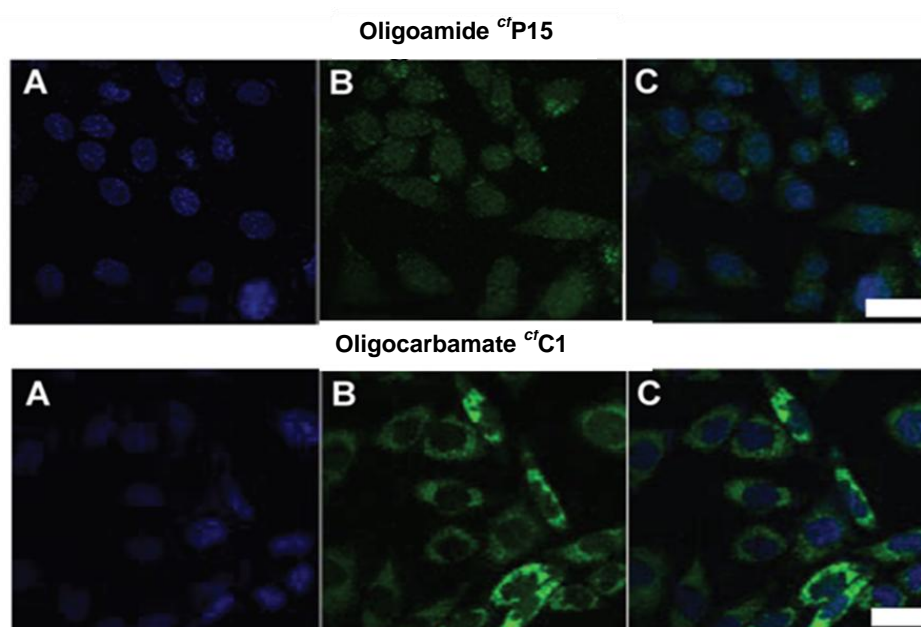

Figure 3.12 Confocal microscopy images of CHO-K1 cells after 4 h incubation at 37 °C with the oligoamide ^{cf}P15 (10 μM) and oligocarbamate ^{cf}C1 (5 μM). (A) Staining with nuclear stain, Hoechst 33342. (B) Fluorescence image. (C) Merged images. Scale bar: 20 μm.

Confocal studies carried out in HeLa cells at 37°C, 10 μM concentration of oligoamide ^{cf}P15 and oligocarbamate ^{cf}C1 showed high fluorescent intensity near the nucleus as well as significant intensity within the nucleus for oligocarbamate, Whereas, low fluorescence intensity was observed in the case of oligoamide control ^{cf}P15. It confirms that, the oligocarbamate ^{cf}C1 showed good cytoplasmic as well as nuclear entry over oliogamide ^{cf}P15 counterpart in the variety of cell types studied.
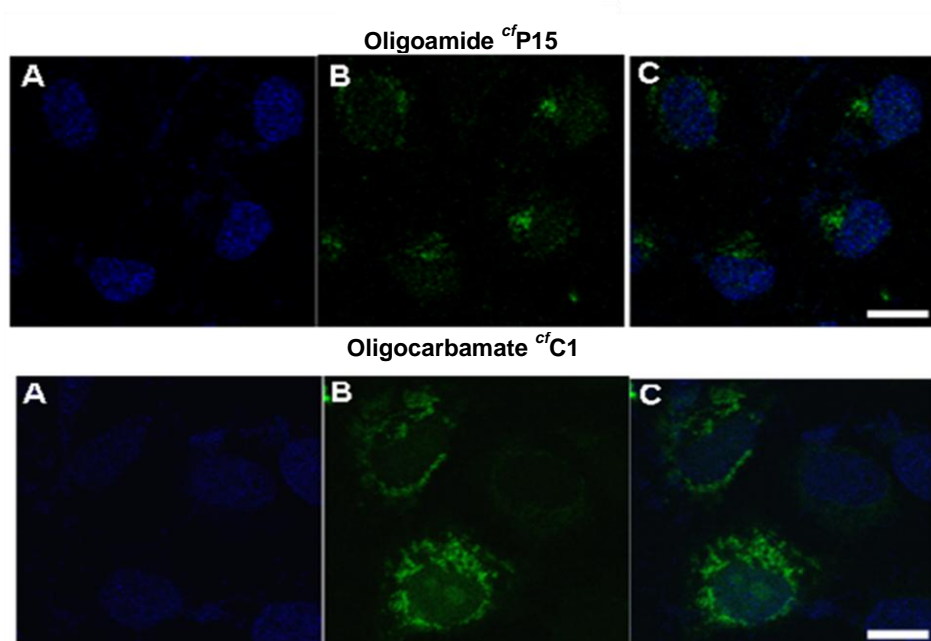
Figure 3.13 Confocal microscopy images of HeLa cells after incubation at 37°C with the oligoamide ^{cf}**P15** and oligocarbamate ^{cf}**C1** (10 μM each). **A**. staining with nuclear stain, Hoechst 33342. **B**. fluorescence image and **C**. merged image. Scale bar: 10μm.

3.3.4.2b Confocal microscopy study of oligomer ^{cf}C1 at low temperature (4°C) incubation

The entry of the oligomer ^{cf}**C1** at 4°C was also checked by confocal microscopy. Majority of the cells showed significant uptake of the oligomer ^{cf}**C1** (Figure 3.14), confirming the energy-independent entry pathway, as indicated by the FACS analysis.
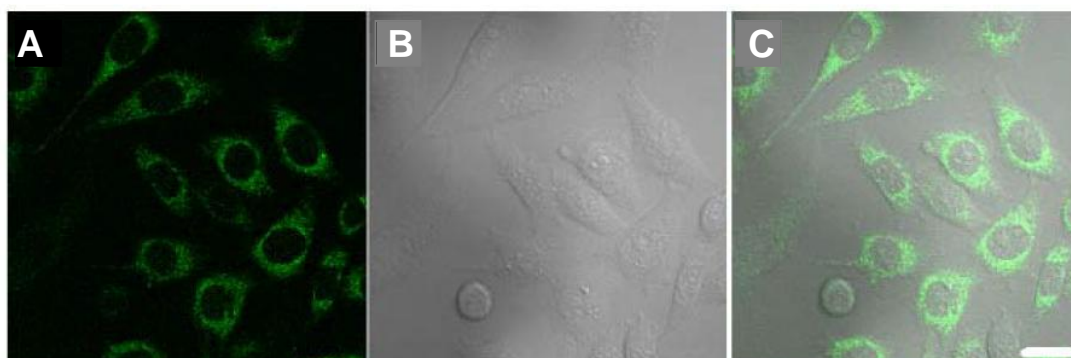

Figure 3.14 Confocal microscopy images showing uptake of *cf*-(r-ahx-r)$_4$-NH$_2$ (^{cf}**C1**) (5μM) in CHO-K1 cells at 4°C after incubation for 1h. **A**. Fluorescence image **B**. DIC image and **C**. merged image. Scale bar:20μm.

3.3.4.2c Confocal microscopy analysis of octaarginine oligocarbamate analogue

In order to compare the difference and localization in cell uptake of reported octaarginine oligocarbamate (^{cf}**C3**) with newly synthesized oligocarbamates, confocal studies were carried out in separate experiments by incubating 5 μM of control oligomer ^{cf}**C3** at 37°C, with CHO-K1 cells, where nucleus was stained with Hoechst 33342 (Figure 3.15).
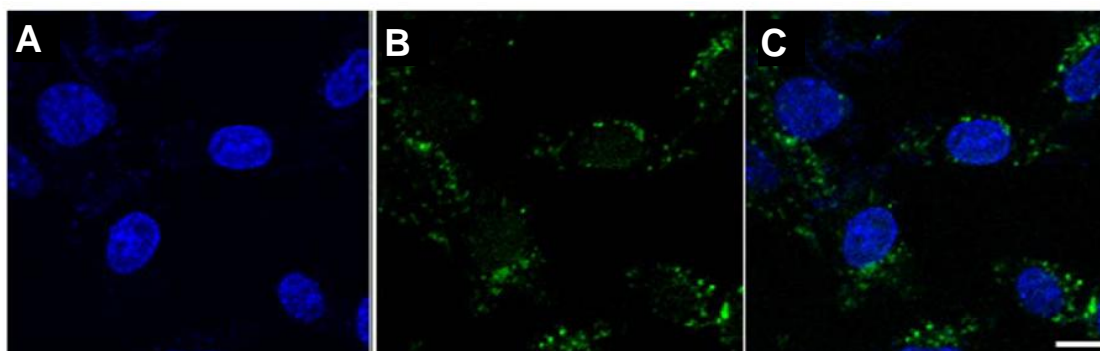

Figure 3.15 Confocal microscopy images of CHO-K1 cells showing uptake of to *cf*-(r)$_8$ –NH$_2$ (^{cf}**C3**). Labeled oligomer (5μM) was added to the cells in serum-free media and incubated at 37°C for 4h. Hoechst 33342 (0.3 μg/mL) was added during the last 30min of incubation. Cells were washed thrice with ice cold PBS(+) containing heparin (1mg/mL). Imaging was done at room temperature, **A**. staining with nuclear stain, Hoechst 33342. **B**. fluorescence image and **C**. merged image. Scale bar 10μm.

Confocal microscopic picture shown in Figure 3.15, clearly demonstrated that very less amount of oligomer entering cells compared to ^{cf}**C1** (Figure 3.14) and majority of cell-entered oligomer was located near nuclear membrane.

3.3.4.2d Confocal analysis of oligocarbamate ^{cf}C1, incubation in the presence of sodium azide

In order to gain the mechanism of cell uptake for oligocarbamate ^{cf}**C1**, the confocal microscopic analysis (Figure 3.16) was performed after incubation of cells with 5 μM concentration oligomer ^{cf}**C1** in the cell medium containing 25 mM of sodium azide. It is known that, the cell uptake studies carried out in the presence of sodium azide inhibits the energy-dependent cell entry of oligomers *via* ATP depletion pathway.
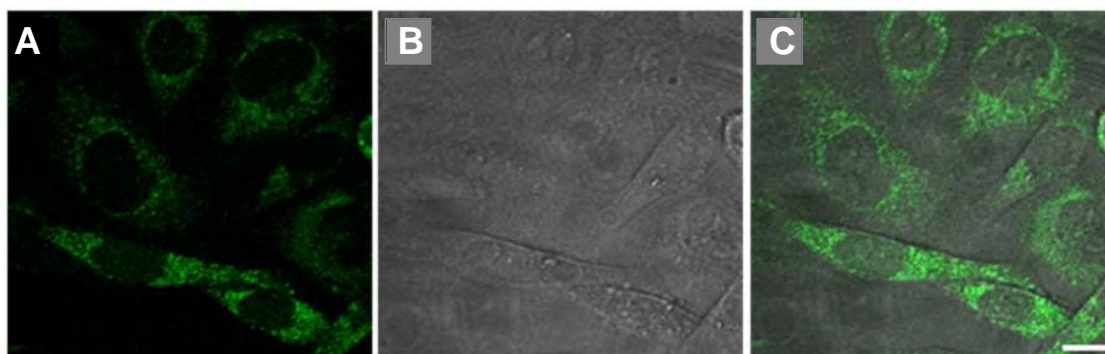
Figure 3.16 Confocal microscopy images showing uptake of *cf*-(r-ahx-r)$_4$-NH$_2$ (*^{cf}*C1) (5µM) in CHO-K1 cells in presence sodium azide (25mM) . **A**. Fluorescence image **B**. DIC image and **C**. merged image. Scale bar 10µm.

Confocal images shown in Figure 3.16 clearly indicate no apparent inhibition in cellular uptake for oligomer *^{cf}*C1, hence it suggested energy-independent mechanisms, most likely by direct translocation into cytoplasm, thereby reducing endosomal entrapment.

3.3.4.3. Cytotoxicity measurement of synthesized oligomers in cell

To evaluate the cytotoxicity of synthesized oligomers we assessed their cytotoxicity by cell viability assay by incubating the oligomers with cells at 5 and 10 µM concentration with CHO-K1 cells for 4 h and cell viability was assayed after 4 h and for oligomer *^{cf}*C1 additionally after 24 h (Figure 3.17).
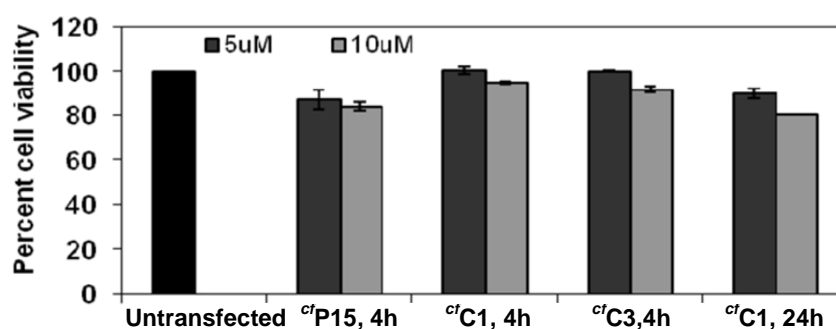

Figure 3.17 Cell Viability Assay in CHO-K1 cells after 4h/24h upon incubation with oligomers.

As clearly seen from the Figure 3.17, none of the oligomers was found toxic to cells as cell viability was found above 90% even after incubation of cells with oligomers *^{cf}*C1 for 24h at the concentration studied. In another experiment, oligoamide *^{cf}*P15 and

oligocarbamate ^{cf}**C1** was incubated at 5 and 10 μM concentration with HeLa cells for 4h and cell viability was measured after 4h Figure 3.18. Again, these oligomers were found non-toxic to HeLa cells at the higher (10 μM) concentration studied.
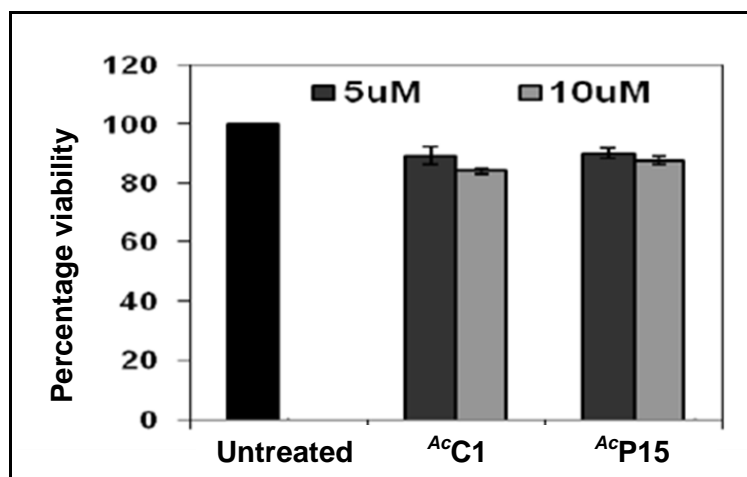

Figure 3.18 Cell Viability Assay in HeLa cells after 4h incubation with oligomers.

3.3.5 Applications of synthesized oligomers as a molecular transporter

To test the applicability of synthesized oligocarbamate as a molecular transporter in comparison to its oligoamide counterpart, additionally we synthesized non-fluorescent oligomers (^{Ac}**P15**, ^{Ac}**C1** and ^{Ac}**C2** listed in Table 3.1).

We tested the synthesized unlabeled oligomers for delivery of different cargo (pDNA, labeled-siRNA, tripeptide, PMO) *in vitro* and *in vivo* experiments. The application of synthesized oligomers was shown by two different strategies, which was used to attach cargo to synthesized oligomers and this section has been divided in following two sub-sections:

Section A: Non-covalent complexation strategy

Section B: Covalent conjugation strategy

3.3.5A Non-covalent complexation strategy

In this section, we present the results for the delivery of negatively charged plasmid DNA (pDNA) and *cf*-labeled siRNA (siGLO) to CHO-K1 cells by charge complexation (non-covalent complexation strategy) with positively charged oligomers (^{Ac}**P15**, ^{Ac}**C1** and ^{Ac}**C2**).

3.3.5A.1 Gel studies of formed complexes

It is well studied that, at physiological pH, guanidine moieties are present in their protonated form and bear one positive charge per guanidine moiety in the oligomer. Hence at physiological pH, oligomers containing guanidine moieties can form electrostatic complexes with negatively charged cargoes such as negatively charged DNA or RNA (represented in terms of Nitrogen/Phosphate ratio; NP ratio) upon pre-mixing in definite charge ratios (Z +/-). The synthesized oligomers ^{Ac}**P15** and ^{Ac}**C1** each contained eight guanidines and hence contains eight positive charges per molecule. Initially to evaluate charge complex formation property of synthesized oligomers (oligoamide ^{Ac}**P15** and oligocarbamate ^{Ac}**C1**) each of them were separately pre-mixed with pDNA, upto the charge ratio 1:10 (pDNA: oligomer). The formed complexes or polyplexes were loaded on agarose gel and analysed by electrophoretic mobility shift assay (Figure 3.19).
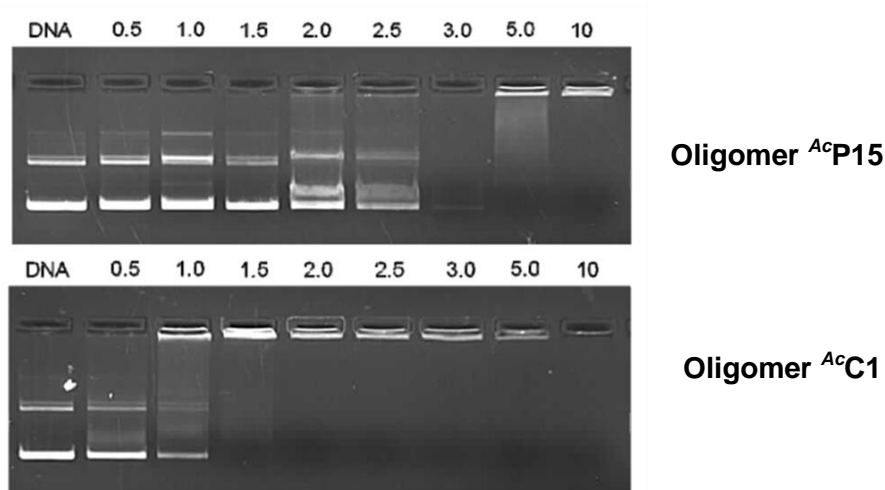

Figure 3.19 Electrophoretic mobility shift assay of pDNA with oligomers ^{Ac}**P15** and ^{Ac}**C1**. Lane 1-Control (only plasmid DNA), Lane 2-9 are the polyplexes formed at different charge ratios or N/P ratio (from 0.5 to 10).

As seen from Figure 3.19, for the oligocarbamate ^{Ac}**C1**, the retarded band was observed at charge ratio 1:1.5 (pDNA : oligomer ^{Ac}**C1**) and shows formation of neutral complex. Whereas in case of control oligomer ^{Ac}**P15,** retarded band was observer at charge ratio 1:3 (pDNA : oligomer ^{Ac}**P15**) and shows formation of neutral complex. The formed complexes above these charge ratios are considered as overall positively

charged complexes. Therefore, charge ratio 1:10 (pDNA: ologomer) was considered suitable for the pDNA cargo delivery applications.

3.3.5A.2 Cell transfection studies

To test the applicability of the oligocarbamates in delivering large size cargo molecules in biologically active form, we carried out pMIR Report plasmid DNA transfection in CHO-K1 cells. Oligomers [Ac]**P15,** [Ac]**C1** and [Ac]**C3** (unlabeled counterparts of [Ac]**P15,** [Ac]**C1** and [Ac]**C3** respectively were chosen to avoid any interference of the *cf* label) were complexed with pDNA (pDNA : oligomers, 1:10) and used to transfect CHO-K1 cells (Figure 3.20).
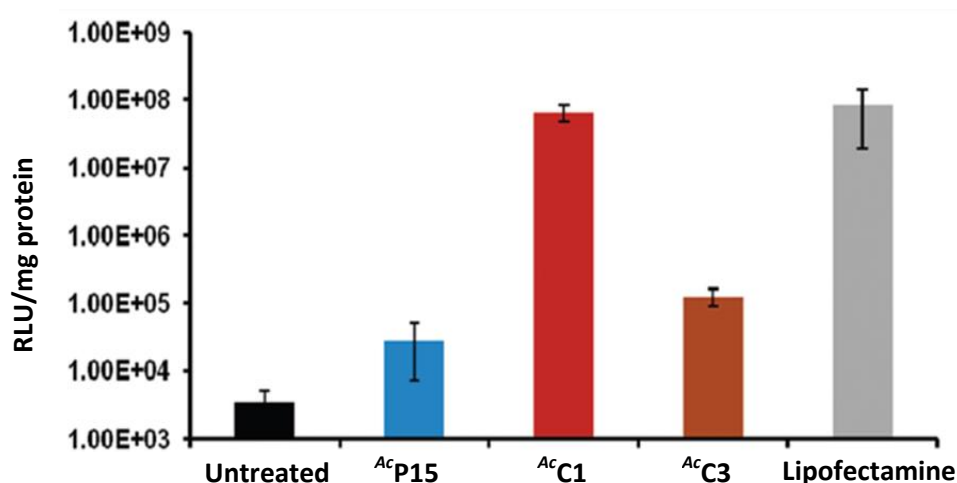

Figure 3.20 Transfection of CHO-K1 cells by pMIR-Report luciferase complexed with unlabeled oligomers [Ac]**P15**, [Ac]**C1**, and [Ac]**C3.**

Along with oligocarbamate [Ac]**C1**, additionally control oligoamide [Ac]**P15** and oligocarbamate [Ac]**C3**, commercially available transfection reagent lipofectamine was also included as an additional reference in transfection experiment. (Despite high transfection efficiency of lipofectamine its *in vivo* application is limited due to high associated cytotoxicity[20]). Results from the transfection experiment clearly demonstrated that oligocarbamate [Ac]**C1** (r-x-r- motif) was superior over control oligocarbamate [Ac]**C3** (r_8_oligocarbamate) and oligoamide [Ac]**P15** (R-X-R-motif) to deliver pDNA to the cells in its active form. The efficiency was found approximately equal or even more than Lipofectamine reagent, more importantly with low cytotoxicity

as shown in Figure 3.21 (cytotoxicity of complexes was checked after premixing of pDNA with oligomers at 1:10 charge ratio of pDNA: oligomer). The cell viability was found approximety 95% in case of oligomer ^{Ac}C1 which was comparable with control oligomer ^{Ac}P15 and ^{Ac}C3. However in case of lipofectamine, cell viability was reduced dramatically upto 55-60%.
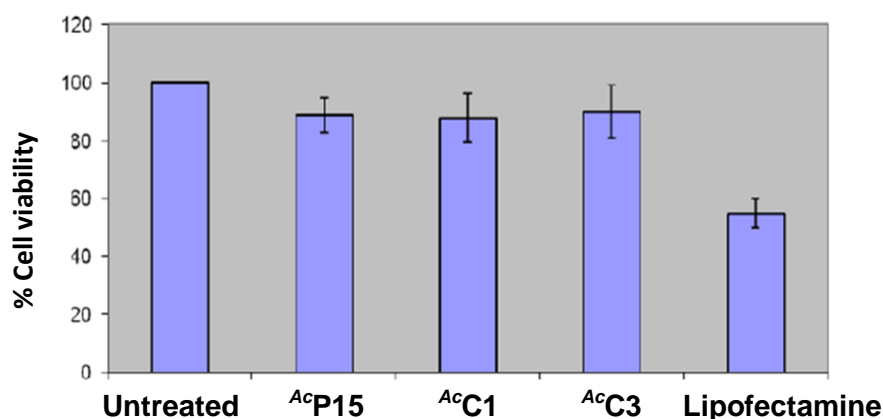

Figure 3.21 Cytotoxicity of pDNA-oligomer complexes.

3.3.5A.3 Delivery of carboxyfluorescein labeled siRNA (siGLO) to cells

Further, transportation of green-labeled siRNA [siGLO Green Transfection Indicator (Thermo Scientifict)] to CHO-K1 cells was tested by non-covalent charge complexation strategy with positively charged oligocarbamate ^{Ac}C1. The cell delivered fluorescent siRNA was quantified by FACS analysis and results were plotted in Figure 3.22. FACS results depicted that siGLO alone (in the absence of oligomer ^{Ac}C1) was unable to cross cell membrane and was detected in very low amount inside the cells. Whereas, when siGLO was tested in cell uptake study after charge complexation with oligomer ^{Ac}C1 at charge ratio 1:10 (siGLO: oligomer ^{Ac}C1), fluorescence was detected in almost 100% cells with high intensity.
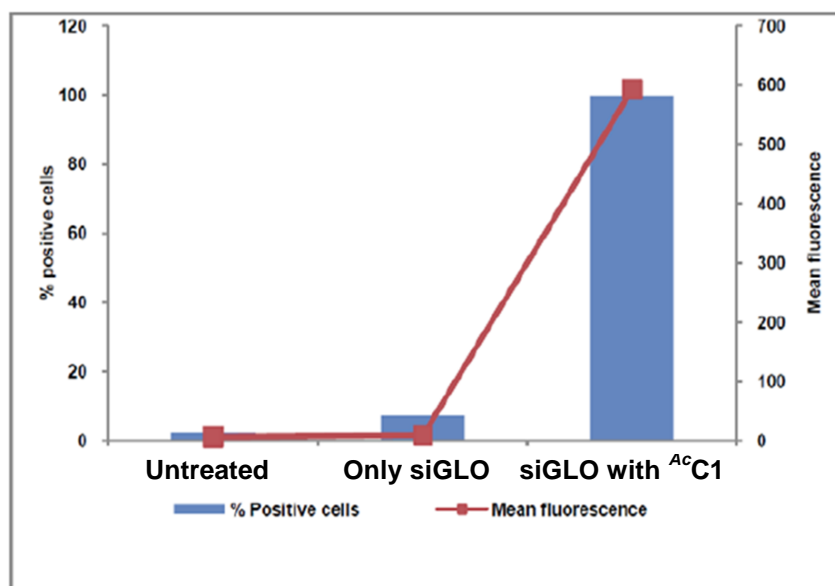
Figure 3.22 FACS analysis of siGLO, siGLO complex with ^{Ac}C1.

3.3.5B Covalent conjugation strategy

In this section, we have synthesized oligomer-cargo conjugates which are synthesized via covalent conjugation strategy and some of these conjugates were tested for cargo delivery application *in vitro* or/and *in vivo*.

3.3.5B.1 Synthesis of Tyroserleutide-oligomer conjugates and their *in vitro* delivery study

Tyroserleutide is known tripeptide for its potent anti-cancer activity consisting a sequence of tyrosine, serine and leucine amino acids. Activity of tyroserleutide can be enhanced, if transported efficiently to the cells. Towards this goal to improve activity of the tripeptide, we covalently conjugated tyroserleutide to our newly synthesized oligocarbamate and as a reference tyroserleutide was also conjugated to oligoamide. To synthesize *cf*-Tyroserleutide-oligoamide (**Conjugate A**) and *cf*-Tyroserleutide-oligocarbamate (**Conjugate B**); The resin attached *N*-terminal Boc-protected (r-ahx-r)$_4$ carbamate and (R-Ahx-R)$_4$ oligoamide was taken (20 mg of each). The oligomers were extended further by sequential coupling of the suitably protected amino acids, Boc-Leu-OH, Boc-Ser(Bzl)OH and Boc-Tyr(Bzl)OH using TBTU, HOBt, and DIPEA in DMF as the coupling reagents, and using the protocols employed for oligoamide synthesis.

Deprotection and coupling reactions were monitored by the Kaiser test. The final coupling was done by using ten equivalents each of 5(6)-carboxyfluorescein, HOBt, DIPCDI in DMF overnight to yield the *cf*-labeled **Conjugates A** and **Conjugate B**.
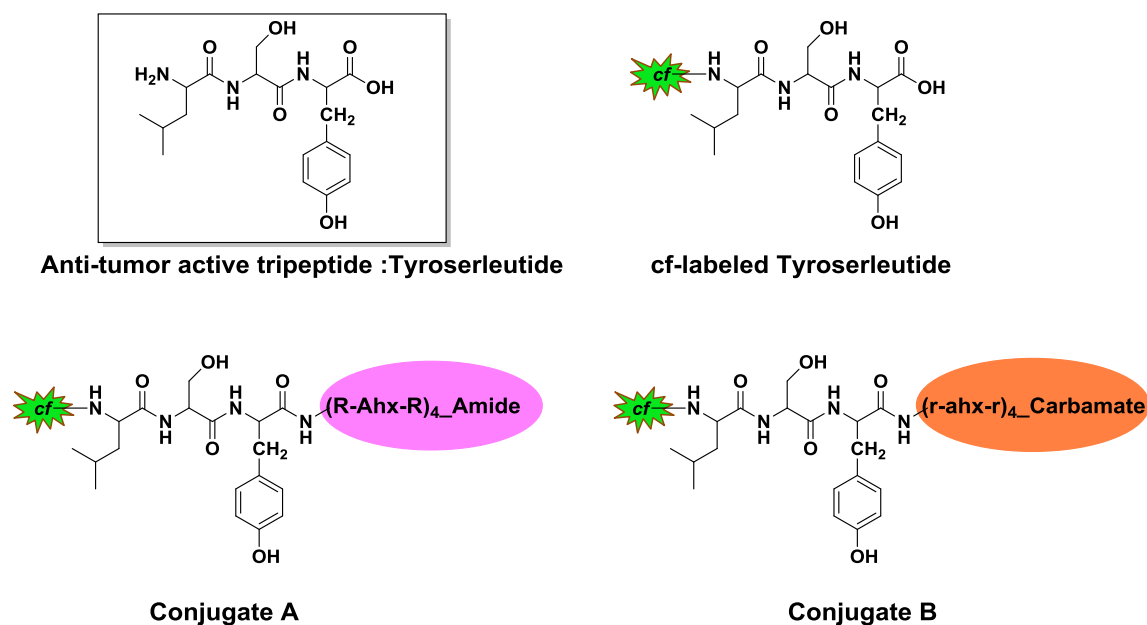

Anti-tumor active tripeptide :Tyroserleutide   **cf-labeled Tyroserleutide**

Conjugate A   **Conjugate B**

Figure 3.23 structures of Tyroserleutide and its covalent conjugates with oligomers.

Additionally control *cf*-labeled tryroserleutide was also synthesized on Merrified resin as a solid support. Further, cleavage of oligomers from solid support and HPLC purification afforded **Conjugate A, B** and control *cf*-tyroserleutide (*cf*P16), their MALDI characterization data is listed in Table 1.2.

Table 1.2 MALDI-TOF mass characterizations of synthesized oligomer and conjugates.

Code	Sequence	Mass (MALDI-TOF)	
		Calcd.	Obsd.
*cf*P16	*cf*-Tyroserleutide-NH$_2$	738.25	738.45
Conjugate A	*cf*-(R-Ahx-R)$_4$-Tyroserleutide-NH$_2$	2439.39	2440.09
Conjugate B	*cf*-(r-ahx-r)$_4$-Tyroserleutide-NH$_2$	2769.51	2769.80

FACS analysis of synthesized conjugates:

FACS analysis was performed after incubation of 5µM of **Conjugate A**, **B** or *cf***P16** (*cf*-tyroserleutide) with CHO-K1 cells for 1h at 37°C and results are shown in Figure 3.24. FACS results demonstrated that, the oligoamide (**Conjugate A**) as well as oligocarbamate (**Conjugate B**) could transport the covalently conjugated *cf*-labeled tyroserleutide to almost 100% of cell whereas, as *cf*-Tyroserleutide (*cf***P16**) alone could not enter cells efficiently. The oligocarbamate showed high transport of tyroserleutide to cells compared to its oligoamide counterpart, as the mean fluorescence intensity inside the cells was very high (when internalized with **conjugate B**). The results of FACS analysis are shown in Figure 3.24.
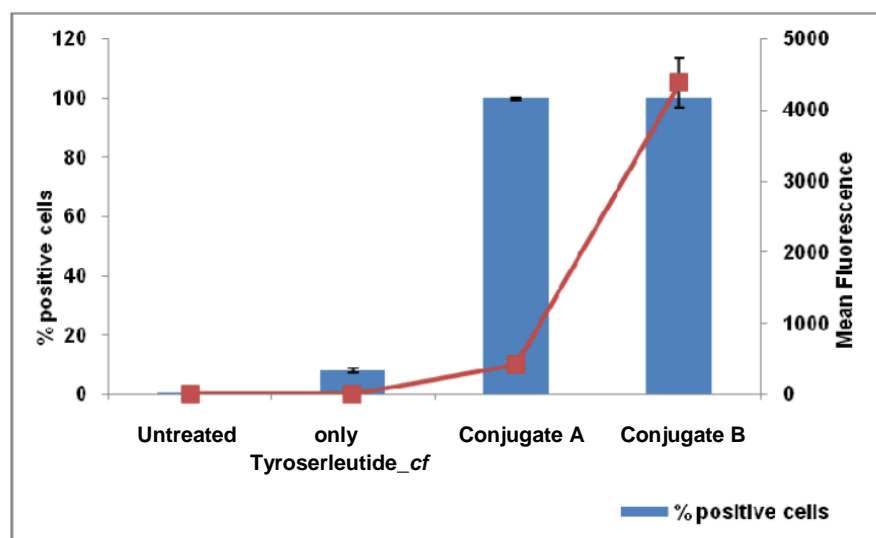

Figure 3.24 FACS analysis showing the uptake of the potential therapeutic tripeptide, Tyroserleutide in comparison to its conjugates with oligomers of the study.

3.3.5B.2. Synthesis of PMO-oligomers conjugate and their *in vitro* and *in vivo* delivery study

Duchenne muscular dystrophy (DMD) is a severe muscle degenerative disorder resulting from mutations that disrupt the DMD gene open reading frame leading to the absence of functional dystrophin protein. DMD is a systemic disease affecting skeletal muscles, as well as heart muscle and brain. Therefore, successful antisense oligonucleotides (AO) exon-skipping therapy will depend critically on effective AO

delivery to all affected tissues. Systemic delivery of 2′-O-methyl phosphorothioate and phosphorodiamidate morpholino oligonucleotides (PMO) have been shown to restore dystrophin protein expression in multiple peripheral muscle groups in dystrophin-deficient *mdx* mice but with low efficiencies even at high doses. More recently, enhanced systemic delivery of PMO AOs has been reported *via* AO conjugation to positively charged, arginine-rich (Arg-rich) CPPs. All of these studies reported significant dystrophin protein restoration in multiple muscle groups at low PMO doses compared with unmodified PMO, with limited dystrophin correction in heart muscle, and improvement of the *mdx* phenotype.

(R-X-R)-type of peptide has been studied by covalent conjugation with AO PMO for exon skipping in DMD disease. Here we synthesized and evaluated the oligocarbamate AO PMO conjugate, initially in the cells and later in animals. Bromoacetylated derivative of the synthesized oligocarbamate was conjugated to AO PMO *via* thiol linkage in the presence of DIPEA in DMF as shown in Scheme 3.3.
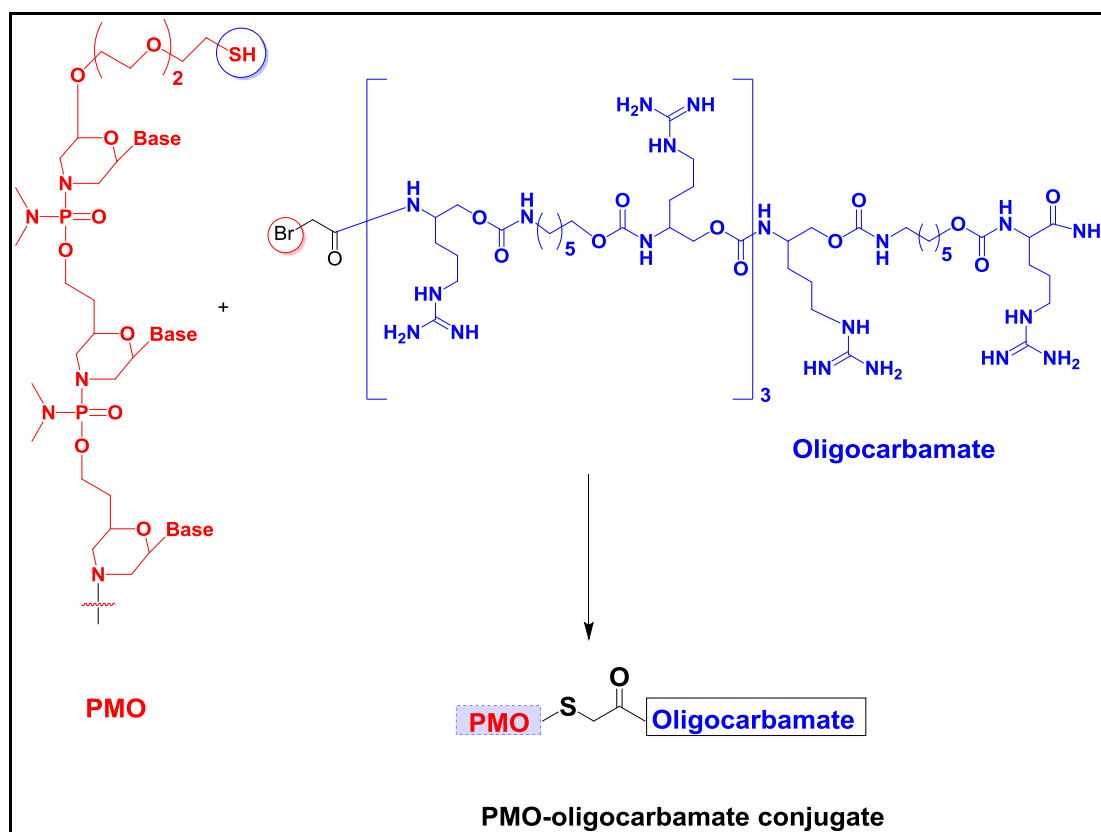
Scheme 3.3 Schematic presentation of covalent attachment of PMO to synthesized oligocarbamate.

HPLC purified PMO-oligocarbamate conjugate was characterized by MALDI-TOF analysis. It was further tested in cell culture for exon skipping using mdx myotubes and free delivery. Initially the concentration of PMO-oligocarbamate conjugate used was in range of 0.25 to 2 µM. Peptide conjugates such as $(R-X-R)_4$-PMO, stearyl-pip6e-PMO, pip9c2-PMO are also been studied as a control along with synthesized oligocarbamate-PMO analogue and their *in vitro* 23 exon skipping activity was plotted and showed in Figure 3.25.
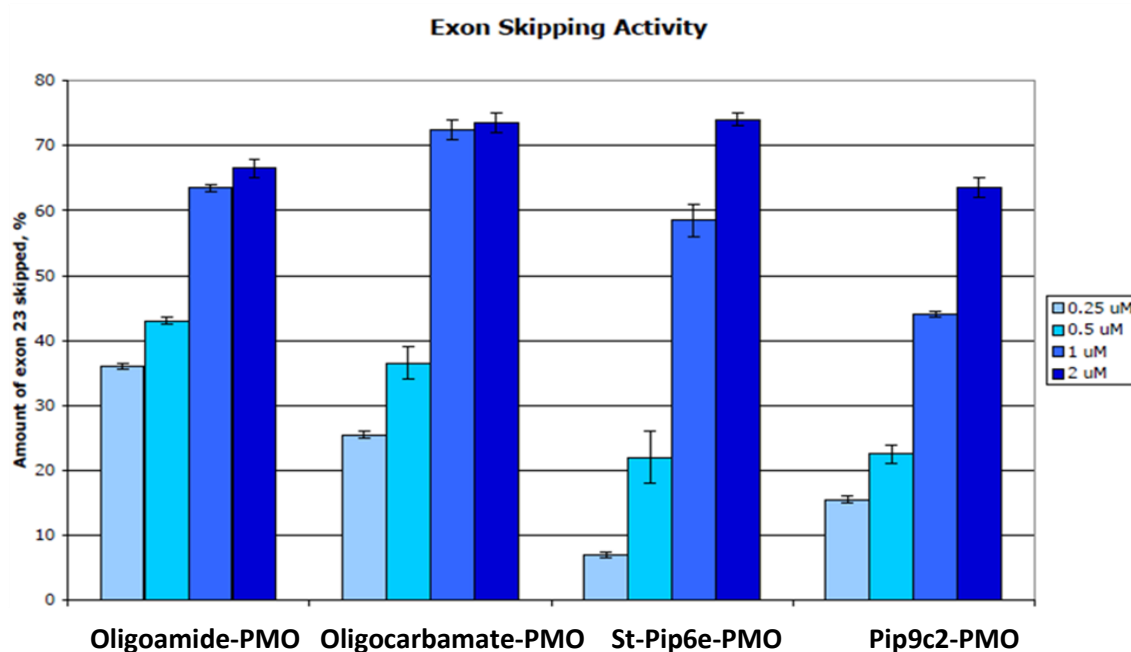
Figure 3.25 Exon skipping activity of oligomer-PMO conjugate *in vitro*.

Results revealed that the newly synthesized oligocarbamate was able to deliver covalently attached PMO to the cells effectively and the delivered PMO showed good exon skipping activity in cell culture. Their cell toxicity was also assayed and up to 20 µM concentrations of both peptide- and oligocarbamate- PMO conjugates showed no loss of cell viability.

We further evaluated the oligocarbamate-PMO conjugate *in vivo* for its intramuscular exon skipping activity in mice. Intramuscular injection of oligocarbamate-PMO was given at TA (tibialis anterior; small muscle of leg) of five

animals at dose 30 μg and three animals at dose 5 μg, (R-X-R)$_4$-peptide PMO conjugate was included as a control in this experiments.

The results of intramuscular exon skipping and dystrophin staining after injection into the tibialis anterior muscles of mdx mices were also been promising, but the activity of oligocarbamate conjugated PMO was found to be less effective than its oligoamide conjugate, the reason for which is not yet clear.

For animal studies, the oligocarbamate had to be synthesized on larger scale and required amounts of oligocarbamate were synthesized and purified. The mdx mice were dosed with 18mg/kg of the (r-x-r)$_4$-Carbamate and [(R-X-R)$_4$-Peptide PMO conjugates (R-Xo-R)-PMO and (R-X-R)-PMO respectively]. Two of the animals were culled immediately after the carbamate-PMO injections and the rest of the animals were culled 48 hours later as their recovery was never complete. After extraction of tissues from these animals, RT-PCR and Immuno staining was performed. IM (intramuscular) administrations of these conjugates showed restoration of dystrophin fibres.

3.3.5B.3 Covalent attachment of Daunomycin to synthesized oligocarbamate

Doxorubicin and Daunomycin are anti-cancer ("antineoplastic" or "cytotoxic") chemotherapy drugs. However, one of the limitations of their clinical use is that systemic administration of an effective dose of these drug results in non-selective cardiac toxicity and myelosuppression. Various methods have been applied in literature to enhance their cell delivery and reduce immunogenicity of this family of drugs. Bidwell III *et al.*[21] attached tat-Elastin-like peptide (tat-ELP) to the doxorubicin in order to minimize nonspecific toxicity, and examined its ability to serve as a macromolecular carrier for thermally targeted delivery. MacKay *et al.*[22] self-assembling chimeric peptide-doxorubicin conjugate nanoparticles in treatment of solid tumour. Ai *et al.*[23] studied biological evaluation of a novel Doxorubicin-peptide conjugate for targeted delivery to EGF receptor-over expressing tumor cells. Similarly there are significant number of literature reports to show the enhancement in activity of doxorubicin, Daunomycin and similar type of drugs when attached or assembled with oligoamides. Here we have attached our synthesized oligocarbamate transporter to the Daunomycin. Initially succinate linker was attached to the exocyclic amino group present in

Daunomycin to get free carboxylic acid end and this free carboxylic acid was coupled to the amino group present in oligocarbamate by peptide coupling reagent afforded Daunomycin-oligocarbamate conjugate analogue as shown in Scheme 3.4. The conjugates were purified and characterized by MALDI-TOF mass spectrometry; their further biological evaluation is in progress.
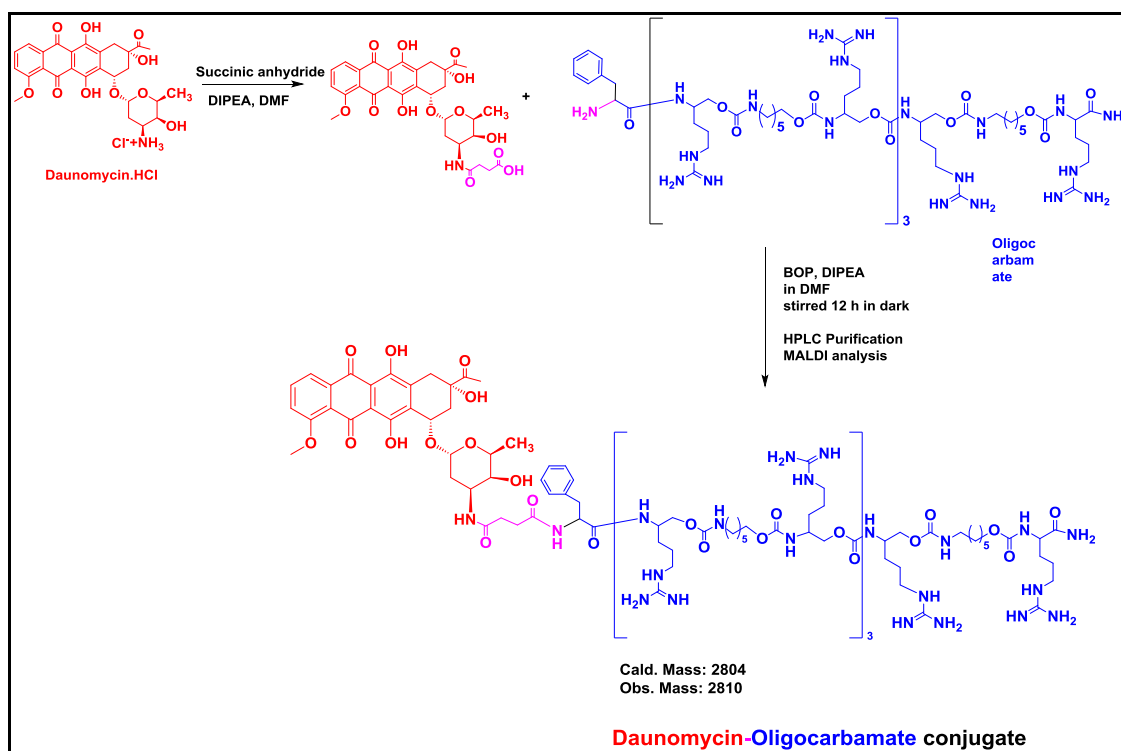
Scheme 3.4: Covalent attachment of Daunomycin to the synthesized oligocarbamate.

3.3.6. Summary and conclusion

- Synthesis of (r-x-r)-type oligocarbamates was accomplished on MBHA resin as solid support by employing *p*-nitrophenyl carbonate activated monomers.

- Structural features of synthesized oligocarbamates were studied by CD and they were found to be less structured in comparison to known $(R-X-R)_4$ oligoamide counterpart.

- Octanol-water partitioning experiment revealed $(r-x-r)_4$-oligocarbamates are amphipathic in nature similar to $(R-X-R)_4$-peptide and could transfer from water (hydrophilic layer) to Octanol (hydrophobic layer) layer upon addition of sodium laurate. The hydrocarbon chain length of X was found to be an important factor.

- FACS analysis carried out at 4 and 37°C in both the cell types (CHO-K1 and HeLa) showed that the oligocarbamate of the present study was superior in cellular penetration property than its oligoamide counterpart at both the temperatures. High cellular uptake was observed even when the experiment was done at low temperature. This suggested energy-independent cellular uptake pathways may be operating for oligocarbamates.

- Confocal microscopic analysis carried out in CHO-K1 and HeLa cells after incubation with oligocarbamate (^{cf}C1) showed high fluorescence intensity from cytoplasm as well as distribution inside the cell nucleus. However, fluorescence intensity was found low in case of control (R-X-R)$_4$-peptide (^{cf}P15).

- Confocal microscopy analysis of oligocarbamate (^{cf}C1) was also carried out after incubation at low temperature and incubation in the presence of sodium azide. In both the experiments, cell uptake of ^{cf}C1 was not affected significantly, supporting energy independent non-endocytotic pathways of cell entry.

- *In vitro* cytotoxicity studies revealed that newly synthesized oligocarbamates are not toxic to cells at concentration studied.

- Electrophoretic mobility shift assay of pDNA after charge complexation with oligomers ^{Ac}C1 and ^{Ac}P15 showed ability to form neutral or positively charged complexes upon premixing with negatively charged oligonucleotides.

- High efficiency in transportation of pDNA, *cf*-labeled siRNA and *cf*-labeled tripeptide (Tyroserleutide) to cells via charge complexation and covalent conjugation strategy respectively revealed applicability of synthesized oligocarbamate.

- Covalent PMO-oligocarbamate conjugate showed good activity *in vitro* as well as *in vivo*, suggesting that the oligocarbamate can be used in antisense oligonucleotide delivery.

- Synthesized oligocarbamate was also been attached covalently to Daunomycin (anticancer drug molecule) via succinate linker.

3.3.7 Experimental

3.3.7.1 Synthesis of compounds/monomer

<u>General Information:</u> All the reagents were purchased from Sigma-Aldrich and used without further purification. DMF, CH_2Cl_2 (dichloromethane), pyridine were dried over P2O5, CaH2, KOH respectively. DMF, CH_2Cl_2 were stored by adding4 Ǻ molecular sieves and pyridine by adding KOH. THF was passed over basic alumina and dried by distillation over sodium. Column chromatography was performed for purification of compounds on silica gel (100- 200 mesh or 60-120 mesh, Merck). TLCs were performed on Merck 5554 silica 60 aluminium sheets. TLCs were performed using petroleum ether-ethyl acetate solvent systems. Compounds were visualized with UV light and/or by spraying with ninhydrin reagent and heating. 1H and 13C NMR (200 MHz) spectra were recorded on a Bruker ACF 200 spectrometer fitted with an Aspect 3000 computer and all the chemical shifts (ppm) are referred to internal TMS for 1H and chloroform-d for 13C NMR. 1H NMR data are reported in the order of chemical shift, multiplicity (s, singlet; d, doublet; t, triplet; q, quartet; br, broad; br s, broad singlet; m, multiplet and/ or multiple resonance), number of protons. Mass spectra were recorded on an AP-QSTAR spectrometer, while MALDI HDMS was obtained on Waters MALDI SYNAPT-HDMS (High Definition Mass Spectroscopy). MALDI-TOF spectra were obtained from a Voyager-De-STR (Applied Biosystems). CHCA (α-Cyano-4- hydroxycinnamic acid) matrix was used to analyze MALDI-TOF samples. UV absorbance was performed on a Varian Cary 300 UV-VIS spectrophotometer. Circular Dichroism (CD) analysis was performed on a JASCO J-715 spectrophotometer using a cell of 10mm pathlength. CD spectra were recorded as accumulations of 5 scans using a scan speed of 200nm/min, resolution of 1.0 nm, band-width 1.0 nm and a response of 1 sec. The spectra were smoothened and plotted using OriginPro 6.1. Flow Cytometry measurements were carried out on Guava® EasyCyteTM System (Guava Technologies) using CytoSoftTM software and FACS-Aria IIIrd (Becton Dickinson). Imaging was done on an inverted LSM510 META laser scanning microscope (Carl Zeiss, Germany) using a Plan- Apochromat 63x 1.4 N.A. lens and the 488-nm line of an argon laser for carboxyfluorescein and 405 nm diode for Hoechst. The cytotoxicity of

the synthesized oligomers was determined by the CellTiter-Glo® Luminescent Cell Viability Assay system (Promega). Luminescence was measured by integration over 10s in Orion microplate luminometer (Berthold Detection System, Germany).

3.3.7.1a Experimental procedure and spectral data

(S)-*tert*-butyl-(1-hydroxy-5-(3-(mesitylsulfonyl)guanidino)pentan-2-yl)carbamate: (16)
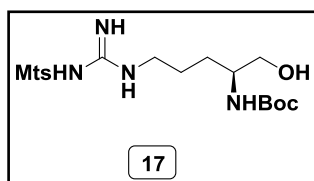
In a dry 100 mL round bottom flask equipped with magnetic bar, under argon atmosphere, $NaBH_4$ (0.30 g, 7.9 mmol) was added in 3:4 mixture of solvents THF: EtOH (40 mL). To this, slowly, LiCl (0.33 g, 7.9 mmol) was added at ice-cold conditions. The reaction mixture was stirred for 30 min., formation of milky solution confirms *in situ* generation of $LiBH_4$. The compound **16** (1.50 gm, 3.19 mmol) dissolved in ethanol (15 mL) was added drop-wise. The reaction mixture was stirred for a further 3h and then allowed to warm to room temperature. The reaction was monitored by TLC. Solvent evaporated in vacuo and the crude residue re-dissolved in water. The reaction mixture was neutralized by adding aq.NH_4Cl, followed by extraction of the water layer by ethyl acetate (3 x 20 mL). Brine washes (3 x 25 mL) were given followed by separation of layers. The combined organic layers was dried over Na_2SO_4. Solvent evaporated in vacuo and the crude compound was purified by silica gel column chromatography (10% Pet-ether/EtOAc) to give title compound **17** (1.27 g, 89%) as white foam.

Molecular formula: $C_{20}H_{34}N_4O_5S$; **Molecular weight:** 442.57

^{1}H NMR (200 MHz, $CDCl_3$) δ: 6.88 (s, 2H), 6.42 (bs, 2H), 5.18 (m, 1H), 3.52 (m, 3H), 3.19 (m, 2H), 2.62 (s, 6H), 2.26 (s, 3H), 1.53 (m, 3H), 1.39 (m, 10H).

^{13}C NMR (50 MHz, $CDCl_3$) δ: 156.8, 156.5, 141.15, 141.11, 138.0, 131.7, 79.7, 64.9, 52.1, 41.1, 28.8, 28.5, 25.7, 23.0, 20.9

^{13}C DEPT (50 MHz, $CDCl_3$) δ: *positive peaks*: 131.7, 52.2, 28.5, 23.0, 20.9; *negative peaks*: 64.9, 41.1, 28.8, 25.6

MALDI-HDMS: Calulated for $C_{20}H_{34}N_4O_5SNa$: 465.2142, found: 465.2163 (M+ Na).

(S)-*tert*-butyl-(5-(3-((4-methoxy-2,3,6-trimethylphenyl)sulfonyl)guanidino)-1-(((4-nitrophenoxy)carbonyl)oxy) pentan-2-yl) carbamate: (17)
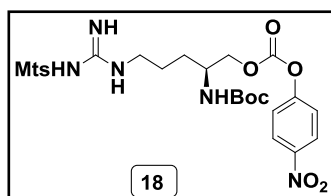
In a dry 100 mL round bottom flask equipped with magnetic bar, alcohol **17** (0.44 g, 1.0 mmol) was dissolved in dry CH_2Cl_2 (10 mL). In ice-cold conditions and under argon atmosphere, dry pyridine (161 μL, 2.0 mmol) was added by syringe and the reaction mixture stirred for 30 min. at 0°C. *p*-Nitrophenyl chloroformate (0.24 g, 1.2 mmol) was added to the reaction under anhydrous conditions and the mixture was stirred for 3h. The solvent was evaporated at room temperature in vacuo to give the crude product, which was further purified by flash silica gel column chromatography (30% EtOAc/Pet-ether) to give title compound **18** (0.48 g, 75.3%) as white foam.

Molecular formula: $C_{27}H_{37}N_5O_9S$; **Molecular weight:** 607.68

^{1}H NMR (200 MHz, CDCl$_3$) δ: 8.26 (d, *J* = 9.1 Hz, 2H), 7.37 (d, *J* = 9.1 Hz, 2H), 6.89 (s, 2H), 6.26 (s, 2H), 4.95 (d, *J* = 8.9 Hz, 1H), 4.22 (m, 1H), 3.92 (m, 1H), 3.23(m, 2H), 2.65 (s, 6H), 2.26 (s, 3H), 1.78 (m, 2H), 1.55 (m, 3H), 1.42 (s, 9H).

^{13}C NMR (50 MHz, CDCl$_3$) δ: 156.5, 156.2, 155.5, 152.5, 145.4, 141.0, 137.9, 131.6, 125.4, 121.9, 80.1, 71.0, 49.0, 40.9, 28.7, 28.4, 25.6, 23.0, 20.9.

^{13}C DEPT (50 MHz, CDCl$_3$) δ: *positive peaks*: 131.6, 125.4, 121.9, 48.9, 28.4, 23.0, 20.9; *negative peaks*: 71.0, 40.9, 28.6, 25.6.

MALDI-HDMS: Calculated for $C_{27}H_{37}N_5O_9SK$, 646.1944, found: 646.1957 (M+K).

tert-butyl-(6-(((4-nitrophenoxy)carbonyl)oxy)hexyl)carbamate: (23)
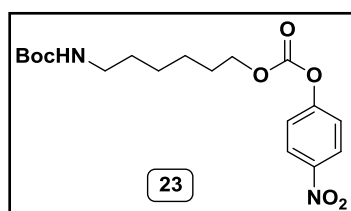
In a dry 100 mL round bottom flask equipped with magnetic bar, Boc-amino alcohol **22** (1.00 g, 4.6 mmol) was dissolved in dry CH_2Cl_2 (30 mL). In ice-cold conditions and under argon atmosphere, dry pyridine (0.74

mL, 9.2 mmol) was added by syringe and the reaction mixture stirred for 30 min at 0°C. *p*-Nitrophenyl chloroformate (1.10 g, 5.5 mmol) was added to the reaction vessel in portions under anhydrous conditions and the mixture was stirred for 3 h. The solvent evaporated in vacuo to obtain the crude product, which was further purified by flash silica column chromatography (25% EtOAc/Pet-ether) to give title compound. Further crystallization from CH_2Cl_2 afforded compound **23** (1.40 g, 82%) in crystalline form.

Molecular formula: $C_{18}H_{26}N_2O_7$; **Molecular weight:** 382.41

^{1}H NMR (200 MHz, CDCl$_3$) δ: 8.28 (d, *J* = 9.2 Hz , 2H), 7.39 (d, *J* = 9.2 Hz, 2H), 4.52 (bs, 1H), 4.29 (t, *J*= 6.57 Hz, 2H), 3.18 (m, 2H), 1.84 (m, 2H,), 1.61 (s, 2H), 1.45 (m, 13H).

^{13}C NMR (50 MHz, CDCl$_3$) δ: 156.0, 155.6, 152.6, 145.3, 125.3, 121.8, 79.1, 69.5, 40.4, 30.0, 28.4, 26.3, 25.4.

^{13}C DEPT (50 MHz, CDCl$_3$) δ: *positive peaks*: 125.3, 121.9, 28.4; *negative peaks*: 69.5, 40.4, 30.0, 26.3, 25.4.

MALDI-HDMS: Calculated for $C_{18}H_{26}N_2O_7Na$, 405.1632, found: 405.1612 (M+Na).

tert-butyl (3-(((4-nitrophenoxy)carbonyl)oxy)propyl)carbamate: (25)
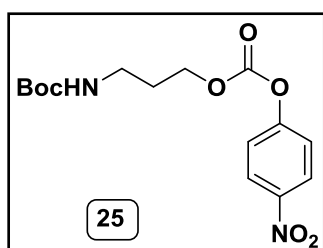
In a dry 100 mL round bottom flask equipped with magnetic bar, Boc-amino alcohol **24** (1.00 g, 5.7 mmol) was dissolved in dry CH_2Cl_2 (30 mL). In ice-cold conditions and under argon atmosphere, dry pyridine (0.92 mL, 11.4 mmol) was added by syringe and the reaction mixture stirred for 30 min at 0°C. *p*-Nitrophenyl chloroformate (1.30 g, 6.8 mmol) was added to the reaction under anhydrous conditions and the mixture was stirred for 3h. The solvent evaporated in vacuo and obtained crude product was further purified by flash silica column chromatography (25% EtOAc/Per-ether) to give title compound **25** (1.65 g, 86%) as a white powder.

Molecular formula: $C_{15}H_{20}N_2O_7$; **Molecular weight:** 340.33

¹H NMR (200 MHz, CDCl₃) δ: 8.28 (d, *J* = 9.2 Hz, 2H), 8.14 (d, *J* = 9.2 Hz, *p*-nitrophenol), 7.38 (d, *J* = 9.2 Hz, 2H), 6.97 (d, *J* = 9.2 Hz, *p*-nitrophenol), 4.81 (bs, 1H), 4.36 (t, 2H, *J* = 6.19, 6.07 Hz), 3.31 (q, 2H, *J* =6.57, 6.44 Hz,), 1.96 (m, 2H), 1.46 (s, 9H).

¹³C NMR (50 MHz, CDCl₃) δ: 156.4, 155.5, 152.6, 145.4, 125.4, 112.9, 80.0, 66.9, 37.2, 28.4; 162.9, 140.9, 126.2, 115.7 (*p*-nitrophenol).

¹³C DEPT (50 MHz, CDCl₃) δ: *positive peaks*: 126.2, 125.4, 121.9, 115.7; *negative peaks*: 66.9, 37.2, 29.1.

MS (ESI) : *m/z* calculated for C₁₅H₂₀N₂NaO₇, 363.11, found: 363.14 (M+ Na)

3.3.7.2 Procedures for oligomer synthesis and cleavage

3.3.7.2a Peptide synthesis

The oligoamide sequence *cf*-(R-Ahx-R)₄-NH₂ (*cf***P15**), *Ac*-Phe-(R-Ahx-R)₄-NH₂ (*Ac***P15**) was synthesized using MBHA resin (loading value 0.5 mmol/g) as solid support by standard Boc- protection strategy. Peptides were synthesized on a 25 μmol scale. Deprotection of Boc- group was carried out by 50% TFA in CH₂Cl₂followed by neutralization by 5% DIPEA in CH₂Cl₂. All coupling reactions were performed using three equivalents each of Boc- protected monomer, HOBt, TBTU and DIPEA in DMF for 4h at room temperature. Successive deprotection, neutralization and coupling steps were carried out as iterative cycles until the desired length of oligomers were synthesized. Deprotection and coupling reactions were monitored by the Kaiser test.

To synthesized carboxyfluorescent (*cf*) labeled oligomer *cf***P15** final coupling was done by using ten equivalents each of 5(6)-carboxyfluorescein (*cf*), HOBt, DIPCDI (diisopropyl carbodiimide) in DMF overnight.

For oligomer *Ac***P15**, a portion of resin-supported *N*-terminal Boc-protected (R-Ahx-R)₄ oligoamide was extended further by cleaving the *N*-terminal Boc group and coupling with phenylalanine using three equivalents of each Boc-phenylalanine, TBTU, HOBt and DIPEA in DMF. Finally, the terminal amine was capped after Boc

deprotection by using ten equivalents of Ac$_2$O and DIPEA in DMF to yield Oligomer ^{Ac}**P15**.

To synthesize the (R-Ahx-R)$_4$ oligoamide-tyroserleutide conjugate (Conjugate **A**), a portion of resin-supported *N*-terminal Boc-protected (R-Ahx-R)$_4$ oligoamide (20mg) was taken and extended further by sequential coupling of the suitably protected amino acids, Boc-Leu-OH, Boc-Ser(Bzl)OH and Boc-Tyr(Bzl)OH using TBTU, HOBt, and DIPEA in DMF as the coupling reagents, and using the protocols employed for oligoamide synthesis. Deprotection and coupling reactions were monitored by the Kaiser test. The final coupling was done by using ten equivalents each of 5(6)-carboxyfluorescein, HOBt, DIPCDI in DMF overnight to yield *cf*-labeled Conjugate **A**.

The tripeptide sequence *cf*-Tyr-Ser-Leu-NH$_2$ was synthesized using Boc-Leu-OH, Boc-Ser(OBzl)OH and Boc-Tyr(OBzl)OH and employing the same protocol as mentioned above for oligoamide synthesis. This was followed by a final coupling with CF, using ten equivalents each of 5(6)-carboxyfluorescein, HOBt, DIPCDI in DMF overnight to yield the *cf*-labeled tripeptide, *cf*-Tyroserleutide.

3.3.7.2b Oligocarbamate synthesis

The carbamate sequences *cf*-(r-ahx-r)$_4$-NH$_2$ (^{cf}**C1**), *cf*-(r-ahx-r-r-apr-r)$_2$ -NH$_2$ (^{cf}**C2**), *cf*-(r)$_8$ -NH$_2$ control (^{cf}**C3**), *Ac*-Phe-(r-ahx-r)$_4$ -NH$_2$ (^{Ac}**C1**) and *Ac*-Phe-(r)$_8$ -NH$_2$ control (^{Ac}**C3**) were synthesized on MBHA resin (0.5 mmol/g) as a solid support by the Boc-protection strategy. The oligomers were synthesized on a 25 μmol scale. Attachment of the first arginine residue to the solid support was by a regular amide linkage, formed using HOBt, TBTU and DIPEA as the coupling reagents. Further couplings with the appropriate carbonate monomers afforded carbamate linkages. Accordingly, deprotection of Boc- group was carried out with 50% TFA in CH$_2$Cl$_2$ followed by neutralization by 5% DIPEA in CH$_2$Cl$_2$. Three equivalents each of *p*-nitrophenylcarbonate activated monomer and DIPEA were added in DMF and allowed to react for 3 h. Successive deprotection, neutralization and coupling steps were performed by iterative cycles until desired length of oligomers was synthesized.

To synthesize the (r-ahx-r)$_4$ oligocarbamate-tyroserleutide conjugate (Conjugate **B**), a portion of resin-supported *N*-terminal Boc-protected (r-ahx-r)$_4$-carbamate (20mg)

was taken and extended further by sequential coupling of the suitably protected amino acids, Boc-Leu-OH, Boc-Ser(Bzl)OH and Boc-Tyr(Bzl)OH using TBTU, HOBt, and DIPEA in DMF as the coupling reagents, and using the protocols employed for oligoamide synthesis. Deprotection and coupling reactions were monitored by the Kaiser test. The final coupling was done by using ten equivalents each of 5(6)-carboxyfluorescein, HOBt, DIPCDI in DMF overnight to yield the *cf*-labeled Conjugate **B**.

For oligomer ^{Ac}**C1** and ^{Ac}**C3** a portion of resin-supported *N*-terminal Boc-protected (r-ahx-r)$_4$ and (r-ahx-r-r-apr-r)$_2$ -NH$_2$ oligocarbamates was extended further by cleaving the *N*-terminal Boc group and coupling phenylalanine using three equivalents of each Boc-phenylalanine, TBTU, HOBt and DIPEA in DMF. Finally, the terminal amine was capped after Boc deprotection by using ten equivalents of Ac$_2$O and DIPEA in DMF to yield Oligomer ^{Ac}**C1** and ^{Ac}**C3**.

3.3.7.2c Cleavage of oligomers from the solid support and purification by HPLC

All oligomers including oligoamides and oligocarbamates were cleaved from the MBHA solid support using a mixture of TFMSA-TFA and 1, 2-ethanedithiol and thioanisole as scavengers to yield ʻCʼ -terminal amide in oligomer. The purity of the oligomers was assessed by RP-HPLC, followed by purification. Pure oligomers were obtained after RP-HPLC on a C18 column with a water/acetonitrile gradient containing 0.1%TFA. The fractions of pure oligomer were concentrated by lyophilization, their identity confirmed by MALDI-TOF mass spectrometry and their concentration determined from their absorbance, using the molar absorption co-efficient of *cf* at 490nm for carboxyfluorescein-labeled oligomers and at 259nm for phenylalanine-labeled oligomer.

3.3.7.3 Procedures for Cell uptake studies (FACS, confocal microscopy)

FACS Analysis

The oligomers were conjugated with carboxyfluorescein as a model cargo at their 'N'-termini prior to cleavage from the solid support and purification. The oligomers were characterized by MALDI-TOF analysis. The concentration of the oligomers was calculated using the molar absorption co-efficient of carboxyfluorescein at 490nm. CHO-K1 cells were seeded in 24-well plates at a density of 50,000 cells/well and incubated for 24 hours. The fluorescently tagged oligomers were added to the cells at concentrations of 3μM and 5μM in 300μL of serum free medium. For measuring uptake in the presence of serum, 5μM oligomers were added in 300μL of medium containing 10% FBS. After 1h of incubation at 37°C or 4°C (37°C for serum studies), cells were washed with PBS containing heparin (1mg/mL) and with trypan blue in PBS. Cells were then collected by trypsinization and resuspended in PBS and placed on ice. Flow Cytometry measurements were carried out on Guava® EasyCyte^{TM} System (Guava Technologies) using CytoSoft^{TM} software. 10,000 live cells were used for each analysis at room temperature.

FACS measurements at 4°C or 37°C, subsequent to treating the cells with oligomers at the same temperature were carried out using the same protocols as mentioned above, but on a FACS-Aria IIIrd (Becton Dickinson) instrument, while maintaining the temperature at 4°C or 37°C respectively.

The uptake experiments were repeated to include an acid wash step (0.2 mol/l acetic acid and 0.2 mol/l NaCl) that quenches fluorescence of carboxyfluorescein that is externally bound to the cell membrane.

Confocal microscopy

Cells were seeded at a density of 1.2 x 105 in 35 mm μ-dishes (ibidi, Germany) and incubated for 24 hours. *cf*-labeled oligomers (10 μM; Oligomer ^{cf}**C1** at 5 μM) were added to the cells in serum-free media and incubated at 37°C for 4h. Hoechst 33342 (0.3 μg/mL) was added during the last 30 min of incubation. Cells were washed thrice with ice cold PBS(+) containing heparin (1 mg/mL). Imaging was done at room temperature

on an inverted LSM510 META laser scanning microscope (Carl Zeiss, Germany) using a Plan-Apochromat 63 x 1.4 N.A. lens and the 488-nm line of an argon laser for carboxyfluorescein and 405 nm diode for Hoechst.

3.3.7.4 Azide inhibition studies

Cells were pretreated with sodium azide at a final concentration of 25 mM for 30 min at 37°C, followed by incubation with the labeled oligomers in the presence of sodium azide.

3.3.7.5 Cytotoxicity studies

The toxicity of the synthesized oligomers was determined by the CellTiter-Glo® Luminescent Cell Viability Assay system (Promega). Cells were seeded in 96-well plates 1 day before treatment. Cells were then treated with different concentrations of the oligomers for 4h in serum-free media, and the cell viability was assayed according to the manufacturer᾽s protocol. Alternatively, cells were replenished with complete media, and the cell viability was assayed after 24h.

3.3.7.6 Octanol water partitioning

The concentration of oligomers was determined by UV absorbance and diluted with water to get a final concentration of 10μM each. To an aqueous solution of oligomers ^{cf}**P15,** ^{cf}**C1 and** ^{cf}**C3** (300 μL each) taken separately in sample vials (three sets), octanol (300 μL) was added. In another set of vials containing Oligomers ^{cf}**P15,** ^{cf}**C1 and** ^{cf}**C3** (10μM each), lauric acid in octanol (10 mM solution, 7.2 μL, 3.0 equiv per guanidine) was added, followed by a solution of sodium hydroxide in water (10 mM solution, 7.2 μL, 3.0 equiv per guanidine). Similarly, in yet another set of vials containing Oligomers ^{cf}**P15,** ^{cf}**C1 and** ^{cf}**C3** (10μM each), lauric acid in octanol (10 mM solution, 14.4 μL, 6.0 equiv per guanidine) was added, followed by a solution of sodium hydroxide in water (10 mM solution, 14.4 μL, 6.0 equiv per guanidine). The mixtures were shaken for one minute, centrifuged (~4000 rpm for 1 min) and photographed.

3.3.8 Appendix B

Compound and characterization	Page No.
Compound 17: ^{1}H, ^{13}C NMR, ^{13}C DEPT, MALDI HDMS	164-165
Compound 18: ^{1}H, ^{13}C NMR, ^{13}C DEPT, MALDI HDMS	166-167
Compound 23: ^{1}H, ^{13}C NMR, ^{13}C DEPT, MALDI HDMS	168-169
Compound 25: ^{1}H, ^{13}C NMR, ^{13}C DEPT, MALDI HDMS	170-171
MALDI-TOF spectra of oligomers	172-177

^{1}H NMR (200 MHz; CDCl$_3$) spectrum of compound **17**:
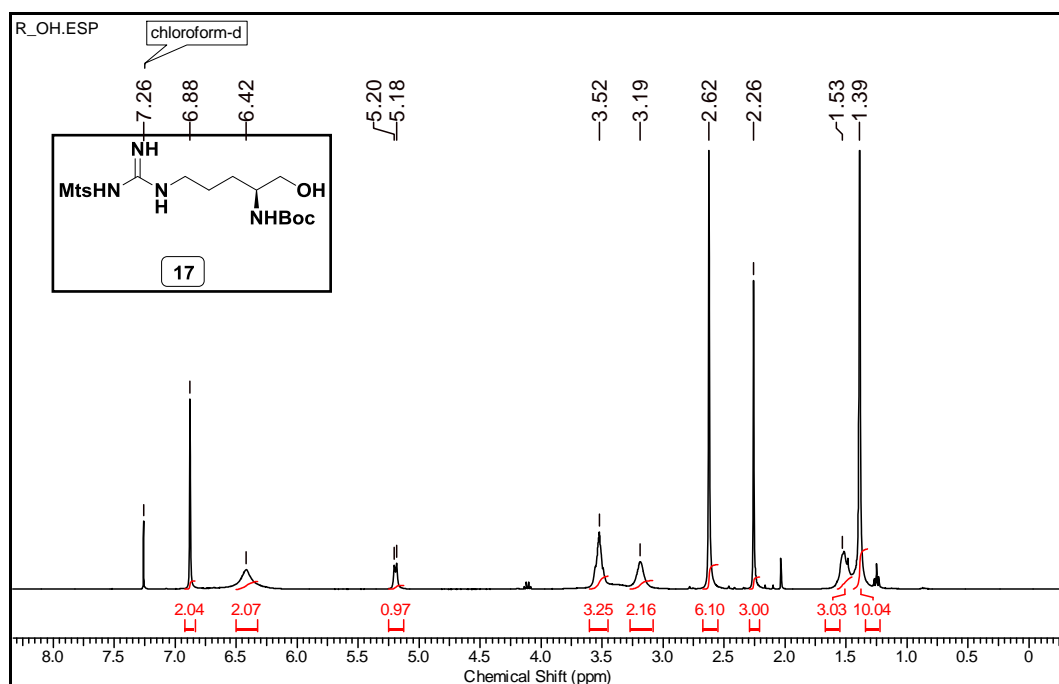
^{13}C NMR (50 MHz; CDCl$_3$) spectrum of compound **17**:
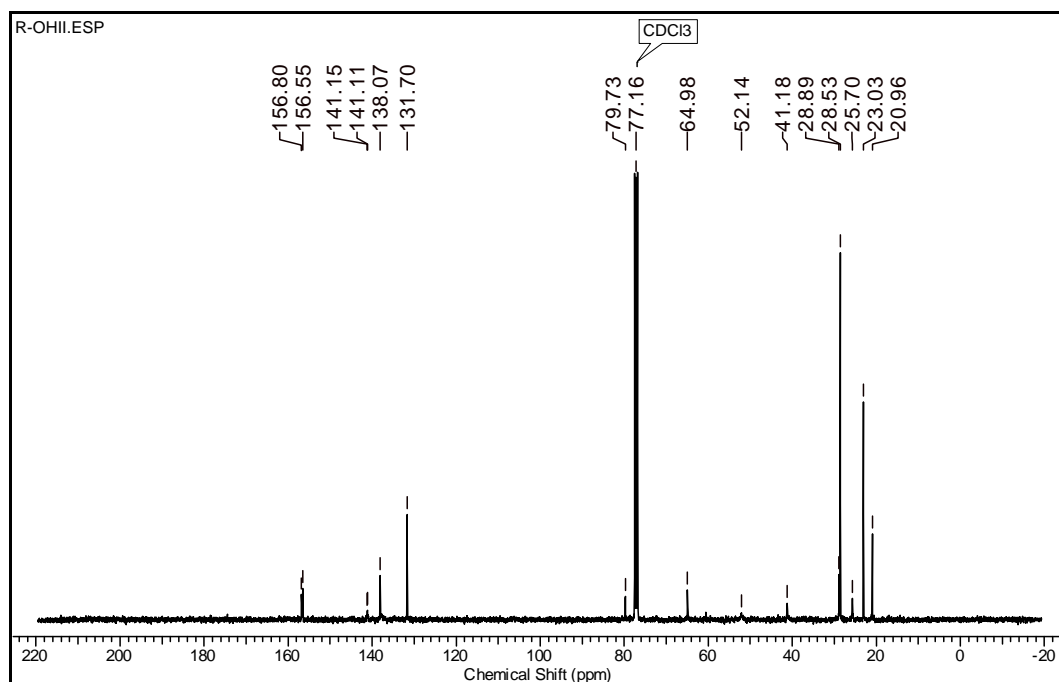
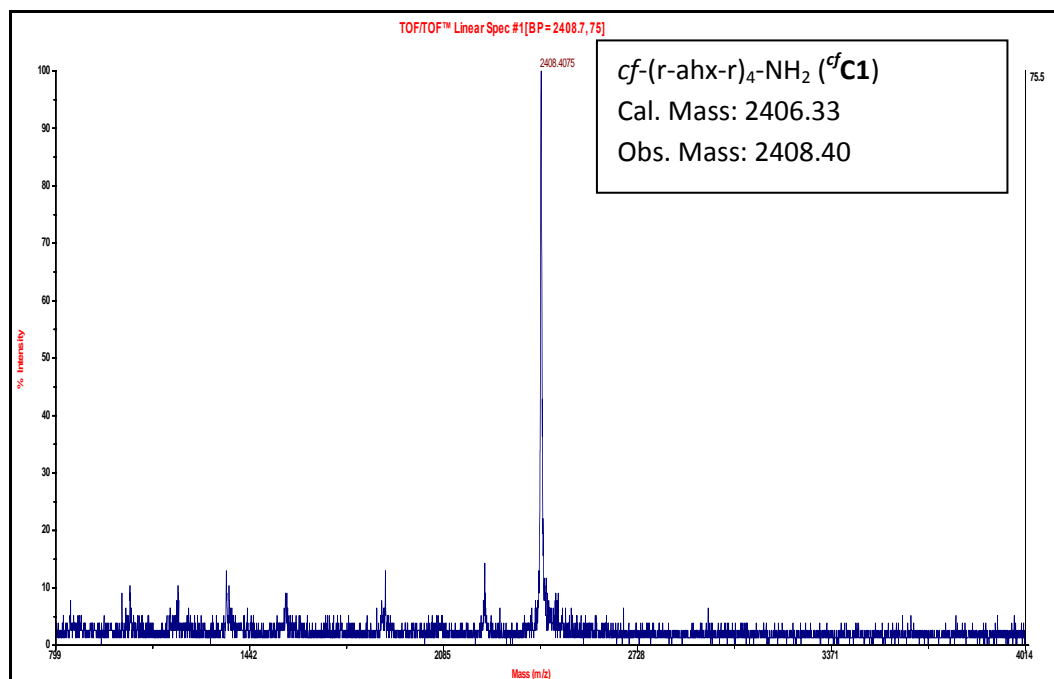^{13}C DEPT (50 MHz; CDCl$_3$) spectrum of compound **17**:

R-OHIII.ESP

—131.70
—64.96
—52.21
—41.16
—28.89
—28.52
—25.69
—23.03
—20.97

Chemical Shift (ppm)

MALDI HDMS spectrum of compound **17**:

DHB
300911-96-2A H9 SEEMA -I 4 (0.083) Cm (2:24)
TOF MS LD+
449

465.2163
365.1645
381.1433
481.2006
466.2253
366.1713
387.1683
367.1723
409.1602
443.2329
467.2195
482.2026

m/z
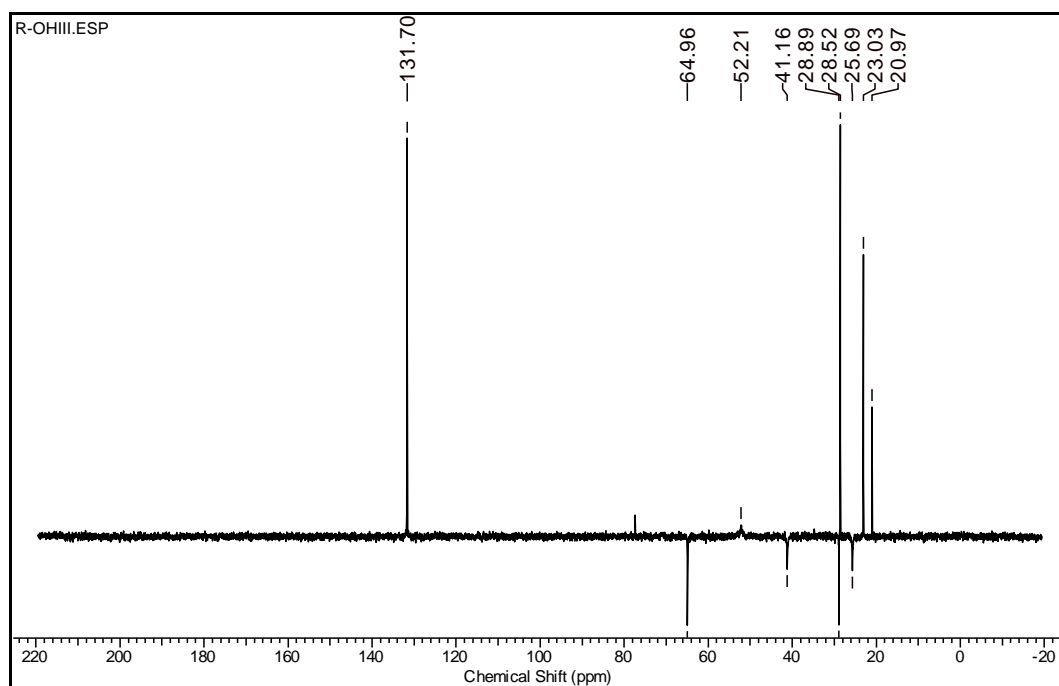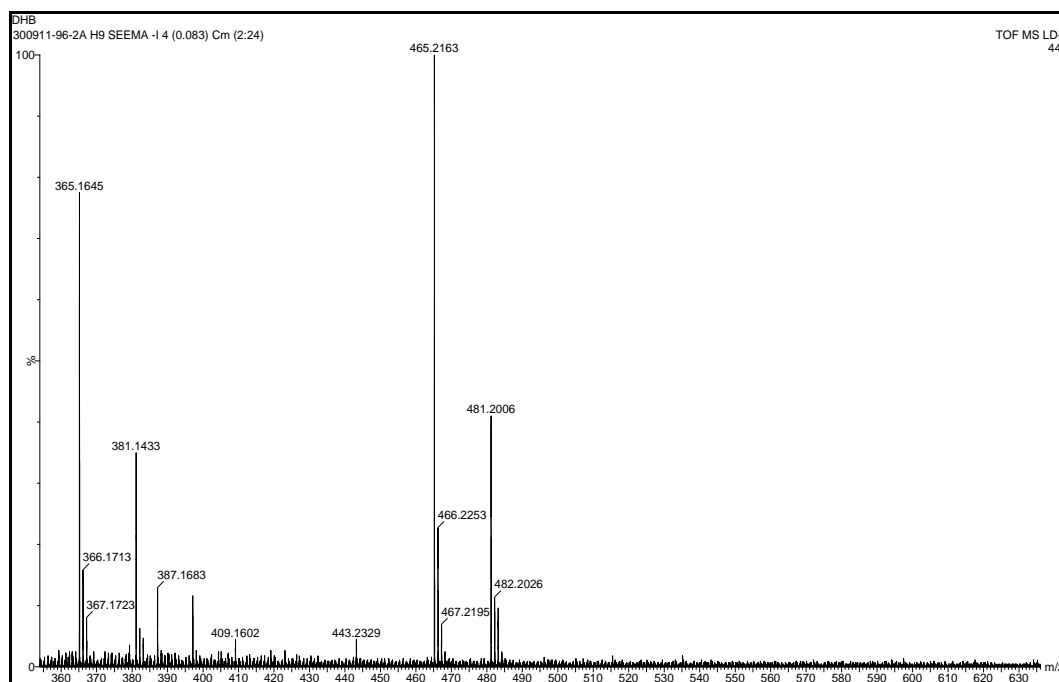
1H NMR (200 MHz; CDCl3) spectrum of compound **18**:
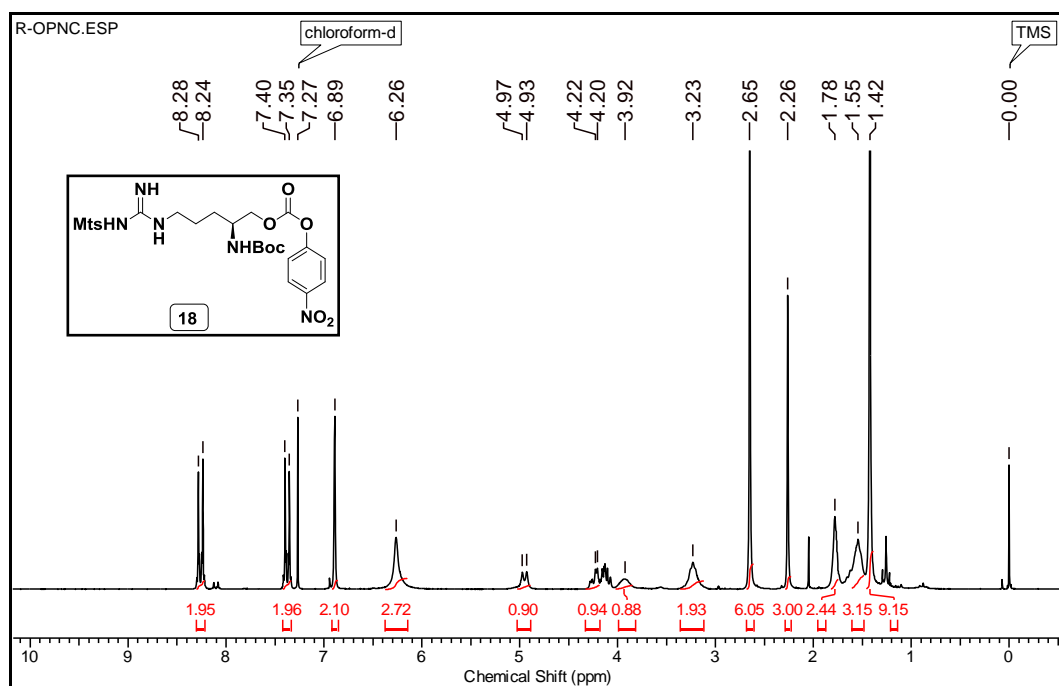
13C NMR (50 MHz; CDCl3) spectrum of compound **18**:
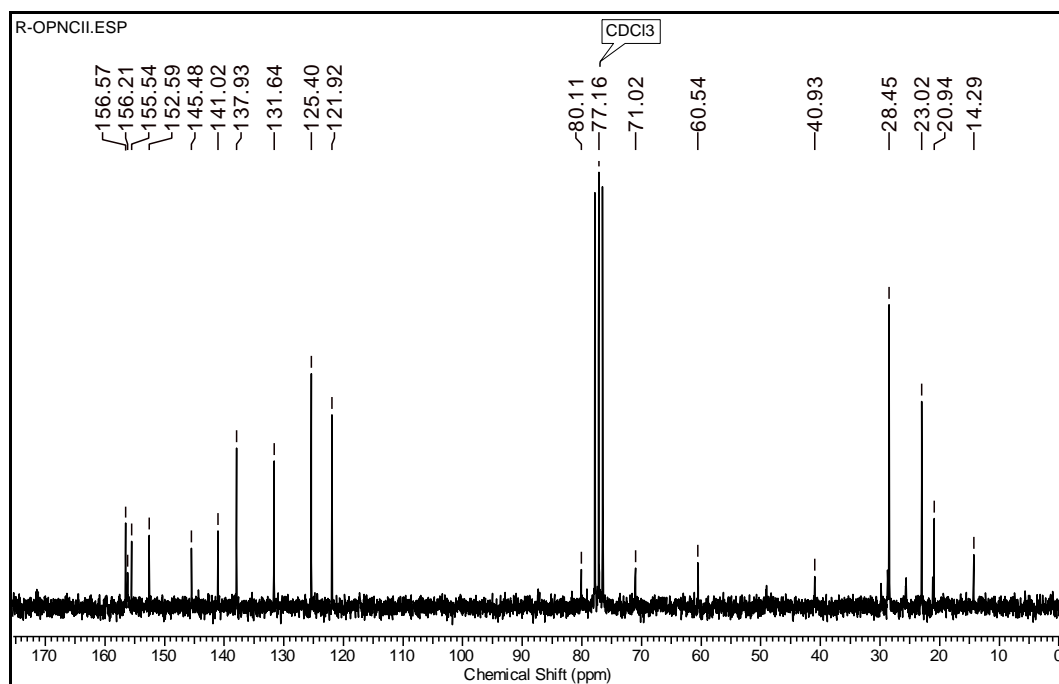
^{13}C DEPT (50 MHz; CDCl$_3$) spectrum of compound **18**:
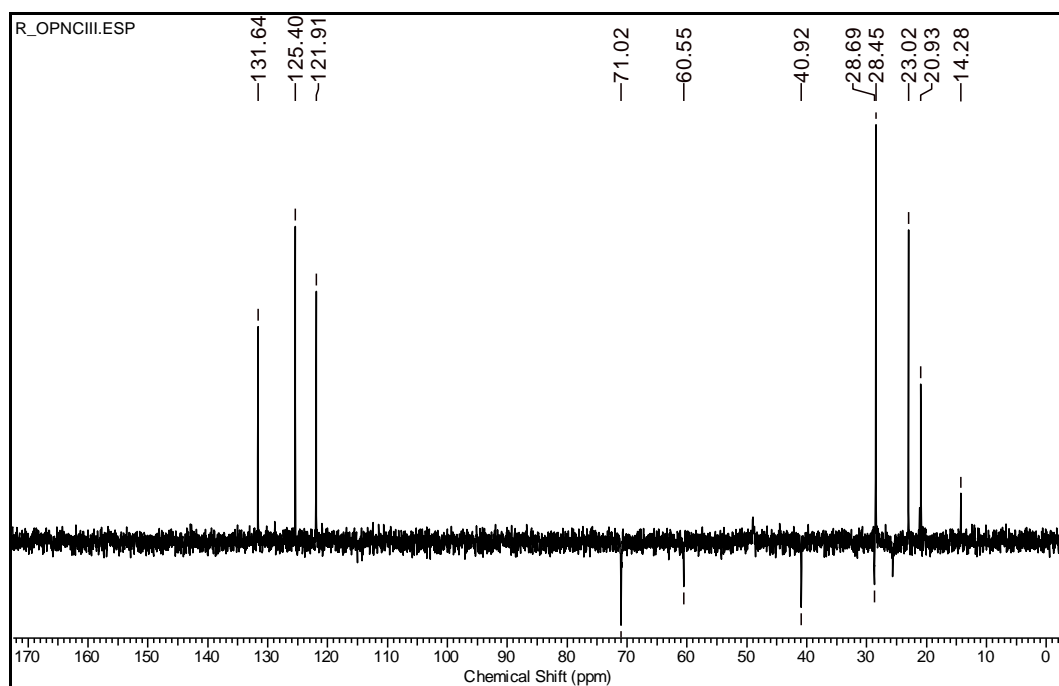
MALDI HDMS spectrum of compound **18**:
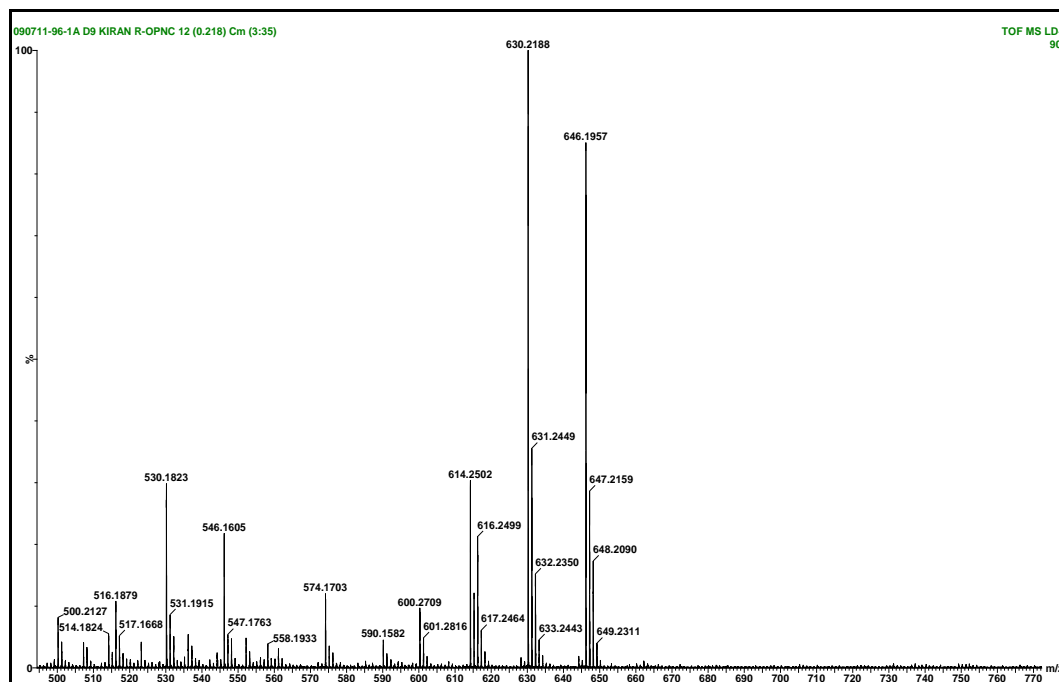
^{1}H NMR (200 MHz; CDCl$_3$) spectrum of compound **23**:
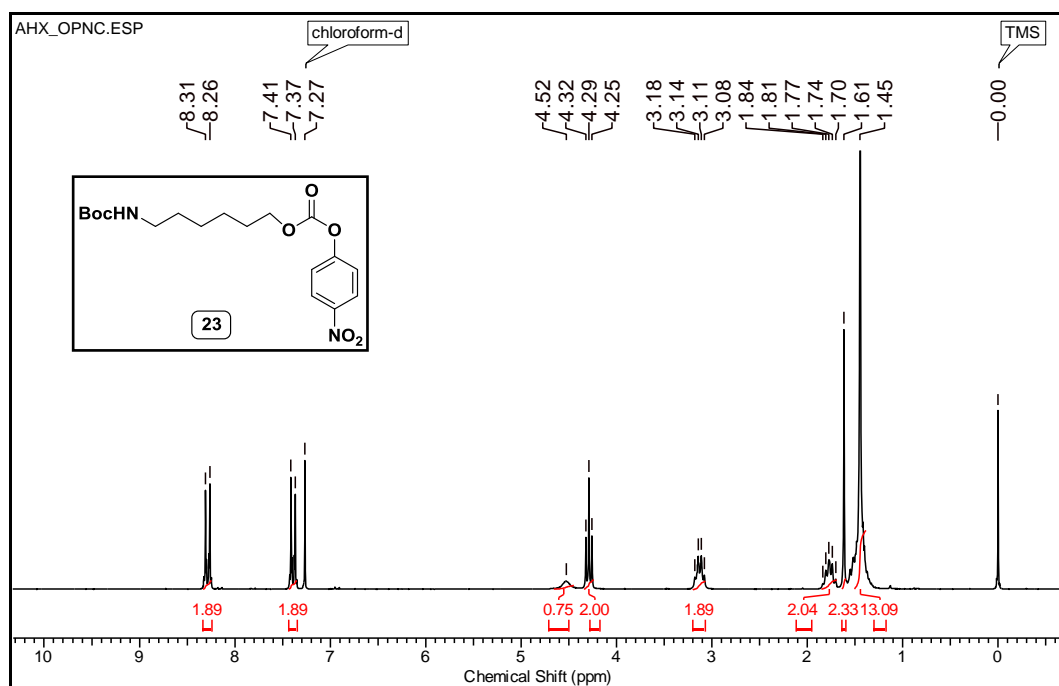
^{13}C NMR (50 MHz; CDCl$_3$) spectrum of compound **23**:
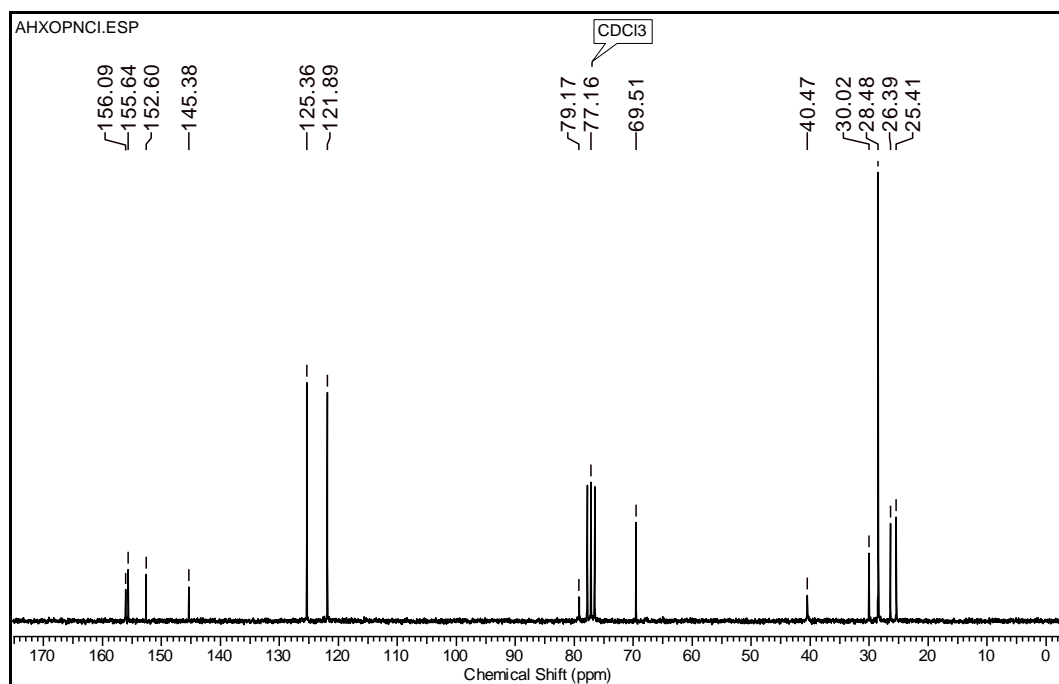
^{13}C DEPT (50 MHz; CDCl$_3$) spectrum of compound **23**:
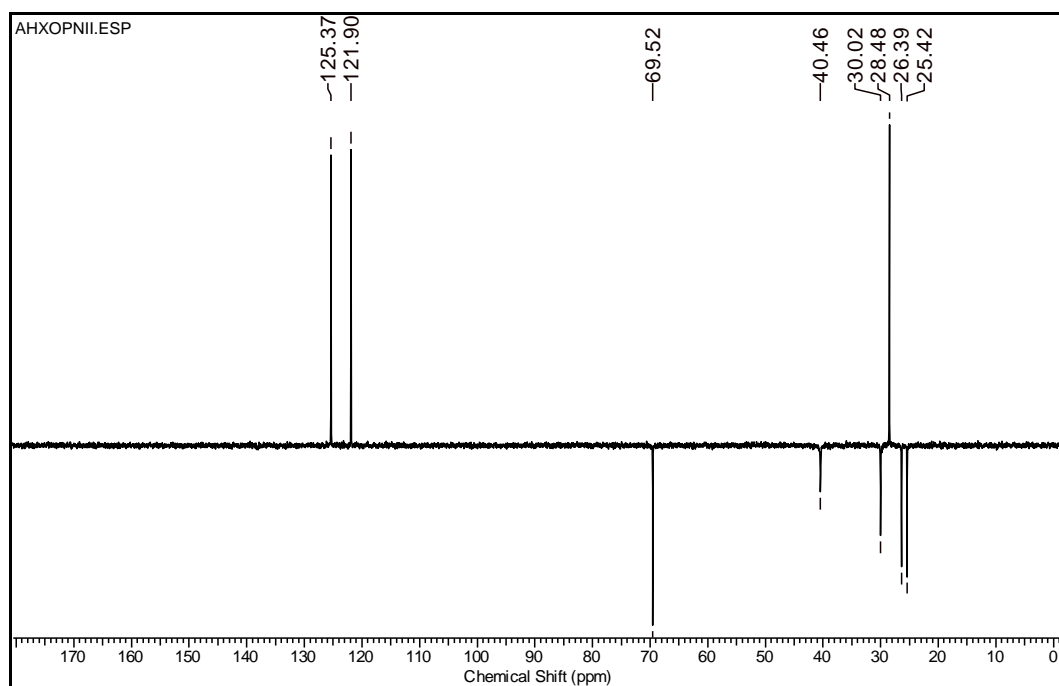
MALDI HDMS spectrum of compound **23**:
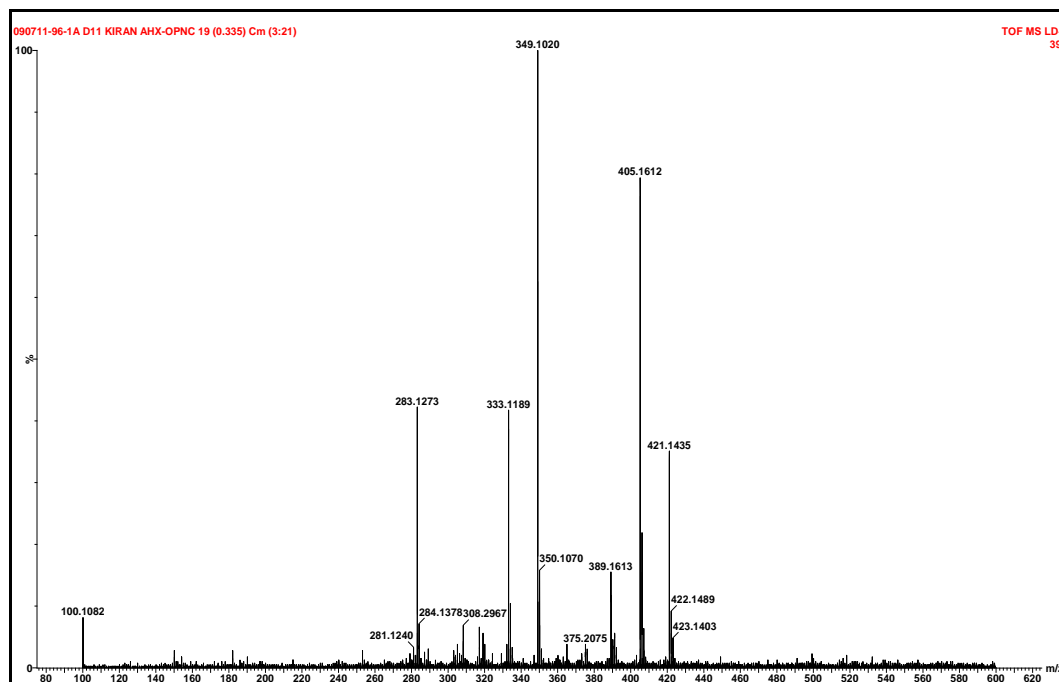
^{1}H NMR (200 MHz; CDCl$_3$) spectrum of compound **25**:
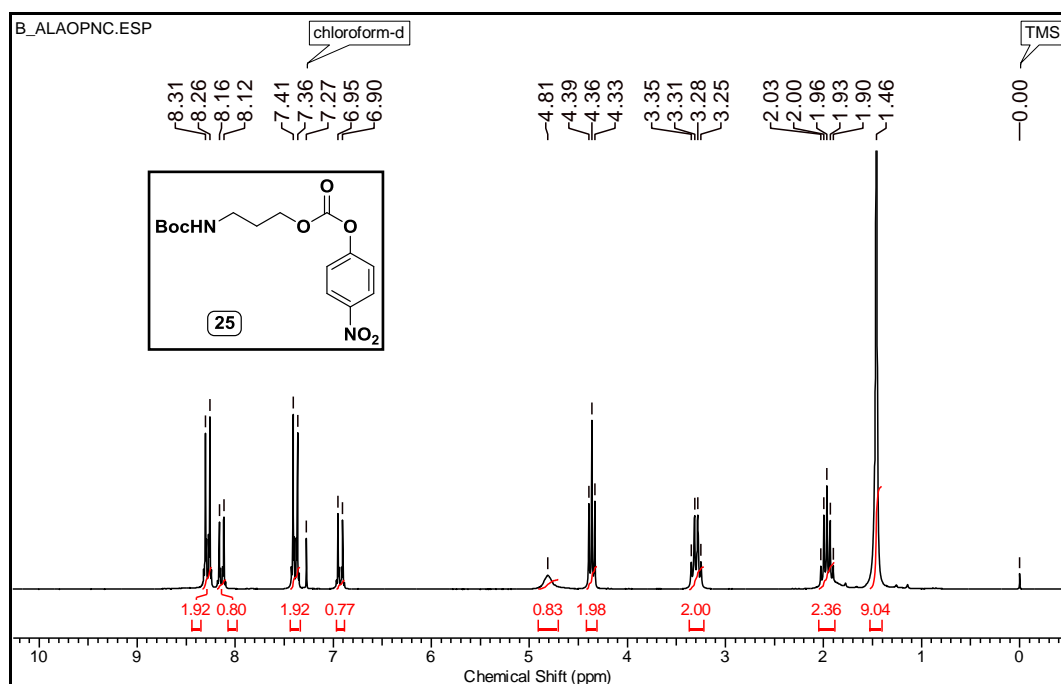
^{13}C NMR (50 MHz; CDCl$_3$) spectrum of compound **25**:
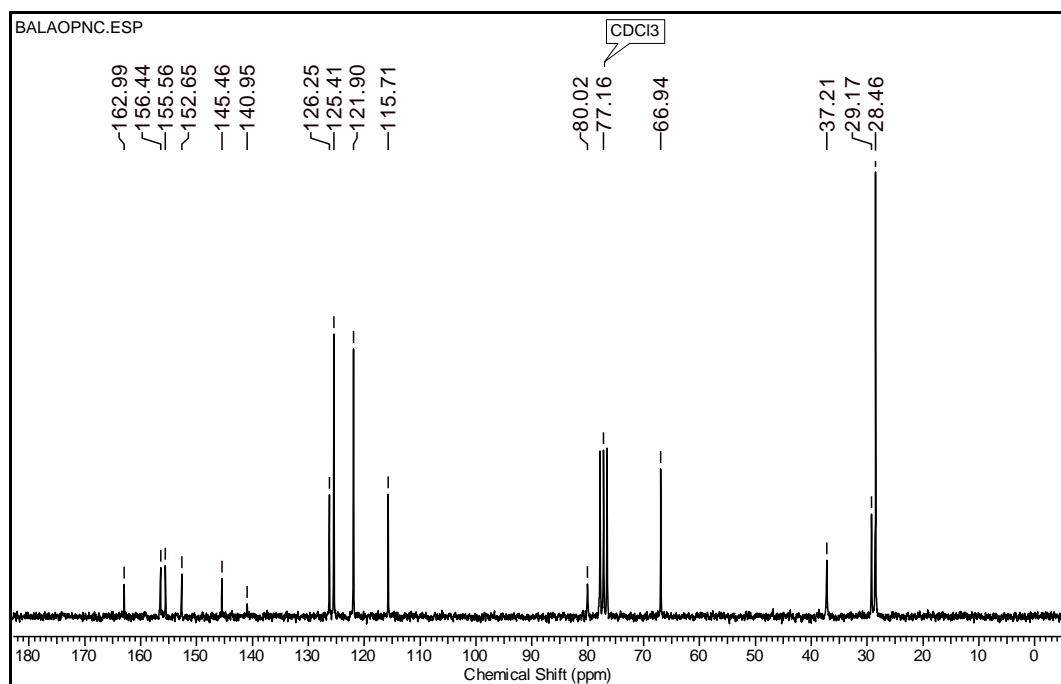
^{13}C DEPT (50 MHz; CDCl$_3$) spectrum of compound **25**:
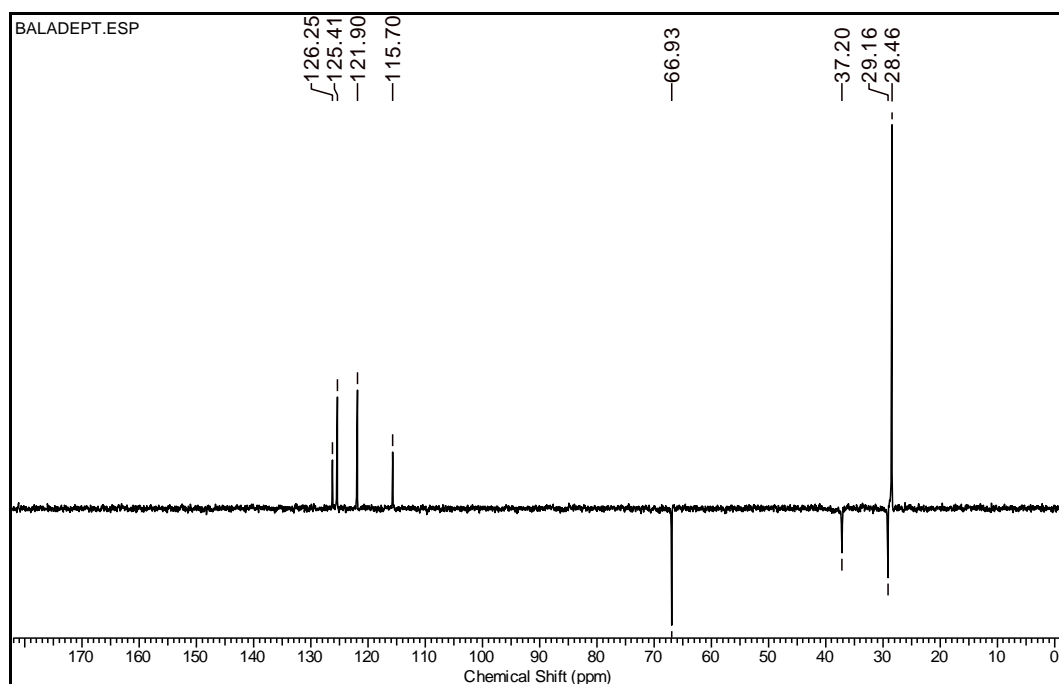
MALDI HDMS spectrum of compound **25**:
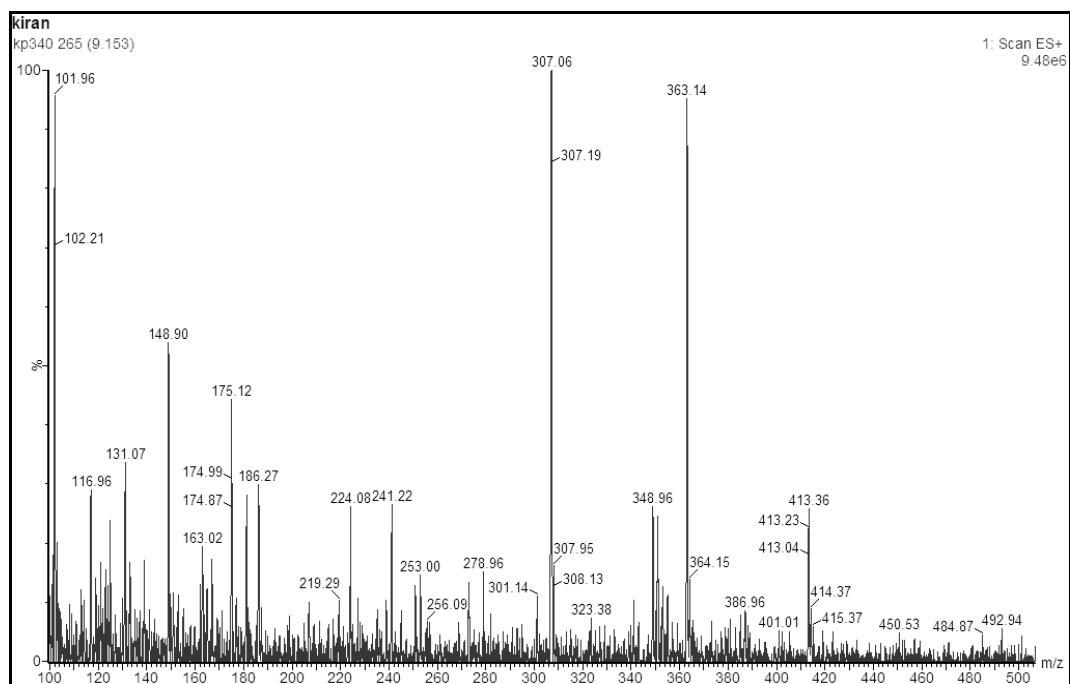
MALDI-TOF spectrum of *cf*-(R-Ahx-R)$_4$ -NH$_2$ (*^{cf}*P15):

cf-(R-Ahx-R)$_4$ -NH$_2$ (*^{cf}*P15)
Cal. Mass: 2076.21
Obs. Mass: 2077.35

MALDI-TOF spectrum of *cf*-(r-ahx-r)$_4$-NH$_2$ (*^{cf}*C1):
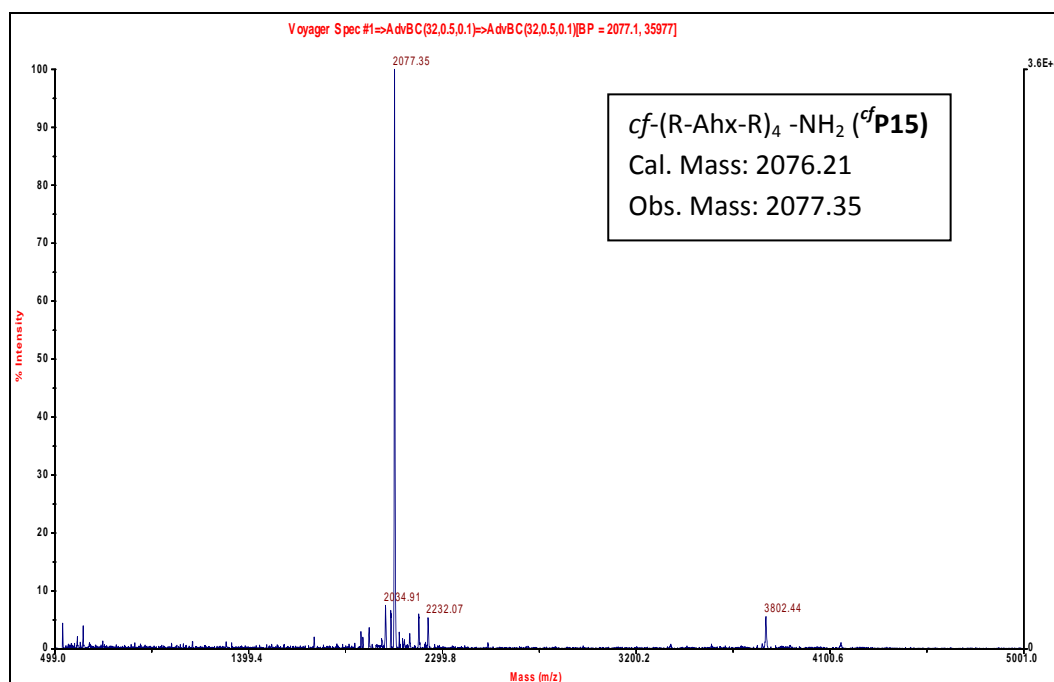
cf-(r-ahx-r)$_4$-NH$_2$ (*^{cf}*C1)
Cal. Mass: 2406.33
Obs. Mass: 2408.40

MALDI-TOF spectrum of *cf*-(r-ahx-r-r-apr-r)$_2$ -NH$_2$ (*cf*C2):
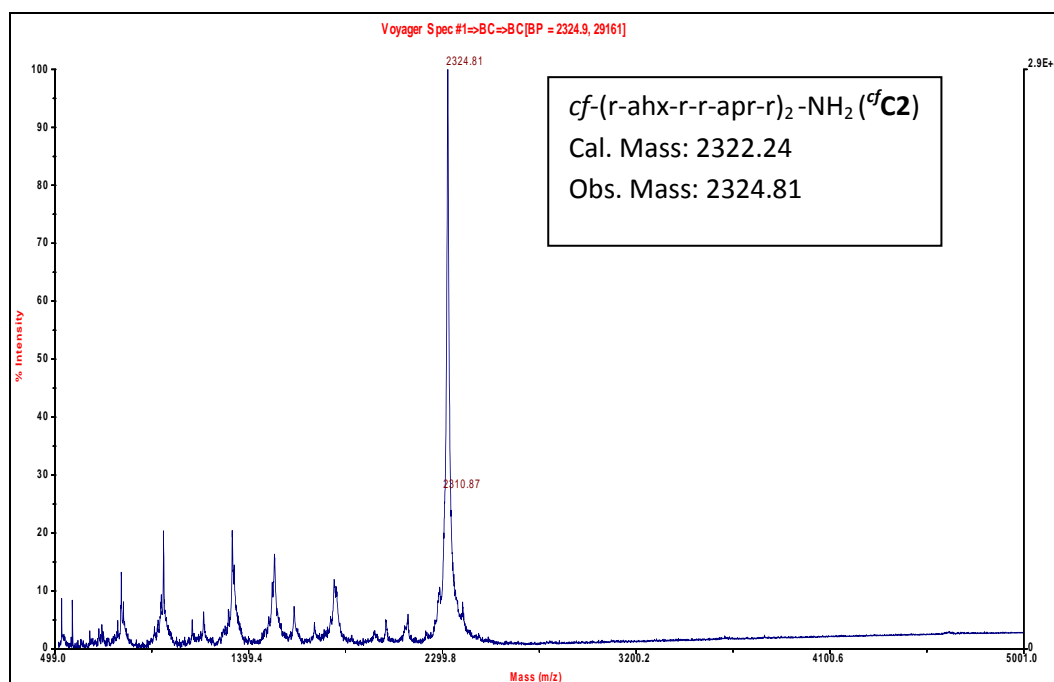
MALDI-TOF spectrum of *cf*-(r)$_8$ –NH$_2$ control (*cf*C3):
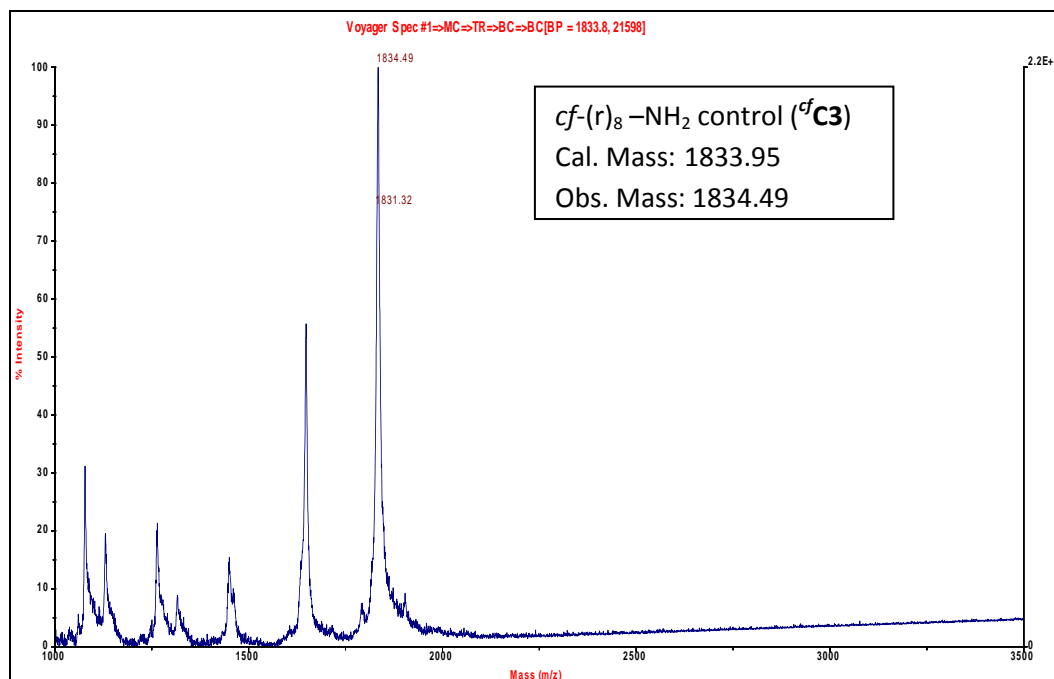
MALDI-TOF spectrum of *Ac*-Phe-(r-ahx-r)$_4$ -NH$_2$(^{Ac}**C1**):
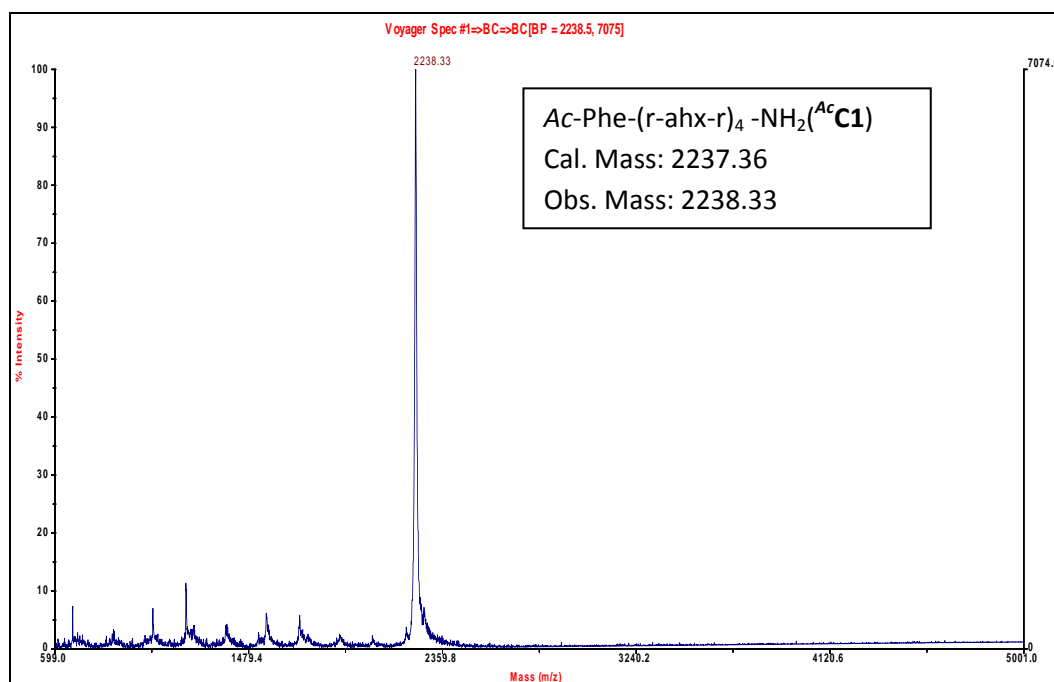
MALDI-TOF spectrum of *Ac*-Phe-(R-Ahx-R)$_4$ -NH$_2$ control (^{Ac}**P15**):
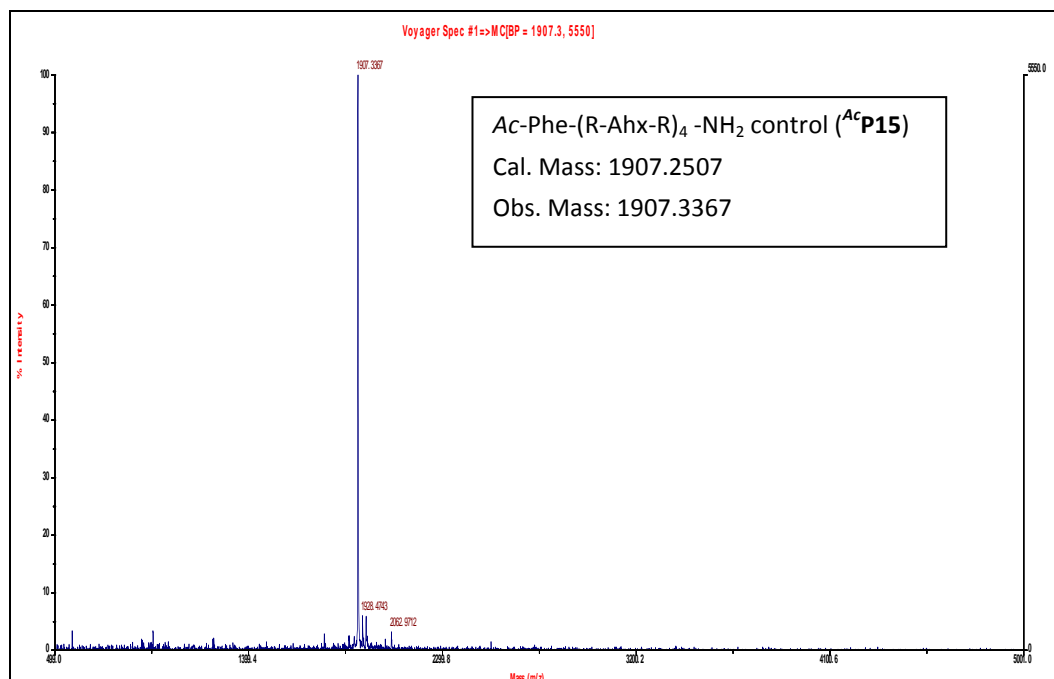
MALDI-TOF spectrum of *Ac*-Phe-(r)$_8$-NH$_2$ control (^{Ac}**C3**):
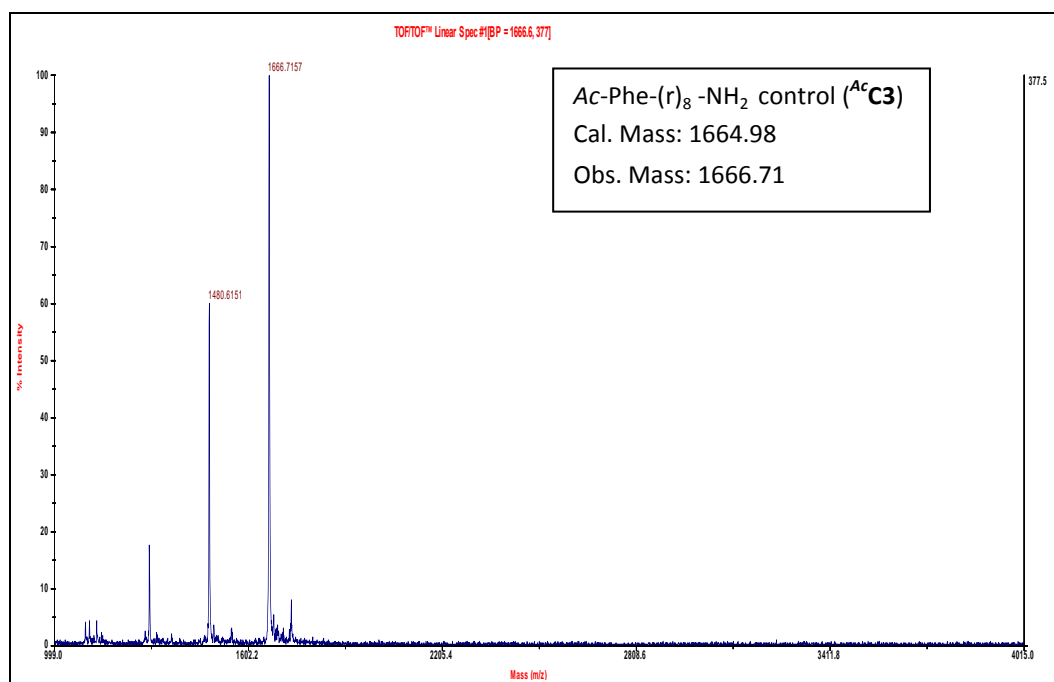
Ac-Phe-(r)$_8$-NH$_2$ control (^{Ac}**C3**)
Cal. Mass: 1664.98
Obs. Mass: 1666.71

MALDI-TOF spectrum of *cf*-Tyroserleutide-NH$_2$ (^{cf}**P16**):

cf-Tyroserleutide-NH$_2$ (^{cf}**P16**)
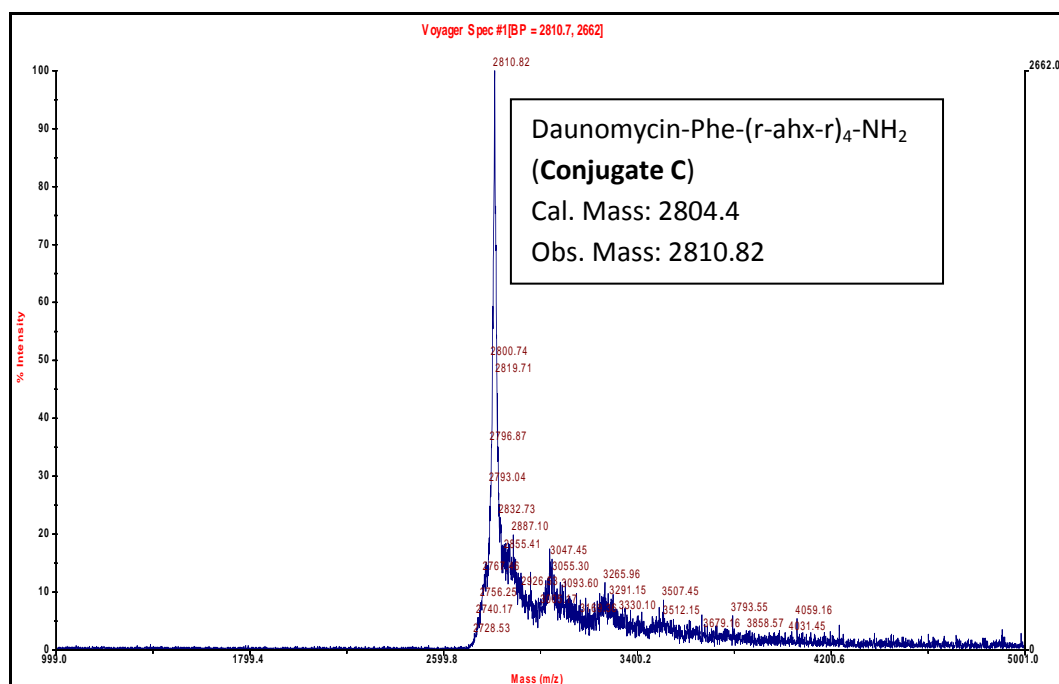Cal. Mass: 738.25
Obs. Mass: 738.45
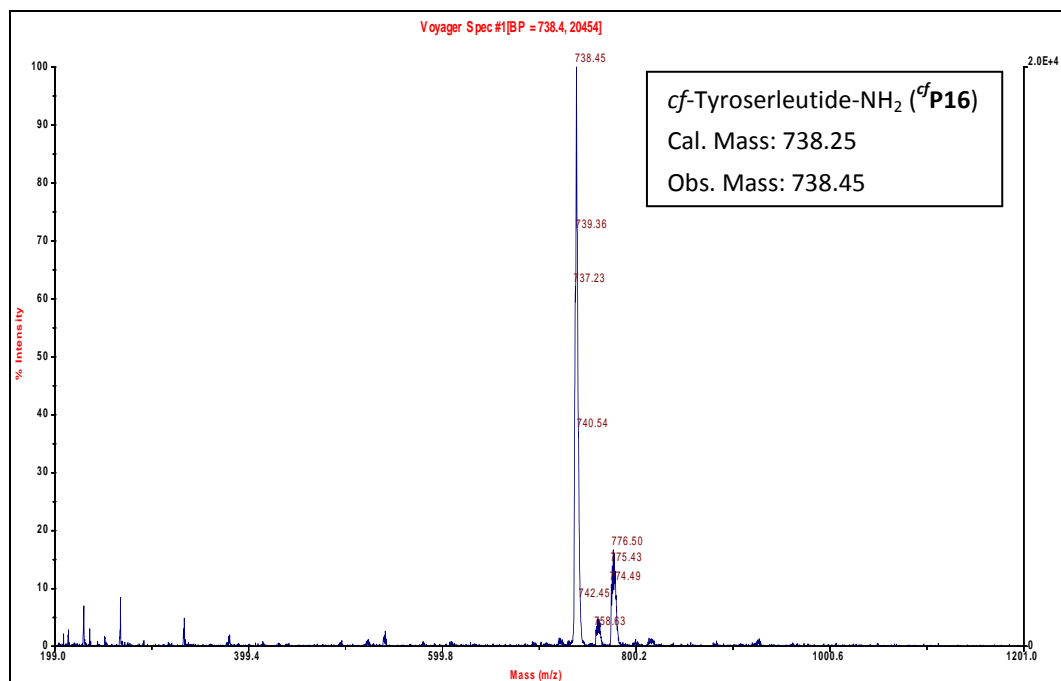
MALDI-TOF spectrum of *cf*-(R-Ahx-R)$_4$-Tyroserleutide-NH$_2$ (**Conjugate A**):
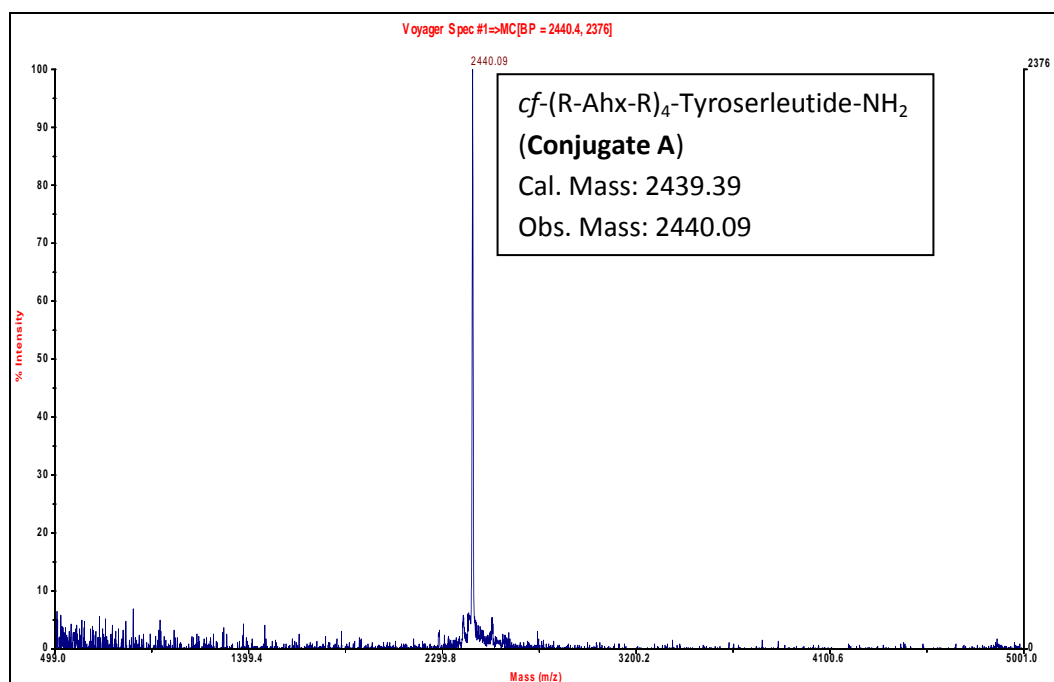
MALDI-TOF spectrum of *cf*-(r-ahx-r)$_4$-Tyroserleutide-NH$_2$ (**Conjugate B**):
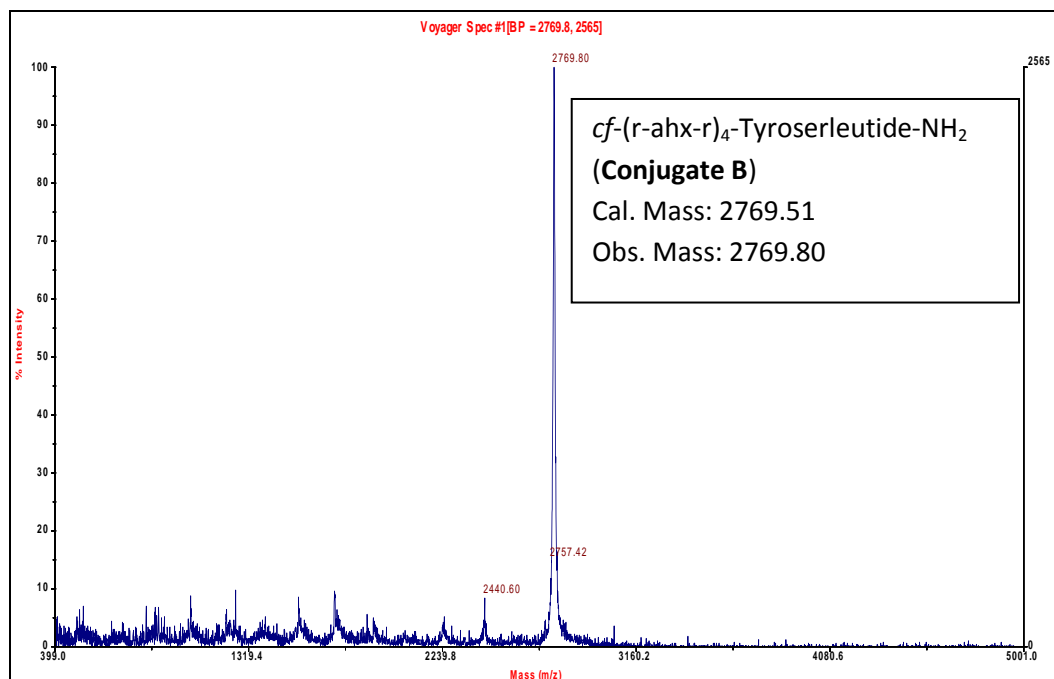
MALDI-TOF spectrum of Daunomycin-Phe-(r-ahx-r)$_4$-NH$_2$ (**Conjugate C**):

3.3.9 References

1. (a) Jin, E.; Zhang, B.; Sun, X.; Zhou, Z.; Ma, X.; Sun, Q.; Tang, J.; Shen, Y.; Van Kirk, E.; Murdoch, W.; Radosz, M. Acid-active cell-penetrating peptides for in vivo tumor-targeted drug delivery. *Journal of the American Chemical Society* **2013,** *135*, 933-940. (b) Madani, F.; Lindberg, S.; Langel, U.; Futaki, S.; Gräslund, A. Mechanisms of cellular uptake of cell-penetrating peptides. *Journal of Biophysics* **2011,** *2011*, 414729. (c) Shiraishi, T.; Nielsen, P. Improved cellular uptake of antisense peptide nucleic acids by conjugation to a cell-penetrating peptide and a lipid domain. *Methods in Molecular Biology (Clifton, N.J.)* **2011,** *751*, 209-221. (d) Schmidt, N.; Mishra, A.; Lai, G.; Wong, G. Arginine-rich cell-penetrating peptides. *FEBS Letters* **2010,** *584*, 1806-1813. (e) Turner, J.; Arzumanov, A.; Gait, M. Synthesis, cellular uptake and HIV-1 Tat-dependent trans-activation inhibition activity of oligonucleotide analogues disulphide-conjugated to cell-penetrating peptides. *Nucleic Acids Research* **2005,** *33*, 27-42. (f) Johnson, R.; Harrison, S.; Maclean, D. Therapeutic applications of cell-penetrating peptides. *Methods in Molecular Biology (Clifton, N.J.)* **2011,** *683*, 535-551.

2. Abes, S.; Moulton, H.; Clair, P.; Prevot, P.; Youngblood, D.; Wu, R.; Iversen, P.; Lebleu, B. Vectorization of morpholino oligomers by the (R-Ahx-R)4 peptide allows efficient splicing correction in the absence of endosomolytic agents. *Journal of Controlled Release* **2006,** *116*, 304-313.

3. (a) Abes, R.; Moulton, H.; Clair, P.; Yang, S.-T.; Abes, S.; Melikov, K.; Prevot, P.; Youngblood, D.; Iversen, P.; Chernomordik, L.; Lebleu, B. Delivery of steric block morpholino oligomers by (R-X-R)4 peptides: structure-activity studies. *Nucleic Acids Research* **2008,** *36*, 6343-6354. (b) Said Hassane, F.; Saleh, A.; Abes, R.; Gait, M.; Lebleu, B. Cell penetrating peptides: overview and applications to the delivery of oligonucleotides. *Cellular and Molecular Life Sciences : CMLS* **2010,** *67*, 715-726.

4. Sebbage, V. Cell-penetrating peptides and their therapeutic applications. *Bioscience Horizons* **2009,** *2*.

5. (a) Wender, P.; Mitchell, D.; Pattabiraman, K.; Pelkey, E.; Steinman, L.; Rothbard, J. The design, synthesis, and evaluation of molecules that enable or enhance
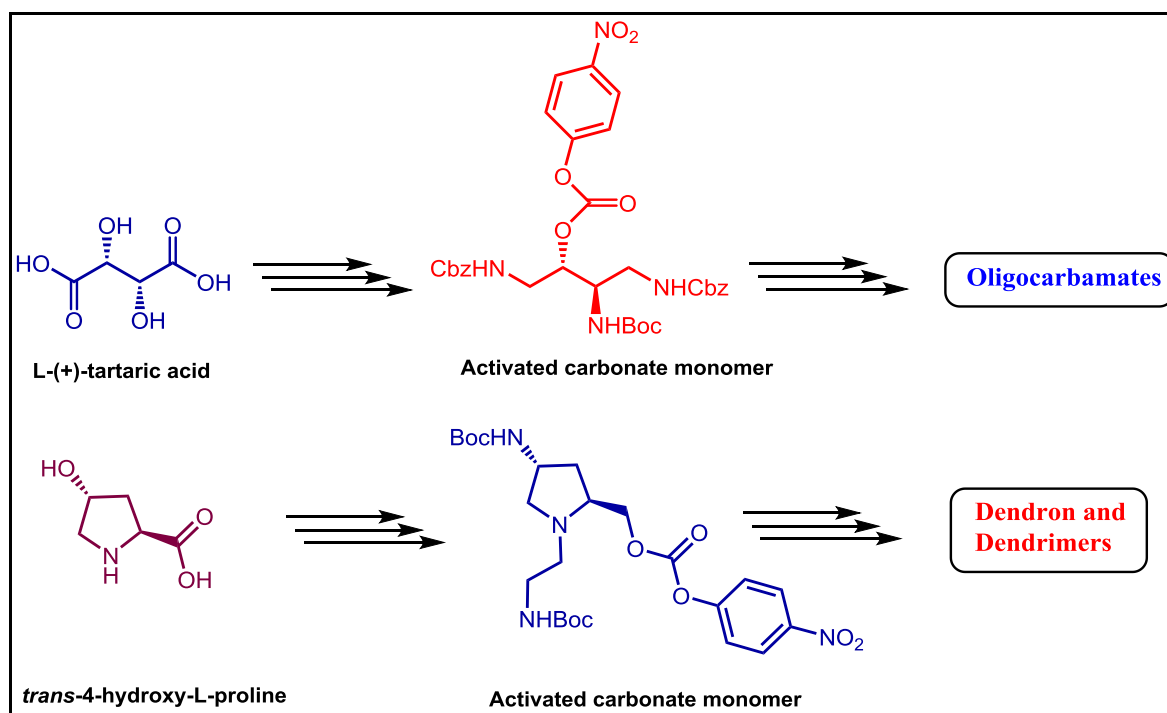
cellular uptake: peptoid molecular transporters. *Proceedings of the National Academy of Sciences of the United States of America* **2000,** *97*, 13003-13008. (b) Huang, W.; Seo, J.; Lin, J.; Barron, A. Peptoid transporters: effects of cationic, amphipathic structure on their cellular uptake. *Molecular BioSystems* **2012,** *8*, 2626-2628. (c)Schröder, T.; Schmitz, K.; Niemeier, N.; Balaban, T.; Krug, H.; Schepers, U.; Bräse, S. Solid-phase synthesis, bioconjugation, and toxicology of novel cationic oligopeptoids for cellular drug delivery. *Bioconjugate Chemistry* **2007,** *18*, 342-354.

6. Tamilarasu, N.; Ikramul, H.; Tariq, M. R. High Affinity and Specific Binding of HIV-1 TAR RNA by a Tat-Derived Oligourea. *Journal of the American Chemical Society* **1999,** *121*.

7. Cooley, C.; Trantow, B.; Nederberg, F.; Kiesewetter, M.; Hedrick, J.; Waymouth, R.; Wender, P. Oligocarbonate molecular transporters: oligomerization-based syntheses and cell-penetrating studies. *Journal of the American Chemical Society* **2009,** *131*, 16401-16403.

8. Wender, P.; Rothbard, J.; Jessop, T.; Kreider, E.; Wylie, B. Oligocarbamate molecular transporters: design, synthesis, and biological evaluation of a new class of transporters for drug delivery. *Journal of the American Chemical Society* **2002,** *124*, 13382-13383.

9. Lee, K.-H.; Oh, J.-E. Design and synthesis of novel antimicrobial pseudopeptides with selective membrane-perturbation activity. *Bioorganic & Medicinal Chemistry* **2000,** *8*, 833-839.

10. Cho, C.; Moran, E.; Cherry, S.; Stephans, J.; Fodor, S.; Adams, C.; Sundaram, A.; Jacobs, J.; Schultz, P. An unnatural biopolymer. *Science (New York, N.Y.)* **1993,** *261*, 1303-1305.

11. Warrass, R.; Wiesmüller, K.; Jung, G. Cyclic oligocarbamates. *Tetrahedron letters* **1998,** *39*, 2715-2716.

12. Gait, M. J.; Jones, A. S.; Walker, R. T. Synthetic analogues of polynucleotides. Part XII. Synthesis of thymidine derivatives containing an oxyacetamido- or an oxyformamido-linkage instead of a phosphodiester group. *Journal of the Chemical Society, Perkin Transactions 1* **1974**, 1684-1686.

13. Coull, J. M.; Carlson, D. V.; Weith, H. L. Synthesis and characterization of a carbamate-linked oligonucleoside. *Tetrahedron Letters* **1987,** *28*, 745-748.

14. Mungall, W.; Kaiser, J. Carbamate analogues of oligonucleotides. *The Journal of Organic Chemistry* **1977,** *42*, 703-706.

15. Ralf, W.; Peter, W.; Karl-Heinz, W.; Günther, J. Oligocarbamates as MHC class I ligands. *Letters in Peptide Science* **1998,** *5*.

16. (a) Madhuri, V.; Kumar, V. A. Design, synthesis and DNA/RNA binding studies of nucleic acids comprising stereoregular and acyclic polycarbamate backbone: polycarbamate nucleic acids (PCNA). *Organic & Biomolecular Chemistry* **2010,** *8*, 3734-3741. (b) Kotikam, V.; Fernandes, M.; Kumar, V. A. Comparing the interactions of DNA, polyamide (PNA) and polycarbamate nucleic acid (PCNA) oligomers with graphene oxide (GO). *Physical Chemistry Chemical Physics* **2012,** *14*, 15003-15006.

17. Darryl, W. H.; Des, W. C. A simple water/octanol partition system for bioconcentration investigations. *Environmental Science & Technology* **1989,** *23*.

18. Chambers, J.; Simon, S.; Berger, E.; Sklar, L.; Arfors, K. Endocytosis of beta 2 integrins by stimulated human neutrophils analyzed by flow cytometry. *Journal of Leukocyte Bbiology* **1993,** *53*, 462-469.

19. Richard, J.; Melikov, K.; Vives, E.; Ramos, C.; Verbeure, B.; Gait, M.; Chernomordik, L.; Lebleu, B. Cell-penetrating peptides. A reevaluation of the mechanism of cellular uptake. *The Journal of Biological Chemistry* **2003,** *278*, 585-590.

20. (a) Tönges, L.; Lingor, P.; Egle, R.; Dietz, G.; Fahr, A.; Bähr, M. Stearylated octaarginine and artificial virus-like particles for transfection of siRNA into primary rat neurons. *RNA (New York, N.Y.)* **2006,** *12*, 1431-1438. (b) Breunig, M.; Lungwitz, U.; Liebl, R.; Goepferich, A. Breaking up the correlation between efficacy and toxicity for nonviral gene delivery. *Proceedings of the National Academy of Sciences of the United States of America* **2007,** *104*, 14454-14459.

21. Bidwell, G.; Fokt, I.; Priebe, W.; Raucher, D. Development of elastin-like polypeptide for thermally targeted delivery of doxorubicin. *Biochemical Pharmacology* **2007,** *73*, 620-631.

22. MacKay, J.; Chen, M.; McDaniel, J.; Liu, W.; Simnick, A.; Chilkoti, A. Self-assembling chimeric polypeptide-doxorubicin conjugate nanoparticles that abolish tumours after a single injection. *Nature Materials* **2009,** *8*, 993-999.

23. Ai, S.; Duan, J.; Liu, X.; Bock, S.; Tian, Y.; Huang, Z. Biological evaluation of a novel doxorubicin-peptide conjugate for targeted delivery to EGF receptor-overexpressing tumor cells. *Molecular Pharmaceutics* **2011,** *8*, 375-386.

CHAPTER 4

Design and synthesis of novel oligocarbamates and monomer synthesis for dendron and dendrimers

L-(+)-tartaric acid   Activated carbonate monomer   Oligocarbamates

trans-4-hydroxy-L-proline   Activated carbonate monomer   Dendron and Dendrimers

In Section A, we describe the synthesis of a novel carbonate monomer containing two amino groups which could further converted to guanidine functionality in solution phase and substitute to on solid phase oligocarbamate synthesis and synthesized consecutive (r-x-r)$_n$-type oligocarbamates where consecutive ' r-r' groups was replaced by synthesized monomer.

In Section B, we have designed and synthesized para-nitrophenyl activated monomer which will be suitable to synthesise variety of dendrons, dendrimers, (r-x-r)-type dendrimers, etc. by solid phase synthesis containing polycarbamate linkages. Our strategy for synthesis of p-nitrophenyl activated monomer was shown in this section.

Section A: Synthesis of tartaric acid-derived novel di-guanidine carbonate monomer and its incorporation in oligocarbamate

4A.1 Introduction

Many cell-penetrating peptides derived from natural sources e.g. tat,[1] pAntp,[2] etc. or synthetic peptides made up of only natural amino acids e.g. polyarginines,[3] polylysines,[4] chimaric peptides,[5] etc. are found efficient to deliver cargo *in vitro*. However, these classes of peptides have limitations for *in vivo* applications due their rapid metabolic degradation, low membrane permeability, and toxicity.[6] Therefore there is always a need of efficient, non-toxic drug delivering candidates, which are stable towards enzymatic cleavage.

Table 4.1 Representative examples of arginine rich oligomers reported in literature.

Name	Sequence*	number of X
Oligoarginine		
R_8	RRRRRRRXB	1
r_8	rrrrrrrrXB	1
R_9	RRRRRRRRRXB	1
RX, RXR and RB Panel		
$(RX)_8$	RX RX RX RX RX RX RX RX B	8
$(rX)_8$	rX rX rX rX rX rX rX rX B	8
$(RXR)_4$	RXR RXR RXR B	5
$(rXR)_4$	rXR rXR rXR rXR B	5
$(rXr)_4$	rXr rXr rXr rXr	5
$(RB)_8$	RB RB RB RB RB RB RB RB B	0
$(rB)_8$	rB rB rB rB rB rB rB rB B	0

*The peptide sequences are written from *N*- to *C*-terminus; R= L-arginine; r = D-arginine; X = 6-aminohexanoic acid; B = β-alanine

As discussed in the earlier chapter, there were significant efforts done in the literature to synthesize different enzymatically stable cell-penetrating oligomers. These strategies included the replacement of L-amino acids in natural peptides by D-amino

acids, incorporation of un-natural or modified amino acids in peptide sequences, replacement of peptide linkages by carbamate,[7] carbonate[8] or urea,[9] etc. Arginine rich peptides such as (RXR)$_n$-type, in which two arginines (RR) are at consecutive positions and are separated by an unnatural amino acid containing hydrocarbon chain, showed most effective cell penetration properties. Some important arginine rich peptides, reported in literature, are shown in Table 4.1. In chapter 3 we discussed the rxr-type of oligocarbamate analogues that were superior in cell penetration and cargo delivery properties over their peptide counterparts.

4A.2 Rationale, design and objectives of the present work

In this section we describe the synthesis of a novel carbonate monomer containing two amino groups which can further be converted to guanidine functionalities and can substitute consecutive 'r-r' groups in (r-x-r)$_n$-type oligocarbamates. Using the synthetic monomer, the guanidine-oligocarbamates could be synthesized using solid phase synthesis methodology. The two amino or guanidino functionalities in the designed monomer were envisioned to be fetched from the carboxylate functionalities present in the inexpensive starting material, L (+) tartaric acid. After appropriate functional group transformations, we synthesized a monomeric unit (Scheme 4.1) which is suitable for oligocarbamate synthesis *via* Boc-chemistry protocol on solid support; our synthetic strategy is depicted in Scheme 4.2. This is a completely new strategy to bring two consecutive guanidines in the same unit in a stereodefined fashion where the oligocarbamate with desired number of guanidines could be synthesized in less number of repetitive cycles.

4A.3 Synthesis, results and discussion

4A.3a Synthesis of monomer

The synthesis of the monomer unit was accomplished starting from naturally occurring L-tartaric acid. According to a reported procedure, the acetonide protection of diol and esterification of the two carboxylic groups in **26** was carried out in a single step to get compound **27** by using 2, 2-dimethoxyproponane, MeOH and catalytic amount of *p*-toluenesulphonic acid. The diester was reduced to corresponding diol compound **28** by

using in situ generated LiBH$_4$. The primary hydroxyl groups in compound **28** were converted to their mesyl derivatives to give dimesylate compound **29**, which were further converted to diazido derivative **30** by treatment with sodium azide. Reduction of azide groups in compound **30** was carried out by hydrogenation using Pd/C in methanol to get compound **31**. The free amines were protected by Cbz-groups by using Cbz-Cl, sodium bicarbonate in water-dioxane to get di-cbz-acetonide compound **32**. Later, acetonide group was deprotected by refluxing compound **32** in MeOH in the presence of catalytic amount of *p*-toluenesulphonic acid to get free secondary diol compound **33**.
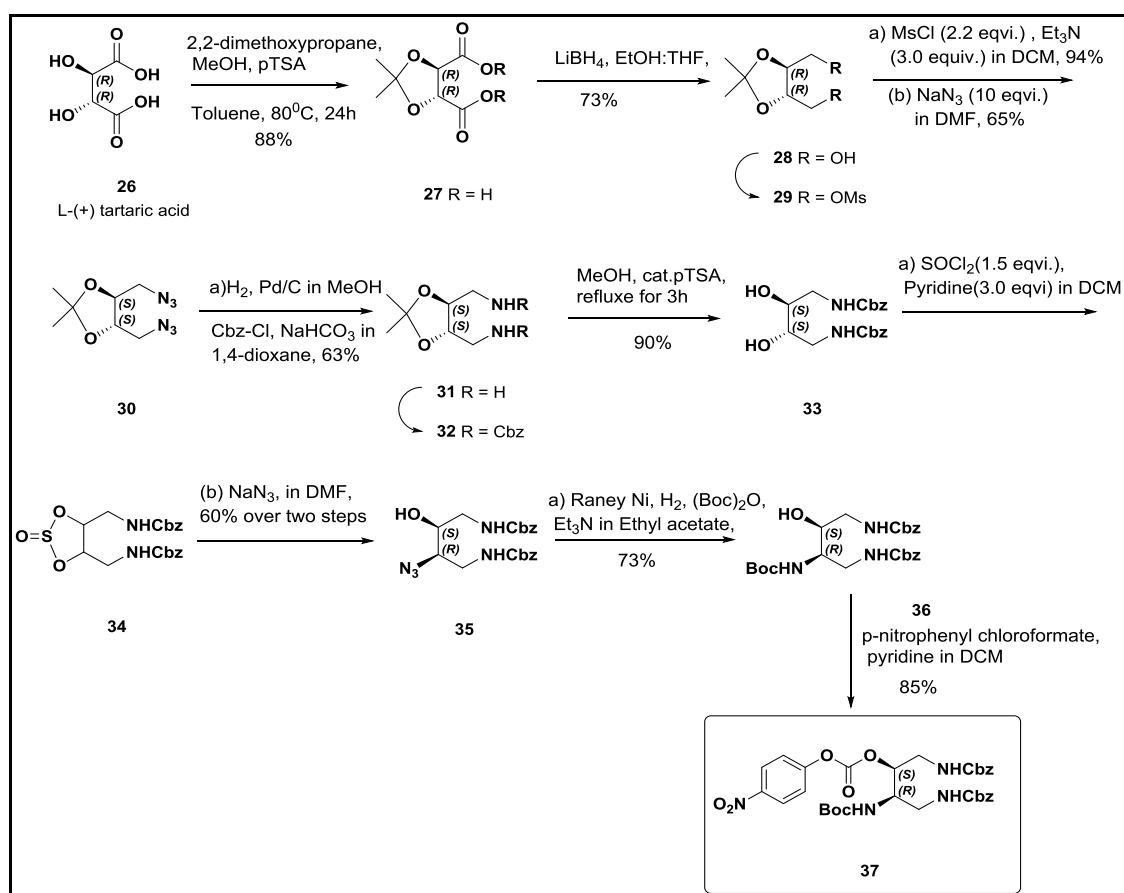
Scheme 4.1 Synthesis of diguanidino-precursor monomer for oligocarbamate.

Further the diol compound **33** was treated with thionyl chloride in the presence of pyridine in CH$_2$Cl$_2$ to get cyclic sulphate compound **34**, which was further treated with sodium azide in DMF to get azido alocohol compound **35**. The azide group in the compound **35** was further reduced to amine by Raney Nickel and the formed amine was protected by Boc using Boc-anhydride in ethyl acetate containing Et$_3$N to get compound

36. Later, free hydroxyl group was converted to its activated carbonate **37** by using *p*-nitrophenyl chloroformate in CH_2Cl_2 and pyridine.

4A.3b Solid phase oligocarbamate synthesis

Synthesized monomer **37** was further incorporated in oligocarbamate sequence at appropriate positions in conjunction with *p*-nitrophenyl activated Boc-aminopropanol (motif of β-alanine; Compound **25**, Chapter 3) and desired oligocarbamate was synthesized *via* solid phase oligocarbamate synthesis protocol (Scheme 3.2, Chapter 3). To facilitate the concentration determination of oligomer by UV measurement we attached phenylalanine at the *N*-terminal of oligocarbamate. The *N*-terminal was acetylated using acetic anhydride in presence of DIPEA. Further, the oligocarbamate ^{Ac}**C4**$_{NH_2}$ was cleaved from solid support to get oligocarbamate in solution containing eight free amino groups. This oligocarbamate was further purified by HPLC and subsequently conversion of free amines to guanidines was accomplished in solution phase by using 1-*H*-pyrazole-1-carboxamidine hydrochloride reagent. Further HPLC purification of crude reaction mixture was performed to get oligocarbamate ^{Ac}**C4**$_{gua}$ having required eight guanidino functionalities. The synthetic scheme is depicted in Scheme 4.2, the HPLC profile of oligocarbamates is shown in Figure 4.1 and MALDI-TOF mass characterization values are tabulated in Table 4.2.
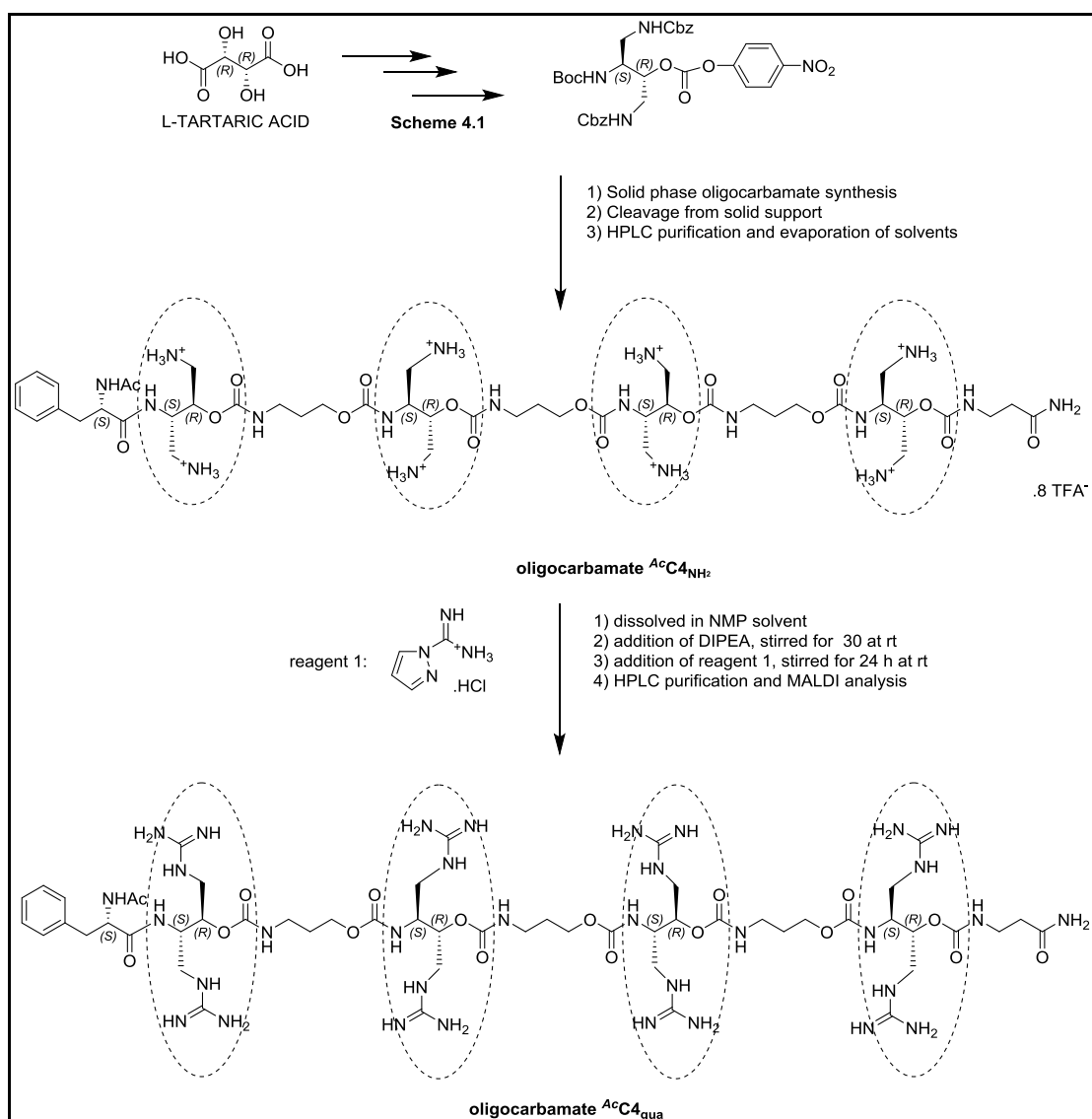
Scheme 4.2 Schematic presentation for synthesis of oligocarbamates ^{Ac}C4$_{NH2}$ and ^{Ac}C4$_{gua.}$
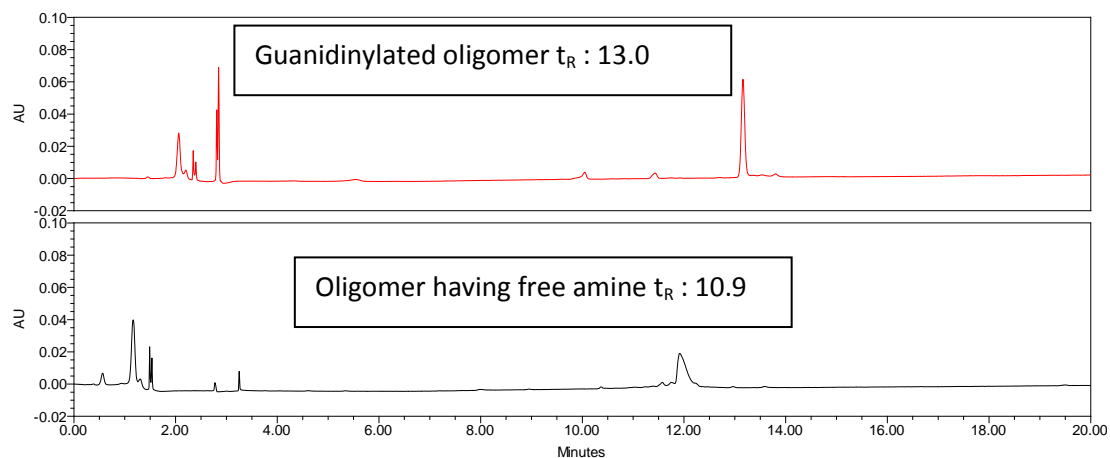
Figure 4.1 comparative HPLC chromatograms of free amines and guanidinylated oligocarbamates.

Table 4.2 MALDI-TOF characterization of synthesized oligocarbamates

Oligomer	MALDI-TOF	
	Calcd.	Obsd.
Oligocarbamate $^{Ac}C4_{NH_2}$	1160.63	1163.79
Oligocarbamate $^{Ac}C4_{gua}$	1496.80	1501.4

Further biological applications to deliver negatively charged cargoes such as siRNA, pDNA to cells *via* non-covalent conjugation strategy using synthesized oligocarbamates are underway.

4A.4 Summary and conclusion

- Design and synthesis of novel *p*-nitrophenyl activated carbonate monomer was accomplished by appropriate functional group transformation, starting from inexpensively available L (+) tartaric acid.
- Synthesized monomeric unit was incorporated on solid support and desired oligocarbamate was synthesized using Boc-chemistry protocol.
- Eight free amines in synthesized oligocarbamate were successfully guanidinylated in solution phase.
- Synthesized oligocarbamates were purified by HPLC and characterized by MALDI-TOF mass analysis and their biological evaluation for cargo delivery applications are in progress.

Section B: Synthesis of 4-hydroxyproline-derived monomer for incorporation in carbamate linked dendron and dendrimer

4B.1 Introduction

In addition to structural diversity of cell-penetrating peptides, cell-penetrating dendrimers are one of the important cell delivery vectors that have been studied in the literature.[10] Dendrimers are a family of nano-sized, three-dimensional polymers characterized by a unique tree-like branching architecture and compact spherical geometry in solution.
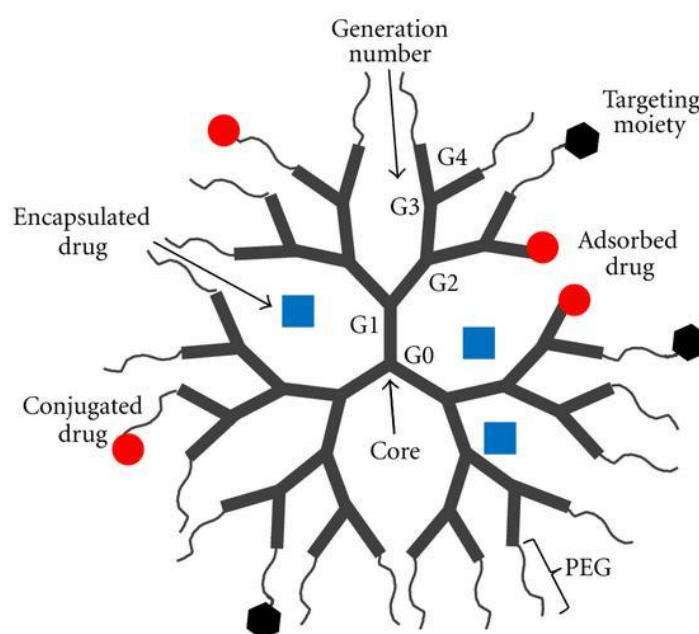
Figure 4.2 Combination drug delivery systems based on dendrimers: concurrent delivery of water-soluble and -insoluble drugs by adsorption to the surface (ionic interaction), encapsulation within hydrophobic microcavities inside branching clefts or direct covalent conjugation to the surface functional groups.[11]

Over the past three decades, several synthetic strategies were developed to generate multiple dendrimer families with versatile chemical compositions, which are sought for a variety of applications in chemistry, biology, and medicine.[12] One of the advantages of this type of cell delivery vector is that large numbers of functional groups can be projected in 3-D space which could be important factor for cell-penetration and drug delivery applications.

4B.1.1 Dendrimer families

According to structure, design and applications, dendrimers can be divided in different families of which some of them are discussed herein.

4B.1.1a PAMAM dendrimer

Poly(amidoamine) (PAMAM) dendrimers were the first synthesized and commercialized dendrimer family.[13] Duncan and co-workers reported that G1-G4 of PAMAM-NH$_2$ dendrimers are cytotoxic upon incubation for 72 h with three different cancer cell lines resulting in IC$_{50}$ values ranging from 50-300 μg/mL.[14]

4B.1.1b Amino acid based dendrimers

Amino acid based dendrimers are developed by using the properties of chirality, hydrophobicity and hydrophilicity present in amino acids. Additionally, variety of functional groups could be decorated around the dendrimer surfaces by using different functional groups present in amino acids e.g. amines and guanidines in lysine and arginine amino acids respectively to improve the cell uptake efficiency of dendrimers.[15]

4B.1.1c Glycodendrimers

These dendrimers are basically designed and synthesized to study the multivalent ligand-receptor interactions, for recognition and targeting specific cells.[16]

4B.1.1d Hydrophobic Dendrimers

Hydrophobic dendrimers are basically designed to carry hydrophobic drug molecules to cells. These types of dendrimers are basically made up of hydrophobic interior which allows the hydrobhobic drugs to get encapsulated and hydrophilic outer surface which helps in solubilising these complexes which makes them suitable for *in vivo* administration. Newkome *et al.* used this concept and developed unimolecular micelles using dendrimers with hydrophobic interiors and a hydrophilic surface, which were used to solubilize and encapsulate hydrophobic guest molecules including lipophilic probes (e.g., diphenylhexatriene), dyes (e.g., pinacyanol chloride), and fluorescence markers (e.g., chlortetracycline).[17]

4B.1.1e Biodegradable Dendrimer

To use high molecular weight dendrimer as drug carrier, dendrimers should get excreted from the body after delivering a drug to the site of action. Therefore the biodegradable dendrimer emerged as a new tool having property of high accumulation and retention in tumor tissue and also allows fast and safe clearance of fragments of biodegraded polymers.[18] These types of dendrimers are usually composed of ester groups in polymers which can be hydrolysed and/or enzymatically cleaved by esterase enzymes at physiological pH.[19]
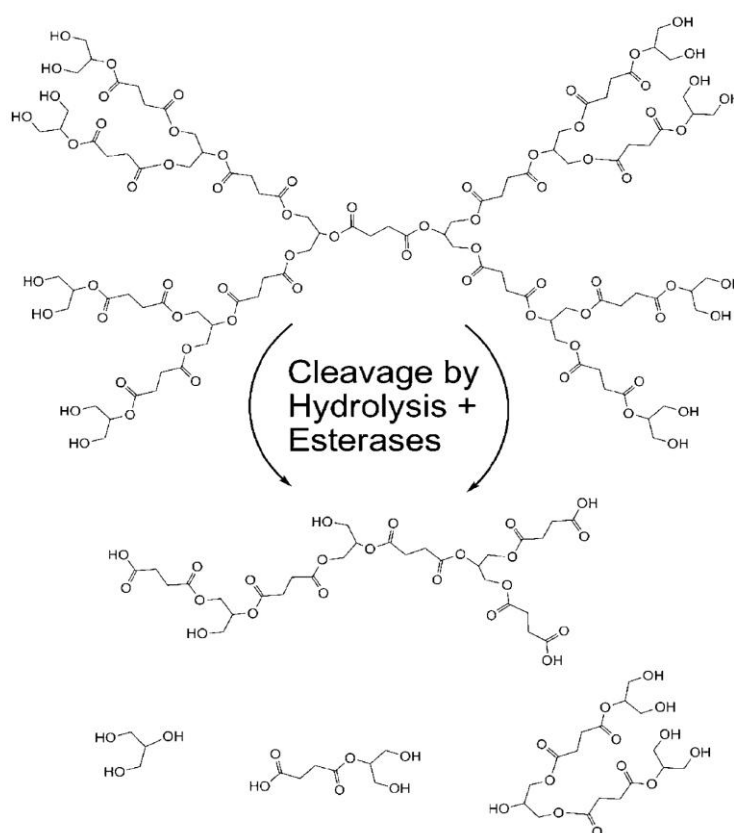
Figure 4.3 Cleavage of a polyester dendrimer by hydrolysis and tissue esterases. Degradation reduces the dendrimers to small molecular weight polymer units that are rapidly excreted with urine to minimize exposure time-dependent carrier toxicity

4B.1.1f Polycarbamate/urea-based, click chemistry inspired dendrimers

Peerlings *et al.* reported fast and efficient syntheses of polycarbamate/urea-based dendrimers by AB-CD2 strategy. The reactivity difference of the two isocyanate functionalities of the AB building block allows them to construct dendrimers without

the necessity of activation or deprotection steps.[20] Roey *et al.* reported dendrons which were built with a multi-enzymatic triggering mechanism, which initiates their biodegradation through a self-destructive chain fragmentation to release a reporter group from the focal point. The dendritic backbone was constructed from polycarbamate linkages, which are stable to hydrolysis and enhance the dendrons' solubility in water. The degradation could readily take place under physiological conditions on enzymatic triggering.[21]

Recently, Divya *et al.* reported the construction of glycoporphyrin dendrimers by the use of azide-alkyne click chemistry.[22] They synthesized porphyrin-cored glycodendrimers containing 8, 12, 16, and 24 β-D-glucopyranose units at the periphery by convergent methodology using click chemistry.

4B.2 Rationale, design and objectives of the present work

Only few examples of dendrimers containing polycarbamate linkages have been reported in literature.[20-21] However the cell uptake and cargo delivery studies for these dendrimers were not studied in details. Successful use of RXR-type dendrimers containing oligoamide bonds was studied by Saleh and co-authors,[23] who showed the applicability of these dendrimers in oligonucleotide delivery to cells. In view of successes met with RXR-type peptides and report of rxr-type oligocarbamates in the present work as good delivery vectors, synthesis of oligocarbamate based dendridic structure was thought about. Herein, we have designed and synthesized *para*-nitrophenyl activated monomer which will be suitable to synthesize a variety of dendrons, dendrimers, rxr-type dendrimers, etc. by solid phase synthesis containing polycarbamate linkages. We envisioned the synthesis of hydrophobic dendrons and dendrimers which can have hydrophobic interior core and surfaces can be decorated by variety of groups such as free amines or guanidines. Our strategy for synthesis of *p*-nitrophenyl activated monomer is depicted in Scheme 4.3.

4B.3 Synthesis, result and discussion

The synthesis of desired carbonate monomer was accomplished by *trans*-4-hydroxy-L-Proline as a starting material. The synthesis of compound **6** in Scheme 4.3 is

shown in Scheme 1.1; Chapter 1. Further the reduction of azide group in compound **6** to the free amine by using Palladium on charcoal (15% w/w) in the presence of hydrogen gas atmosphere. The subsequent Boc protection of 4-position free amine was carried out by Boc-anhydride, Et$_3$N in Ethylacetate to give di-Boc alcohol compound **39**. The free hydroxyl group was further activated as its *para*-Nitrophenyl active carbonate.
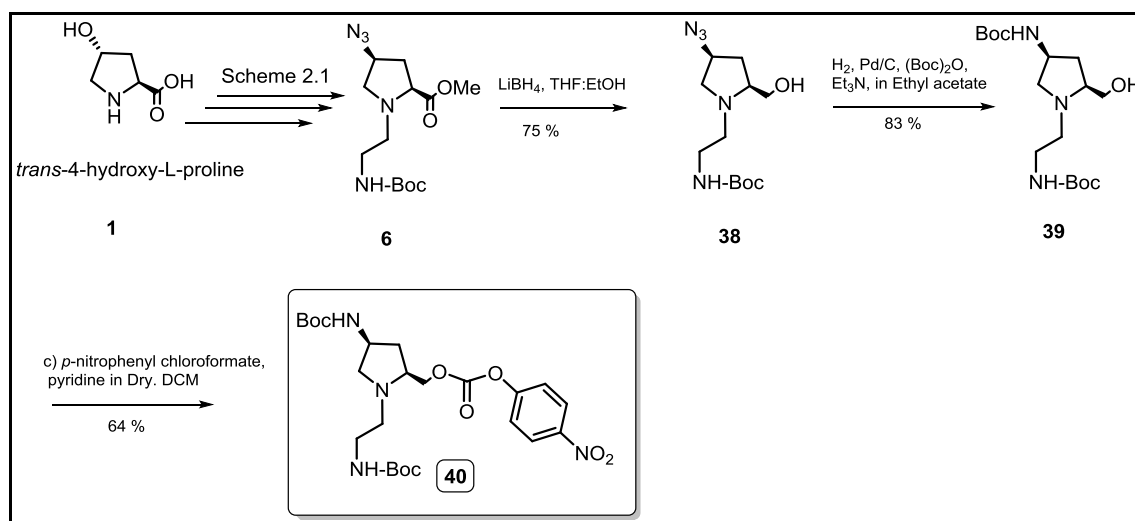
Scheme 4.3 Synthesis of *p*-nitrophenyl activated monomer.

Synthesis of various dendrons and dendrimers would be undertaken from synthesized novel monomer **40**. It would be possible to explore and use this monomer in combination with earlier synthesized spacer monomers (*p*-nitrophenyl activated monomer of Boc-aminopropropanol or Boc-aminohexanol, Chapter 3) to synthesize novel (r-x-r)-type of dendrons and dendrimers.

4B.4 Summary and conclusion

- A novel monomeric unit from easily accessible *trans*-4-hydroxy proline as a starting material was designed and synthesized.

- *para*-Nitrophenyl activated monomer a building block can further use to build various dendrons and dendrimers was synthesized.

➕ Hydrophobic interior and surface pendant group anchoring is envisioned in planned dendrons and dendrimers, and those can further explored in drug delivery applications.

4.1 Experimental

4.1.1 Experimental procedure and spectral data

(2*S*,3*S*)-2,3-O-isopropylidene-1,4-diol: (28)
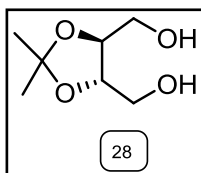
To a dry 1000 ml round bottom flask equipped with big magnetic bar, under argon atmosphere, $NaBH_4$ (10.3 g, 0.27 mol) was added in 3:4 mixture of solvents THF: EtOH (100 ml). To this, slowly, LiCl (11.5 g, 0.27 mol) was added at ice-cold conditions. The reaction mixture was stirred for 30 min., formed a milky solution confirms *in situ* generation of $LiBH_4$. The dimethyl ester compound **27** (20 g, 0.091 mol) dissolved in ethanol (50 mL) was added drop-wise. The reaction mixture was stirred further 3 h and then allowed to warm at room temperature. The reaction was monitored by TLC. Solvents were evaporated under reduced pressure and the residue was re-suspended in water. The reaction mixture was neutralized by adding dil. HCl. Solvents evaporated in vacuo to give the crude product which was purified by column chromatography (90% EtOAc/Pet-ether) to give the title diol compound **28** (10.2 g, 68%) as yellow liquid.

Molecular formula: $C_7H_{14}O_4$; **Molecular weight:** 162.19

^{1}H NMR (400MHz, $CDCl_3$) δ: 4.00 (s, 2H), 3.79 (m, 4H), 1.86 (bs, 2H), 1.44 (s, 6H)

^{13}C NMR (100 MHz, $CDCl_3$) δ: 109.25, 78.0, 61.9, 26.9

(2*S*,3*S*)-2,3-O-isopropylidene-1,4-diazidobutane: (30)
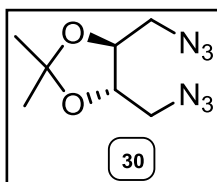
To a oven dried 250 mL round bottom flask equipped with magnetic bar, containing of acetonide diol (5.0 g, 0.03 mol), pyridine (20 mL) was added under argon atmosphere. Mesyl chloride (5.0 ml, 0.06 mol) was added drop wise at ice coild condition, formed reaction mixture was stirred further for 30 min at ice cooled condition. The reaction was monitored by TCL. Water and ethyl acetate were added to the reaction mixture and formed layers were separated. The organic layer was washed by water (3 x 100 mL), further brine (100 mL) was added to the organic layer and separated organic layer was

dried over Na_2SO_4. Solvents were evaporated to give dimesyl compound **29** as a pale-yellow liquid.

Formed dimesyl compound **29** was further divide into three round bottom flasks (each contains 3.0 g, 0.009 mol of compound) and dissolved them in dry DMF and allow to react further with sodium azide (1.5 g, 0.02 mole to each of three flasks) at 70°C for 6h. Reaction was monitored by TLC. Upon completion of reactions, contained of all three flasks were combine, water (100 mL) and ethyl acetate (100 mL) was added into it and layers were separated. Water layer was extracted with ethyl acetate (2 x 100 mL). Brine (100 mL) was added to organic layer and combined organic layers was dried over Na_2SO_4. Solvents evaporated in vacuo to give the crude product which was purified by column chromatography to give the title diazide compound **30** as white solid (4.8 g, 73% yield).

Molecular formula: $C_7H_{12}O_6O_2$; **Molecular weight:** 212.2

^{1}H NMR (200MHz, $CDCl_3$) δ: 4.05 (m, 2H), 3.53 (m, 4H), 1.47 (s, 6H)

^{13}C NMR (50 MHz, $CDCl_3$) δ: 110.3, 76.8, 51.5, 26.7

Dibenzyl(((4S,5S)-2,2-dimethyl-1,3-dioxolane-4,5- iyl)bis(methylene))dicarbamate: (32)
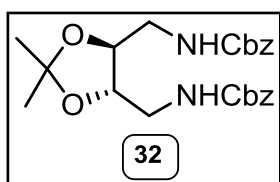
The diazide compound **30** (3.0 g, 0.014 mol) was dissolved in dry. MeOH was transferred to the parr hydrogenation flask; 10 % palladium on charcoal (600 mg, 20% w/w) was added carefully to it. The flask containing reaction mixture was shook on parr shaker apparatus for 6h under hydrogen gas atmosphere (65 psi). Reaction was monitored by TLC. The reaction mixture was filtered through celite. The solvent evaporated in vacuo to give diamine compound. The formed diamine compound was further dissolved by addition of water: 1, 4-dioxane (1:1, 30 mL) into a 250 ml round bottom flask and $NaHCO_3$ (5.7 g, 0.068 mol) was added to it. After 15 min. benzyl choloroformate (5.0 ml, 0.032 mol) which was dissolved in 1, 4-dioxane was added dropwise to the above formed solution at ice-cold condition. Reaction was monitored by TLC. The solvent 1, 4-dioxane was evaporated in vacuo and reaction mixture was

neutralized by addition of dil.HCl. Ethyl acetate (100 mL) was added to it and layers were separated and water layer was extracted with ethyl acetate (3 x 100 mL), combined organic extracts were dried over Na_2SO_4. Solvents evaporated in vacuo to give the crude product, which was purified by column chromatography to give the title acetonide dibz compound **32** (4.2 g, 69% over two steps) as yellow powder.

Molecular formula: $C_{23}H_{28}N_2O_6$;   **Molecular weight:** 428.4

^{1}H NMR (200MHz, $CDCl_3$) δ: 7.34 (m, 10H), 5.28 (m, 2H), 5.11 (s, 4H), 3.80 (s, 2H), 3.41 (m, 4H), 1.36 (s, 6H)

^{13}C NMR (50 MHz, $CDCl_3$) δ: 156.5, 136.2, 128.3, 128.0, 108.9, 66.7, 42.0, 26.8

dibenzyl ((2S,3S)-2,3-dihydroxybutane-1,4-diyl)dicarbamate: (33)
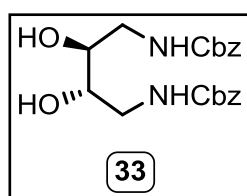
In oven dried round bottom flask equipped with magnetic bar acetonide compound **32** (3.0 g, 7.0 mmol) was dissolved in dry. MeOH (20 mL), catalytic amount of *p*-toluene sulphonic acid (150 mg) was added. Refluxed the above formed reaction mixture for 10h, white precipitated formed in reaction mixture indicative of completion of reaction and it was confirmed by TLC. Solvents evaporated in vacuo to give the crude product which was purified by column chromatography to give the title diol compound **33** (2.5 g, 92%) as white solid.

Molecular formula: $C_{20}H_{24}N_2O_6$; **Molecular weight:** 388.4

^{1}H NMR (200MHz, MeOD-d4) δ: 7.34 (m, 10H), 5.08 (s, 4H), 3.60 (m, 2H), 3.27 (m, 4H)

^{13}C NMR (100 MHz, MeOD-d4) δ: 159.3, 138.4, 129.6, 128.9, 71.6, 67.6, 49.9

dibenzyl ((2S,3S)-2-azido-3-hydroxybutane-1,4-diyl)dicarbamate: (35)
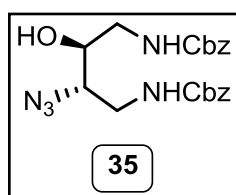
The compound **35** was synthesized from compound **33** by literature reported procedure in details, to 250 mL round bottom flask containing stirred solution of **33** (4.0 g, 10.3 mmol) in 25ml

dry CH_2Cl_2 and anhydrous pyridine (2.07 mL, 25.0 mmol) at 0°C, thionyl chloride (1.6 mL, 22.0 mmol) was added drop wise. The temperature of reaction mixture was allowed to attend room temperature in 2 h. The CH_2Cl_2 (20 mL) and saturated NaCl (40 mL) were added to the reaction mixture. Formed layers were separated, the aqueous phase was extracted thoroughly with CH_2Cl_2 (2 x 50 mL). The combined organic layers were dried over anhydrous Na_2SO_4. The solvent was removed in vacuo to give the crude compound **34** quantitatively as brown oil, which was used in next reaction, without further purification.

To a solution of compound **34** in DMF (30 mL) at room temperature, sodium azide (3.3 g, 51.5 mmol) was added and the mixture was stirred at room temperature for 5 h. The solvent was evaporated in vacuo; the residue was dissolved in EtOAc (50 mL), washed with saturated NaCl (3 x 30 mL), and dried over anhydrous Na_2SO_4. Solvents evaporated in vacuo to give the crude product which was purified by column chromatography (25 % EtOAc/Pet-ether) to give the title azido alcohol compound **35** (2.8 g, 66% over two steps) as viscous oil.

Molecular formula: $C_{20}H_{23}N_5O_5$; **Molecular weight:** 413.4

^{1}H NMR (500MHz, CDCl$_3$) δ: 7.33 (m, 10H), 5.42 (bs, 2H), 5.1 (m, 4H), 3.64 (m, 1H), 3.51 (m, 2H), 3.36 (m, 2H), 3.24 (m, 1H)

^{13}C NMR (125 MHz, CDCl$_3$) δ: 157.7, 157.1, 136.2, 135.8, 69.8, 67.3, 66.9, 63.6, 43.6, 41.2

MS (ESI): *m/z* calculate 413.4; found: 436.1(M+Na)

dibenzyl tert-butyl ((2S,3S)-3-hydroxybutane-1,2,4-triyl)tricarbamate: (36)
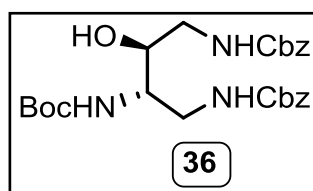
The azide alcohol compound **35** (2.0 g, 4.8 mmol) was dissolved in MeOH in 50 mL of round bottom flask under atmosphere of nitrogen gas. To that, freshly prepared Raney nickel (300 mg, 15% by weight) was added carefully. The reaction was stirred under a hydrogen atmosphere at room temperature for 2h. Reaction was monitored by TLC. The reaction mixture was filtered through celite and solvent

evaporated in vacuo to give the crude amine compound, which was further dissolved in dry. CH_2Cl_2 (50 mL) and triethylamine (1.34 ml, 9.6 mmol) was added to it. After 15 min., $(Boc)_2O$ (1.3 g, 6.2 mmol) which was added drop wise to the above formed reaction mixture at ice-cold condition and stirred for 3h. Reaction was monitored by TLC. Solvents were evaporated in vacuo and water(100 mL) was added to reaction mixture and neutralized by aq. NH_4Cl. Solvent CH_2Cl_2 (100 mL) was added and layers were separated. Water layer was extracted with CH_2Cl_2 (3 x 50 mL), combined organic extracts were dried over Na_2SO_4. Solvents evaporated in vacuo to give the crude product which was purified by column chromatography to give the title compound **36** (2.0 g, 86% over two steps) as white powder.

Molecular formula: $C_{25}H_{33}N_3O_7$; **Molecular weight:** 487.5

^{1}H NMR (200MHz, MeOH-d4) δ: 5.08 (s, 4H), 3.57 (m, 4H), 3.11 (m, 2H), 1.43 (s, 9H)

^{13}C NMR (125 MHz, $CDCl_3$) δ: 158.1, 156.2, 136.2, 136.0, 128.4, 128.0, 79.8, 77.2, 71.4, 67.1, 66.9, 53.1, 43.6, 41.7, 28.2

MS (ESI): *m/z* calculate 487.5; found: 510.18 (M+Na)

dibenzyl tert-butyl ((2S,3S)-3-(((4-nitrophenoxy)carbonyl)oxy)butane-1,2,4-triyl)tricarbamate: (37)
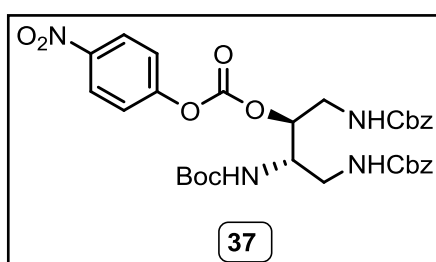
To the stirring solution of Boc alcohol compound **36** (1.0 g, 2.0 mmol) in dry CH_2Cl_2 (15 mL) , pyridine (0.45 mL, 6.0 mmol) was added at ice cold condition. Powdered *p*-nitrophenyl chloroformate (0.64 g, 3.0 mmol) was added in portion to the above formed reaction and stirred the reaction mixture for 3h at 0°C, reaction was monitored by TLC. Solvents evaporated in vacuo to give the crude product which was purified by column chromatography to give the title compound **37** (0.9 g, 76%) as yellow foam.

Molecular formula: $C_{32}H_{36}N_4O_{11}$; **Molecular weight:** 652.6

^{1}H NMR (200MHz, CDCl$_3$) δ: 8.21(d, 2H), 7.42 (d, 2H), 7.31 (m, 10H), 5.71 (m, 1H), 5.49 (m, 1H), 5.10(m, 4H), 3.95 (m, 2H), 3.11(m, 2H), 1.42 (s, 9H)

^{13}C NMR (100 MHz, CDCl$_3$) δ: 157.7, 157.1, 156.5, 155.5, 151.7, 145.4, 136.4, 135.9, 128.5, 128.4, 128.3, 128.09, 128.00, 125.2, 122.1, 80.5, 77.4, 67.2, 66.8, 50.4, 41.6, 39.1, 28.22

MS (ESI): *m/z* calculate 652.6; found: 675.14 (M+Na)

tert-butyl (2-((2S,4S)-4-azido-2-(hydroxymethyl)pyrrolid in-1-yl)ethyl)carbamate: (38)
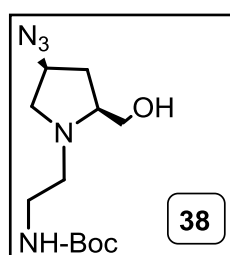
In a dry 100 mL round bottom flask equipped with magnetic bar, under argon atmosphere, NaBH$_4$ (0.80 g, 22 mmol) was added in 3:4 mixture of solvents THF: EtOH (70 mL). To this, slowly, LiCl (0.9 g, 22 mmol) was added at ice-cold conditions. The reaction mixture was stirred for 30 min., formed milky solution confirmed *in situ* generation of LiBH$_4$. The 4-azido methyl ester of *N*-alky proline compound **6** (2.0 gm, 5.5 mmol) dissolved in ethanol (15 mL) was added drop-wise. The reaction mixture was stirred for 3 h and then allowed to warm to room temperature. The reaction was monitored by TLC. Solvent evaporated in vacuo and the residue was re-dissolved in water. The reaction mixture was neutralized by adding aq.NH$_4$Cl, followed by extraction of the water layer with ethyl acetate (3x 20 mL). Brine washes (3x 25 mL) were given and the combined organic layers were dried over Na$_2$SO$_4$. Solvent evaporated in vacuo to give the crude product which was purified by column chromatography (45% EtOAc/Pet-ether) to give the title azido alcohol compound **38** (1.2 g, 75%).

Molecular formula: C$_{12}$H$_{23}$N$_5$O$_3$; **Molecular weight:** 285.3

^{1}H NMR (200MHz, CDCl$_3$) δ: 5.0 (bs, 1H), 3.99 (m, 1H), 3.65 (m, 6H), 3.25 (m, 4H), 2.55 (m, 5H), 2.00 (m, 1H), 1.45 (s, 9H)

^{13}C NMR (100 MHz, CDCl$_3$) δ: 156.0, 79.3, 64.2, 61.5, 59.0, 53.1, 39.2, 33.6, 28.3

MS (ESI): *m/z* calculate 285.3; found:307.9 (M+Na)

tert-butyl ((3S,5S)-1-(2-((tert-butoxycarbonyl)amino)ethyl)-5-hydroxymethyl)pyrrolidin-3-yl)carbamate: (39)
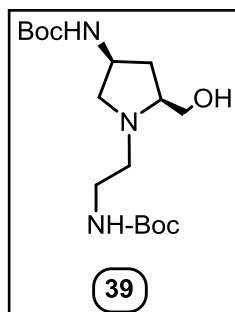
In oven dried 100 mL round bottom flask containing compound **38** (2.0 g, 7.0 mmol) was dissolved in ethyl acetate (15 mL). The (Boc)₂O reagent (3.8 g, 17.5 mmol) and Et₃N (2.5 mL, 21 mmol) were added to it. Then carefully Palladium on charcoal (300 mg, 15% w/w) was added and stirred the reaction mixture for next 6h in hydrogen gas atomosphere pressure. Reaction was monitored by TLC. Filtered the reaction mixture through celite and crude reaction mixture was further purified through column chromatography (3% MeOH/CH₂Cl₂) to afforded the gummy liquid compound **39** (2.1 g, 83%).

Molecular formula: $C_{17}H_{33}N_3O_3$; **Molecular weight:** 359.25

¹H NMR (200MHz, CDCl₃) δ: 5.51 (bs, 1H), 5.13 (bs, 1H), 4.11 (m, 1H), 3.72 (m, 1H), 3.13 (m, 5H), 2.61 (m, 5H), 1.7 (m, 1H) 1.43 (d, 18H)

¹³C NMR (100 MHz, CDCl₃) δ: 156.4, 155.4, 79.2, 78.8, 64.1, 61.2, 53.5, 48.8, 39.5, 35.3, 28.3

MS (ESI): *m/z* calculate 359.25; found: 360.02 (M+H)

tert-butyl((3S,5S)-1-(2-((tert-butoxycarbonyl)amino)ethyl)-5-((((4-itrophenoxy) carbonyl)oxy) methyl)pyrrolidin-3-yl)carbamate: (40)
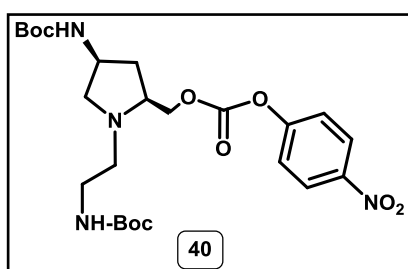
To the stirring solution of Boc alcohol compound **39** (1.0 g, 2.7 mmol) dry CH₂Cl₂ (10 mL), pyridine (0.4 mL, 5.5 mmol) was added at 0°C. Powdered *p*-nitrophenyl chloroformate (0.8 g, 4.0 mmol) was added in portion to above formed reaction and continued the reaction for next 3h at 0°C, reaction was monitored by TLC. Solvents evaporated in vacuo to give the crude product which was purified by column chromatography to give the title compound **40** (0.9 g, 64%) as gummy compound, which was dried and stored in refrigerator as it was found little unstable at room temperature and in solvent.

Molecular formula: $C_{24}H_{36}N_4O_9$; **Molecular weight:** 524.5

^{1}H NMR (200MHz, CDCl$_3$) δ: 832 (m, 2H), 7.4 (m, 1H), 5.25 (m, 1H), 4.87 (m, 1H), 4.14 (m, 4H), 3.10 (m, 5H), 2.49 (m, 2H), 1.70 (m, 1H), 142 (m, 18H)

^{13}C NMR (100 MHz, CDCl$_3$) δ: 156.3, 155.3, 152.5, 145.3, 125.2, 121.7, 79.3, 70.9, 61.2, 59.7, 49.1, 39.1, 35.7, 29.6, 28.3

4.1.2 Appendix C

Compound and characterization	Page No.
Compound **28**:^{1}H, ^{13}C NMR, ^{13}C DEPT	203-204
Compound **30**: ^{1}H, ^{13}C NMR, ^{13}C DEPT	204-205
Compound **32**:^{1}H, ^{13}C NMR, ^{13}C DEPT	206-207
Compound **33**:^{1}H, ^{13}C NMR, ^{13}C DEPT	207-208
Compound **35**:^{1}H, ^{13}C NMR, ^{13}C DEPT	209-210
Compound **36**:^{1}H, ^{13}C NMR, ^{13}C DEPT	210-211
Compound **37**:^{1}H, ^{13}C NMR, ^{13}C DEPT	212-213
Compound **38**:^{1}H, ^{13}C NMR, ^{13}C DEPT	213-214
Compound **39**:^{1}H, ^{13}C NMR, ^{13}C DEPT	215-216
Compound **40**:^{1}H, ^{13}C NMR, ^{13}C DEPT	216-217
MALDI-TOF spectra of oligomer	218

^{1}H NMR (400 MHz; CDCl$_3$) spectrum of compound **28**:
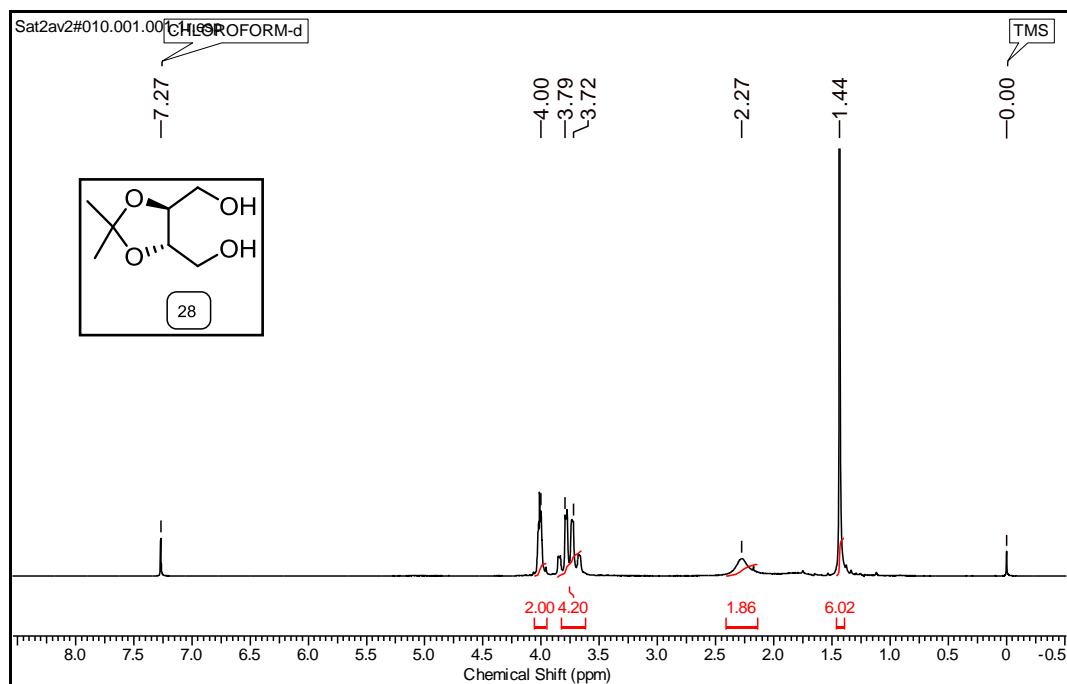
^{13}C NMR (100 MHz; CDCl$_3$) spectrum of compound **28**:
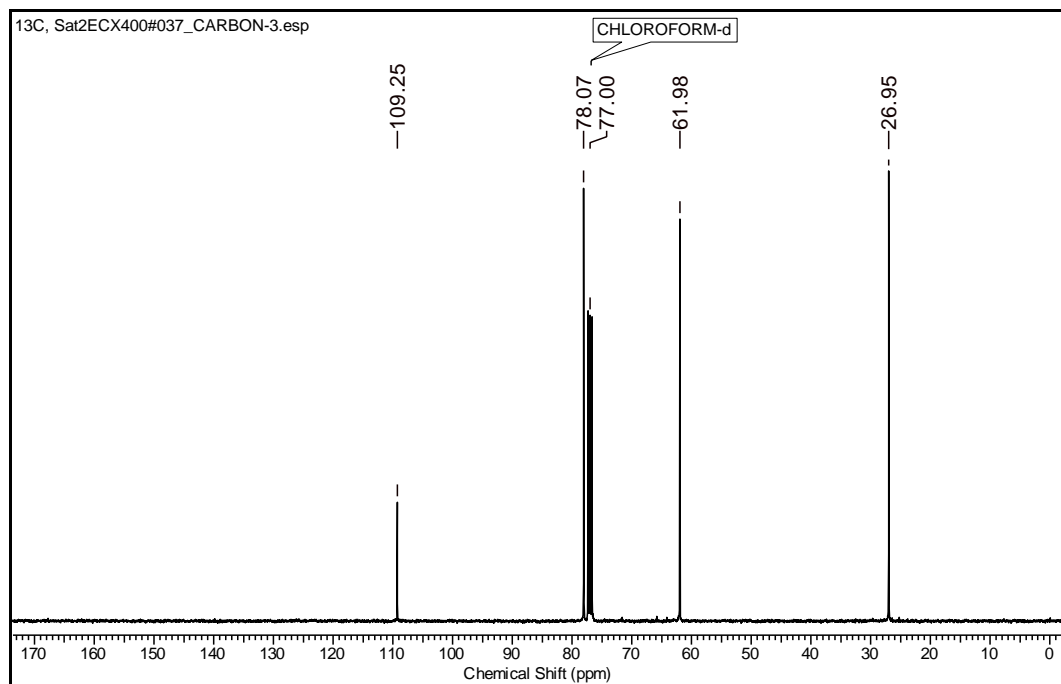
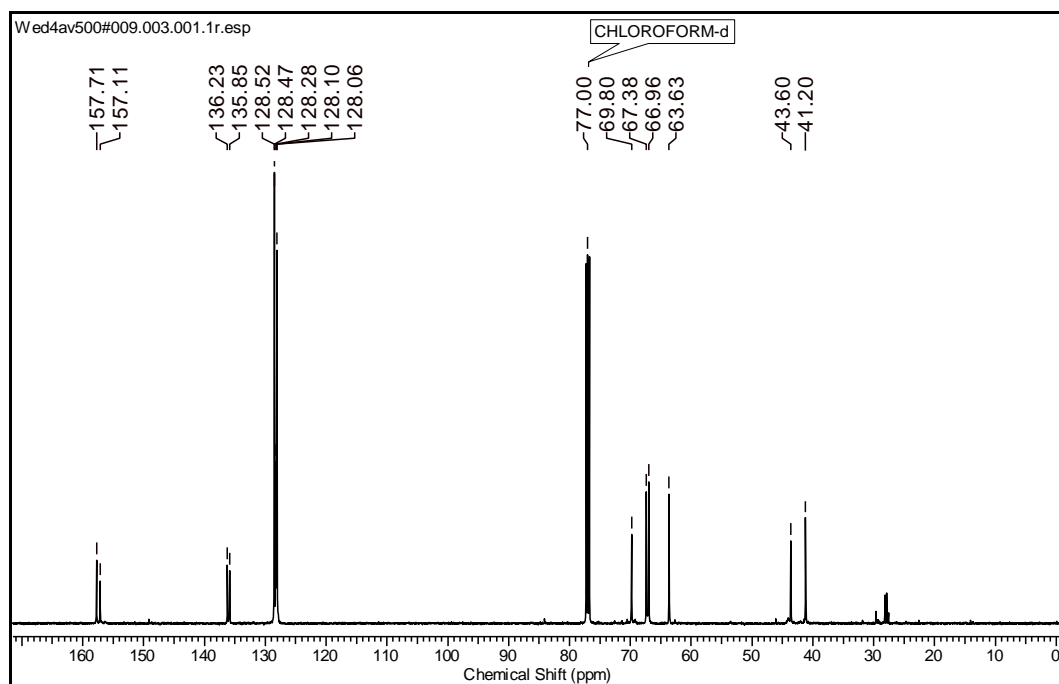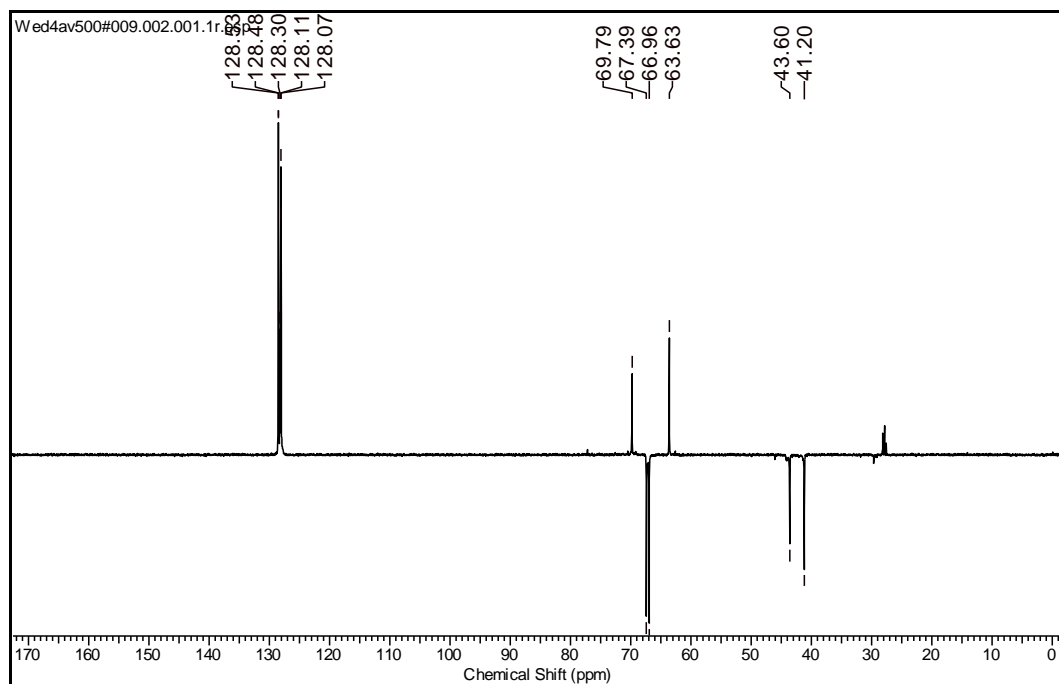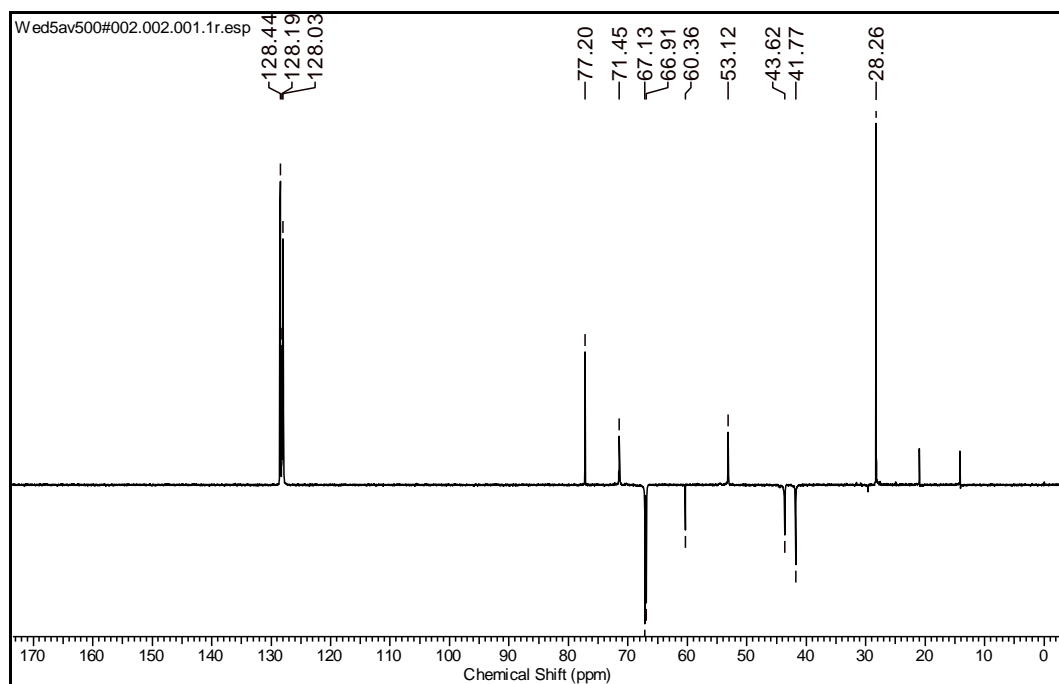^{13}C DEPT (100 MHz; CDCl$_3$) spectrum of compound **28**:

Sat2ECX400#037_DEPT135-3.jdf

—78.01
—61.93
—26.90

170 160 150 140 130 120 110 100 90 80 70 60 50 40 30 20 10 0
Chemical Shift (ppm)

^{1}H NMR (200 MHz; CDCl$_3$) spectrum of compound **30**:

Fri5av2#010.001.001.1r.esp

—7.27
4.05
4.05
3.60
3.53
3.38
3.30
—1.47
—0.00

30

2.00   4.10   6.00

8.5 8.0 7.5 7.0 6.5 6.0 5.5 5.0 4.5 4.0 3.5 3.0 2.5 2.0 1.5 1.0 0.5 0
Chemical Shift (ppm)
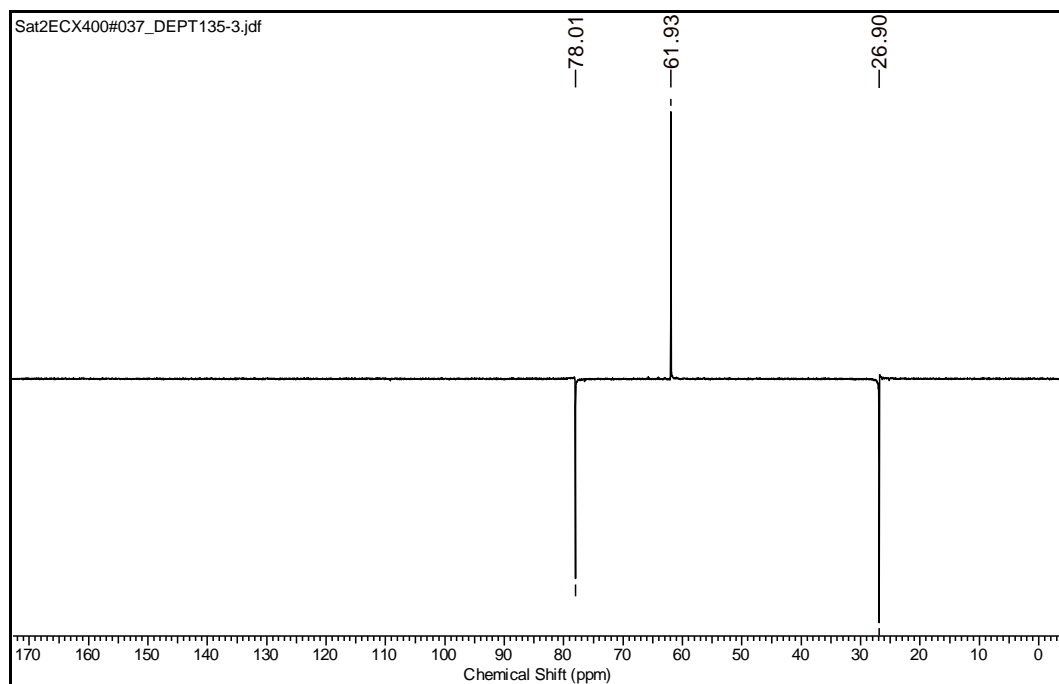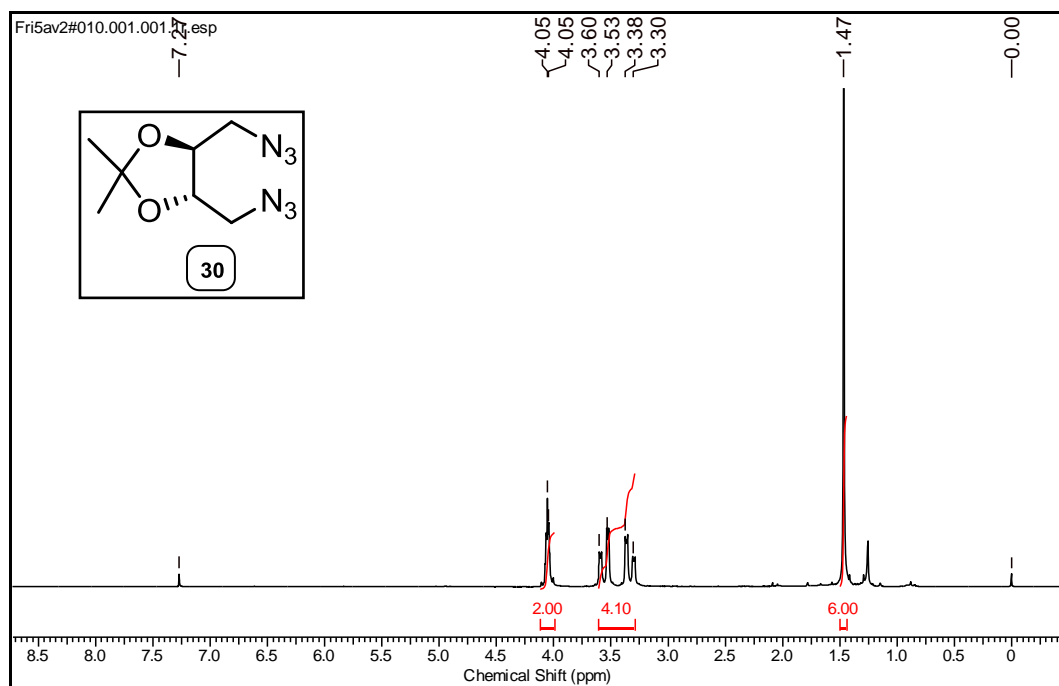
^{13}C NMR (50 MHz; CDCl$_3$) spectrum of compound **30**:
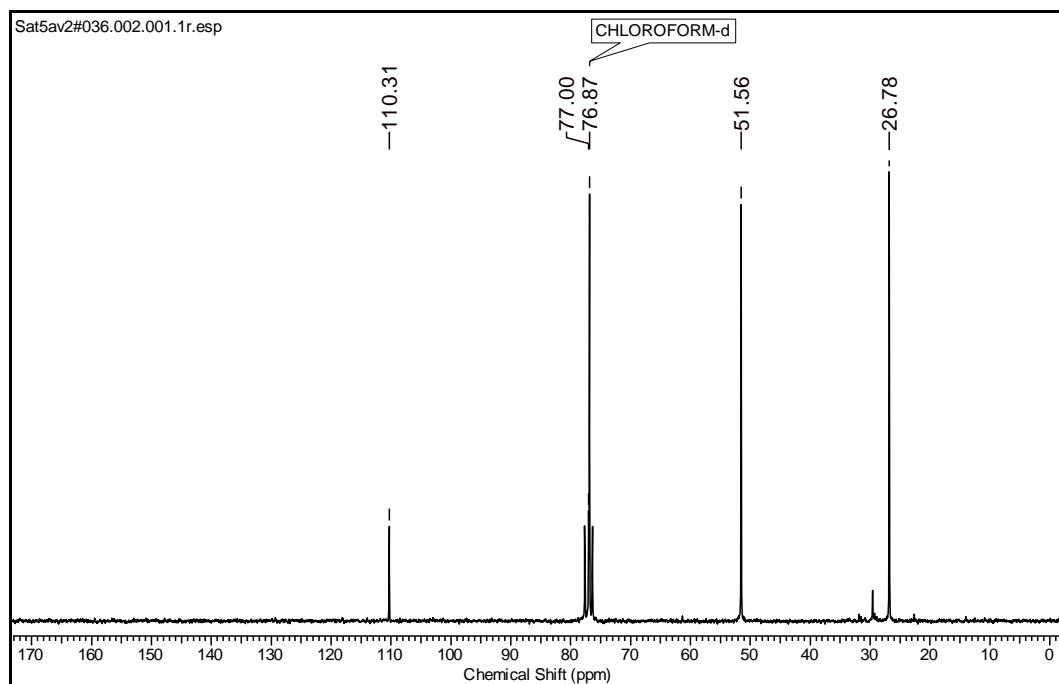
^{13}C DEPT (50 MHz; CDCl$_3$) spectrum of compound **30**:
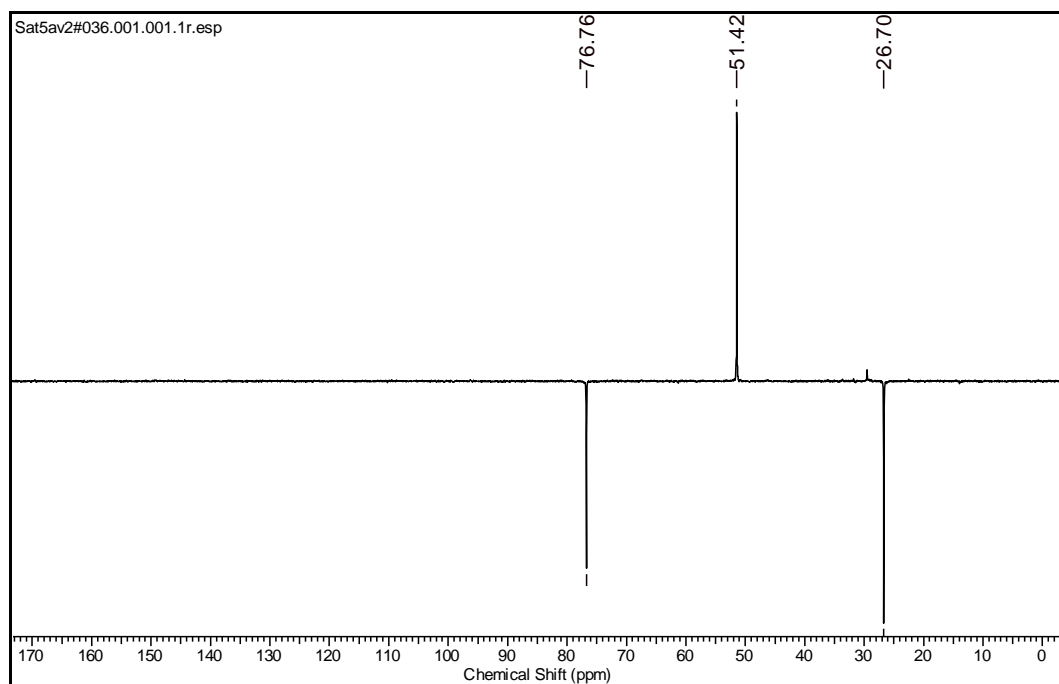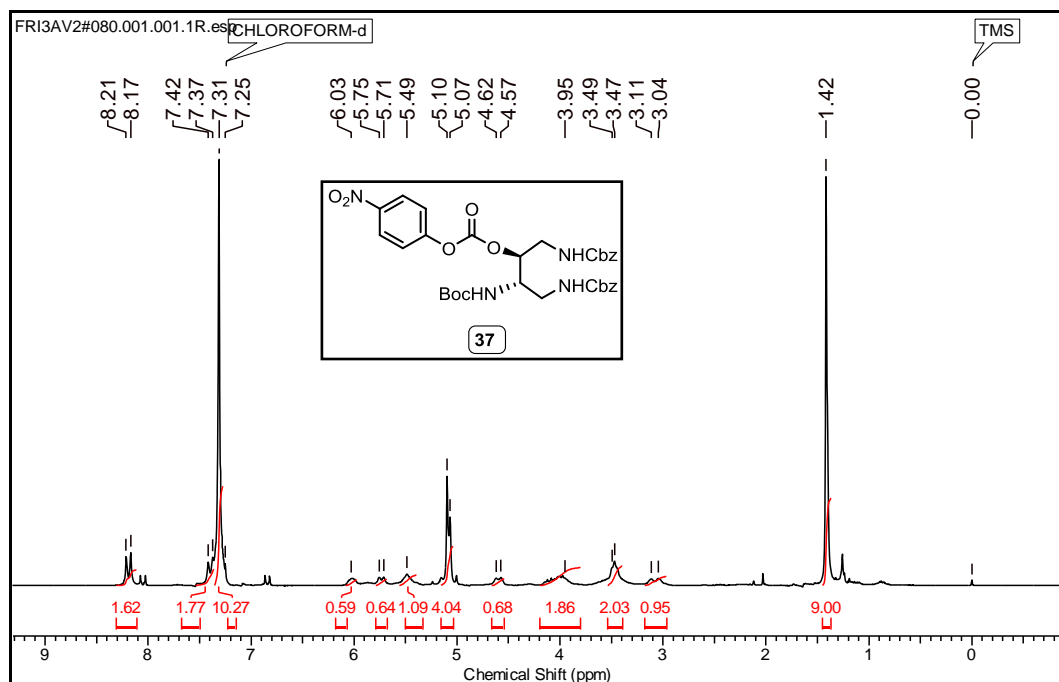
^{1}H NMR (200 MHz; CDCl$_3$) spectrum of compound **32:**
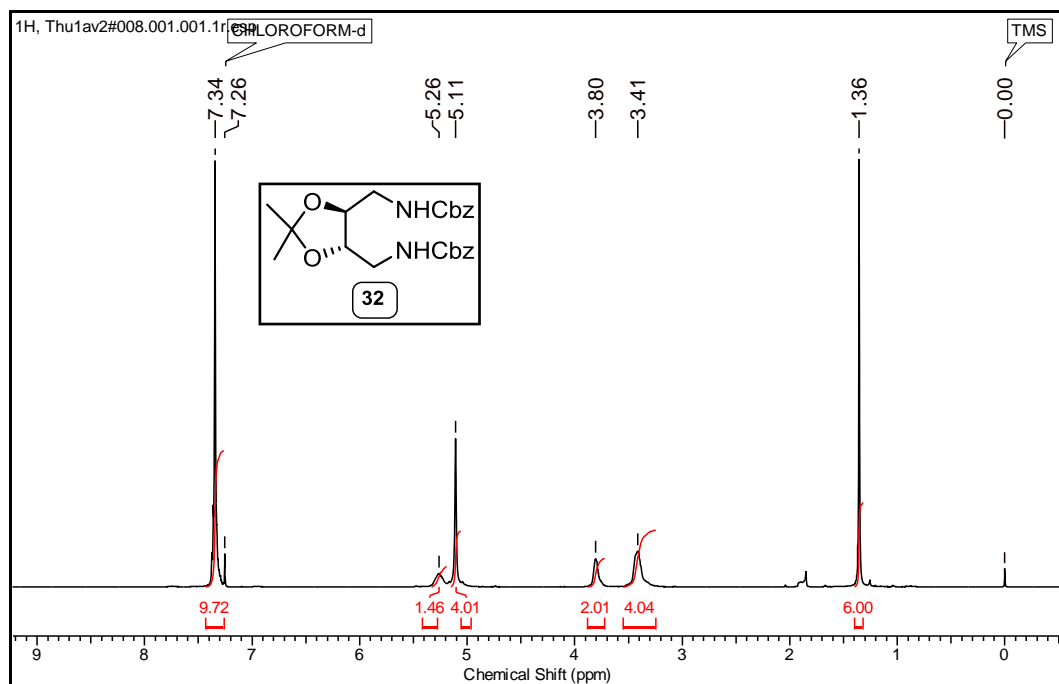
^{13}C NMR (50 MHz; CDCl$_3$) spectrum of compound **32**:
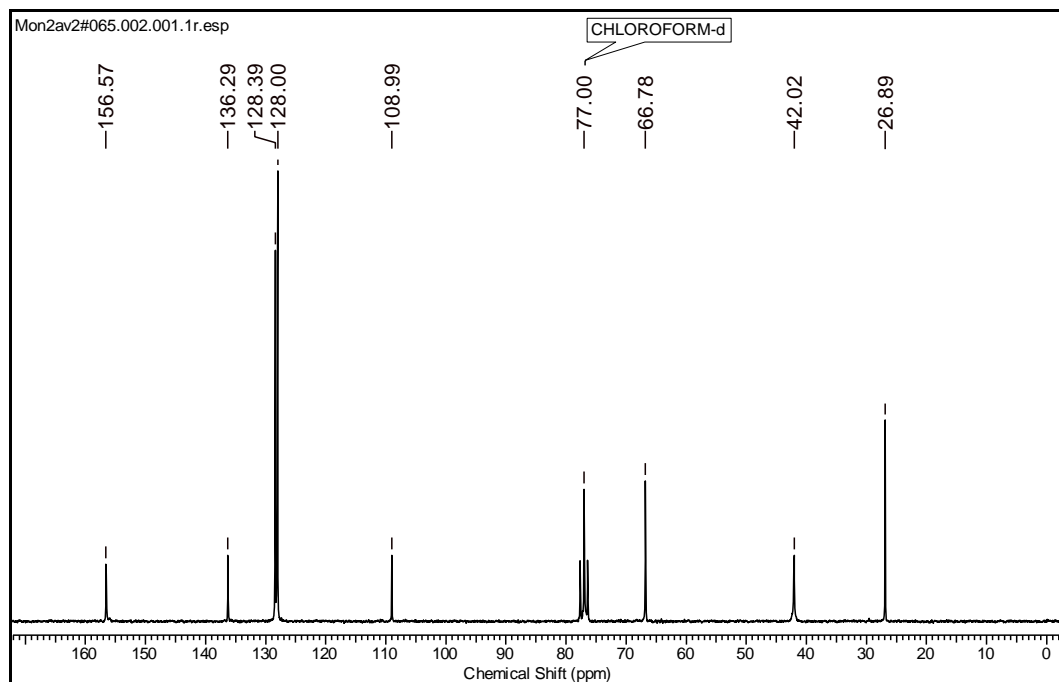
^{13}C DEPT (50 MHz; CDCl$_3$) spectrum of compound **32**:
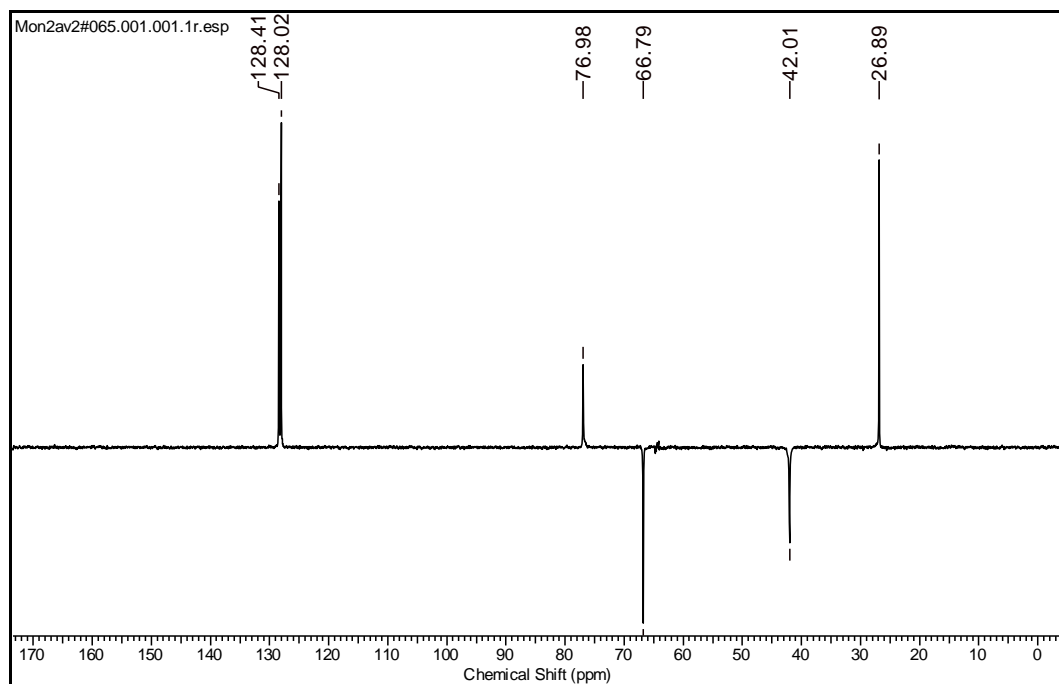
^{1}H NMR (200 MHz; CDCl$_3$) spectrum of compound **33:**
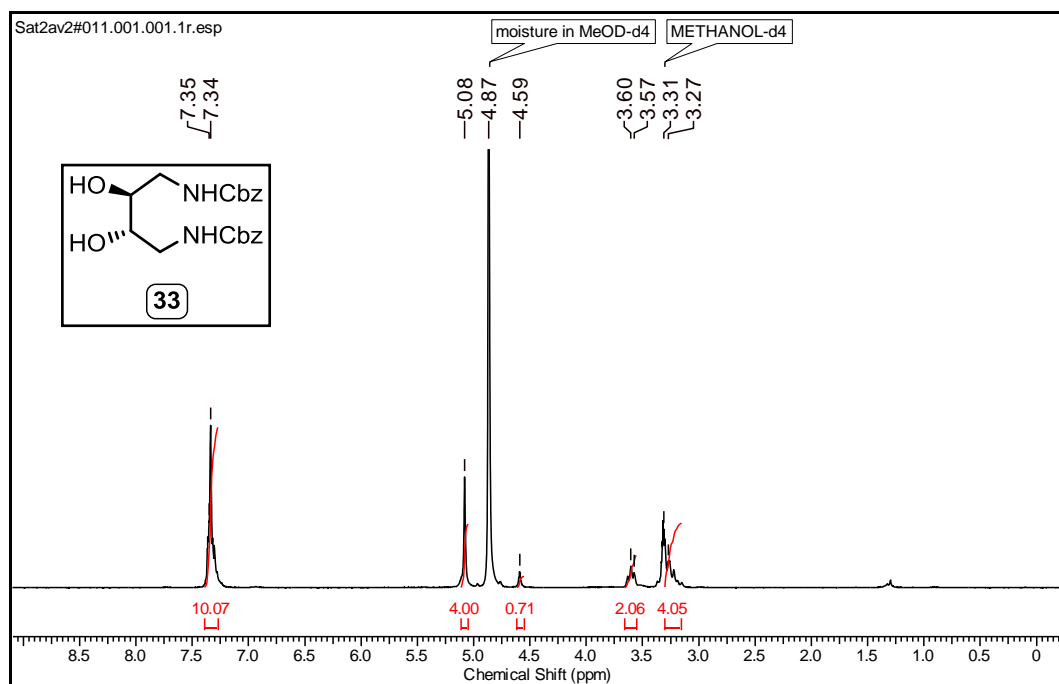
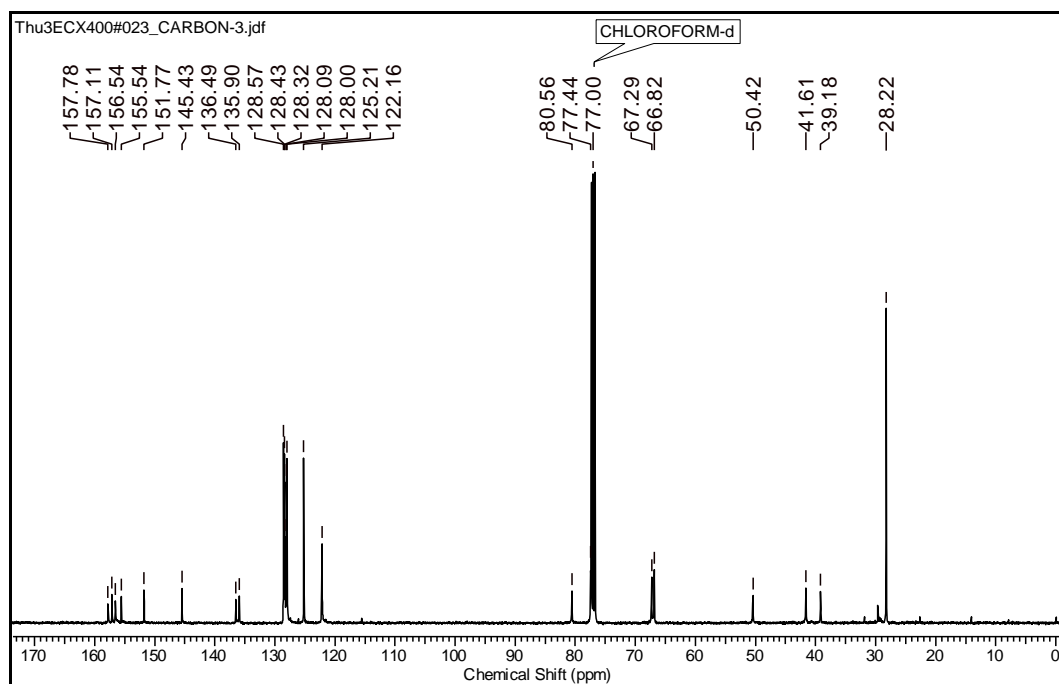^{13}C NMR (50 MHz; CDCl$_3$) spectrum of compound **33**:
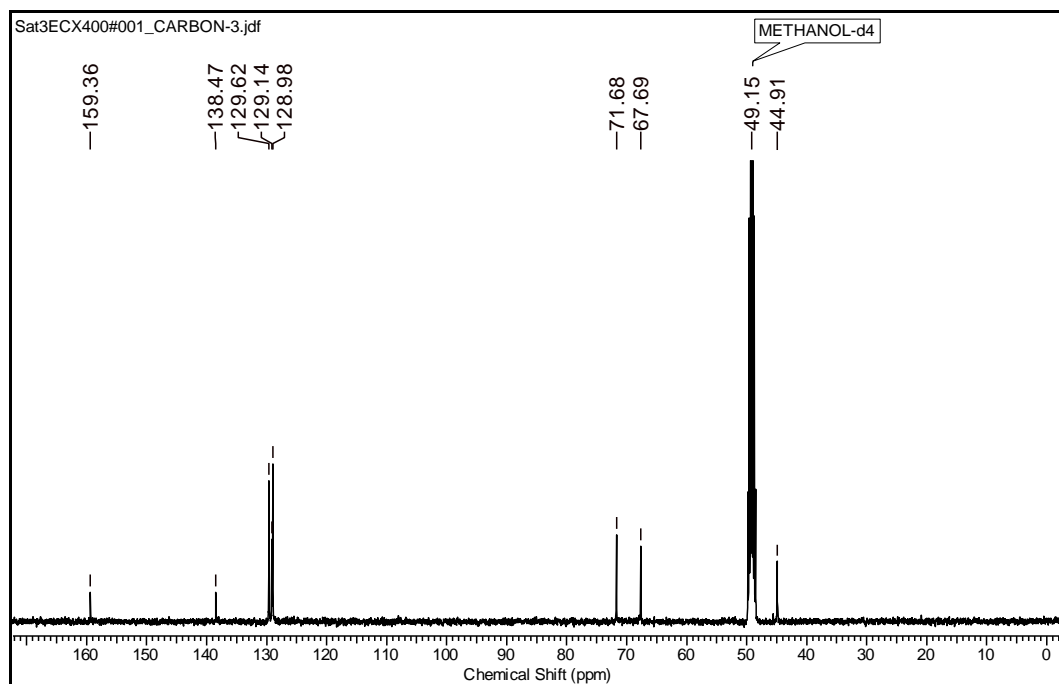
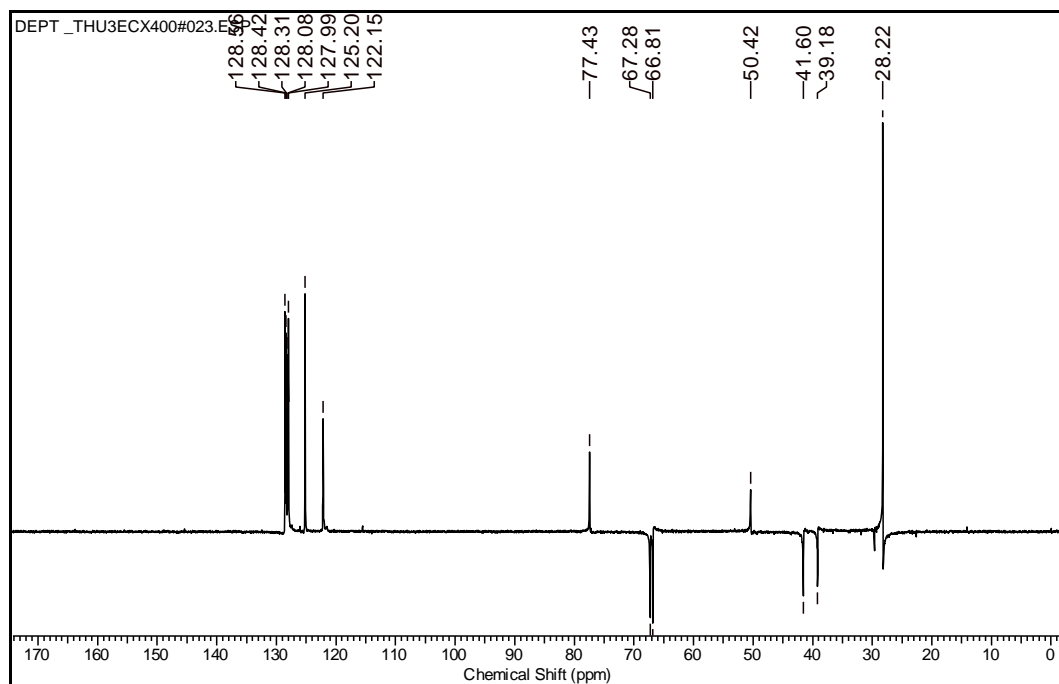

^{13}C DEPT (50 MHz; CDCl$_3$) spectrum of compound **33**:
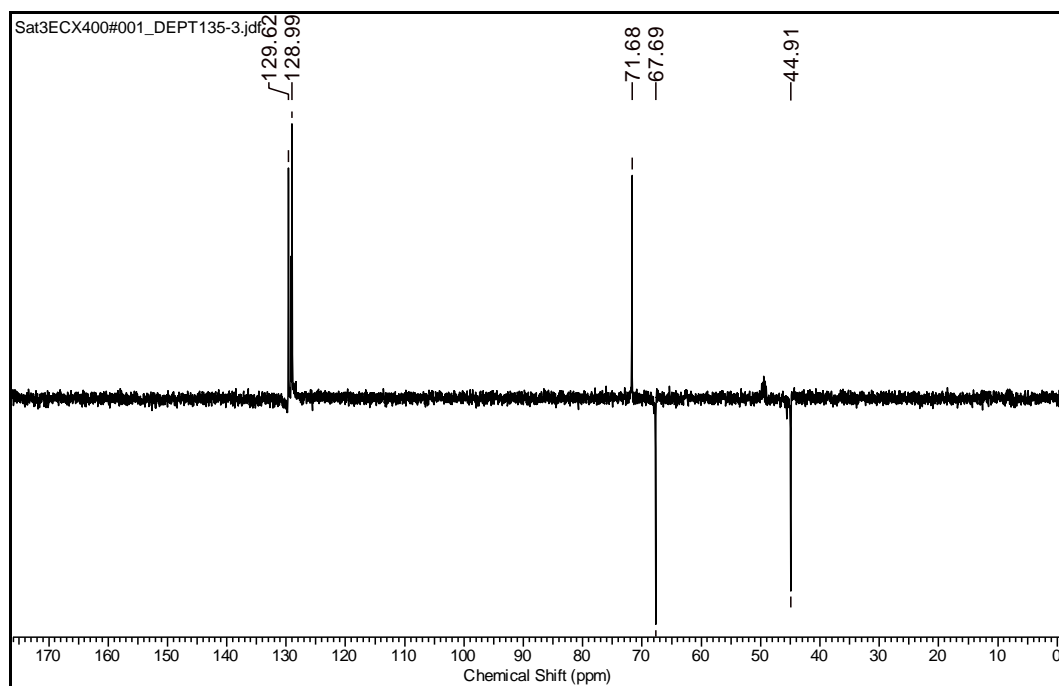
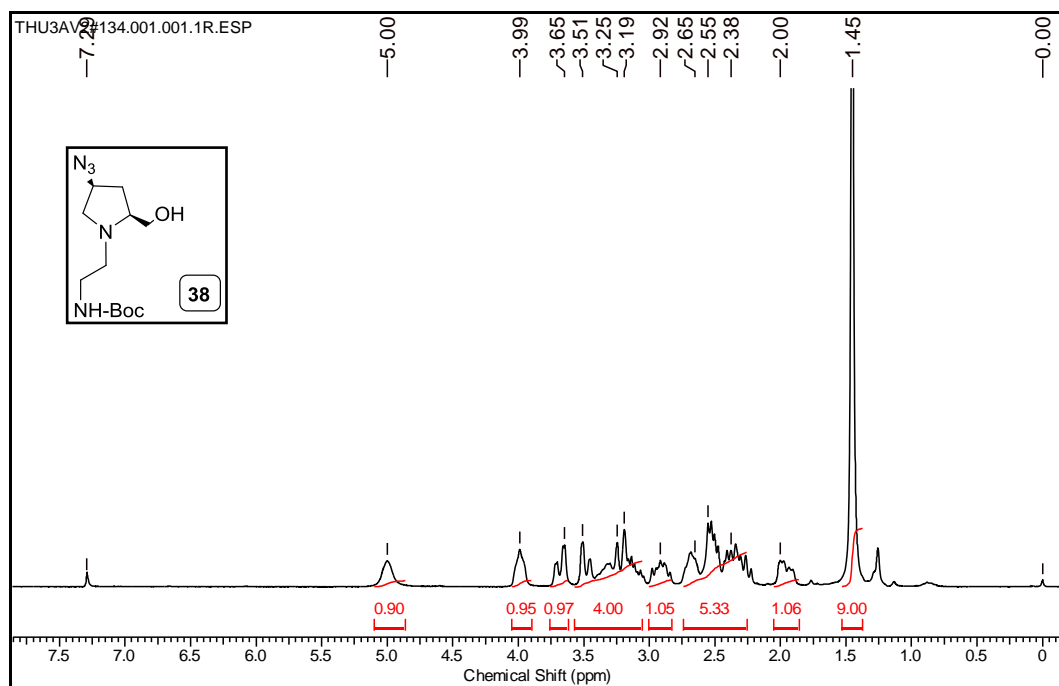## ^{1}H NMR (500 MHz; CDCl$_3$) spectrum of compound **35:**
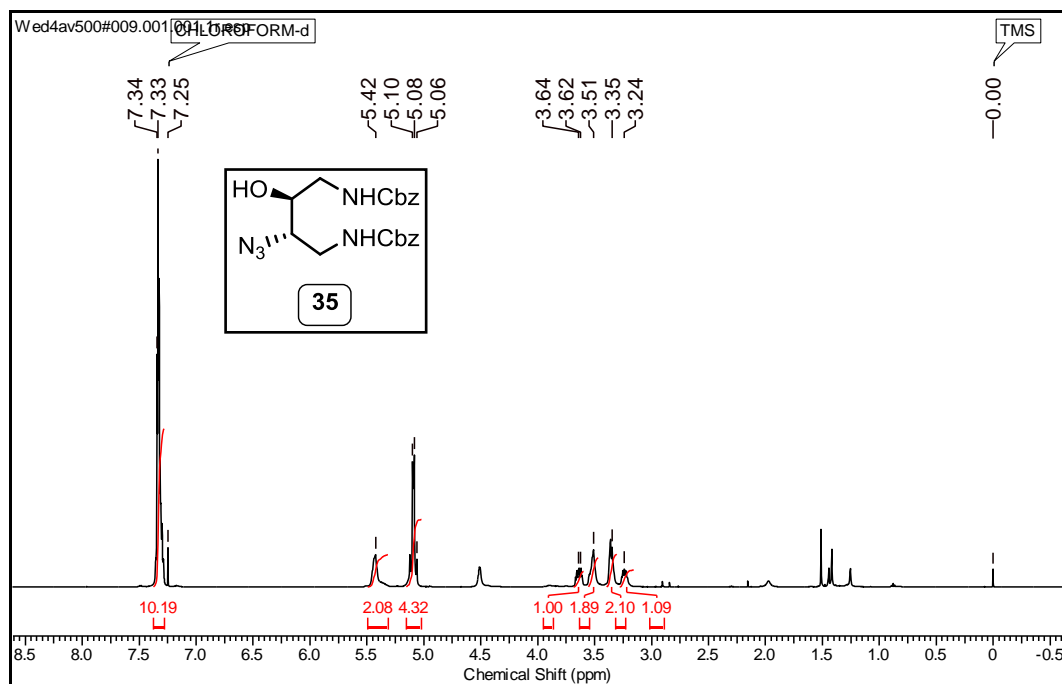
^{13}C NMR (125 MHz; CDCl$_3$) spectrum of compound **35**:

^{13}C DEPT (50 MHz; CDCl$_3$) spectrum of compound **35**:

Wed4av500#009.002.001.1r.esp

128.83
128.48
128.30
128.11
128.07
69.79
67.39
66.96
63.63
43.60
41.20

^{1}H NMR (200 MHz; CDCl$_3$) spectrum of compound **36**:

MOn5av2#058.001.001.1r.esp

moisture in MeOD-d4   METHANOL-d4

5.08
4.92
3.57
3.50
3.40
3.31
3.11
3.04
1.43

HO   NHCbz
BocHN   NHCbz
36

4.10   0.52   4.04   2.01   9.00
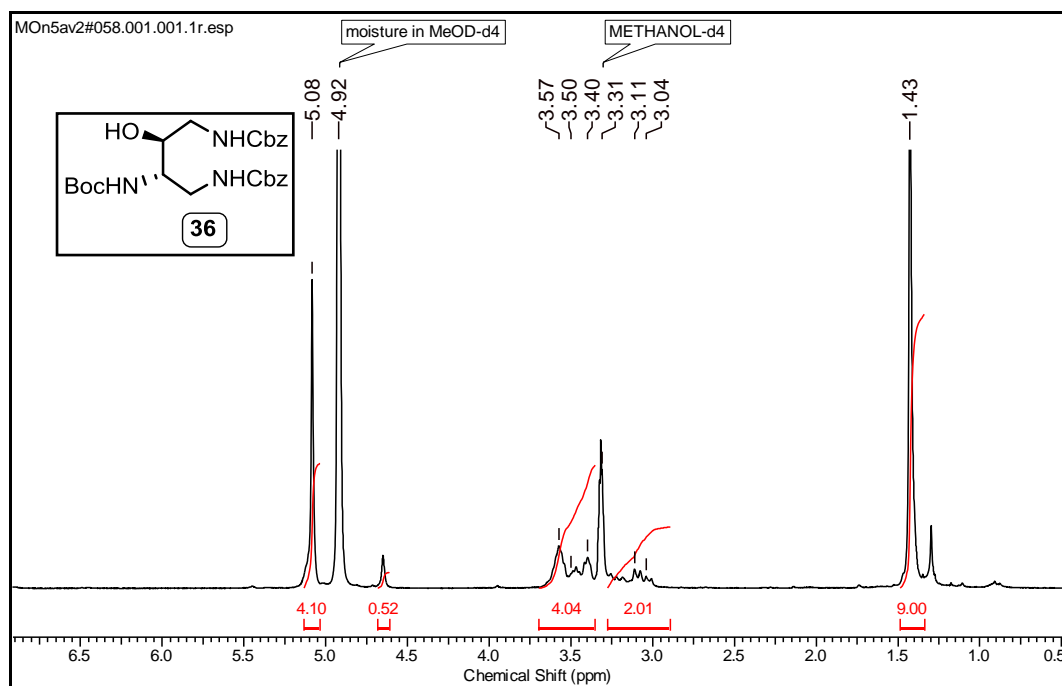
^{13}C NMR (50 MHz; CDCl$_3$) spectrum of compound **36**:
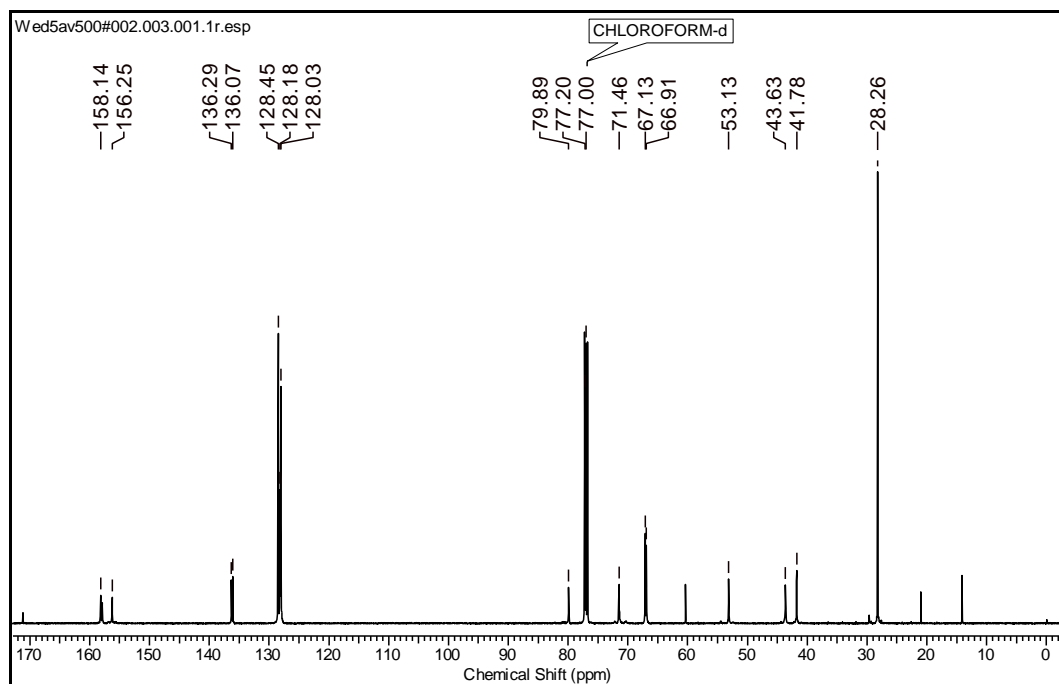
^{13}C DEPT (50 MHz; CDCl$_3$) spectrum of compound **36:**

¹H NMR (200 MHz; CDCl₃) spectrum of compound **37**:

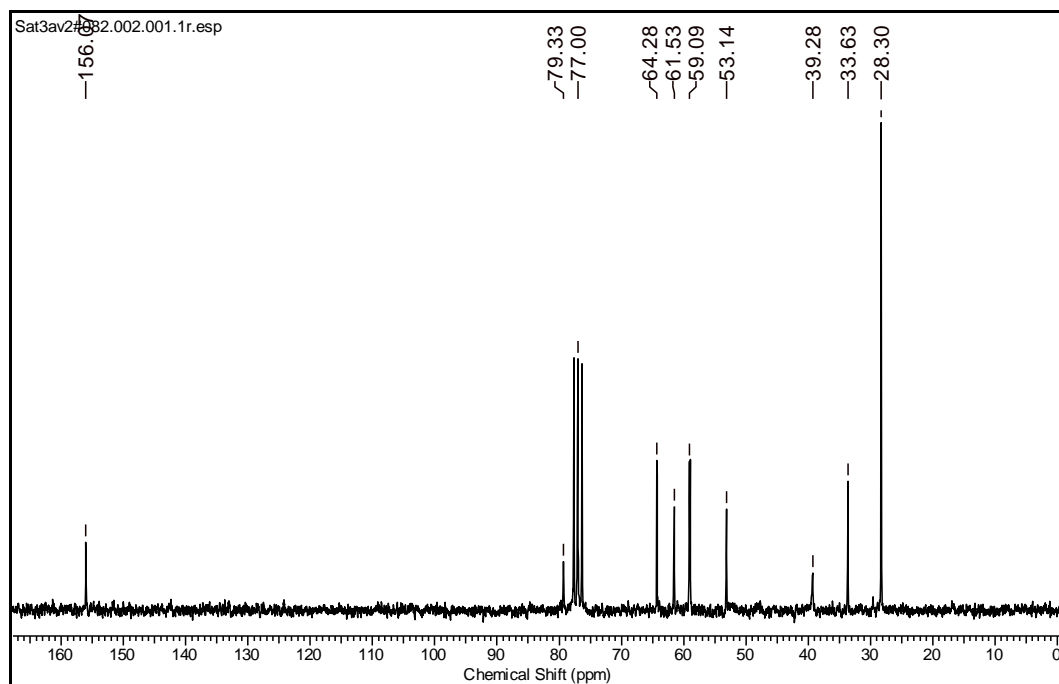## ¹³C NMR (100 MHz; CDCl₃) spectrum of compound **37**:

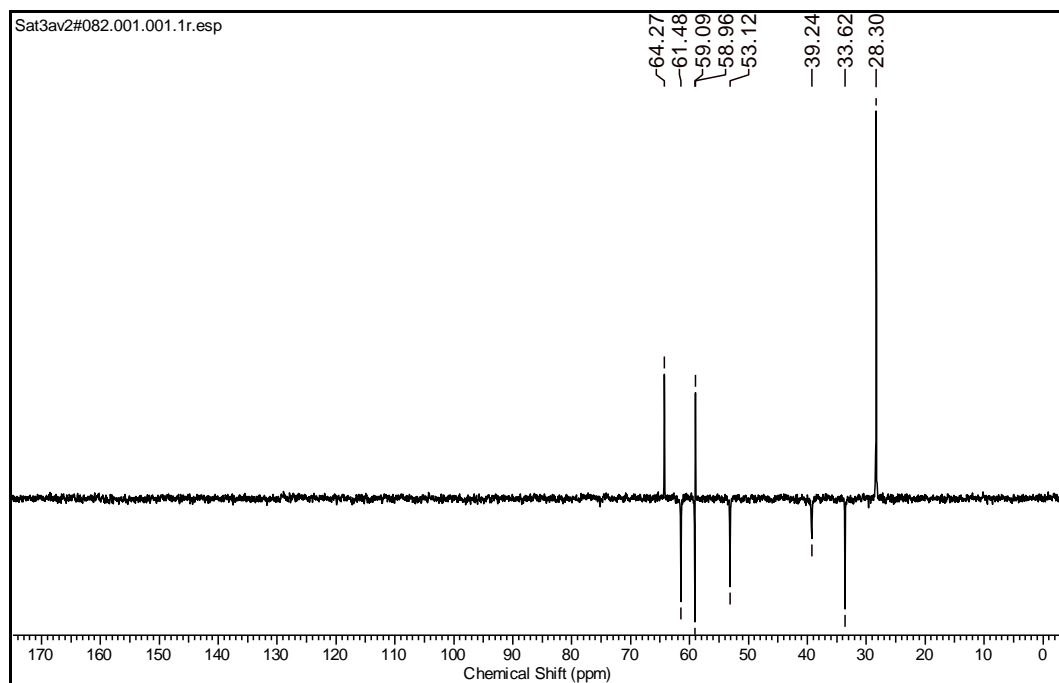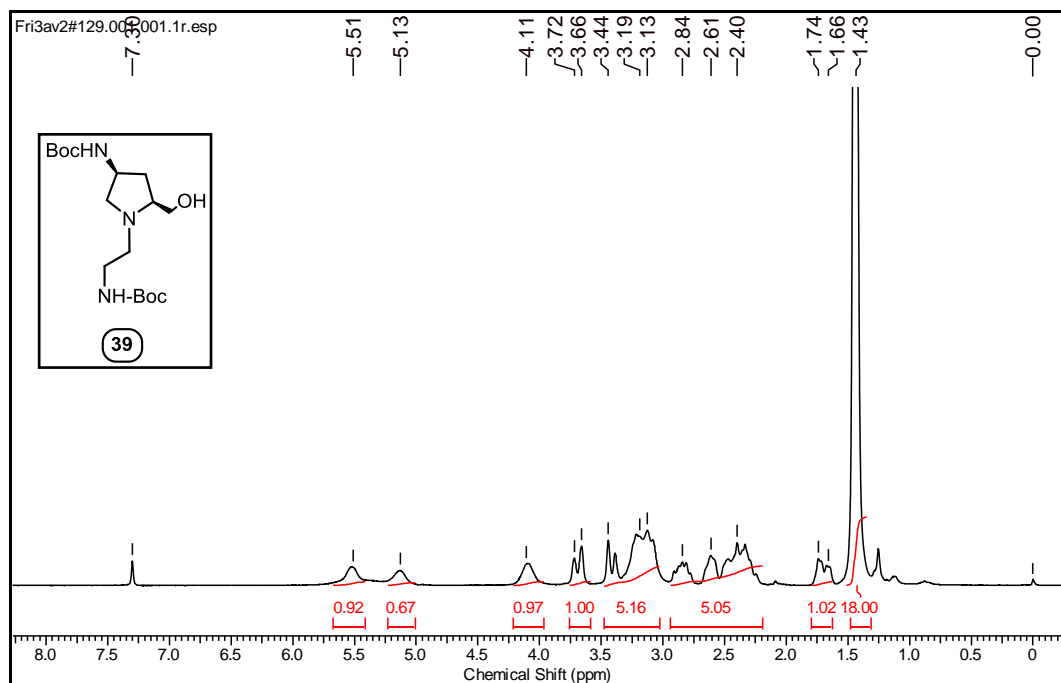## ^{13}C DEPT (100 MHz; CDCl$_3$) spectrum of compound **37**:

^{1}H NMR (200 MHz; CDCl$_3$) spectrum of compound **38**:

^{13}C NMR (100 MHz; CDCl$_3$) spectrum of compound **38**:
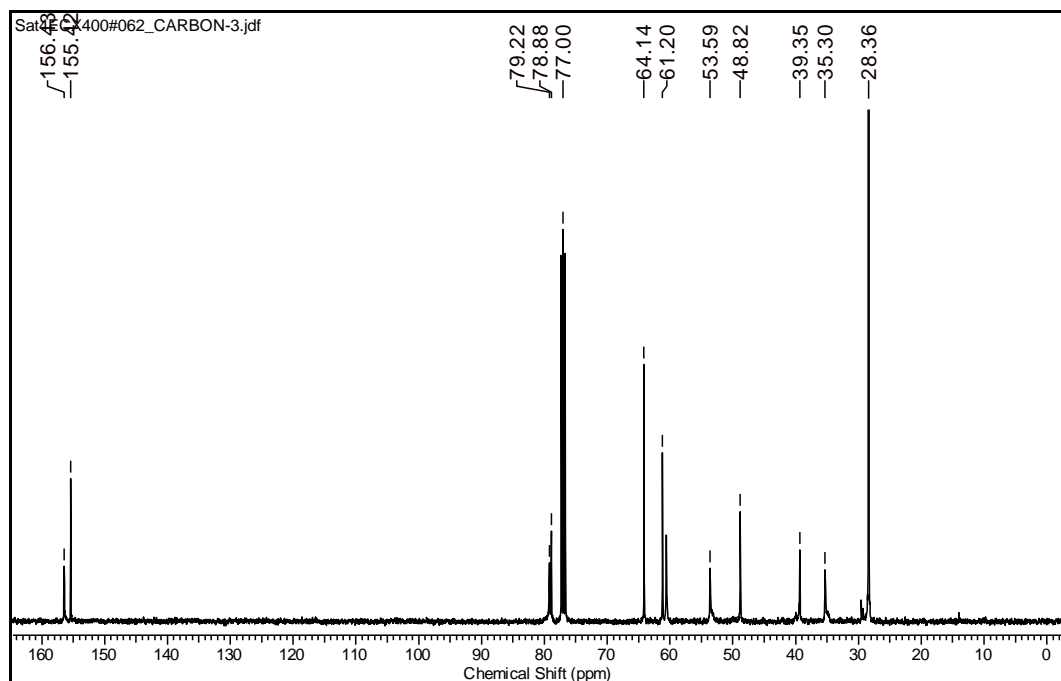

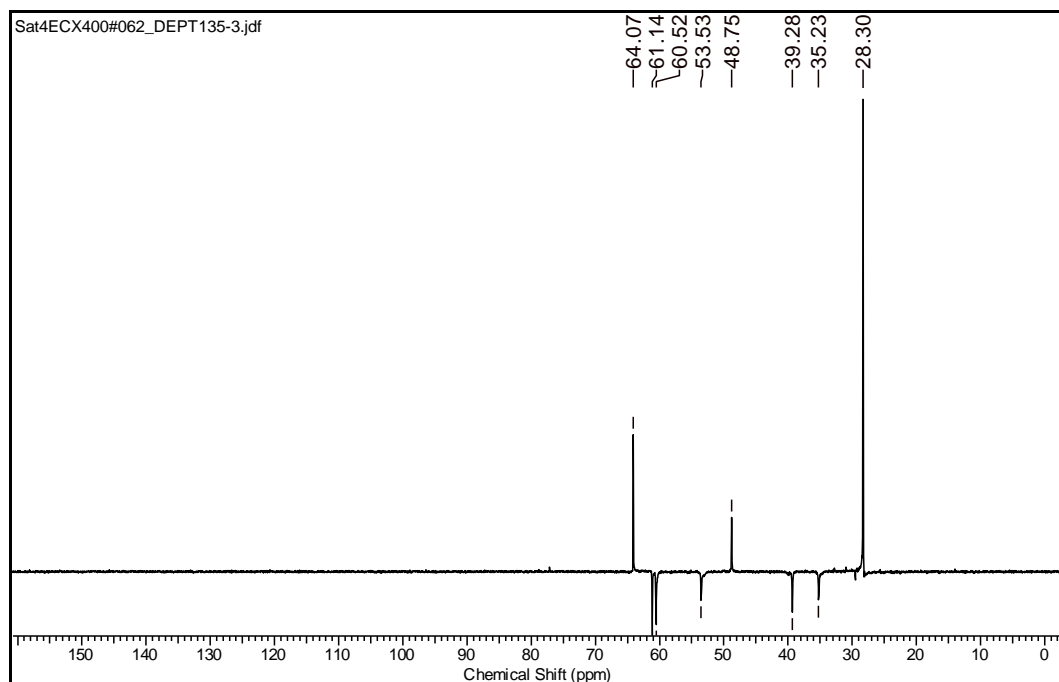## ^{13}C DEPT (100 MHz; CDCl$_3$) spectrum of compound **38**:

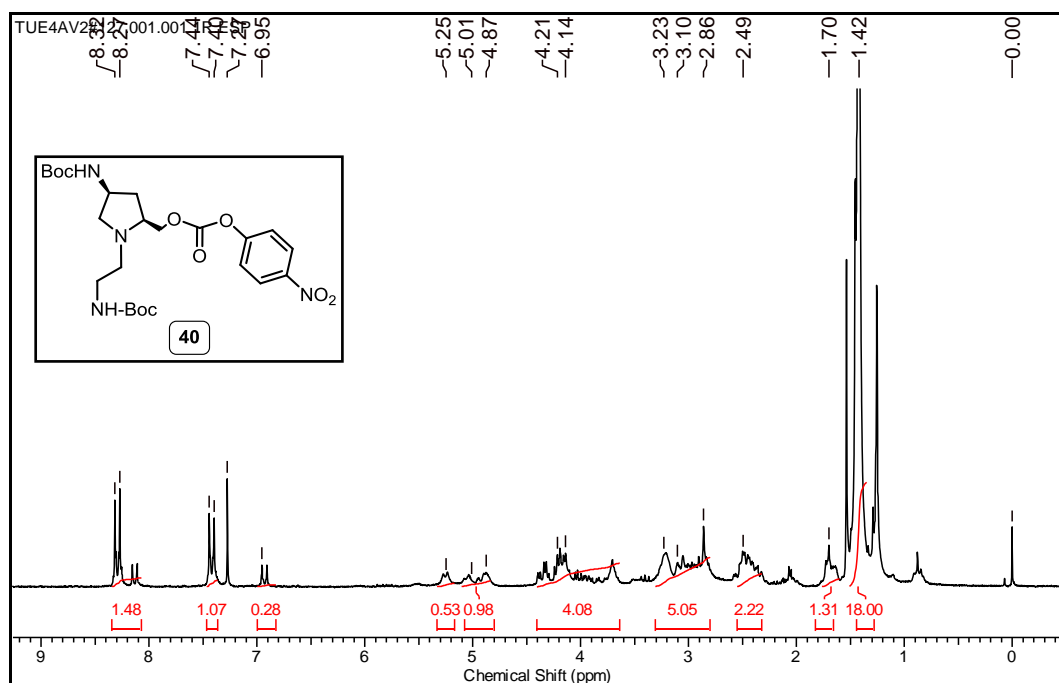^{1}H NMR (200 MHz; CDCl$_3$) spectrum of compound **39:**

^{13}C NMR (100 MHz; CDCl$_3$) spectrum of compound **39**:
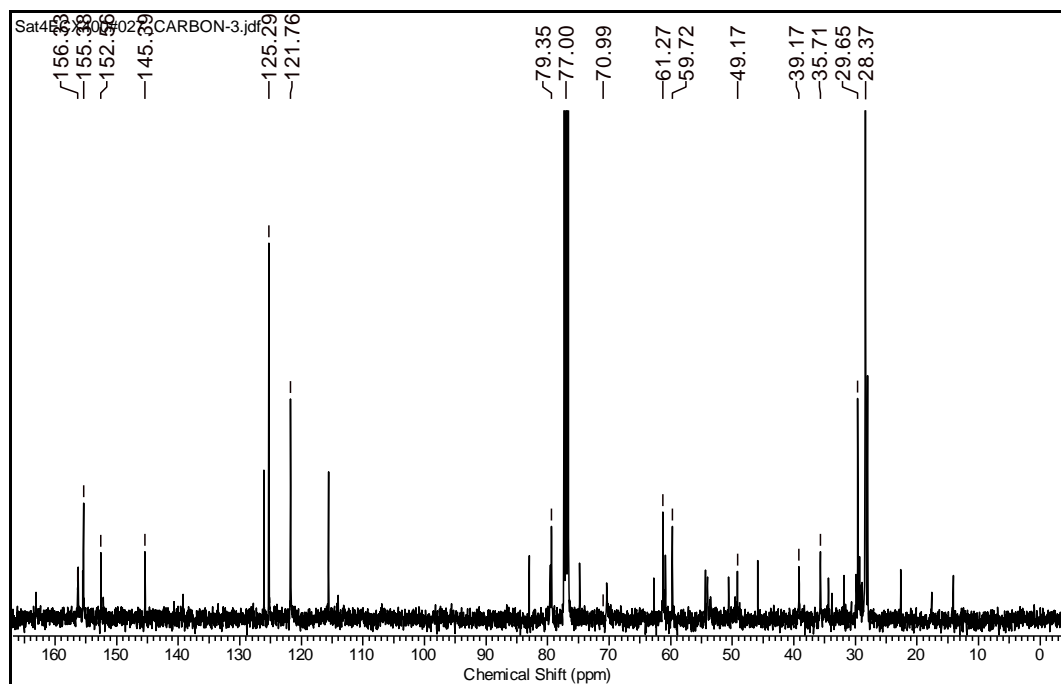
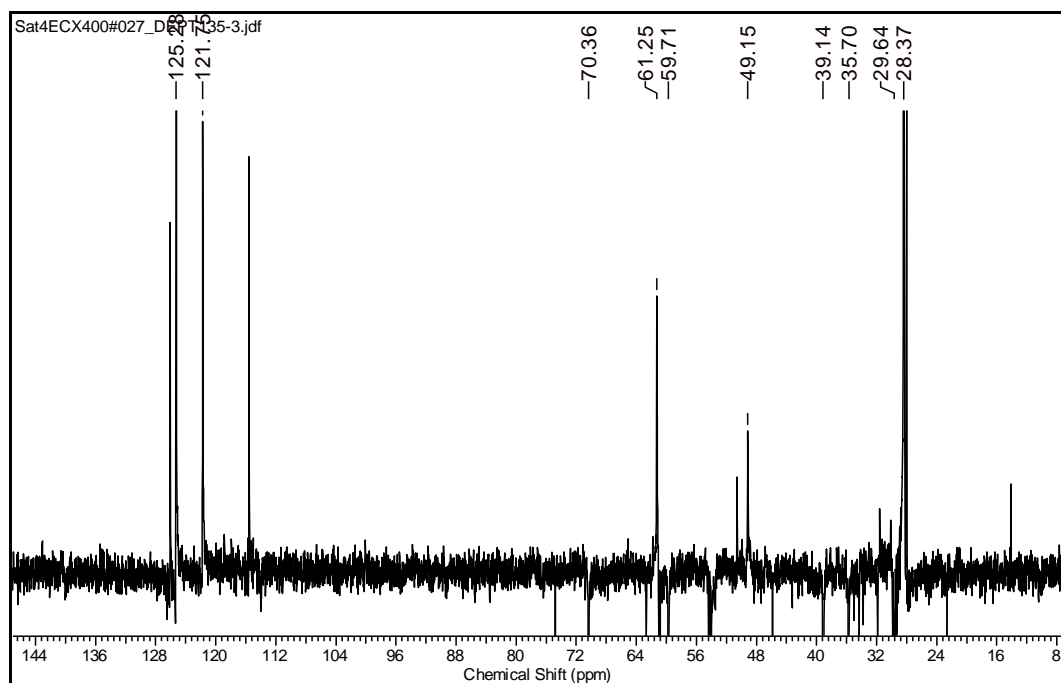## ^{13}C DEPT (100 MHz; CDCl$_3$) spectrum of compound **39**:

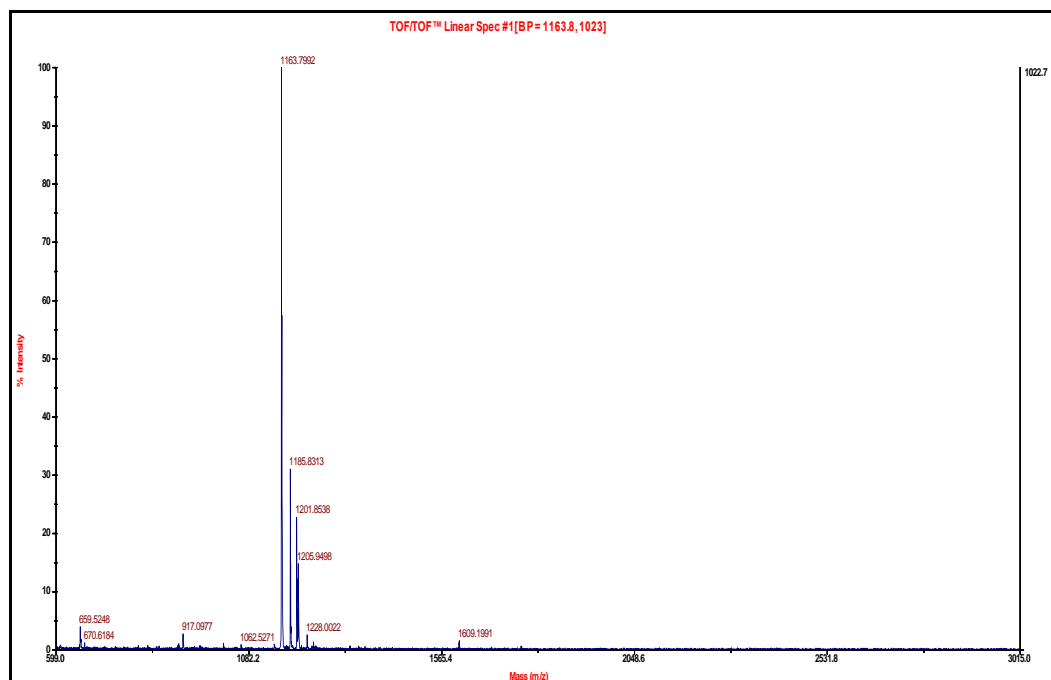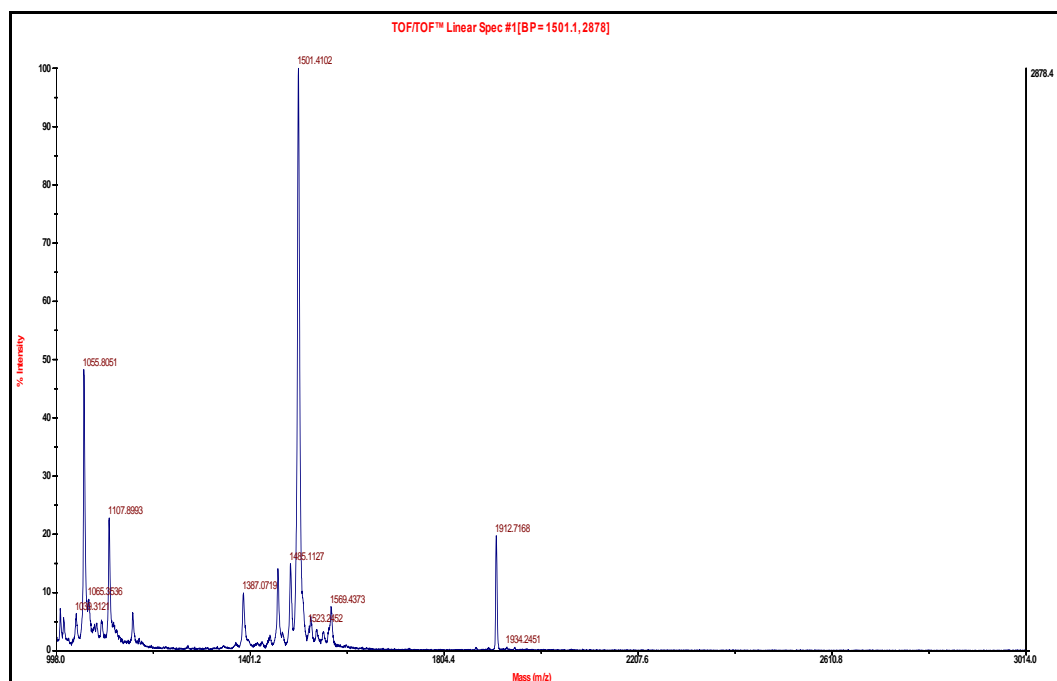## ^{1}H NMR (200 MHz; CDCl$_3$) spectrum of compound **40:**

^{13}C NMR (100 MHz; CDCl$_3$) spectrum of compound **40**:

^{13}C DEPT (100 MHz; CDCl$_3$) spectrum of compound **40**:

Maldi spectrum of Oligocarbamate ^{Ac}C4$_{NH}$:

Maldi spectrum of Oligocarbamate ^{Ac}C4$_{gua}$:

4.2 References

1. Fawell, S.; Seery, J.; Daikh, Y.; Moore, C.; Chen, L.; Pepinsky, B.; Barsoum, J. Tat-mediated delivery of heterologous proteins into cells. *Proceedings of the National Academy of Sciences of the United States of America* **1994,** *91*, 664-668.

2. (a) Derossi, D.; Joliot, A.; Chassaing, G.; Prochiantz, A. The third helix of the Antennapedia homeodomain translocates through biological membranes. *The Journal of Biological Chemistry* **1994,** *269*, 10444-10450. (b) Théodore, L.; Derossi, D.; Chassaing, G.; Llirbat, B.; Kubes, M.; Jordan, P.; Chneiweiss, H.; Godement, P.; Prochiantz, A. Intraneuronal delivery of protein kinase C pseudosubstrate leads to growth cone collapse. *The Journal of Neuroscience* **1995,** *15*, 7158-7167.

3. Schmidt, N.; Mishra, A.; Lai, G. H.; Wong, G. C. L. Arginine-rich cell-penetrating peptides. *FEBS Letters* **2010,** *584*, 1806-1813.

4. Naik, R. J.; Chandra, P.; Mann, A.; Ganguli, M. Exogenous and Cell Surface Glycosaminoglycans Alter DNA Delivery Efficiency of Arginine and Lysine Homopeptides in Distinctly Different Ways. *Journal of Biological Chemistry* **2011,** *286*, 18982-18993.

5. Mäe, M.; Langel, Ü. Cell-penetrating peptides as vectors for peptide, protein and oligonucleotide delivery. *Current Opinion in Pharmacology* **2006,** *6*, 509-514.

6. Farrera-Sinfreu, J.; Giralt, E.; Royo, M.; Albericio, F. Cell-Penetrating Proline-Rich Peptidomimetics. In *Peptide Characterization and Application Protocols*, Fields, G., Ed. Humana Press: 2007; Vol. 386, pp 241-267.

7. (a) Wender, P.; Rothbard, J.; Jessop, T.; Kreider, E.; Wylie, B. Oligocarbamate molecular transporters: design, synthesis, and biological evaluation of a new class of transporters for drug delivery. *Journal of the American Chemical Society* **2002,** *124*, 13382-13383. (b)Patil, K.; Naik, R.; Rajpal; Fernandes, M.; Ganguli, M.; Kumar, V. Highly efficient (R-X-R)-type carbamates as molecular transporters for cellular delivery. *Journal of the American Chemical Society* **2012,** *134*, 7196-7199.

8. Cooley, C.; Trantow, B.; Nederberg, F.; Kiesewetter, M.; Hedrick, J.; Waymouth, R.; Wender, P. Oligocarbonate molecular transporters: oligomerization-based syntheses and cell-penetrating studies. *Journal of the American Chemical Society* **2009,** *131*, 16401-16403.

9. Tamilarasu, N.; Huq, I.; Rana, T. M. Targeting RNA with peptidomimetic oligomers in human cells. *Bioorganic & Medicinal Chemistry Letters* **2001,** *11*, 505-507.

10. (a) Medina, S.; El-Sayed, M. Dendrimers as carriers for delivery of chemotherapeutic agents. *Chemical Reviews* **2009,** *109*, 3141-3157. (b) Tamis, D.; Jean-Louis, R. Peptide Dendrimers as Artificial Enzymes, Receptors, and Drug-Delivery Agents. *Accounts of Chemical Research* **2006,** *39*. (c) Jun, H. L.; Anjan, N. Combination Drug Delivery Approaches in Metastatic Breast Cancer. *Journal of Drug Delivery* **2012,** *2012*.

11. Lee, J. H.; Nan, A. Combination Drug Delivery Approaches in Metastatic Breast Cancer. *Journal of Drug Delivery* **2012,** *2012*, 17.

12. (a) Tomalia, D. A.; Naylor, A. M.; Goddard, W. A. Starburst Dendrimers: Molecular-Level Control of Size, Shape, Surface Chemistry, Topology, and Flexibility from Atoms to Macroscopic Matter. *Angewandte Chemie International Edition in English* **1990,** *29*, 138-175. (b) Gillies, E. R.; Fréchet, J. M. J. Dendrimers and dendritic polymers in drug delivery. *Drug Discovery Today* **2005,** *10*, 35-43. (c) Boas, U.; Heegaard, P. M. H. Dendrimers in drug research. *Chemical Society Reviews* **2004,** *33*, 43-63.

13. Esfand, R.; Tomalia, D. A. Poly(amidoamine) (PAMAM) dendrimers: from biomimicry to drug delivery and biomedical applications. *Drug Discovery Today* **2001,** *6*, 427-436.

14. Duncan, R.; Izzo, L. Dendrimer biocompatibility and toxicity. *Advanced Drug Delivery Reviews* **2005,** *57*, 2215-2237.

15. (a) Choi, J. S.; Lee, E. J.; Choi, Y. H.; Jeong, Y. J.; Park, J. S. Poly(ethylene glycol)-block-poly(l-lysine) Dendrimer: Novel Linear Polymer/Dendrimer Block Copolymer Forming a Spherical Water-Soluble Polyionic Complex with DNA. *Bioconjugate Chemistry* **1998,** *10*, 62-65. (b) Choi, J. S.; Nam, K.; Park, J.-y.; Kim, J.-B.; Lee, J.-K.; Park, J.-s. Enhanced transfection efficiency of PAMAM dendrimer by surface modification with l-arginine. *Journal of Controlled Release* **2004,** *99*, 445-456.

16. Turnbull, W. B.; Stoddart, J. F. Design and synthesis of glycodendrimers. *Reviews in Molecular Biotechnology* **2002,** *90*, 231-255.

17. Newkome, G. R.; Moorefield, C. N.; Baker, G. R.; Saunders, M. J.; Grossman, S. H. Unimolecular Micelles. *Angewandte Chemie International Edition in English* **1991,** *30*, 1178-1180.

18. (a) Lim, J.; Guo, Y.; Rostollan, C. L.; Stanfield, J.; Hsieh, J.-T.; Sun, X.; Simanek, E. E. The Role of the Size and Number of Polyethylene Glycol Chains in the Biodistribution and Tumor Localization of Triazine Dendrimers. *Molecular Pharmaceutics* **2008,** *5*, 540-547. (b)Gillies, E. R.; Dy, E.; Fréchet, J. M. J.; Szoka, F. C. Biological Evaluation of Polyester Dendrimer: Poly(ethylene oxide) "Bow-Tie" Hybrids with Tunable Molecular Weight and Architecture. *Molecular Pharmaceutics* **2005,** *2*, 129-138.

19. (a) Goodwin, A. P.; Lam, S. S.; Fréchet, J. M. J. Rapid, Efficient Synthesis of Heterobifunctional Biodegradable Dendrimers. *Journal of the American Chemical Society* **2007,** *129*, 6994-6995. (b)Grinstaff, M. W. Biodendrimers: New Polymeric Biomaterials for Tissue Engineering. *Chemistry – A European Journal* **2002,** *8*, 2838-2846.

20. Peerlings, H. W. I.; Benthem, R. A. T. M. V.; Meijer, E. W. Fast and convenient construction of carbamate/urea-based dendrimers with a diisocyanate building block. *Journal of Polymer Science Part A: Polymer Chemistry* **2001,** *39*.

21. Roey, J. A.; Doron, S. Self-immolative dendrimer biodegradability by multi-enzymatic triggering *Chemical Communications* **2004,** 1614

22. Divya, K.; Vinod, K. T. Click Chemistry Inspired Synthesis of Glycoporphyrin Dendrimers. *The Journal of Organic Chemistry* **2013,** *78*.

23. Saleh, A.; Arzumanov, A.; Abes, R.; Owen, D.; Lebleu, B.; Gait, M. Synthesis and splice-redirecting activity of branched, arginine-rich peptide dendrimer conjugates of peptide nucleic acid oligonucleotides. *Bioconjugate Chemistry* **2010,** *21*, 1902-1911.